

THE ROLE OF EXTRACELLULAR VESICLES IN RADIATION LEUKAEMOGENESIS

DPhil in Oncology



ERIC RUTTEN
KEBLE COLLEGE

Table of Contents

1. Introduction 9

1.1 Acute Myeloid Leukaemia and radiation 9

1.2 Extracellular vesicles 19

1.3 Vesicles involved in bystander response 22

1.4 Micro RNAs, a regulatory cargo shuttled by EVs 24

1.5 Murine models 27

1.6 Research aims 31

2. Materials and Methods 34

2.01 Ethical Considerations 36

2.02 Irradiation Protocols 36

2.03 Period and location of studies performed 37

2.04 Subjects of study 37

2.05 Murine models 39

2.06 Blood Testing and Flow Cytometry: 45

2.07 Schedule 1 techniques used 45

2.08 Bone Marrow Extraction: 45

2.09 Radiation end points and experimental design 46

2.10 Serum-free techniques for tissue culture: 47

2.11 Bone marrow-derived Macrophage culture: 51

2.12 Bone marrow-derived Mesenchymal stem cell culture: 52

2.13 Murine HSPC culture: 53

2.14 Extracellular vesicle purification: 55

2.15 miRNA extraction from cellular and EV sources: 57

2.16 miRNA analysis by nCounter: 58

2.17 Lysine level assay: 62

2.18 Aldehyde and Aldh activity assay: 63

2.19 Free fatty acid level assay: 63

2.20 Gene expression assay: 63

3. Extracellular vesicle landscape of the bone marrow 66

3.01 Immediate post-radiation response; the miRNA landscape of CBA mice 24 hours post radiation insult 66

3.02 Late effects in transgenic mch/GFP CBA mice; the miRNA landscape in IR-induced AML 78

3.03 Comparison of irradiated mice to preleukaemic, non-irradiated mice 105

3.04 Strain Dependent Variation on Radiation Signature and Potential Dose Dependent Responses 108

3.05 Chromosomal locations of differentially regulated miRNAs 110
3.06 Discussion 113
4. Cell-type specific miRNA responses to radiation: Breaking down the larger picture 123
4.01 BM-derived macrophage response to ionising radiation 123
4.02 BM-derived mesenchymal stem cell (MSC) response to ionising radiation 141
4.03 Chromosomal distributions of DE miRNA in BM macrophages and MSCs 156
4.04 Discussion and implications 159
5. Metabolic effects and gene dysregulation in progenitor cells 165
5.01 Lysine dysregulation in progenitor cells 165
5.02 Effect of radiation on aldehyde and fatty acid concentrations 167
5.03 Differential expression of miRNA-targeted genes in progenitor cells 171
5.04 Discussion and potential implications 175
6. Discussion 177
6.1 Summary of key findings and context within the research 177
6.2 Extracellular Role in the Radiation Damage Response and Oncogenesis 183
6.3 Limitations of the study 204
6.4 Future research and implications 207
6.5 Hypotheses and Conclusions 215
7. References Cited 223
8. Appendix 259

List of Tables and Figures

1. Introduction 9

Figure 1.01: The Linear Non-Threshold model. 10

Figure 1.02: Relative Risk of solid cancer vs exposure. 11

Figure 1.03: AML risk summary plot vs weighted dose. 11

Figure 1.04: Role of extracellular vesicles in normal homeostasis of the bone marrow microenvironment. 24

Figure 1.05: The importance of PU.1/Sfpi1 and the mCh/GFP CBA mouse. 29

Figure 1.06: SPM CBA mouse. 30

2. Materials and Methods 34

Figure 2.01: High level overview of experimental planning and processes 35

Figure 2.02: A transgenic murine model for clonal expansion tracking 40

Figure 2.03: Non-preleukaemic mouse 41

Figure 2.04: Preleukaemic mouse 42

Figure 2.05: Classical AML disease progression in CBA-strain Mus musculus and Homo sapiens. 44

Figure 2.06: Growth curves of different combinations of complete or conditioned media with Panexin Basic or CD, compared to baseline RPMI medium, in MLP3. 49

Figure 2.07: Comparative staining of macrophages. 51

Figure 2.08: Abbreviated conceptual workflow of the nCounter probe hybridization process. 60

Figure 2.09: General experimental workflow. 65

3. Extracellular vesicle landscape of the bone marrow 66

Figure 3.01: Heatmap graphical representation of murine miRNA, isolated from bone marrow, 24 hours post radiation exposure 67

Table 3.01: Dysregulated miRNA in 24 hours post IR WT-CBA mice. 69

Table 3.02. MiRNAs correlating with the dose. 70

Table 3.03: Overlapping miRNA across 0.1Gy and 3Gy-irradiated CBA mice 24 hours post radiation exposure 71

Figure 3.02: Venn diagram showing the involved pathways and intersections between the four conserved miRNAs at 0.1 and 3Gy 73

Table 3.04: Targeted pathways as predicted by KEGG in sham vs 3Gy WT CBA mice, 48 hours post radiation exposure. 74

Table 3.05. Common pathways between differentially expressed miRNAs 76

Figure 3.03. Common pathways between differentially expressed miRNAs from bone marrow-derived extracellular vesicles 77

Figure 3.04: Heatmap showing the miRNA expression patterns in CBA mCh/GFP mice TBI at 3Gy. 79

Table 3.06: List of differentially regulated miRNA in sham vs low clonal expansion (<30%) CBA mCh/GFP mice. 81

Table 3.07: KEGG-predicted targeted pathways in sham vs low clonal expansion mch/GFP CBA mice. 87

Table 3.08: List of differentially regulated miRNA in sham vs high clonal expansion (>30%) CBA mCh/GFP mice. 89

Table 3.09: KEGG-predicted pathways in sham vs high clonal expansion CBA mch/GFP mice. Table continued on page 94. 93

Table 3.10: Gene targets of miRNA associated with AML development in the KEGG database. 96

Figure 3.05: Gene target overlaps of the Wnt, Hippo, MAPK and FoxO signalling pathways in high clonal expansion mCh/GFP mice 97

Figure 3.06: Overlaps in interacting miRNA between common genes 98

Figure 3.07: EV vs cellular miRNA 100

Table 3.11: KEGG-predicted pathways targeted by statistically relevant miRNA in EVs vs BM cells in irradiated CBA mCh/GFP with >30% clonal expansion in the myeloid compartment. 101

Table 3.12: Statistically relevant miRNA enriched in EVs and their predicted biological function. 102

Figure 3.08: Genetic and miRNA overlap between metabolic pathways 104

Figure 3.09: Heat map of preleukaemic EVs vs SPM-derived EVs 107

Table 3.13: Statisfically significant miRNA, determined by both p-value and FDR being sub 0.05, when comparing different doses of irradiation to sham controls in C57BL/6J Ldlr KO mice 108

Figure 3.10: Heat map of BM-derived EVs from 0Gy, 0.5Gy, 2Gy, and 4Gy 109

Table 3.14: Genomic locations of differentially regulated miRNA across murine data sets, sourced from miRDB. 111

Figure 3.11: Number of miRNAs per chromosome as combined score, 48 hours post IR in WT CBA mice, and 12 months post IR in high clonal expansion CBA mCh/GFP mice. 112

Figure 3.12: Hypothetical interaction pathway for miR-302c, miR-497a, miR-181c and miR-128 during AML progression after initial IR insult 120

4. Cell-type specific miRNA responses to radiation: Breaking down the larger picture 123

Table 4.01: Differentially regulated miRNAs in 2Gy vs 0Gy BM-derived macrophages, and their suspected or confirmed biological interactions 124

Figure 4.01: Irradiated and unirradiated murine BM-derived macrophage EV miRNA. 128

Table 4.02: miRNA-gene interactions in the KEGG database acute myeloid leukaemia pathway. 130

Table 4.03: KEGG-predicted pathways associated with differentially expressed miRNA in 2Gy vs 0Gy BM-derived murine macrophages. Created using DIANATools miRPath v.3. 131

Figure 4.02: Significant pathways of differentially expressed genes (DE) in BM-derived macrophages 132

Figure 4.03: Volcano plot showing statistically significant DE miRNA and their fold changes with respect to 0Gy control in BM-derived macrophages. 133

Figure 4.04: Significant pathways of differentially expressed genes (DE) in BM-derived Macrophages. 139

Figure 4.05: Gene target overlap between up- and downregulated miRNA gene targets of the FoxO pathway in BM-derived macrophages. 140

Table 4.04: Differentially regulated miRNAs in 2Gy vs 0Gy MSCs, and their suspected or confirmed biological interactions 142

Table 4.05: miRNA-gene interactions in the KEGG database proteoglycans in cancer pathway. 144

Figure 4.06: BM mesenchymal stem cell signalling network gene target overlap and regulating miRNA 146

Figure 4.07: Notch signalling pathway interactome with downregulated miRNA in BM-derived mesenchymal stem cells 149

Figure 4.07: Irradiated and unirradiated BM-derived MSC EV miRNA. 151

Table 4.06: KEGG-predicted pathways associated with differentially expressed miRNA in 2Gy vs 0Gy BM-derived murine mesenchymal stem cells 152

Figure 4.07: Significant pathways of differentially expressed genes (DE) in BM-derived MSCs. 153

Figure 4.08: Volcano plot showing statistically significant DE miRNA and their fold changes with respect to 0Gy control in BM-derived macrophages. 154

Figure 4.09: Gene Ontology (GO) terms for DE miRNA gene targets in MSCs 155

Table 4.07: Genomic locations of differentially regulated miRNA across murine data sets, sourced from miRBase 157

Figure 4.10: Number of miRNAs per chromosome as combined score, in macrophages, and mesenchymal stem cells 158

5. Metabolic effects and gene dysregulation in progenitor cells 165

Figure 5.02 Aldehyde concentration in BM-derived MSCs and murine HSCs 168

Figure 5.03 Fatty acid concentration in conditioned media. 170

Figure 5.06 Fasn expression in BM-derived MSCs and HSCs. 174

Figure 5.07: Pictorial summary of metabolic data 175

6. Discussion 177

Table 6.1: Subdivision of miRNAs into known pro-oncogenic, anti-oncogenic or unknown categories 197

Table 6.2: Gene targets of select miRNA. 198

Figure 6.01: Possible pathways for EV export and miRNA profile composition. 203

Figure 6.03: Flowchart showing the experimental process for FACS-assisted determination of EV-induced chromosomal damage in human PBMCs 209

Figure 6.03: List of different techniques which can be used to study cancer cell metabolism. 214

Figure 6.04: Overview of processes in rAML development and which sections of the process have been studied 215

Figure 6.05: Hypothetical regulatory interaction network in early-stage post-IR response within the bone marrow 217

Figure 6.06: Hypothetical pathway for the development of AML over time 218

Figure 6.07: Simplified overview of some of the hypotheses generated during this research. 222

7. References Cited 223

8. Appendix 259

Figure A.01: Lineage depleted and adaptive media-derived EVs. 260

Figure A.02: Staining of different EV samples with ALIX, TSG101 and CD63. 261

Table 3.01a: Hippo pathway gene targets 262

Table 3.01b: MAPK pathway gene targets 263

Table 3.01c: Wnt pathway gene targets 264

Table 3.01d: FoxO pathway gene targets 265

Figure 4.01A: Notch signalling in mesenchymal stem cells 266

Acknowledgements

I would like to express my deepest gratitude to my supervisors, Dr. Christophe Badie and Dr. Mark Hill, for their invaluable guidance, patience, and feedback throughout my doctoral project, from research planning to thesis writing. I would also like to thank Dr. Lourdes Cruz-Garcia for helping me so much on a day-to-day basis, training me in so many essential protocols, and helping me with scientific considerations and planning. My gratitude extends to all the members of the Cancer and Biomarkers group at UKHSA, and I would like to personally thank Dr. Grainne O'Brien, Dr. Rosie Finnon, and Paul Finnon for all their help. This endeavour would not have been possible without our kind, dedicated collaborators at the National Public Health Institute of Hungary, especially Dr. Katalin Lumniczky and Dr. Tünde Szatmári, and my co-author on our paper published on LEUTRACK, Ilona Barbara Csordás.

I would also like to thank my family for their support throughout these years. Their unwavering faith in me has kept me motivated throughout the entire DPhil project, and I could not have done it without them.

Abstract

Ionising radiation is an increasingly more important part of our world, with many opportunities for exposure to the public, such as occupational, environmental, and clinical. Reduction of accumulated dose is essential to prevent deleterious stochastic effects arising from radiation exposure. Stochastic effects arising from radiation include cancer, especially acute myeloid leukaemia (AML), a highly aggressive cancer of the bone marrow. To understand and establish exposure thresholds as well as potential biomarkers thereof, the mechanisms of AML must be studied. At low doses of ionising radiation, non-targeted effects, such as the bystander effect, are highly represented. One route by which bystander effects act is via extracellular vesicles (EVs), small signalling particles produced by cells. EVs are a rapidly growing field of interest, both from a mechanistic and clinical point of view. Using a combination of murine models, including CBA and a transgenic CBA mouse allowing for tracking of AML progression, we analysed the EV miRNA content of irradiated murine BM and preleukaemic BM. We then analysed the miRNA content of BM-derived subpopulations, such as macrophages and mesenchymal stem cells, 48 hours post radiation. We tested the metabolic effect of radiation derived EVs on recipient cells, analysing impact on lysine levels, fatty acids, and free aldehydes, and gene expression. There is a conserved EV miRNA signature in transgenic CBA mice with high levels of clonal expansion, as well as dysregulation of lysine, fatty acid and aldehyde metabolism. EVs showed a mixed profile of pro-tumour and tumour-suppressant miRNA content, often with more tumour-suppressant miRNA overexpressed in radiation derived EVs. These findings demonstrate promise for the development of a miRNA-based post exposure biomarker panel, as well as offering insights into little studied routes of EV influence on metabolic processes in radiation injury response and oncogenesis, opening up opportunities for future research into both biomarkers and clinical targets.

1. Introduction

1.1 Acute Myeloid Leukaemia and radiation

Ionising radiation (IR) is a constant in our lives. Every single organism on Earth is exposed to IR in some form, such as exposure to radon gas, consumption of radionuclides, cosmic ray radiation penetrating through the atmosphere (especially at high altitudes), and these are just the natural sources of ionising radiation (WHO). We are also exposed to ionising radiation through occupational exposures; according to the IAEA, this primarily occurs in mining, milling, medical and research institutions, and in nuclear fuel cycle facilities (IAEA, 2002), with the IAEA raising concerns that the increasing use of IR-dependent medical procedures has concurrently resulted in a rapid increase in the number of occupationally exposed workers (IAEA, 2022), with as of 2022 over 24 million people worldwide being monitored for potential or actual IR exposure. Further sources of exposure include medical and diagnostical, although there is still debate as to how significant this is on average: in the USA, patient exposure averages at around 3 mSV per year from background radiation alone, while chest X-ray exposure is 0.1 mSV and CT scans 5-15 mSV (Akram & Chowdhury, Statpearl, 2022; Health Physics Society; Harvard Health), note that these are Effective Doses. In the case of CT scans, this falls in the lower range of exposures for which epidemiological data for increased cancer risk exists (Mercuri *et al.,* 2011, Canadian Medical Association Journal). As such, a single medical exam is unlikely to pose significant risk, but repeated exposures and accumulated dose may. Another source of exposure still are nuclear events, both deliberate and accidental, as has occurred in survivors of the atom bomb and radiation accidents such as Chernobyl and Fukushima. Epidemiological studies of these cohorts has yielded the linear non-threshold model (LNT), which is of particular import to the analysis in this thesis. The LNT model extrapolates from higher doses into lower doses in an attempt to estimate cancer risk, based on the postulate that all IR, no matter the dose, is harmful, and this effect is cumulative and contributes to an increased cancer risk over the course of a lifetime (Yanovskiy *et al.,* 2019, Dose Response). The BEIR

VII phase 2 reports as well as the ICRP 2007 publication 103 report both demonstrate an increase in relative cancer risk correlating to dose. As such, cancer risk is a major concern in environmental, medical, occupational, and accidental exposures, making understanding of stochastic effects of paramount importance. Especially given a renewed interest in manned space missions, and the associated cosmic ray exposure, further understanding of radiation cancer mechanisms and potential ways to mitigate or avoid them are necessary for safe space exploration.

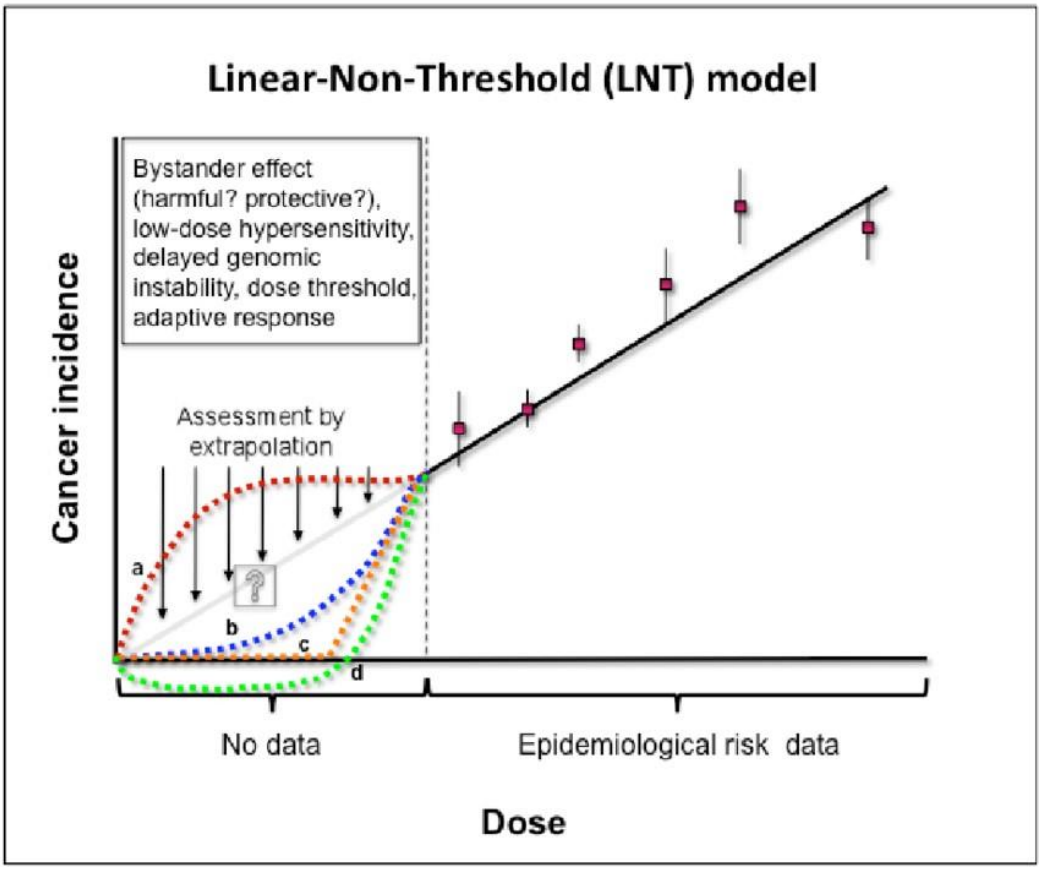


Figure 1.01: The Linear Non-Threshold model. Reproduced from Mancuso *et al.,* 2012, Current Molecular Medicine.

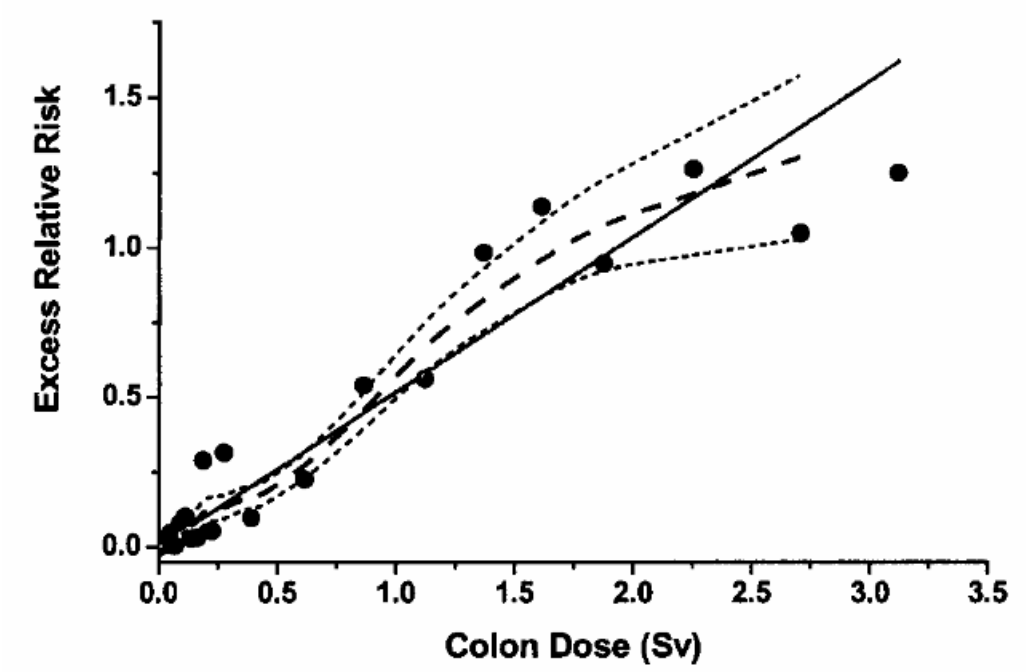


Figure 1.02: Relative Risk of solid cancer vs exposure. Reproduced from *Health Risks from Exposure to Low Levels of Radiation: BEIR VII Phase 2 (2006).*

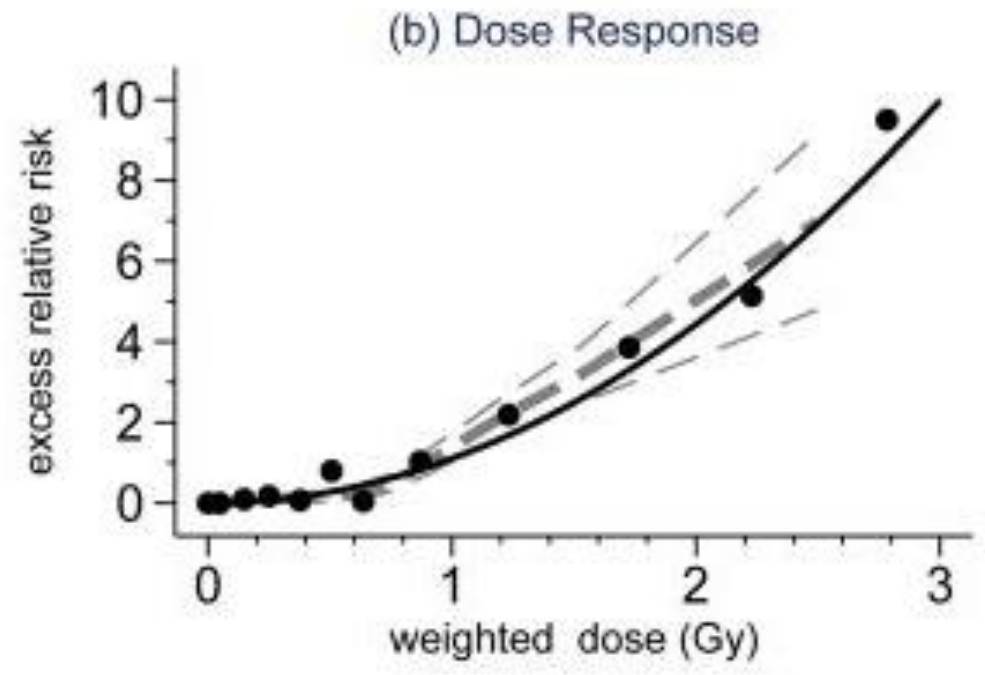


Figure 1.03: AML risk summary plot vs weighted dose. Reproduced and modified from Hsu *et al.,* 2013, Radiation Research. Solid black represents the pure fitted quadratic dose response curve.

Cancers are a leading concern in modern medicine, accounting for nearly 10 million deaths in 2020 (WHO). The unique and variant compositions of cancers, including difficulties in the critical stages of clinical treatment, which comprise avoidance, detection, and treatment, mean that cancer remains to this day a complex issue tackled by many research groups the world over. Despite many promising recent advancements in the field of cancer research and treatment, such as BioNTech's RNA vaccines, a versatile technology repurposed to deal with the current coronavirus pandemic, it will likely remain an issue for many years to come.

The most common cancers are breast, lung, colon & rectum (WHO), so called solid tumours, which are treated by primarily 3 main techniques: surgical excision of a primary tumour, chemotherapeutical suppression of the cancer, and radiotherapeutical targeting and elimination of cancerous tissue. Often a combination of all three methods is utilized. However, the difficulty begins especially with the lattermost treatment course, radiotherapy. Radiotherapy is an incredibly powerful technique for the treatment of solid tumours. Recent advancements in the technology such as Cyberknife, carbon ion, proton and FLASH techniques result in much higher sparing of healthy tissues than chemotherapy, notorious for systemwide deleterious effects. The reality is, however, that radiotherapy is somewhat of a double-edged sword. Leukaemia, particularly acute myeloid leukaemia (AML), is a major secondary cancer after radiation exposure, such as is the case after treatment of a primary cancer by radiotherapy and is also highly prevalent in atomic bomb survivors (Hsu *et al.,* 2013); less than 1% of *de novo* total cancer cases are AML (Cancer Research UK, 2019). This is not to say that AML is an inevitable outcome of radiation injury, but nevertheless it poses a significant concern as a potential long-term post-exposure risk.

Evidently, avoiding long term consequences of radiation exposure, among these medically necessary ones such as radiotherapy, dubbed stochastic effects, is preferential. The treatment of one cancer only to occur another is not an ideal outcome in any circumstance. The current paradigm with ionising-radiation (IR) induced AML is that IR directly damages

cells, whether via DNA double strand breaks (DSB) or reactive oxygen species generation. These DSB include complex DSB, which include additional strand-breaks and/or base damage within a few base pairs, decreasing the probability of faithful repair (Mavragani *et al.,* 2017, Cancers). It is important to note that the amount of DNA lesions produced by e.g. 1Gy of radiation is significantly smaller than that produced natively by a cell on a day-by-day basis: circa 40 DSB, 1000 single-strand breaks, >2000 base damages, and 30 DNA-DNA crosslinks are produced by Gy, compared to circa 50,000 endogenous DNA lesions (Hill, 2020, Clinical Oncology). What makes them unique is their ability to cause clustered, complex damage vs distributed endogenous damage, as mentioned previously. Increasing dose results in increasing complexity, but even at low LET, 20-50% of induced DSB are complex and thus resistant to repair (Hill, 2020, Clinical Oncology). At both high and low LET, these clusters of damage can be caused from two sources: direct damage done by radiation tracks, or short-range indirect effects in the form of free radicals. Indirect effects will be further expanded on later in this section (*idem)*. Especially at low LET, the indirect component of radiation damage is significant, with scavenging of free radicals being effective at reducing ensuing damage (*idem).* Besides DSB and DNA damage clusters, however, IR can also induce chromosomal rearrangements and aberrations due to mis-repair, which represent an early marker for late effects and stochastic effects (Durante & Formenti, 2018, Frontiers in Oncology), some of which can survive cell division (asymmetric aberrations) and pass down generations, contributing to radiation-induced genomic instability. As such, radiation exposure, even at low doses, can cause a wide variety of genomic damage to an organism, both immediate and long term, which can drive the development of stochastic effects such as cancer.

IR, in the short-term post-exposure, triggers a normal tissue response, operating mainly on three levels: signalling, immune, and metabolic. Several signalling networks are activated: the ATM pathway is core to DNA damage repair (Jin & Oh, 2019, Pharmacology and Therapeutics). p53 activation induces cell cycle arrest which promotes DNA repair or, upon

failure of DNA repair in cases of extreme damage, cellular apoptosis (Lee *et al.,* 2013, Translational Cancer Research). MAPK mediates multiple radiation-activated pathways initiating a cascade which ultimately regulates cell fate (Munshi & Ramesh, 2013, Genes & Cancer), PI3k/AKT activation is known to enhance oncogenic induction, with inhibition thereof increasing radiosensitivity (Park *et al.,* 2021, Cells).

On an immune level, IR induces systemic inflammation (Lumniczsky *et al.,* 2017, Frontiers in Immunology; Schaue *et al.,* 2015, Seminars in Radiation Oncology) and triggers the innate immune system, activating macrophages, dendritic cells, natural killer (NK) cells and others, with this occurring via induced apoptosis, ATP release into the extracellular space, and macrophage-mediated phagocytosis of damaged, irradiated cells (Boopathi *et al.,* 2023, Cancers).

Finally, radiation disrupts normal tissue metabolism, e.g. via oxidative stress induced by ROS, an immediate effect occurring within 10^{-12} s post radiation (Menon *et al.,* 2016, Frontiers in Oncology; Azzam *et al.,* 2012, Cancer Letters). This in turn activates ROS scavenging pathways to deal with oxidative stress. While studied in the context of a disease state, radiation-resistant tumour cells reroute existing metabolic pathways to clear out ROS at an enhanced rate, suggesting that in normal tissue this is the case as well (Read *et al.,* 2022, Molecular Carcinogenesis). Interestingly, radiotherapy increased blood glucose levels in patients treated for glioblastoma multiforme (Duma *et al.,* 2019, Radiation Oncology). Post IR exposure, normal tissue exhibits an upregulation in glucose transferases and an increase in rates of aerobic glycolysis, mediated by HIF1α (Lall *et al.,* 2014, Cell Death & Differentiation) and suppression of pyruvate kinase (Zhang *et al.,* 2019, Breast Cancer Research and Treatment). This in turn creates a surplus of glycolytic intermediates available for alternative pathways, e.g. the pentose phosphate pathway, important for cellular anabolism in proliferating cells (Chiara de Santis *et al.,* 2018, Frontiers in Oncology). IR has also been demonstrated to alter the lipid profile of many different types of cancers (Yuan *et al.,* 2021, Frontiers in Cell and Developmental Biology) although it must

be noted that unlike normal tissue, cancerous cells possess the ability to synthesize fatty acids *de novo* (Ookhtens *et al.,* 1984, American Journal of Physiology). Lipid peroxidation (particularly that of polyunsaturated fatty acids) is induced by IR as a result of generated ROS, which in turn alters membrane-bound protein activity (Reisz *et al.,* 2014, Antioxidants & Redox Signalling). Further involvement of IR can be found in other metabolic pathways, for example the lysine degradation pathway, found at all time points (3, 14, and 30 days) post radiation with a 5Gy single dose to the head and neck region in mice, using extracted salivary glands as tissue material (Buss *et al.,* 2023, PLoS One). IR therefore dysregulates metabolism on multiple levels, mostly mediated by the immediate generation of ROS causing a reaction cascade via aggressive oxidation of metabolic or cytosolic targets, with this in turn triggering ROS-defense mechanisms and damage repair.

It is this last response, the dysregulation of metabolism, which is of particular interest in the latter chapters of this thesis. Direct intervention in signalling networks prior to irradiation is a tricky affair, with dysregulation having potentially unforeseen consequences due to signalling cascades, and such direct intervention requiring precise delivery mechanisms, for example targeted drugs; as such, potential clinical intervention into dysregulated signalling networks must occur post-radiation exposure. Metabolism, on the other hand, can be regulated by non-invasive means such as dietary control, and provided such a diet does not negatively impact health in terms of overall nutrient intake, can be a means of mitigating the effect of radiation. Lysine degradation, and the dysregulation thereof, is a commonly affected pathway seen during this research. A form of dietary control would be a lysine-restrictive diet, thus minimizing the available pool of lysine and mitigating post-radiation increase. This has the potential to improve radiotherapy outcomes in terms of normal tissue protection and sensitization of targeted tissue, and further reaching, a public health boon to mitigate stochastic cancers occurring due to natural radiation exposure. Metabolism plays a key role in tissue response to radiation which necessitates further

research and is a major target for non-invasive clinical intervention, as well as drug targets for therapeutic intervention in post-exposure or after IR therapy scenarios.

Haematopoietic cells that do not undergo apoptosis after this initial damage have an enhanced probability to become leukaemic cells, eventually undergoing clonal expansion and displacing normal, non-leukaemic cells from the bone marrow niche (Camacho *et al.,* 2017, Hematology). The apparent radiosusceptibility of the bone marrow as a tissue, given its preponderance of highly pluripotent stem cells *vis a vis* other body tissues, is the major reason why AML is such a highly represented radiation cancer outcome when compared to other potential stochastic effects, and currently lacks prophylactic measures in terms of after IR care. Iodine pills are famously issued after or immediately prior to suspected radiation exposure incidents to protect the thyroid from absorbing radioactive isotopes, a measure which is lacking in AML, with no equivalent technique existing or widely practiced. While iodine pills do not impact the mechanism of thyroid carcinogenesis, they do mitigate its progress due to preventing the accumulation of radioactive iodine in the thyroid, which would serve as internal IR emitters.

Drawing a parallel here is apt as the knowledge that radioactive iodine accumulates in the thyroid was necessary before iodine tablets could be thought of as a preventative measure. It is important to note that it is not because such a measure is impossible for AML that it does not exist. It is worth to stress that the iodine prophylactic method was developed due to a mechanistic understanding of how thyroid cancer is incurred post radiation-exposure, mediated via the absorption of radioactive iodine-131, a major radioisotope found in fission products, and a major component of the radiological danger posed by the Chernobyl disaster. As such, a greater mechanistic understanding of the progression of AML post-IR could potentially lead to the development of a similar prophylactic protective measure targeting oncogenic mechanisms rather than accumulation of internal emitters. Even if such a thing is not possible, understanding of the essential pathways and progression of the disease would allow for the development of alternate radiotherapy regimens specifically

designed to mitigate the impact, perhaps in combination with another treatment, on said pathways, thus reducing the risk of secondary cancer development. Indeed, a major part of this rationale is the ability to predict if there is even a risk of said secondary cancer developing in the first place, which leads us to the research topic in question.

It has long been known that radiation-damaged cells can potentially communicate their damaging effects to non-radiation damaged cells, the so-called “bystander effect”. Generally speaking, the bystander effect refers to when non-irradiated cells respond to radiation. This non-irradiated radiation response is typically similar to a direct radiation response: increased apoptosis, micronucleation, DNA damage and mutation, changes in protein levels or activity, and potential oncogenic transformation (Marin *et al.,* 2014, Reports of Practical Oncology and Radiotherapy). The first, and historically best known, of the mechanisms causing this response is the generation of free radicals via water radiolysis (Daguenet *et al.,* 2020, Nature). However, more recent research in the past decade has demonstrated that multiple mechanisms exist, as distal non-irradiated cells can also exhibit indirect effects of radiation. Three types of non-targeted effect are defined by the United Nations Scientific Committee on the Effects of Atomic Radiation (UNSCEAR): the radiation-induced bystander effect, defined by the transmission of radiation effects from irradiated cells to neighbouring non-irradiated cells, the abscopal effect, referring to a local systemic effect extending outside of the directly irradiated area, and the cohort effect, defined as the interaction between irradiated cells within an irradiated volume or area in cases of heterogeneous radiation, where high dose and low dose irradiated cells interact and communicate effects to one another, although this lattermost type of indirect damage does not directly concern us for this research (all of the above cited from Daguenet *et al.,* 2020, Nature).

These types of indirect damage occur via multiple mechanisms: the aforementioned production of ROS via water radiolysis, for more local effects, immune responses and inflammation, which can be responsible for distal effects, and finally, and of major import to

this research, extracellular vesicles, which will be expanded on in chapter 1.2 of this introduction and is the primary focus of this research.

These indirect effects are often responsible for non-classical dose responses, i.e. non-linear. Unlike classic dose response in direct effects, which involves a linear increase in radiation effects, indirect effects are more pronounced at low radiation doses, swiftly plateau, and then actually decline with dose past this plateau threshold (Desouky *et al.,* 2015, Journal of Radiation Research and Applied Sciences). A further type of indirect effect is not location dependent but time dependent, an effect called radiation-induced genomic instability (RIGI). Progeny of irradiated cells exhibit higher levels of chromosomal rearrangement and other mutations even multiple generations after the initial radiation event, demonstrating a lasting effect that radiation has on an organism well beyond the direct (Morgan, 2011, Health Physics). Thus a singular radiation effect in fact causes a cascade of multiple secondary events; bystander, abscopal, cohort, and RIGI, mediated by a host of mechanisms including ROS, immune function, inflammation, and EV signalling, a sequence of events which may be compounded by repeated exposures. The wide-ranging systematic effect may cause a shift of the stable state of intercellular signalling to another, and study of how this shift occurs and what it entails is important for a deeper understanding of IR-induced late effects and their potential mitigation or avoidance.

A potential discrepancy exists then between the ability of a radiation dose to cause cancer, and its actual direct effects. This led to the development and discovery of the indirect effects, as mentioned already, which is the propagation of radiation effects by directly affected cells to cells not directly impacted, thus spreading the effect. Direct effects dominate at high dose/high LET radiation, but at lower doses, as previously mentioned, indirect effects dominate- and these latter effects may persist for long periods of time. Given that typical human exposures, or out-of-field radiotherapy doses, are low LET, this indirect damage is of particular importance in radiation protection. Besides ROS, the propagation has other aspects in terms of the propagation of the genomic mutation effects, which can

be exported in a variety of ways, shuttling RNA out of a cell which can cause potentially oncogenic signalling cascades in recipient cells. RNA export is not a trivial process, but instead mediated by extracellular vesicles. These will be expanded on in the proceeding section, but extracellular vesicles are key to the research question of this thesis, which is their role in the post-IR oncogenic process of AML development. In the understanding of the mechanistic processes, of which vesicles are an essential part, lies the potential for a prophylactic treatment as with iodine, or early detection methodology. This is critical to the development of a safer radiotherapeutical regimen and rationale, and thus mitigate the possibility of treatment of one cancer only causing another.

1.2 Extracellular vesicles

Exosomes and microvesicles are a class of small, biologically active lipid nanoparticles (Raposo & Stoorvogel, 2013, Journal of Cellular Biology), often grouped together under the label Extracellular Vesicles (EVs), secreted from the cellular membrane. Although their biogenesis pathways are distinct (Akers *et al.,* 2013, Journal of Neuro-Oncology; Abels & Breakefield, 2016, Cellular and Molecular Neurobiology), the lack of distinguishing markers has rendered separation traditionally difficult. There is no consensus on the definition of exosome and microvesicle size, with some groups maintaining that there is a size overlap between both groups (Krause *et al.,* 2018, Journal of Extracellular Vesicles) while others contend the size thresholds are distinct (Kastelowitz & Yin, 2014, ChemBiochem; Raposo & Stoorvogel, 2013, Journal of Cellular Biology). As such, exosome size definition can vary from 30nm to either 120nm or 150nm in size, while microvesicles are variably from 100/150nm in size to 1,000nm, and they tend to be classified depending on their biogenesis pathways.

Historically, exosomes and microvesicles were considered as ‘cellular garbage’ (Vidal, 2019, Traffic), responsible for the removal of waste products from cells, being relatively unregulated blebbing of cellular membrane bubbles containing said products for disposal into the intercellular space and ferrying away into the bloodstream and were thus mostly

dismissed as being of any significant importance. Exosomes were first identified in reticulocytes in two papers published within a week of each other, Harding *et al.* in the Journal of Cell Biology, and Pan & Johnstone in Cell, in 1983. They were initially thought to be a means for reticulocytes to shed their excess cellular machinery and complete their maturation into erythrocytes; early research by the Stahl lab focused on the role of exosomes within reticulocytes. In 1996, Raposo *et al.* demonstrated the action of exosomes in B lymphocytes, and soon afterwards, in 1998, Zitvogel *et al.* demonstrated that dendritic cells produce exosomes, later demonstrated, in 2002, to also provoke T cell response (Thery *et al.,* 2002, Nature Immunology). These findings soon demonstrated that exosomes were not unique to reticulocytes and were in fact a ubiquitous feature of cells throughout the body. Their ability to cause a T cell response, and the later discovery that exosomes contain both mRNA and miRNA in human mast cells (Valadi *et al.,* 2007, Nature Cell Biology) led to a dramatic increase in interest in exosomes and microvesicles, as well as their reclassification into a signalling molecule and not merely a cellular waste disposal mechanism.

EVs are typically involved in intracellular communication (Tetta *et al.,* 2013, Endocrine; Paolicelli *et al.,* 2018, Neuroscience) (figure 1.04), with different types of cargo being shuttled between cells: mRNA, proteins, and miRNA (Valadi *et al.,* 2007), among others. Previous research (Johnson *et al.,* 2016, Blood; Johnson *et al.,* 2017, Journal of Extracellular Vesicles; Pando *et al.,* 2018, Leukaemia Research) has shown that EVs may be involved in oncogenesis, as well as leukaemogenesis within the bone marrow (BM) (Kumar *et al.,* 2018, Leukemia), with cancer cells secreting EVs that promote immune escape, tumour progression and remodel the microenvironment to be pro-oncogenic (Miyazaki *et al.,* 2018, Oncogenesis).

In radiation response, EVs have been shown to modulate radiation damage response on a systemic level, but are also dose dependent, although not linearly as with DNA damage induction (Szatmári *et al.,* 2017, Frontiers in Immunology). Instead, EV effects peak at lower

doses, although this was studied in the context of IR-induced damage (i.e. at lower doses, suspected EV-mediated damage was more prevalent than complex DSB breaks induced by direct radiation, rather than increasing linearly with dose). EV release does appear to be linearly dose-responsive in terms of quantity released, with the number of EVs released increasing with X-ray dose. EV ability to promote repair has been reported to be inversely proportional with dose, with an increase in damage induction (which does not necessarily agree with what we have observed during this research, as demonstrated in later sections of this thesis) (Jokar *et al.,* 2022, Bioengineering). Containing a complex array of various molecular cargoes, EVs play multiple roles throughout normal tissue, allowing for intercellular communication to affect distant targets, not bound by cell-cell contact, and potential organ crosstalk.

The established phenotype of EV response to radiation is a dose-dependent upregulation in EV secretion from irradiated cells. Sources variably report an induction of damage (Szatmári *et al.,* 2017, Frontiers in Immunology) to promoting wound healing and being significant drivers, repressing cellular senescence to accelerate regeneration (Dai *et al.,* 2022, Burns & Trauma) as a consequence of this increased EV release. Due to this duality in functions and observation, it is most probable that different EV cargo incur different effects, with this varying by dose, tissue, and model.

An EV-centric view, especially within the context of miRNA cargo, connecting initial radiation damage response to AML leukaemogenesis has not been proposed, to the best of this writer's knowledge. Within the existing AML disease state, EVs are able to regulate and even *de novo* confer chemoresistance (Barzegar *et al.,* 2021, Iranian Journal of Pharmaceutical Research; Nehrbas *et al.,* 2020, Frontiers in Oncology) and have been observed to confer and enhance radioresistance in other cancers (Yang *et al.,* 2022, Cell Communication and Signalling). Tumour-derived EVs support maintenance of stemness, resistance to differentiation, proliferation, and suppression of apoptosis in haematologic malignancies (Sun *et al.,* 2022, Journal of Clinical Investigation). Within the cancer disease

state, EVs play an important support and survival role, conferring and enhancing chemo- and radioresistance, enabling cancer cell survival, while also accelerating disease progression by supporting aberrant proliferation, suppression of apoptosis and maintenance of stemness.

To summarise, EVs have been variably described in the literature to significantly induce damage post-IR and/or to substantially accelerate post-IR wound healing. A linking and initial leukaemogenic role for EVs has not been characterized. Within the developing AML, EVs then support and enhance cancer survival and increase the cancer's capability to robustly deal with external stress.

It is important to note that EVs are by no means a completely researched, well-known area of study, and much remains unclear, in particular their role in disease progression, just how important they are in the establishment of the disease, and how consistent a part they play in oncogenesis. Answering these three questions is therefore paramount to answer the ultimate question of what can EVs contribute to clinical treatment of disease and management of radiation risk in general, and if they can serve as biomarkers of disease risk and progression, or even serve as a route for clinical intervention and treatment. In a wider context, this could also elucidate how EVs could be applied to mitigating the effects of occupational, environmental, and accidental/acute exposure to radiation.

1.3 Vesicles involved in bystander response

In recent years it has been shown that EVs are affected by ionising radiation (IR), with their secretion composition changing (Jelonek *et al.,* 2016, Protein and Peptide Letters), suggesting that EVs play a role in systemic stress response. It has been further demonstrated that EVs are also involved in mediating bystander response signals in the bone marrow and spleen (Szatmári *et al.,* 2017, Frontiers in Immunology).

The bystander effect describes the propagation of radiation effects from cells directly damaged by IR to cells that were not exposed to ionising damage, via cellular

communication and the transfer of free radicals. This replicates the effects of radiation damage in otherwise radiation-naïve cells. It has been demonstrated that the miRNA cargo of EVs is modified post-IR (Szatmári *et al.,* 2019, International Journal of Radiation Biology), with these miRNAs being associated with known bystander pathways.

It is currently unknown how the EVs factor into this oncogenic process; whether the transcriptional regulation effect of their miRNA cargoes is a major driver behind tumour development, or if EVs merely have an attenuating role, with the most important mechanisms behind tumour development lying in other pathways. Finally, currently no 'irradiation exposure miRNA signature' exists, and the cell population(s) responsible for this signature (if specific) has/have not been identified.

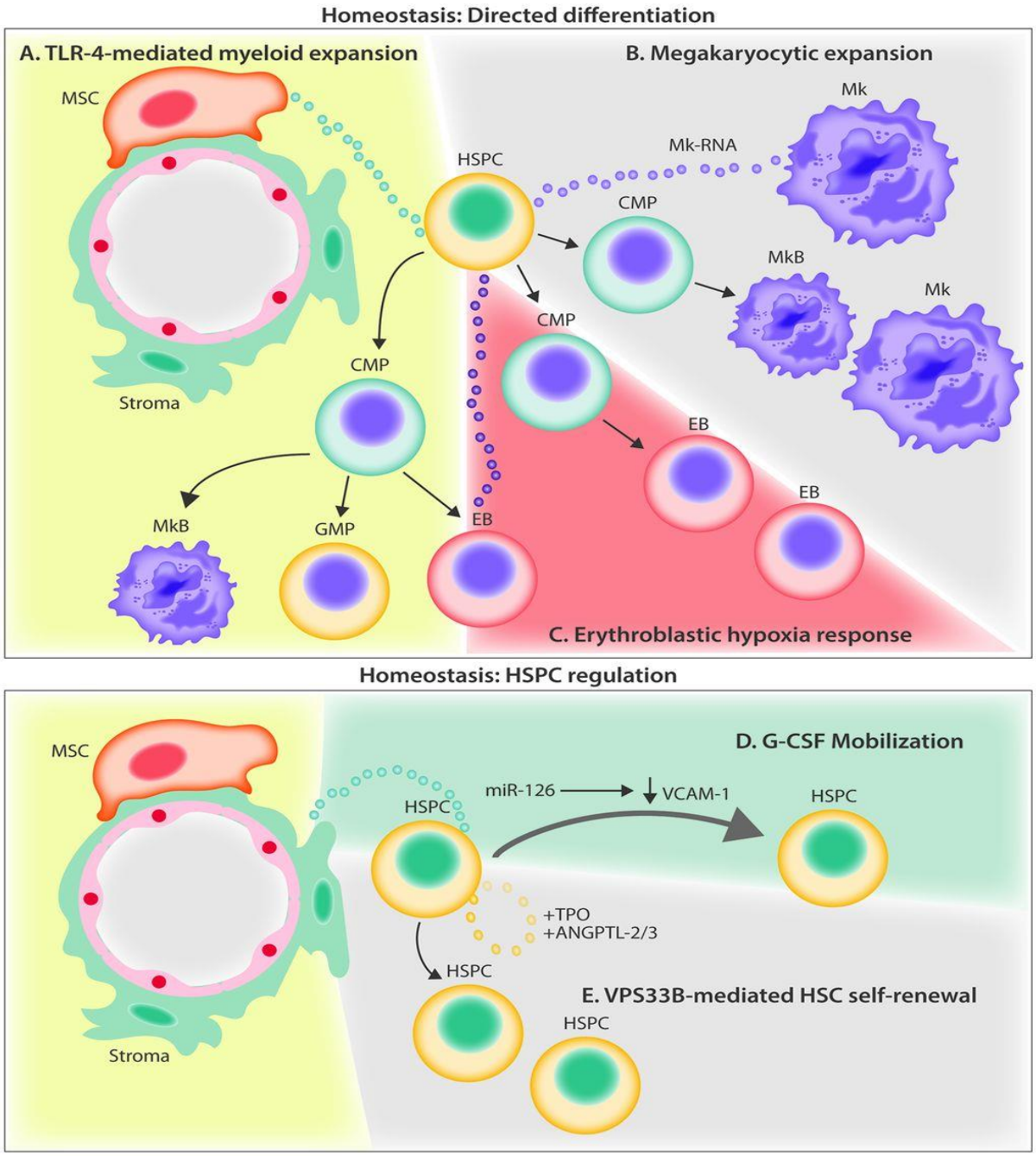


Figure 1.04: Role of extracellular vesicles in normal homeostasis of the bone marrow microenvironment. Figure reproduced from Butler *et al.,* 2018, Haematologica.

1.4 Micro RNAs, a regulatory cargo shuttled by EVs

Micro RNAs, or miRNAs for short, are non-coding RNAs that are characterized by their short length, on average 22 nucleotides, and their ability to regulate gene expression. MiRNAs have 3 biogenesis pathways: a canonical (dominant) pathway and two non-canonical pathways. The canonical pathway begins with the formation of a pri-miRNA,

freshly described from a gene. This pri-miRNA is then processed into a hairpin pre-miRNA, a process performed by the microprocessor complex, a multi-protein assembly consisting of RNA binding protein DiGeorge Syndrome Critical Region 8 (DGCR8) and Drosha, which is a ribonuclease III enzyme. This pre-miRNA is then exported into the cytoplasm by an exportin 5/RanGTP complex, and further processed by Dicer, an RNase III endonuclease. This final cleavage produces a mature miRNA (Jacob *et al.,* 2018, Frontiers in Endocrinology).

The nomenclature of miRNA is important as well. A typical miRNA follows the following naming convention: XXX-miR-YYY-5/3p. The initial three letters, such as hsa and mmu, determine the species of origin of the miRNA in question. Hsa is for human, while mmu is for murine; more specifically, hsa stands for *Homo sapiens,* mmu is for *Mus musculus,* rno would be *Rattus norvegicus,* etc. The number (YYY) distinguishes which miRNA is being referred to. In some instances, a number might have a letter suffix, e.g. miR-451a and miR-451b. This indicates that both are members of the 451 family. In rarer instances one might also see a numeral suffix, e.g. miR-515-1 and miR-515-2. Generally speaking, miRNA are derived from a singular gene locus, but in instances where multiple gene loci create the same mature miRNA, this numeral suffix is used to distinguish between the loci. Finally, the final part of the name, 5p or 3p, states the directionality of the miRNA with reference to its pre-miRNA, as final cleavage by Dicer results in two possible miRNA, one derived from the 3' arm of the hairpin, referred to as 3p, and the 5' arm of the hairpin, referred to as 5p. As such, e.g. miR-701-5p and miR-701-3p are derived from the same gene locus.

Some exceptions to this nomenclature exist, which will be seen in chapter 3, such as *let-7.* These exceptions to the rules refer to some of the first miRNA discovered, typically in *Caenorhabtidis elegans.* These miRNAs are not somehow unique when compared to other miRNA, their unusual naming convention arises from the fact that they were named before the accepted nomenclature was established and were often referred to as their given names in mutation screens; as a matter of ease of use, their names were not changed.

miRNAs act by binding the 3' UTR of their target miRNA, although cases of binding to the 5' UTR as well as promoter regions have also been seen (Xu *et al.,* 2014, BMC Bioinformatics). First, mature miRNAs bind with Argonaute, forming a miRNA silencing complex (miRISC). The miRISC complex then binds to its target mRNA, usually in the 3' UTR, although as mentioned sometimes in the 5' UTR and promoter regions. This binding promotes the deadenylation and decapping of the target mRNA, resulting in degradation of the transcript and thus translational repression via depletion of the mRNA pool within a cell, thus miRNA acts, generally speaking, as an mRNA silencer. In rare instances and other specific conditions however, miRNA can in fact upregulate translational expression, e.g in quiescent cells or specific stress conditions such as amino acid starvation (Jacob *et al.,* 2018, Frontiers in Endrocrinology; Truesdell *et al.,* 2012, Scientific Reports; Orom *et al.,* 2008, Molecular Cell). Therefore, while miRNAs generally act as translational repressors, environmental conditions within the cell can change this, rendering absolute statements as to the impact of miRNAs on their targeted mRNA and pathways difficult without experimental evidence and validation.

miRNAs play an extremely important role in EV-mediated intercellular communication. miRNAs are packaged into EVs within the cell, through four potential mechanisms, although their precise mode of action remains unclear. These are, 1) mediated by neural sphingomyelinase 2 (nSMase2), 2) a pathway dependent on sumoylated heterogeneous ribonucleoproteins, 3) a critical sorting signal contained within the 3' end of mature miRNA, and 4) an entire miRISC complex may be sorted or act in preferential sorting of miRNAs into EVs (Zhang *et al.,* 2015, Genomics, Proteomics & Bioinformatics). Regardless of the method of miRNA sorting, EVs contain higher levels of miRNA when compared to their parent cells (Goldie *et al.,* 2014, Nucleic Acids Research) which are also of a different profile when compared to their parent cells (Valadi *et al.,* 2007, Nature Cell Biology). These two facts served to spur substantial interest in EVs as a transportation method for miRNAs,

meaning that a route existed for miRNAs to exert their post-transcriptional regulation outside of their cell of origin.

In the context of radiation and disease progression, this makes EV-mediated miRNAs a focal area of interest with regards to the aforementioned bystander effect. However, it is important to remember that EVs contain a multitude of cargo, not only limited to miRNAs. As such, miRNAs are only one piece of a larger signalling and regulation network in which EVs play a crucial role, and further research into these other cargoes, e.g. proteins, lncRNAs, mtDNA, is required to fully appreciate their true impact in radiation-induced bystander effects and ultimately tissue late effects, especially within the bone marrow haematopoietic signalling network.

1.5 Murine models

There is a rising need for biomarkers of radiation dose and biomarkers for radiation-induced malignancies, including cancers (Singh *et al.,* 2016, Expert Review of Molecular Diagnostics; Hall *et al.,* 2017, Mutation Research) globally, especially in the context of nuclear disasters past and future and growing IR exposure to the public. Epidemiology studies demonstrate that IR exposure leads to an increased risk of both leukaemia and solid tumour development (Hall *et al.,* 2017, Mutation Research). Serum miRNAs may be a source of biomarkers for dosimetry (Tomasik *et al.,* 2018, Oncotarget); combined, this illustrates the need for markers of risk and irradiation, which may lead to markers of oncogenic development and progression.

Traditionally, one of the primary challenges with regards to animal research into radiation-induced cancers is firstly the stochastic nature of radiation-induced damage, with only a minority percentage (strain-dependent) of exposed animals going on to develop late effects, but also manifold other issues. These include strains that have a high background incidence of tumours, obfuscating results, and strains that are extremely resistant to tumour formation, requiring extremely large cohorts to gain sufficient animals for a study. The final problem

typically facing researchers is the difficulty in gauging how many animals have developed cancer before they are culled, and post-mortem dissection or other confirmation diagnoses their malignancies, present or not. This last issue necessarily complicates many studies, requiring high levels of power in terms of represented animals to solve. As most laboratories lack methods of non-invasive progression tracking of a malignancy, this means that *in vivo* tracking of cancer progression is impossible for most laboratories and indeed most murine models of such. An additional complication lies in cancers not of interest, e.g. liver tumours, developing in an animal and thus necessitating euthanasia of the individual.

The Cancer Mechanisms and Biomarkers group at UKHSA Harwell possess two unique murine models (figure 1.05 and figure 1.06) (Verbiest *et al.* 2018, Leukemia, O'Brien *et al.,* 2020, Carcinogenesis, Olme *et al.,* 2013, Leukemia Research) which provides an in-depth, specific look at AML. These murine models are based on a CBA strain, which has a low (1/10,000) background rate of AML incidence. The first model (figure 2), referred to as mCh/GFP, allows for the tracking of clonal expansion via tracking of expansion of mCh negative cells in the peripheral blood (Verbiest *et al.,* 2018, Leukemia), the methodology of which is described in chapter 2. This allows for in *vivo* visualisation and tracking of the progress of leukaemic expansion, referred to as 'pre-leukaemia". Pyrosequencing performed on the blood can identify if the cells carry the specific point mutation in Sfpi1 that marks progression into AML. This is a unique model that allows for precise identification and tracking of AML before death.

The second model (figure 1.06), referred to as SPM, is susceptible to AML (manuscript in preparation). With an engineered single point mutation to Sfpi1, a *secondary* event in classic murine AML, the mouse develops a 100% rate of AML incidence, even without irradiation. With a remarkably short and controlled latency of AML development post-irradiation, this is a unique mouse strain allowing for the investigation of EV impact on a known AML latency, something other mouse models lack.

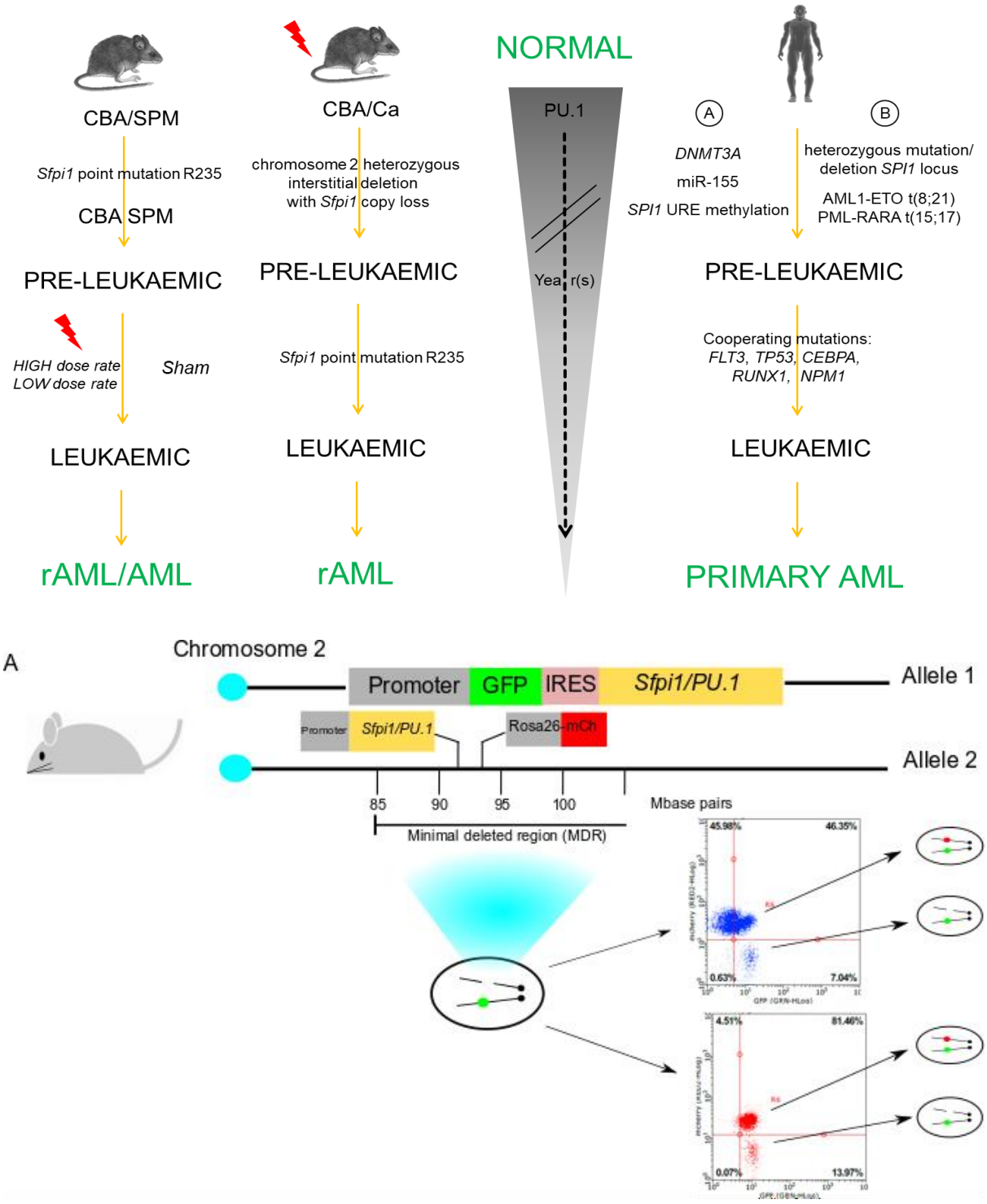


Figure 1.05: The importance of PU.1/Sfpi1 and the mCh/GFP CBA mouse. Low levels of PU.1 in humans correspond to the development of AML; in mice, deletion of one allele of Sfpi1 and mutation of the other leads to an AML. Two fluorescent reporters, mCh and GFP, are engineered into one allele each of Sfpi1, the murine gene that codes for the protein PU.1. In both cases the reporter is linked to Sfpi1 expression. Via flow cytometry testing of the peripheral blood, populations with a deleted mCh can be identified and quantified. (Figures derived from Verbiest *et al.,* 2015, Carcinogenesis and Verbiest *et al.,* 2018, Leukemia).

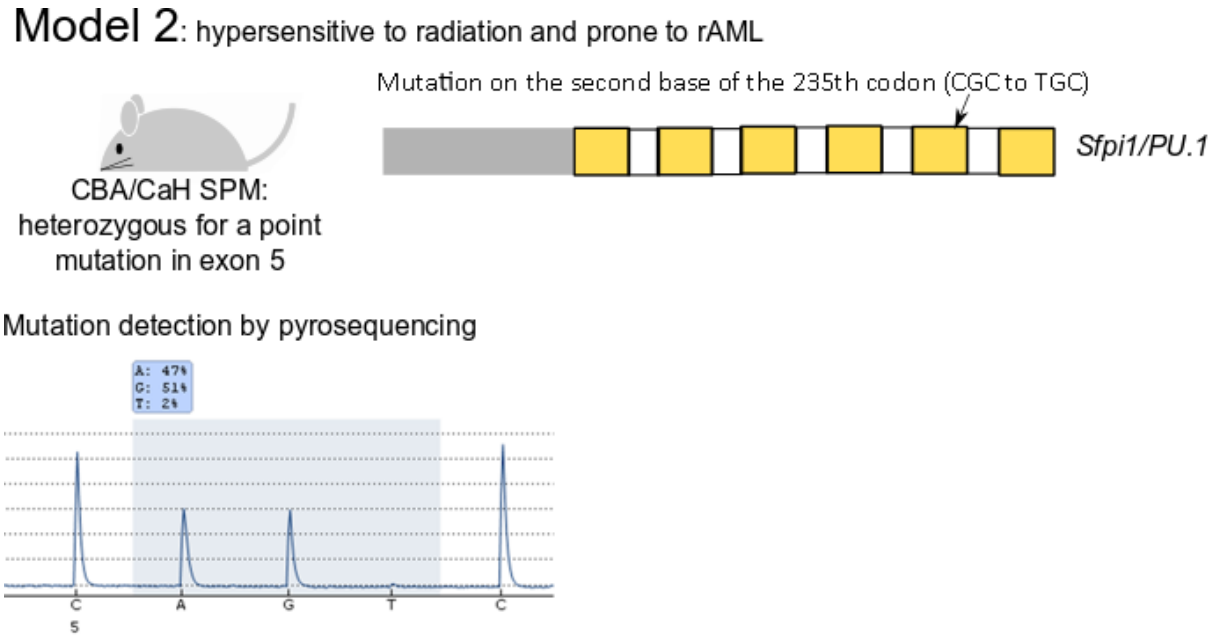


Figure 1.06: SPM CBA mouse. Via a nonsynonymous single point mutation to the second base on codon 235, the strain becomes 100% sensitive to AML development, i.e. 100% of a population, even unirradiated, will eventually develop AML. This mutation is a secondary event in IR-induced leukaemogenesis in genomically normal CBA mice.

The scientific basis of this model, as seen in figure 1.05, is the equivalence of PU.1 **loss of function**. PU.1 is an ETS-family transcription factor encoded by the Sfpi1 gene, critical in myeloid and lymphoid differentiation, which interacts with a variety of regulatory factors, acting either directly or with other transcriptional regulators on a network of circa 3000 genes involved in haematopoiesis, with at least 1000 direct gene targets (Fisher & Scott, 1998, Stem Cells; Burda *et al.,* 2010, Leukemia). It is downregulated in myeloid and lymphoid progenitors, becoming expressed during terminal differentiation. A loss of function thereby favours a long-term pluripotent state, evading differentiation, thus enabling the development of a leukaemic cancer cell. In humans, following an ionising radiation event, epigenetic silencing via DNA methylation is responsible for progressive loss of function (Tatetsu *et al.,* 2007, Cancer Research), with mutations being rare (Sive *et al.,* 2015, Leukemia). In mice, this loss of function following IR progresses along different means, with IR inducing a deletion event in one copy of Sfpi1 in a percentage of irradiated mice. The remaining Sfpi1 copy, in a majority of cases (~85%) suffers a point mutation event, most

likely due to increased transcriptional activity on one allele. This leads to further downregulation of PU.1 activity and the development of AML (Verbiest *et al.,* 2015, Carcinogenesis). As such, while the molecular pathways post-IR with respect to PU.1 function differ in mice and humans, both ultimately result in a loss of PU.1 function. IR, and our murine models, are therefore a proxy for PU.1 loss of function, mimicking the PU.1 loss of function seen in human AML patients. While IR is an initiating event, the true trigger for AML development is downregulation PU.1, massively deregulating haematopoietic differentiation networks and losing a major tumour suppressor.

Using these two models, we avoid some of the traditional issues facing animal research, in that pre-mortem we are cognizant of how many animals are in a state of cancer development, and it also grants us the ability to cull an animal at any stage of cancer development, allowing for the study of multiple stages of development within the same experiment. We can study more precisely the role of EVs within the development of IR-induced AMLs with the confidence that these AMLs are indeed IR-induced, without lengthy post-mortem confirmations other than an optional confirmatory pyrosequencing. These models also allow us to identify which miRNA are critical in AML development, either for use as biomarkers or potential therapeutic targets should they prove to have significant mechanistic involvement. Within a clinical setting, EV miRNA could be used as non-invasive biomarkers of AML development, allowing for further intervention at an early stage. Future work involving this model would allow us to model intervention, with appropriate miRNA therapies being applied at different cancer stages, hopefully to develop a method to retard or interrupt AML development in the bone marrow.

1.6 Research aims

This research aims to clarify the role of EVs in IR-induced AML: establish how the BM responds to IR in terms of EV cargo, how the EV cargo changes during leukaemic development, how these changes in cargo can propagate or favour AML development, and whether these cargo changes can be used to create a replicable signature of IR-induced

AML that serves a biomarker for risk of AML development and/or stage of AML. Ultimately the aim is to establish what potential role EVs play in leukaemia induction and its associated mechanisms.

The importance of this research is manifold. First, the discovery or development of a vesicle-based marker panel would help in assessing radiation exposure. A diagnostic EV-based miRNA panel for hepatocellular carcinoma has been reported (Yang *et al.,* 2022, Frontiers in Cell and Developmental Biology), meaning that this is possible. One problem with current radiological exposure models, e.g. disaster simulations, is the difficulty in large scale processing of mass amounts of samples. The current gold standard for dosimetry is cytogenetics, protocols of which are still carried out by human researchers and have not been fully automated or adapted to high throughput methodology. The development of a marker panel would alleviate this issue; while cytogenetics is, and most likely will remain the gold standard method for years to come (Akkari *et al.,* 2022, Blood), a vesicle-based method based on blood draws and easily automated by microarray would allow for high throughput screening of a large population and allow for rapid estimation of risk, and thus countermeasures, saving precious time versus current cytogenetics-based approaches. Further confirmation could then take place by cytogenetics, but this initial first estimation of risk, done rapidly, could prove essential in mitigation of post-exposure effects.

The other significant, and hopefully more relevant, use of such a panel would be in the treatment of cancer patients receiving radiation as part of their treatment therapy. Significant advances have been made in recent years in terms of radiation methodology and sparing healthy tissues. However, these advances, like much medicine, have yet to be married to a personalized therapy regimen that is the necessary next step for clinical treatment of patients. A marker panel would allow a clinician to assess the potential risk for late-stage effects of radiation, including immune effect, cancer risk and tissue toxicity (of which not much is known with respect to EVs, as the majority of literature focuses on oncogenic or immune modulation by EVs) on a cancer patient, or indeed even give them

cause to consider an alternate regimen to avoid the development of secondary cancers such as AML.

Finally, while this research is still short of establishing this, discovering the importance and mechanics of EVs within the context of oncogenesis could provide another therapeutic target vis a vis cancer therapy or post-radiation exposure treatment. By targeting the relevant miRNA or protecting the pathways they negatively affect, it could be possible to somewhat shield an individual from post-exposure effects; while not desirable in a radiation therapy patient for this same reason, instead targeting pathways the EVs are disrupting and thus promoting oncogenesis might yield higher tumour toxicity with less effect on surrounding healthy tissue.

EVs are a complex, relatively unknown system of intercellular communication, and the field is rapidly evolving. Their use, and ultimate relevance, is still highly debatable. Techniques lack standardization, results are variable, and much remains unclear. It is precisely for this reason that they are deserving of study and further research, as a potential therapeutic marker panel or even target, and could provide an avenue for the further development and implementation of personalized medicine.

2. Materials and Methods

To better understand the procedures described here, a brief summary of the overall study and workflow will be provided. The research question was the impact and importance of BM EVs in IR-induced AML. To investigate this, we used transgenic CBA mice which had fluorescent reporter proteins that allowed us to track clonal expansion. Using these we extracted BM and BM EVs from leukaemic, non-leukaemic and unirradiated CBA mice. BM EVs from irradiated mice were compared against those of non-irradiated mice. Subsequently, BM cells were cultured from BM cells, specifically haemopoietic stem cells, macrophages, and mesenchymal stem cells. These were irradiated *in vitro* and assayed for their BM EV content. They were then further assayed for metabolic function in the form of aldehyde generation, lysine level and fatty acid content, as well as qPCR quantification of related gene expression. This allowed us to establish how BM EVs act in short- and long-term post exposure situations at the whole organism level, and then how they act short-term post exposure at the cell population level in terms of their miRNA content and their metabolic impact.

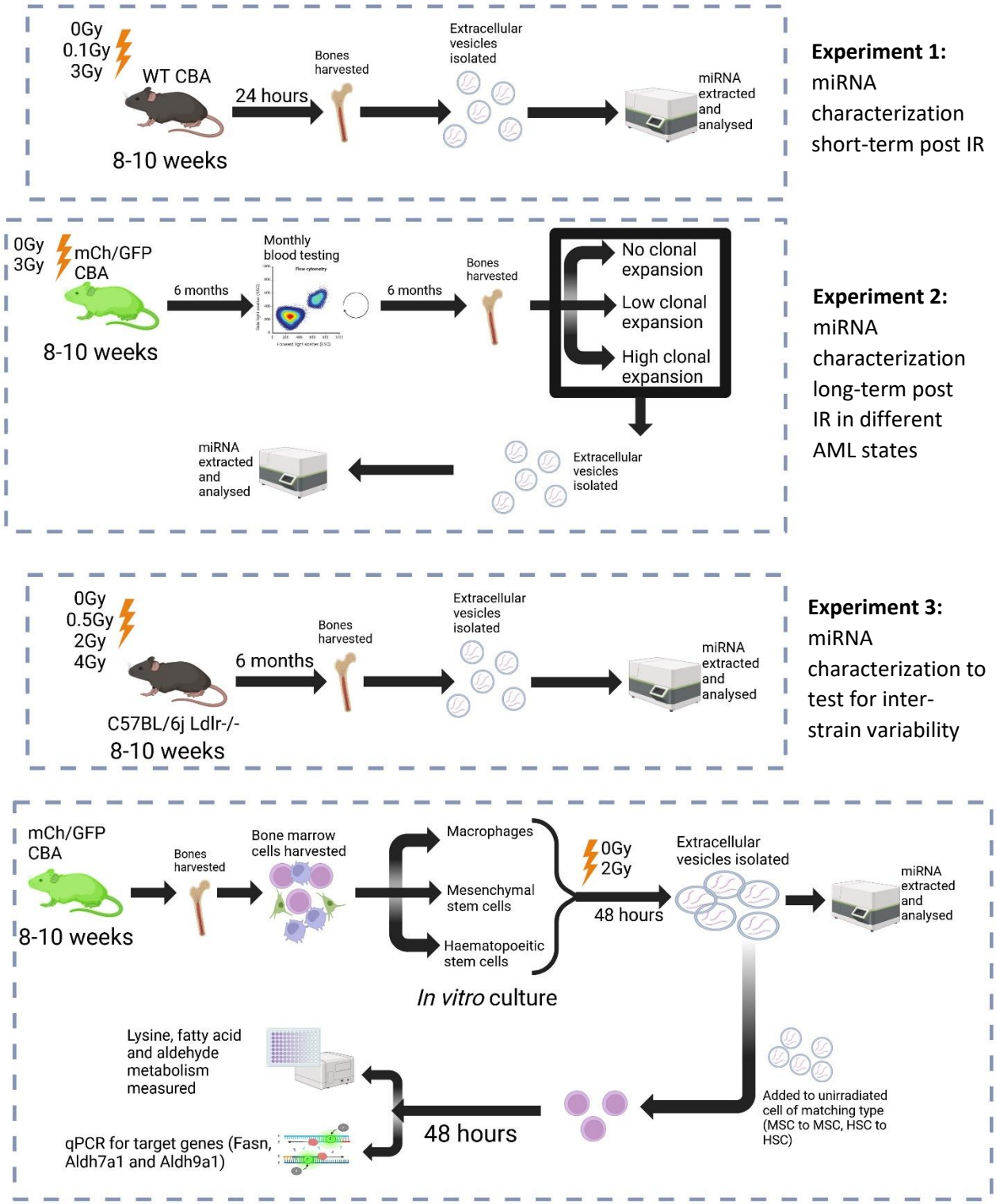


Figure 2.01: High level overview of experimental planning and processes. Created with Biorender.com.

2.01 Ethical Considerations

The study utilized transgenic CBA mice; animals were bred and handled according to the UK Animals (Scientific Procedures) Act, 1986, Amendment Regulations 2012. Animal protocols were reviewed and approved by the local Ethics Committee and the Home Office. Mice were provided with water and food ad libitum. All human-sourced samples were utilized under a licensed distributor's ethics code and were used only for their stated end-point purpose and sourced from anonymized volunteers only. No personal data was included or requested from the volunteers that was not scientifically relevant to the study. No information on identity, gender, ethnicity, or age was collected. No trials on patients or live human tissue were performed. Surgical procedures on mice were limited to tail vein bleeds, once monthly. No major surgeries were performed.

2.02 Irradiation Protocols

All irradiations at UKHSA were performed on an AGO X-ray set (AGO, Reading, UK) running at 250V (constant potential) cabinet irradiator with a Cu/Al filter producing a beam of 1.2mm HVL Cu. High dose rates were delivered at 0.5Gy/min, 13mA, with a 60cm distance from the source. Low dose rates were delivered at 4.9mGy/min, 0.2mA, with a 91cm distance from the source. Mice were anaesthetized and irradiated in an irradiation holder. Cells were irradiated in a monolayer in a T-75, T-25 flask or adherent wells. All cell irradiations were carried out using high dose rate parameters for a total dose of 2Gy unless otherwise stated. All irradiation was performed at room temperature and central to the axis of the chamber at the stated distance.

Irradiations at the Radiobiology and Radiohygiene department, National Public Health Institute, Budapest, Hungary, were performed using X-rays using an X-RAD 225/XLi X-ray source (Precision X-Ray, Madison, CT, USA).

2.03 Period and location of studies performed

All experiments were performed between October 2018 and November 2022. All transgenic CBA mouse animal handling, tissue processing, and cell culturing was done on-site at the United Kingdom Health Security Agency's Centre for Radiation, Chemical, and Environmental Hazards at the Harwell Campus, located in Didcot, Oxfordshire. All post-processing, e.g. RNA and miRNA extraction, quantification, qualification (with the following exception), and analysis was performed on the Harwell Campus site as well. Quantification and qualification of low concentration extracellular vesicle-derived miRNA was performed by Arraystar's in-house RNA sequencing service, located in Rockville, Maryland, the United States of America. Non-transgenic CBA mice were bred, reared and processed in Dr. Katalin Lumniczky's group at the Radiobiology and Radiohygiene department, National Public Health Institute, Budapest, Hungary.

2.04 Subjects of study

The following subjects were used for the study of the function of extracellular vesicles in radiation-induced acute myeloid leukaemia:

1) CBA mice, male and female, 10-12 weeks of age

2) CBA mice, male and female, 6-12 months of age

3) Healthy human volunteers as blood donors

The inclusion and exclusion criteria for mice and human volunteers are summarized in the table on the next page:

Subject	Inclusion Criteria	Exclusion Criteria
CBA mice (10-12 weeks)	**For all *in vivo* experiments and experiments not requiring post-mortem cell culturing:** The mouse had to be a transgenic mCh/GFP marker carrier The mouse had to be part of the list of study-included litter lines **For all *ex vivo* experiments requiring post-mortem cell culturing:** The mouse was either a wild-type or transgenic mCh/GFP.	**For both *in vivo* and *ex vivo* experiments:** The mouse was a transgenic SPM mouse. The mouse had a history or present state of disease. The mouse had any form of leukaemia **Only for *ex vivo* experiments requiring post-mortem cell culturing:** The mouse was previously irradiated.
CBA mice (6-12 months)	**For all *in vivo* experiments and experiments not requiring post-mortem cell culturing:** The mouse was previously irradiated at 10-12 weeks of age The mouse was a transgenic mCh/GFP mouse The mouse had been tested monthly via tail vein bleeds for fluorescent reporter levels since six months post-irradiation up until termination. **For all *ex vivo* experiments requiring post-mortem cell culturing:** The mouse was either wild-type or transgenic mCh/GFP. The mouse was unirradiated.	**For all *in vivo* experiments and experiments not requiring post-mortem cell culturing:** The mouse showed signs of a leukaemia other than acute myeloid leukaemia e.g. lymphoblastic or chronic. The mouse had to be terminated due to a non-leukaemic cancer developing. The mouse had to be terminated due to a non-cancerous disease developing. **For all *ex vivo* experiments requiring post-mortem cell culturing:** The mouse was an SPM transgenic.
Volunteer	The volunteer was healthy and fit as of the time of study.	The volunteer was undergoing treatment for a cancer, leukaemia or otherwise, or previously had cancer and associated treatment. The volunteer was immunocompromised. The patient had an infectious blood disease e.g. HIV.

In addendum, several cell lines were used during the initial development and optimization of the protocols involved in the research study. The inclusion and exclusion criteria were simple; all cell lines were well-known and characterized lines used in other research, and the cell lines were not contaminated with unknown viruses. This was determined based on manufacturer quality certificates and reports and was not assayed on site. Known viral contaminants e.g. HPV were accounted for. Where possible, functional p53 pathways and no viral contamination or excessive genomic mutation from the baseline were preferred as cell lines suitable for testing.

2.05 Murine models

The first strain was a wild-type (WT) CBA mouse, reared in-house and deriving from Harwell stock. These mice were used as a source of cells for *in vitro* culture, via methods described in proceeding sections, as per protocol used. Both genders were used, with 8-10 week old mice being preferred, except where noted otherwise. All wild-type CBA mice were previously unirradiated. WT CBA mice were also used by our collaborators in the National Public Health Center, Department of Radiobiology and Radiohygiene. These were derived from CBA/Ca, not CBA/H, meaning that some level of genetic drift between the two strains since the original CBA strain was derived should be expected and taken into consideration. Both models suffer chromosome 2 aberrations post IR and a propensity for IR-induced AML.

The second strain was a transgenic CBA mouse (see figure 2.02) with constitutively expressed GFP and mCh markers engineered into the mouse's genome, specifically in or near to the Sfpi1/PU.1 gene. GFP was spliced into the region between the promoter and the internal ribosomal entry site (IRES) of allele 1, while mCh was placed after the gene on allele 2, but only a few base pairs distant. The purpose of these two markers was to allow for the *in vivo* tracking of the presence of both Sfp1 alleles. As demonstrated in Verbiest *et al.,* 2015, the deletion of one of these alleles is a preceding event to the development of acute myeloid leukaemia in mice post radiation. Not all mice experience a deletion event

post radiation. In mice that had lost an allele however, 100% of these went on to develop AML Monthly tail vein blood tests, as seen in figures 5 and 6 reveal if both alleles are still present, shown by the presence of both fluorescent markers, or if a population with only single marker expression is present. This is judged by the loss of mCh signal. Loss of GFP signal can also be used, but GFP expression varies with Sfpi1 expression, which is variable or even absent in certain blood cell populations within normal tissue, and thus leads to a false positive for the presence of pre-leukaemic cells in a state of clonal expansion. mCh, on the other hand, has a consistent expression throughout all blood cell populations, due to its location distal to Sfpi1 rather than within the gene itself.

This system does not only allow for the assessment of pre-cancerous state in a live mouse, but also the tracking of the progress of the cancer from nascent to terminal state, determined when the level of clonal expansion in the mouse blood reaches circa 50%, or the mouse shows deleterious symptoms and thus must be ethically euthanized.

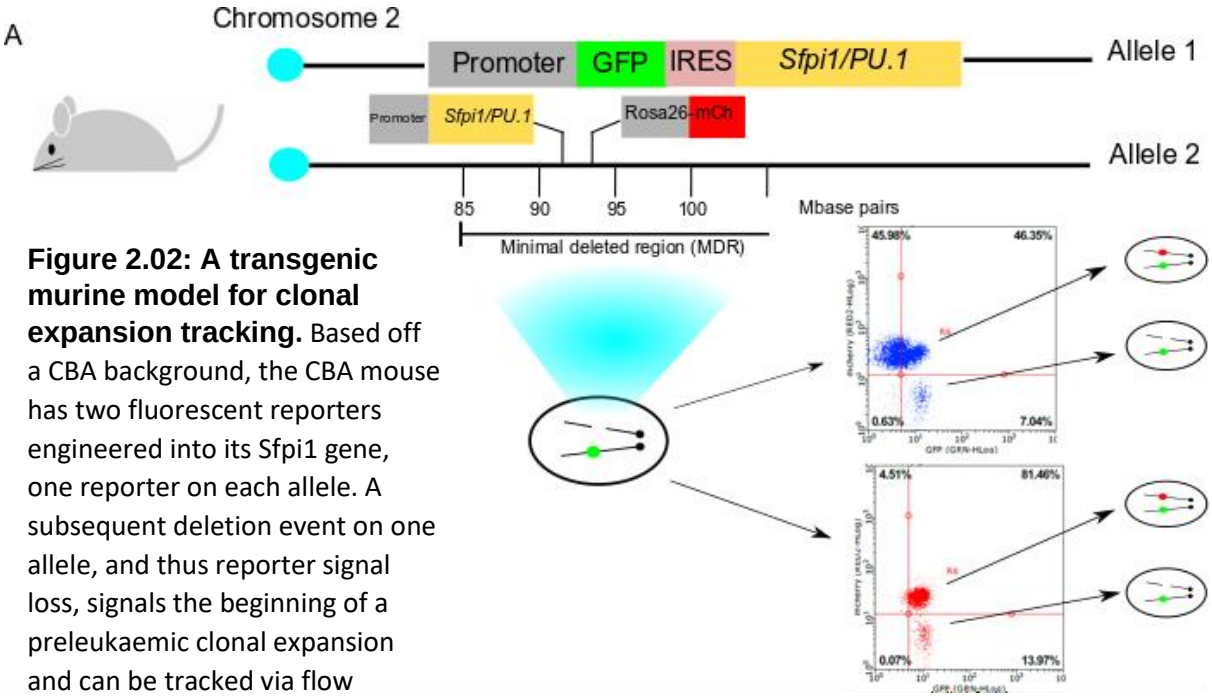


Figure 2.02: A transgenic murine model for clonal expansion tracking. Based off a CBA background, the CBA mouse has two fluorescent reporters engineered into its Sfpi1 gene, one reporter on each allele. A subsequent deletion event on one allele, and thus reporter signal loss, signals the beginning of a preleukaemic clonal expansion and can be tracked via flow cytometry. Modified from Verbiest *et al.,* 2015, Carcinogenesis.

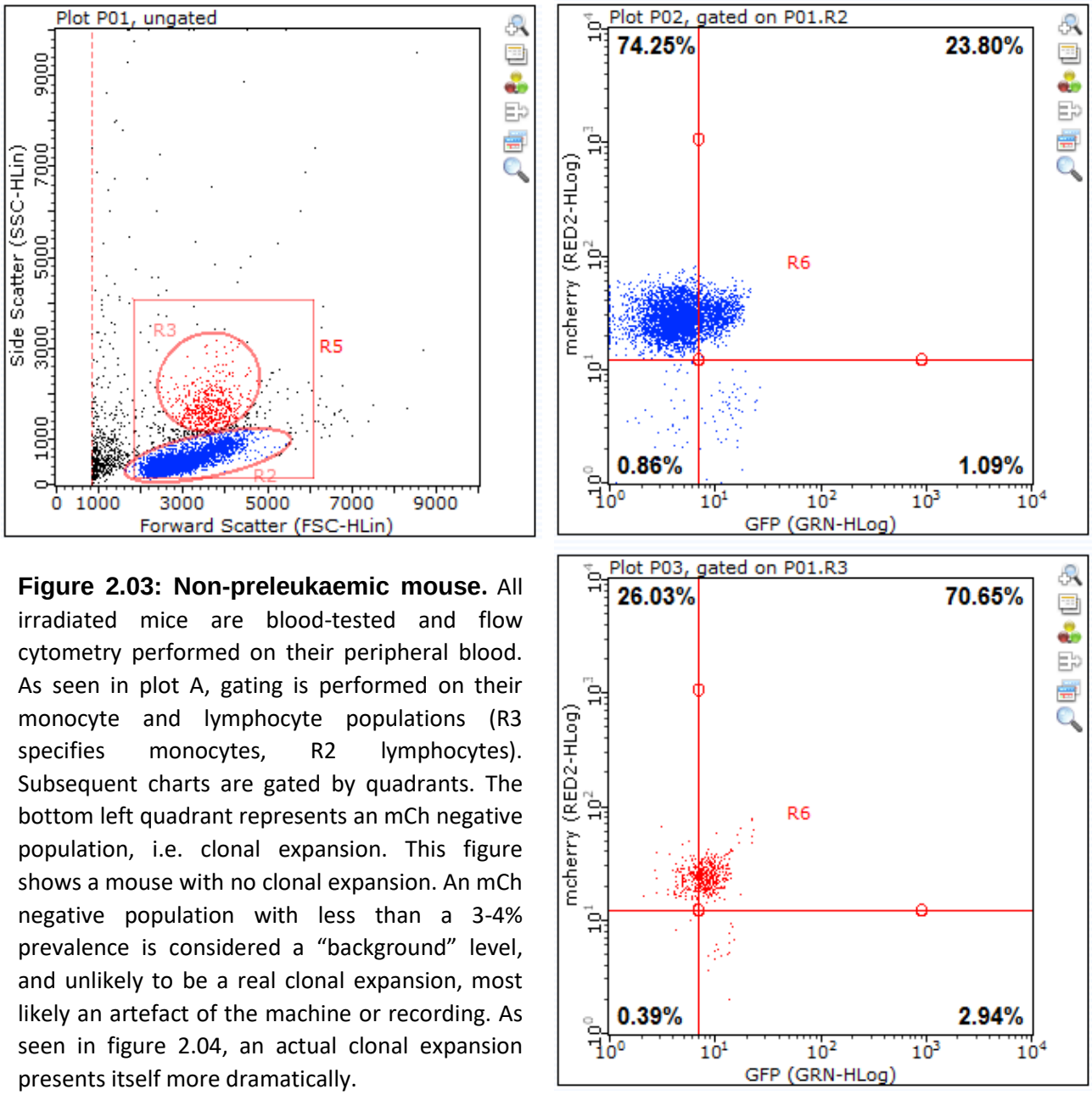


Figure 2.03: Non-preleukaemic mouse. All irradiated mice are blood-tested and flow cytometry performed on their peripheral blood. As seen in plot A, gating is performed on their monocyte and lymphocyte populations (R3 specifies monocytes, R2 lymphocytes). Subsequent charts are gated by quadrants. The bottom left quadrant represents an mCh negative population, i.e. clonal expansion. This figure shows a mouse with no clonal expansion. An mCh negative population with less than a 3-4% prevalence is considered a "background" level, and unlikely to be a real clonal expansion, most likely an artefact of the machine or recording. As seen in figure 2.04, an actual clonal expansion presents itself more dramatically.

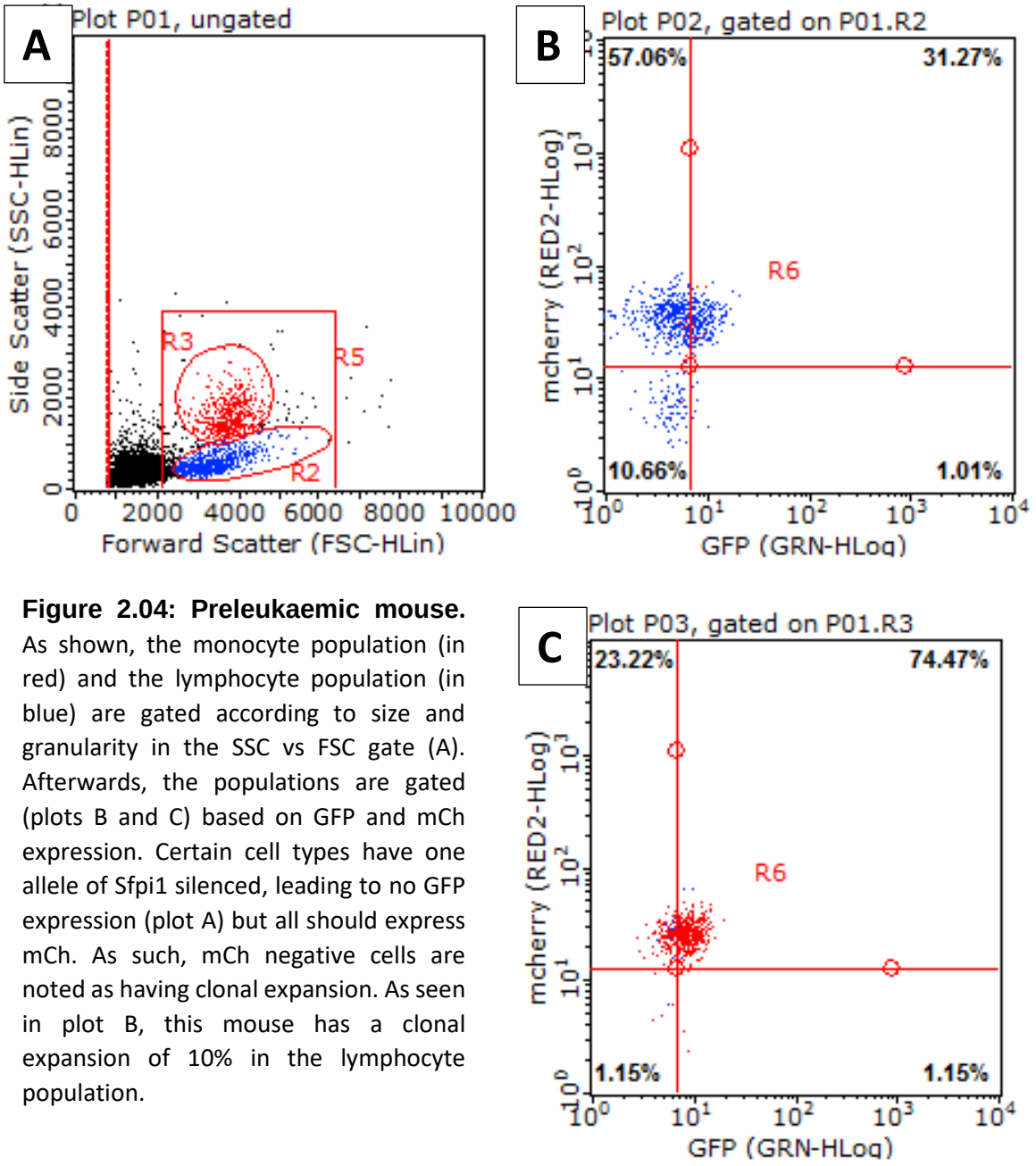


Figure 2.04: Preleukaemic mouse. As shown, the monocyte population (in red) and the lymphocyte population (in blue) are gated according to size and granularity in the SSC vs FSC gate (A). Afterwards, the populations are gated (plots B and C) based on GFP and mCh expression. Certain cell types have one allele of Sfpi1 silenced, leading to no GFP expression (plot A) but all should express mCh. As such, mCh negative cells are noted as having clonal expansion. As seen in plot B, this mouse has a clonal expansion of 10% in the lymphocyte population.

The transgenic CBA mCh/GFP mice were irradiated at 8-10 weeks at a dose of 3Gy using an X-ray source at a dose rate of 0.5Gy/min, and then monitored via monthly tail vein blood tests until one of three end points:

1) The mouse displays terminal symptoms that the project license specifies as reason for ethical euthanasia of the specimen.

2) The mouse reaches circa 50% clonal expansion (as defined by the percentage of non-mCh expressing peripheral blood cells).
3) The mouse reaches 12 months of age post-irradiation.

The culled mice were than harvested as per the protocol described in **Bone Marrow Extraction.** The protocol for blood testing is described in the section **Blood Testing and Flow Cytometry.**

Another murine strain included in the study, and vital to future work on this research question, is another transgenic CBA mouse strain referred to as CBA SPM. As described previously, post-radiation, a percentage of the irradiated mouse population experiences a deletion event of a single Sfpi1 allele, and then goes on to develop AML. This is a slight oversimplification of events. The actual process is shown in figure 2.05, modified from Verbiest *et al.,* 2015, published in Carcinogenesis. After this initial deletion event, the remaining Sfpi1 copy then experiences a point mutation event, specifically to R235. After these two conditions are met, the deletion event and mutation, then AML develops in 100% of these cases.

In the CBA SPM strain, the sequence of these events has been reversed. These mice carry a heterogeneous point mutation at R235 on a single allele of Sfpi1. After an irradiation event, remarkably, 100% of these mice experience a deletion event in the non-mutated Sfpi1 allele. As a consequence, unlike other murine models in which only a (variable) percentage of the population gets a radiation-induced cancer secondary to acute exposure, all irradiated CBA SPM mice get AML within 6 months post radiation insult. In addition, all CBA SPM mice eventually succumb to AML within 12 months without any preceding radiation exposure. The single change to R235 in Sfpi1 is enough to confer a hypersensitivity to radiation and a significant predisposition to the spontaneous development of AML.

All animals were bred and handled according to the UK Animals (Scientific Procedures) Act, 1986, Amendment Regulations 2012. Animal protocols were reviewed and approved by the local Ethics Committee and the Home Office. Mice were provided with water and food ad libitum.

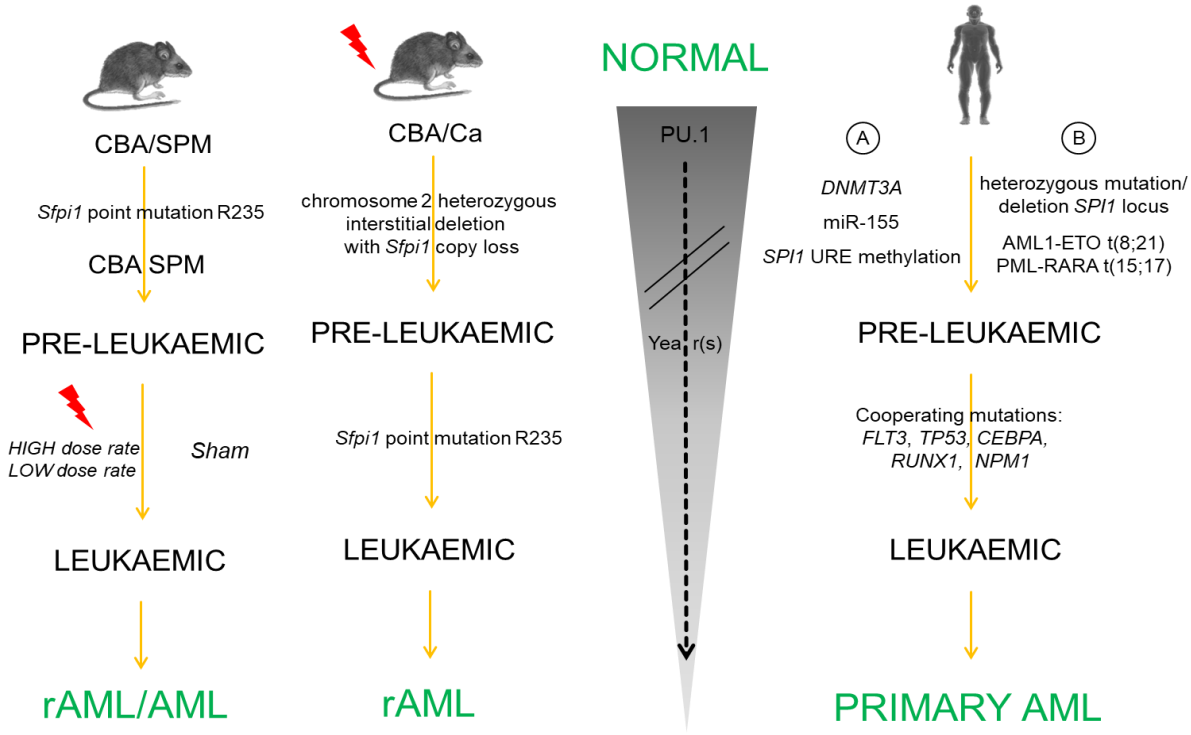


Figure 2.05: Classical AML disease progression in CBA-strain Mus musculus and Homo sapiens. The murine Sfpi1 gene is an analogue to the human PU.1 gene, which is downregulated in AML. In mice, a deletion occurs, having much the same effect. A subsequent mutation event on the remaining allele results in AML development. In CBA/SPM mice, this secondary mutation is present heterozygously prior to irradiation, resulting in 100% deletion of the unmutated allele irrespective of dose or even radiation.

Another strain of mouse was provided to the study by the Cardiovascular Disease group at (then) Public Health England, Radiation Effects department. This strain was a Ldlr KO (henceforth known as Ldlr-/-) high cholesterol model based on a C57BL6/j mouse, and irradiated at 4 doses: 0Gy, 0.5Gy, 2Gy, and 4Gy. The mouse strain was used as a fortuitous opportunity to test strain-dependent signal variability.

2.06 Blood Testing and Flow Cytometry:

mCh/GFP mice were monitored for clonal expansion of the mCh negative population in the peripheral blood from 6 months post-irradiation and every month onwards. Blood samples were taken by tail bleed and subsequently red blood cells were lysed by adding 200µl RBC lysis buffer, incubating for circa 60 seconds until the blood turned clear and was no longer turbid, and was then washed with 20ml of PBS and centrifuged at 1200rpm. The cells were resuspended in PBS and analysed using a GUAVA InCyte flow cytometry machine. Gating was performed on the myeloid and lymphoid cell populations present within the peripheral blood. mCh negative populations of higher than 4-5% represent clonal expansions. Populations above 10% were closely monitored, and these mice considered "pre-leukaemic". Mice with clonal expansion of above 50% were marked for termination as soon as possible, to avoid succumbing to leukaemia. Termination was, whenever possible, performed immediately after the blood testing was done.

2.07 Schedule 1 techniques used

From 2018-2021, a CO_2 chamber was used to asphyxiate the mouse, with secondary confirmation of death via exsanguination performed immediately afterwards. From 2021-2022, the CO_2 chamber system was retired in favour of an anesthetic gas overdose system. With this system, the mice are put into an irreversible coma, and are left in the chamber until they no longer respond to external stimuli with autonomic nervous responses. Secondary confirmation of death was then performed by cervical dislocation, with care taken not to crush the top section of the spine.

2.08 Bone Marrow Extraction:

After culling, the mouse abdomen was opened, and the internal organs removed. The following bones were collected: posterior tibia, posterior femur, pelvis, and spine, with feet, anterior limbs, tail, and ribcage being excluded from collection. The bones were carefully cleaned using sterile paper towels and then placed in a petri dish containing sterile PBS

and placed on ice. Furthermore, the spinal cord was removed from the spine via separation of spine sections and then carefully pulling out the spinal cord.

The bones were then removed from the petri dish and placed in a sterile mortar with approximately 10ml fresh, sterile PBS. The bones were crushed using a pestle, with firm vertical pressure and rocking motions to extract the marrow. The release of the marrow results in the PBS turning a cloudy red. PBS was drawn up using a syringe and a sterile 21G needle (BD Microlance) and dispensed into a 50ml Falcon tube, on ice. The bones were washed and crushed with more PBS until the PBS was no longer turning red and the bones were a pallid colour, indicating the successful extraction of all bone marrow from within.

The Falcon tubes were then centrifuged at 1200rpm in a swinging bucket rotor and the supernatant carefully pipetted out and placed into another, clearly labelled 50ml Falcon and placed on ice. If the cells were being further processed, the cells were resuspended in 5ml fresh PBS and counted using an Incucyte cell counter (Sartorius) at 1:100 dilution and using acridine orange/propidium iodide as a stain.

2.09 Radiation end points and experimental design

The overall flow of the research was as follows:

1) Establish a broad-spectrum view of miRNA expression in EVs in the presence and absence of ionising radiation in both newly irradiated mice, and mice allowed to live 12 months past irradiation.
2) Elucidate how miRNA expression differed between irradiated and control samples, and how it differed between irradiated mice that developed AML and those that did not.
3) Investigate whether individual cell populations that make up the wider bone marrow whole have different EV miRNA than the broad-spectrum view (many pieces make up an average whole) or if all cell populations respond the same way.

4) Investigate how EV-mediated miRNA interacts with cellular function via pathways targeted.
5) Establish if, and how, EV-mediated miRNA affects gene expression and endpoint metabolic output of the pathways found to be affected.

2.10 Serum-free techniques for tissue culture:

The bone marrow was not the only source of extracellular vesicles used for this research. Tissue culture based on bone marrow cells, isolated as described in the previous section, was also performed in order to create population-specific EV samples, rather than the mixed, holistic EV output of the total BM cell population. The aim was to establish what the total "vesiclesome" landscape of the BM was, and then to break it down into constituent, important cell populations to elucidate whether this was representative of all cells, or if different cell types produced different EV signals. In addition, cell lines were also planned for use in accompanying experiments.

However, one major problem with tissue culture vis a vis the production of EVs is the presence of fetal bovine serum (FBS) in nearly every single cell culture methodology. FBS is nigh indispensable for the growth and survival of cells. However, FBS is also completely full of bovine EVs (so-called xeno EVs). Roughly speaking, the proportion of EVs in an average tissue culture vessel with 10^6 cells would be ~1% cell derived EVs and ~99% xeno EVs. This means that most tissue culture methods using FBS are totally unsuited for EV research.

The initial attempt to produce an FBS-free tissue culture protocol was straightforward. Centrifugation to remove EVs from the FBS was impossible given that the laboratory did not have access to an ultracentrifuge. Filtration using a filter insert and a syringe failed to deplete EVs, with significant EV presence found via ExoQuick-TC isolation (described in the EV purification section) still being found. Spin filtration (as described in a following section) was used to deplete FBS of EVs, and this did seem to work in depleting EVs.

However, use of this EV-depleted FBS resulted in ailing, slow-growing and declining cell line tissue cultures, tested using HeLa and HEK293, which failed to establish themselves, indicating that either EVs themselves or a co-precipitated factor are very important in cell maintenance in tissue culture.

An attempt was made to create cell lines capable of growing in EV-depleted FBS-supplemented media via gradual passage-by-passage adaptation of the cells. Two streams were established, with HEK293 being used as a model. In the first stream, the first passage was done with complete FBS. The second passage used media supplemented with a mix of EV-depleted FBS and FBS in a 25:75 ratio. The third passage upped this ratio to 50:50, subsequently 25:75, and finally 100% EV-depleted FBS supplemented media. The second stream was done using the same method, but with the exception that conditioned media was added every passage in a 50:50 ratio to new media, supplemented as described with varying rations of EV-depleted FBS and FBS.

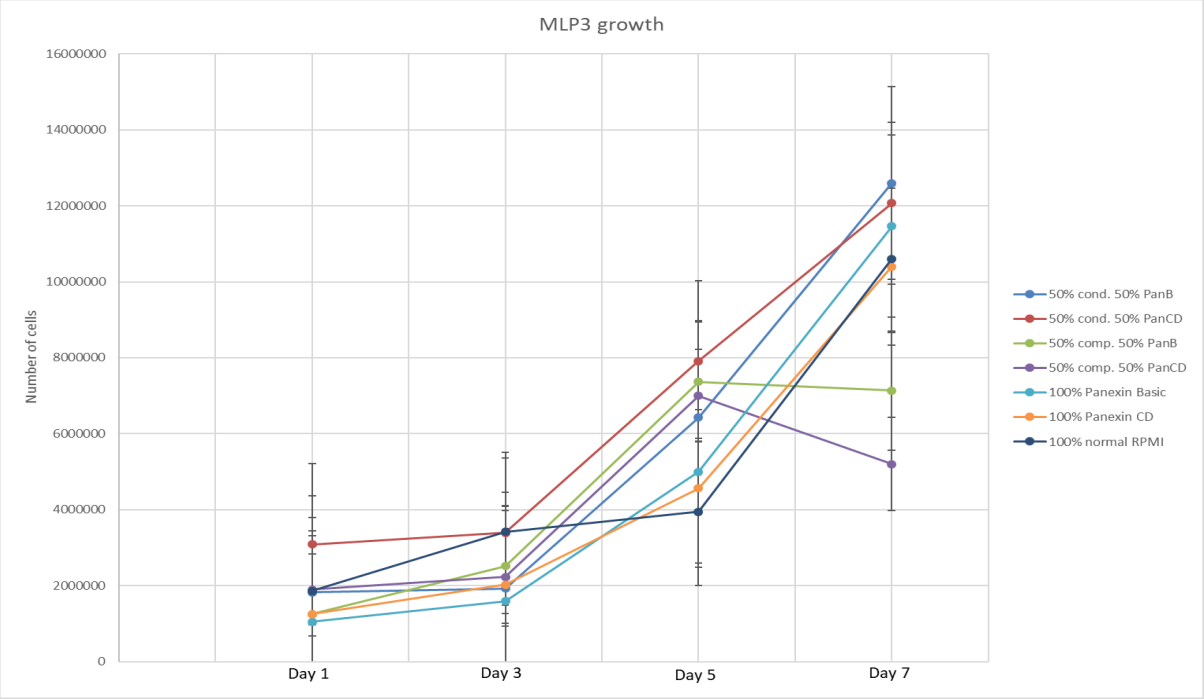


Figure 2.06: Growth curves of different combinations of complete or conditioned media with Panexin Basic or CD, compared to baseline RPMI medium, in MLP3. MLP3 is a suspension culture derived from a murine AML. As seen, 100% Panexin basic, 50% conditioned media/50% Panexin CD, and 50% conditioned media/50% Panexin Basic in fact outperformed baseline RPMI medium with MLP3 over a 7 day growth period.

Both methods resulted in partial success; the second stream, using conditioned media, was generally more successful. However, both streams suffered from long growing times to confluence, and were nowhere near as competitive in terms of growth to standard HEK293 cultures using widely accepted media. As such, it was decided that rather than attempt to create EV-depleted FBS, an EV-free FBS substitute would be used.

Methods using insulin selenium transferrin X were available (and indeed used for a haematopoetic stem cell culture protocol to great success, as described in a future section), but fortuitously a synthetic FBS product had (at the time) recently been developed. Panexin (Pan Biotech) is a “fully defined serum replacement for the cultivation of adherent and non-adherent cells” (Pan Biotech, product description). Three types of Panexin exist- Basic, CD, and BMM, the lattermost of which was specifically developed for the growth of

macrophages. All three types were studied, with HEK293 once again serving as the model. As seen in figure 2.05, Panexin Basic and CD performed at similar levels to FBS, and were therefore of feasible use for the generation of culture-derived EVs, without contamination with xeno EVs. Due to the cost differential vs their similar performance, Panexin Basic was used over CD, and Panexin BMM was used for macrophage cultures.

2.11 Bone marrow-derived Macrophage culture:

The first of these tissue culture methods was the culturing of bone-marrow derived macrophages. Macrophages are suspected to play a major role in EV expression within the bone marrow (Shen *et al.,* 2011). Media was prepared using RPMI1640 (Thermo Fisher Scientific), supplemented with 5% Panexin BMM (Pan Biotech), 50µM β-mercaptoethanol (Sigma-Aldrich), and 2ng/ml recombinant murine GM-CSF (Abcam). Bone marrow was processed as previously described. The cell pellet was subsequently resuspended in 3ml complete media. This was split into 3 and dispensed into 3 T75 adherent tissue culture flasks with 20ml complete media; one animal's worth of cells was thus dispensed into three

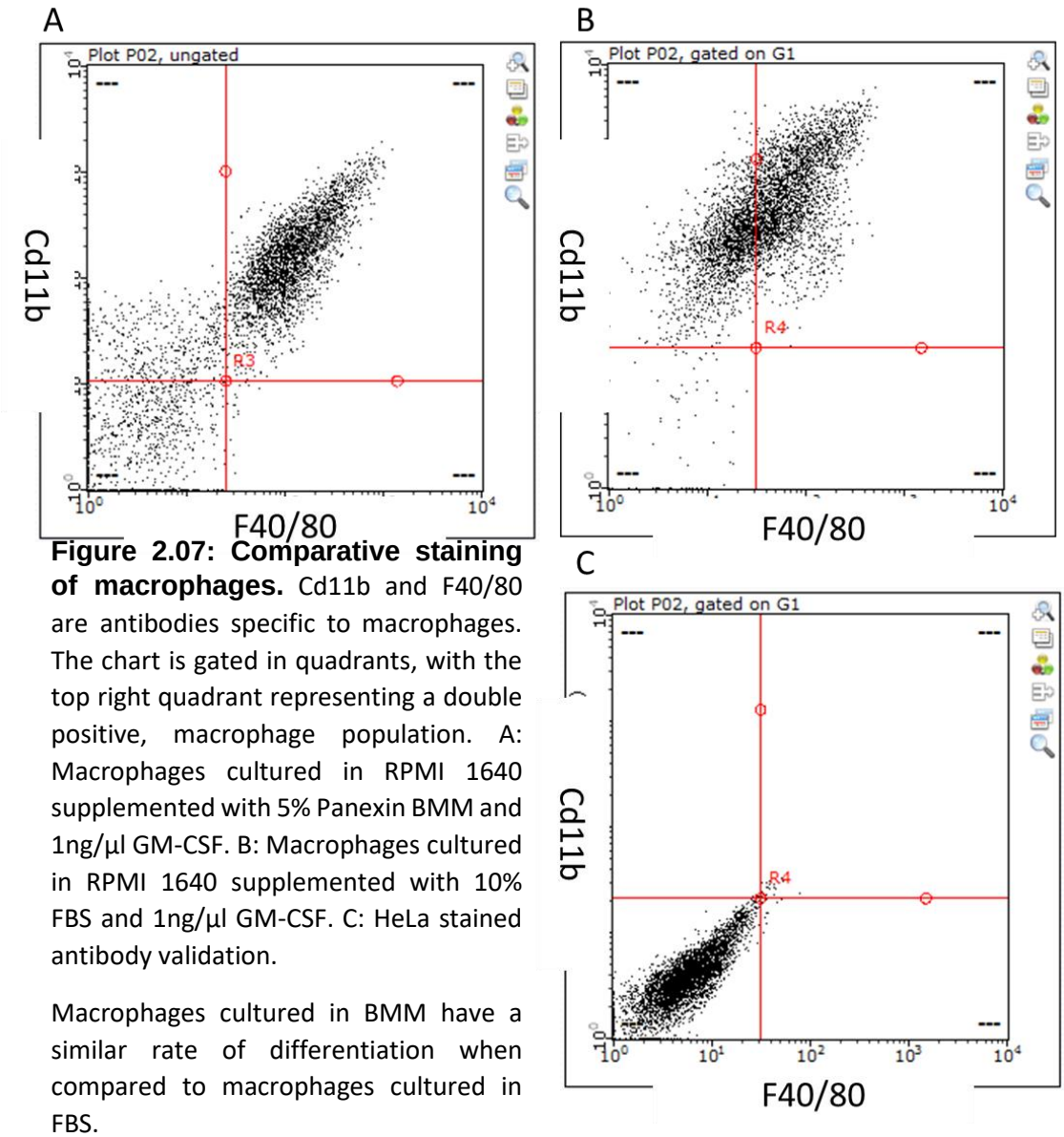


Figure 2.07: Comparative staining of macrophages. Cd11b and F40/80 are antibodies specific to macrophages. The chart is gated in quadrants, with the top right quadrant representing a double positive, macrophage population. A: Macrophages cultured in RPMI 1640 supplemented with 5% Panexin BMM and 1ng/µl GM-CSF. B: Macrophages cultured in RPMI 1640 supplemented with 10% FBS and 1ng/µl GM-CSF. C: HeLa stained antibody validation.

Macrophages cultured in BMM have a similar rate of differentiation when compared to macrophages cultured in FBS.

flasks, and this was scaled accordingly. The cultures were then incubated at 37C 5% CO2 and fed with fresh complete media on days 5 and 7, done by removing 10ml media and adding 10ml fresh media (Eske *et al.,* Journal of Immunological Methods, 2009). Cells were trypsinized and harvested at day 10; after washing twice with PBS, cells were treated with trypsin EDTA for 10-15 minutes and then detached using a cell scraper. The supernatant was kept in a separate 50ml falcon for EV processing.

Cd11b and F40/80 are antibodies that serve as macrophage surface markers, with presence of both being required to positively identify a cell as a macrophage. As seen in figure 2.06, both culturing strategies described presented a significant macrophage population, with Panexin-BMM supplemented cultures showing a purer population of double positive macrophages.

2.12 Bone marrow-derived Mesenchymal stem cell culture:

Mesenchymal stem cells were cultured according to the protocol used by Caroti *et al.,* 2017, published in Nature Scientific Reports. After cell isolation from the bone marrow, the pellet was resuspended in complete media, which consisted of RPMI1640 supplemented with 20% FBS, 2mM glutamine, 10ng/ml bFGF, and 100 units/ml penicillin and 100ug/ml streptomycin. This was then dispensed into T-175 culture flasks (Nunclon, Naperville IL, cat#178883) containing 40ml complete media, such that cell concentration was at 500,000 cells per cm^2, i.e. 8.75 x 10^7 cells. This was then incubated at 37C under hypoxic (5% O_2) conditions. 24 hours after plating, the media was entirely removed, thus discarding any non-adherent cells, and replaced with 30ml fresh complete media. The media was refreshed every 3-4 days.

Once confluence was reached, the culture was rinsed with 4ml 0.25% trypsin-EDTA to remove serum. Another 4ml 0.25% trypsin-EDTA was then added and left for slightly longer, circa 2-3 minutes. The culture was placed under a light microscope and monitored for the detachment of large, senescent cell bodies, identified due to their size and phenotype,

which consisted of an uneven, irregular shape and associated blebbing. Once detachment began to occur, this trypsin wash was removed, and a third volume of 4ml added. This was then placed into the incubator and left for 3-5 minutes for total cell detachment, which was completed via use of a cell scraper. 16ml complete media was added to neutralize the trypsin, and the cells spun down at 1200rpm in a swinging bucket rotor centrifuge, with the supernatant being removed and the cells being resuspended in a fresh volume of complete media. The cells were then counted and split no wider than 1:2. This completed the passaging of p0 to p1.

24 hours after this passaging, the media was completely removed and refreshed. Feeding occurred at the same schedule, every 3-4 days. When cells were confluent, the same passaging procedure as above was used. Once the cells reach p3, their growth would slow down. Cells in p0 to p2 appear more rounded and refractory, and rapidly proliferate. Cells in p3 will begin to change in appearance, to a more spindle-shaped, almost myocytic appearance; during this phase proliferation will slow. Once they have completed this transition, proliferation will accelerate once again. Once this has been passaged to p4 and this phenotypic transition is complete, the cells were ready for further experimentation, having become an MSC-enriched culture capable of long-term proliferation. This culture could survive for almost 2 months, with an upper bound being unknown.

When assays requiring EV collection were performed, the media was changed to RPMI1640 supplemented with 10ng/ml bFGF, 2mM glutamine, 100 units/ml penicillin and 100mg/ml streptomycin, and 20% Panexin Basic as an EV-free serum replacement.

2.13 Murine HSPC culture:

Haematopoetic stem cells (HSCs) were enriched and expanded from a murine BM cell population, adapted from a protocol by Adam C. Wilkinson *et al.,* 2020, published in Nature Protocols.

In order to create a long term, pluripotent HSC culture, a specialized media was required. A complete media was made using Ham's F-12 media (Gibco, Cat #11765-054) supplemented with 10mM HEPES (Gibco, Cat #15630-080), 1X Penicillin-Streptomycin-Glutamine (Gibco, Cat #10378-016), 1X Insulin-Transferrin-Selenium-ethanolamine (ITS-X) (Gibco, Cat #51500-056), which served as an FBS replacement, 100ng/ml recombinant murine thrombopoietin (TPO) (Peprotech, Cat #AF-315-14), 10ng/ml recombinant murine stem cell factor (SCF) (Peprotech, Cat #AF -250-03). In addition, hydrolysed polyvinyl alcohol (PVA) (Sigma, Cat #P8136) was also dissolved in sterile, deionized water at a concentration of 100mg/ml and added to the media such that the final concentration was 1mg/ml.

Once the BM cells were isolated and safely stowed on ice, the cells were then lineage depleted using a RoboSep Fully Automated Cell Separator (StemCell). Cells were resuspended such that their concentration was no greater than $1x10^7$ per ml, and then a high specificity lineage depletion protocol was run using the provided RoboSep lineage depletion kits.

After sorting, the lineage-depleted cells were collected and counted. 1ml of the complete media was placed in each well of a 24 well fibronectin-coated cell culture plate. Two types were used; one was coated with fibronectin in-house (Plates: Corning, Fibronectin: Roche, Cat #10838039001) or pre-coated (Corning, Cat #354411). This was due to a pandemic-induced severe delay in shipment of pre-coated plates; once these were acquired, they were used in preference to the self-coated plates. Into this 1ml of complete media, 5,000 HSCs were placed and then immediately put into an incubator set to 37C, 5%CO_2 and 20% O_2. From day 5 onwards, complete media changes were performed every 2-3 days. This was done by very carefully pipetting the media out using a P1000 pipette and going down along the sides, and carefully removed until the meniscus of the media was at the bottom of the well, ensuring that a very small volume of liquid still covered the cells, which at this point were an adherent monolayer. New media was then slowly pipetted down the side so

that the monolayer, very weakly adherent, was not disturbed and cells were not flushed out into the media. Once the culture reached ~90% confluency, achieved after 3-4 weeks, this was then split 1:2, with the same media conditions as above. Trypsinization was not required, as the monolayer was easily detached from the well surface by vigorous up-and-down pipetting and washing with media.

The stem-ness of these HSCs was confirmed using flow cytometry using the following markers: $Sca1^{+}$, $Ckit^{+}$, $CD150^{+}$, $CD48^{-}$, $CD135^{-}$, and $CD34^{-}$.

2.14 Extracellular vesicle purification:

The supernatant separated from the cellular pellet in the previous section was further spun at 2,000g, to separate larger apoptotic bodies and eliminate most apoptotic body contamination, and the pellet discarded. It is important to note that apoptotic body contamination remains; smaller bodies remain within the sample. As such, it cannot be claimed that using this methodology (as demonstrated via Western Blot analysis) produces pure extracellular vesicle samples. Strictly speaking, the sample is an “extracellular vesicle enriched mixture”. For ease of use, this mixture will be referred to as extracellular vesicles or EVs, but once again this method does not claim to produce a pure sample, only a sample of sufficient amount for the analyses used in this thesis.

Depending on downstream applications, two different extracellular vesicle isolation methods were used. The first method relied on a polyethylglycol precipitation method, via the use of ExoQuick-TC (System Biosciences). The reason this technique was used is because the predecessor and germinating idea of this project, LEUTRACK, an EU CONCERT funded research project on EVs, used ExoQuick-TC in all their methodology, and in order to continue this vein of research and ensure resulting data could be compared, ExoQuick-TC was retained. It should be noted that ExoQuick-TC does have limitations and is commonly regarded as a ‘dirty’ preparation. As such it is important to keep diligent controls and acknowledge the fact that the EV sample is not pure.

Briefly, the clarified supernatant was measured to the nearest 0.1ml. 200µl ExoQuick-TC per ml was carefully pipetted into the supernatant, and the sample mixed by inverting it several times until the viscous ExoQuick-TC and the supernatant were thoroughly mixed. This was then incubated in an upright position using a rack at 4C overnight, for a maximum of 16 hours. The following day, the tube containing the supernatant/ExoQuick-TC mix was carefully removed and then centrifuged for 30 minutes at 1500g. The supernatant was carefully removed, and the resultant EV-enriched pellet resuspended in an appropriate buffer for downstream applications, typically lysis buffer for miRNA extraction.

For samples wherein the EV concentration was suspected to be very low within the supernatant, e.g. cells taken from tissue culture, a variation of this method was performed. From observation, using ExoQuick-TC on samples with low EV concentration per ml seldom yields useable results. Prior to addition of ExoQuick-TC to the clarified sample, the sample was first concentrated using a 10,000 kilodalton (kDa) spin filter (Merck-Millipore), according to the method described in the next paragraph. This super concentrated sample then had ExoQuick-TC added to it and incubated and processed as described previously.

The second method was for samples requiring same-day processing due to the requirements of the experiment in question, or for samples destined to be added back to live cells for secondary effects analysis. Merck-Millipore provides a method for using their 10,000 kDa spin filters to concentrate EVs. 15ml spin filters were used. The spin filter is an insert into a 50ml falcon tube. First, 2ml sterile PBS was added to the spin filter. The filter was then centrifuged at 4,000g in a swinging bucket rotor for 15 minutes. The filtrate was discarded, and the remaining unfiltered PBS pipetted out using a 200µl Gilson pipette, using a sweeping motion. 15ml of the clarified supernatant was then added to the filter and spun at 4000g for 30 minutes. The filtrate was discarded, and the process repeated until all of the supernatant volume was processed. Once all the supernatant was processed, 14ml sterile PBS was added, and a final 4000g spin for 30 minutes was performed. The resulting unfiltered, concentrated, EV-enriched sample was then carefully pipetted out into a 1.5ml

Eppendorf tube. The sides of the filter were washed with a small volume of sterile PBS and added into the Eppendorf tube.

Merck-Millipore states that this sample is analysis-ready; however, for the sake of consistency in instances where the EVs were to be analysed directly, ExoQuick-TC incubation was performed first. Only where indicated was this step skipped due to the extremely low concentration of EVs even after spin filtration, and where further loss could not be tolerated before falling beneath minimum level for analysis parameters.

2.15 miRNA extraction from cellular and EV sources:

miRNA was extracted using two methods: the first with an RNEasy mini kit (Qiagen, Cat #74104) and the second with an miRNEasy mini kit (Qiagen, Cat #217004), both according to manufacturer's instructions. Both processes yield the same total RNA, but both were tested to see if one yielded an appreciably better yield than the other. Both were found to perform identically re: yield, with the exception of low concentration EV samples, in which miRNEasy outperformed RNEasy.

Using the RNEeasy kit, the sample to be extracted, whether it was EVs or cellular (both were treated the same way), were lysed with RLT lysis buffer containing β-mercaptoethanol at a concentration of 10ul/ml. The cells were mechanically lysed using a 25-gauge needle and up-and-down pipetting to mechanically shear the membrane, aided by chemical lysis using RLT buffer. This step was added due to the low yield of miRNA observed when only using vortexing or pipetting to lyse EV samples. 350µl RLT buffer was added to samples, except in the case of cellular samples exceeding 5 x10^6, in which case 600µl RLT was used. After homogenization of the lysate, 1 volume (350 or 600ul) of 70% ethanol was added and well mixed by pipetting. This was *not* centrifuged.

700µl of this ethanol/lysed sample was added to an RNEasy spin column, including any precipitate which may have formed. From observation, high concentrations of RNA tend to yield a milky white precipitate at this stage. The spin column was centrifuged at 8000g for

15s, at which point the flowthrough was discarded and the process repeated with any remaining sample. After all the sample had been run through the spin column, 700µl buffer RW1 was added and washed through using the same conditions as prior. Again, flowthrough was discarded, and 500µl buffer RPE added. After another wash, a second volume of 500µl RPE was added, and spun for 2 minutes. Finally, the collection tube was replaced, and the tube was run empty for 1 minute at full speed (circa 13,000g). The filter was then placed in a sterile 1.5ml Eppendorf and the RNA eluted using 30µl of sterile, deionized water and placed on ice. The filter was retained on ice until the sample was measured using a NanoDrop (ND-2000, ThermoFisher Scientific); if the total yield was greater than 30ug of RNA, a second volume of 30µl water was added, although this was rarely the case.

2.16 miRNA analysis by nCounter:

miRNA derived from both cellular and EV sources was analysed via nCounter, using a murine codeset panel (Nanostring, Catalog #CSO-MMIR15-12). The principle of the nCounter analysis method is conceptually similar to a microarray. 10ng of total miRNA input was used, and the protocol was performed per manufacturer's instructions. While the entire protocol will not be replicated here, a brief summary of the process and the rationale behind it will be provided below.

The nCounter miRNA expression kit contains several different components; broadly speaking this can be split into three different components. A reagent set for the amplification of the miRNA sample and the provided miRNA controls, a reagent set for the hybridization of the amplified miRNA to a fluorescent probe, and a kit containing a glass plate and reagents for the binding of the probe-hybridized miRNA to the wells of the glass cartridge, which will be read by the nCounter machine.

After amplification and purification of the miRNA as indicated in the protocol, the miRNA is then hybridized to a probe. The probes in an nCounter panel consist of a varying number

(depending on the panel purchased) of RNA sequences complimentary to targets of interest. In the case of the murine expression panel, this consisted of roughly 800 different miRNA sequences, covering a broad range of biological activities, e.g. carcinogenesis, metabolic activity, immune function, etc. This short, complimentary sequence is in turn bound to a “codeset”- a series of small, synthetic fluors in linear sequence with different colours, e.g. red-green-blue-green-red. The order and combination of these colours is unique to every sequence, meaning that this codeset is effectively a fluorescent barcode.

This means that after hybridization and binding of the miRNA to the Nanostring input cartridge, which is automatically performed by the NanoString PrepStation, an automated machine for the washing and binding of samples to the glass cartridge, the miRNA can be scanned, and the precise number of individual targets counted by means of this internal barcode. Naturally, the limitation of such a method is that only what is targeted will be reflected in the data; unlike RNA sequencing, wherein the total RNA population is present, any non-hybridized miRNAs, no matter how abundant, will be washed away and not bound to the cartridge, and thus be absent from the final dataset.

The NanoString Reader is then programmed to read the cartridge, which can be modulated for how detailed one wishes the analysis to be. For the purposes of this research, the maximum fields of view, 555, was chosen in order to have a high resolution counting of the hybridized miRNA.

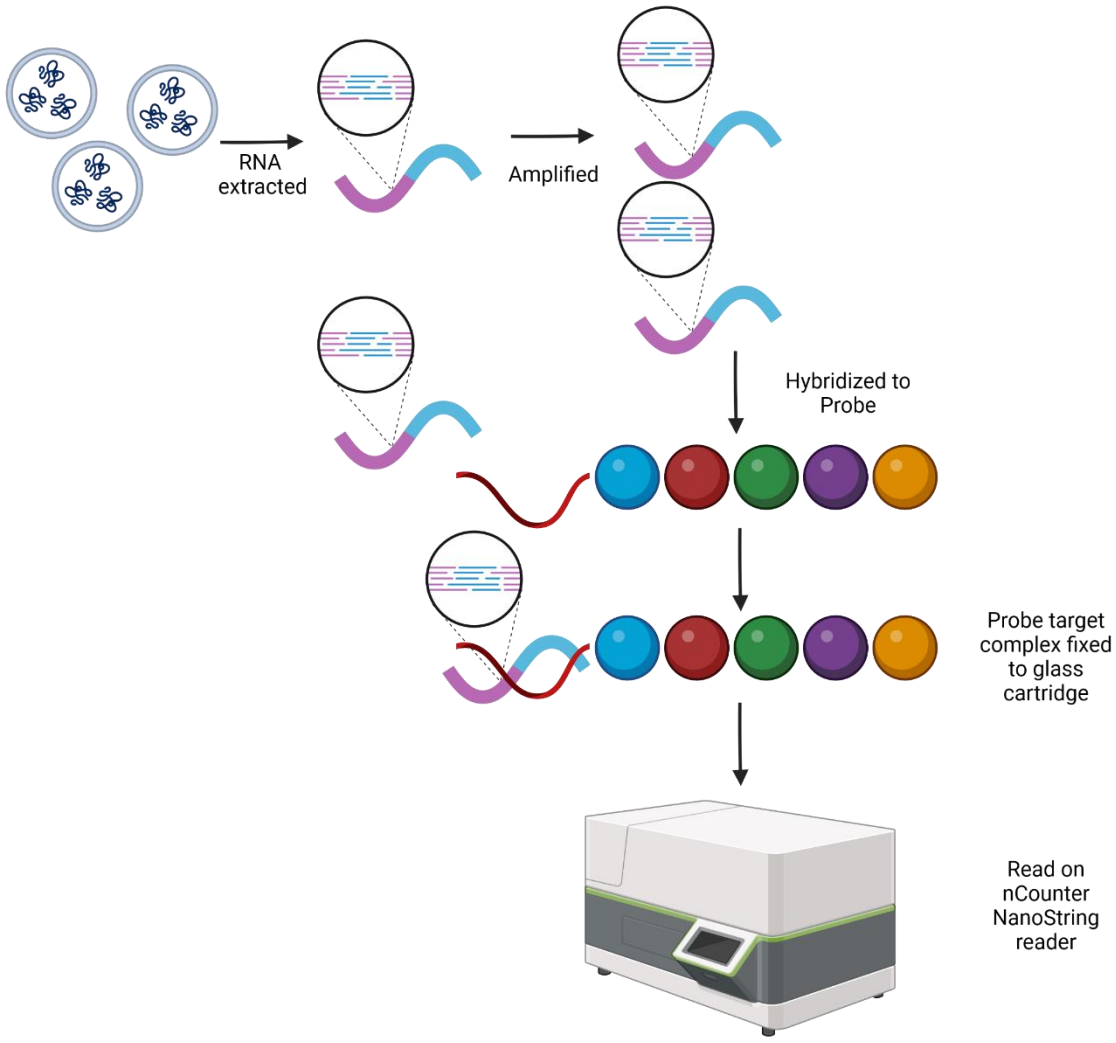


Figure 2.08: Abbreviated conceptual workflow of the nCounter probe hybridization process. miRNA was purified from EVs or cells and then amplified. These amplified and purified miRNAs were then hybridized to a probe with a set of 5 fluors that act as a bar code, creating a probe-target complex which is then affixed to a well within a glass cartridge. This is then read on the NanoString reader, resulting in raw miRNA counts, with identification done automatically by the fluorescent bar code. Created using BioRender.

Once the raw count was obtained, this was fed into the nSolver software, NanoString's proprietary data processing software. This program comes with a suite of features, including but not limited to normalization, statistical analysis, and graphical post-processing (e.g. heat maps). The data was normalized according to the top 100 miRNA expressed, and then

exported into a .cdf format. This was then reformatted for use as an input data file to the BRBArray Tools free suite of statistical tools, an Excel extension specifically built for use with biological data.

The data was then split into multiple groups depending on what was run; if, for example, samples subjected to 0Gy, 0.1Gy, and 3Gy were run, these were split into 3 groups. BRBArray Tools was then used to compare each of the variable groups, in this case 0.1Gy and 3Gy, to the control 0Gy group. This was then used to build a heat map for the graphical expression of the data.

In order to generate a list of significantly differentially expressed miRNA, DIANATOOLS miRPath v2.0 was used, a free browser-based statistical analysis and database package. The data was once again reformatted to be readable as an input by DIANATOOLS, and split into two sets, control vs variable. One limitation of the miRPath software is that it cannot read more than two groups at once, meaning that in the example above, two datasets must be generated, 0Gy vs 0.1Gy, and 0Gy vs 3Gy.

This then uses KEGG analysis to generate a list of significantly differentially expressed miRNA, with p-value and false discovery rate (FDR). miRNA below p=0.05 were chosen and analysed further using the DIANATOOLS suite to generate the list of predicted gene targets and pathways associated, as well as the combined likelihood of all involved miRNA acting in concert, allowing for a prediction of how exactly these differentially expressed miRNA were acting in a biological context.

All Venn diagrams produced from miRNA data were performed using R Statistical Software (v4.4.0; R Core Team 2021). The package used was Gao C, Dusa A (2024). _ggVennDiagram: A 'ggplot2' Implement of Venn Diagram_. R package version 1.5.2, <https://CRAN.R-project.org/package=ggVennDiagram>.

2.17 Lysine level assay:

Analysis of the RNA sequencing derived data (provided by ArrayStar) as well as the nCounter data demonstrated a few key overlapping metabolic pathways. Among these was lysine degradation. In order to see how exactly this was being affected, a threefold approach was decided on. First, the level of lysine would be measured in unirradiated vs irradiated cell populations. Then, the level of lysine would be measured in cells that had been exposed to EVs derived from irradiated cell populations, and if this differed from a control population of the same age but with EVs from a non-irradiated population. Due to issues with sample availability, however, this latter control was not possible for all cell types, meaning that an alternative control with refreshed media but no EVs was used. This is not ideal and in a repeat of this work a control of the former type would be used. The third approach was to analyze how the expression levels of genes specifically targeted by the relevant miRNA were affected, done by qPCR; this will be detailed in a later section.

Firstly, two different BM-derived cell types were used, cultured as described in previous sections. BM-derived murine mesenchymal stem cells, and BM-purified haematopoietic stem cells. Both cell types were cultured to maturity (circa 4 weeks post initiation for MSCs, and 2-3 weeks post-initiation for HSCs). In the case of HSCs, these were divided into 4 categories: Unirradiated, irradiated, unirradiated + refreshed media and unirradiated + irradiated EVs (referred to as bystander + irradiated EVs). In the case of MSCs due to sample availability, as a contamination problem had sharply curtailed the number of available cultures and necessitated a restart and thus significant time pressure, these were separated into three categories: unirradiated, irradiated, and unirradiated + irradiated EVs.

24 hours post irradiation, or 24 hours post EV addition, cells were collected from their culture flasks and tested using a fluorometric lysine level assay kit (Abcam, Cat #ab273311). Fluorescence readings were measured according to manufacturer's instructions on a plate reader and compared to one other. T-test and ANOVA were used to establish significance.

2.18 Aldehyde and Aldh activity assay:

The pathway predictions provided by KEGG in terms of lysine degradation intersected with other pathways in Aldehyde and Aldehyde dehydrogenase being present, serving as a common factor. As such, the level of free aldehydes as well as the activity of aldehyde dehydrogenase was tested. Cell populations were prepared as described in section 2.16. These were irradiated, and subjected to bystander conditions, in the same way. To measure aldehyde levels, cells were lysed in PBS and then processed using a fluorometric aldehyde level kit (Abcam, Catalogue # ab138882) according to manufacturer's instructions, and read on endpoint mode using a plate reader. To measure aldehyde dehydrogenase activity, lysed cells were instead processed using a fluorometric ALDH activity assay (Abcam, Catalogue # ab155894), and read first on endpoint mode, then on kinetic mode with a reading every 2 minutes over the period of one hour. A final endpoint mode reading was then performed.

2.19 Free fatty acid level assay:

Samples were prepared identically to sections 2.16 and 2.17, with the exception that rather than cells being used, supernatant was used in order to identify levels of free fatty acids in the extracellular space. Supernatant was snap frozen in liquid nitrogen before being stored at -80C, and later thawed on ice prior to processing. A free fatty acid quantification kit (Abcam, catalogue #ab65341) was used to quantify free fatty acid levels, according to manufacturer's instructions. This was then read on a microplate reader in endpoint mode.

2.20 Gene expression assay:

The following genes were assessed in murine HSPC and murine MSC samples: Aldh9a1, Aldh7a1, and Fasn. These three genes were found to be commonly involved in all samples tested during this project. Murine HSPCs and murine MSC samples were drawn from the same cell populations tested for lysine, fatty acids and aldehyde levels, with the same conditions: 0Gy, 2Gy, and 0Gy+2Gy derived EVs, with the same timepoints.

Total RNA was extracted as described previously, and then transcribed to cDNA using a high-capacity cDNA Reverse Transcription Kit (Catalog no. 4368814, Applied Biosystems), according to manufacturer's instructions. The concentration of cDNA was then measured, and all samples diluted to the same concentration. qPCR was then carried out using gene-of-interest complimentary primers and SYBR Green, i.e. not in a multiplexed fashion. The primers were validated using randomly selected samples and then subjected to a melting curve, looking for the presence of multiple peaks. If multiple peaks were found, the primer was rejected. Four different primer designs per gene were created, and all of these assessed using the melting curve method, with only those with a single peak then being used for the entire sample set. The level of gene expression was then measured using the delta CT method, and thus quantified and compared to other sets using ANOVA.

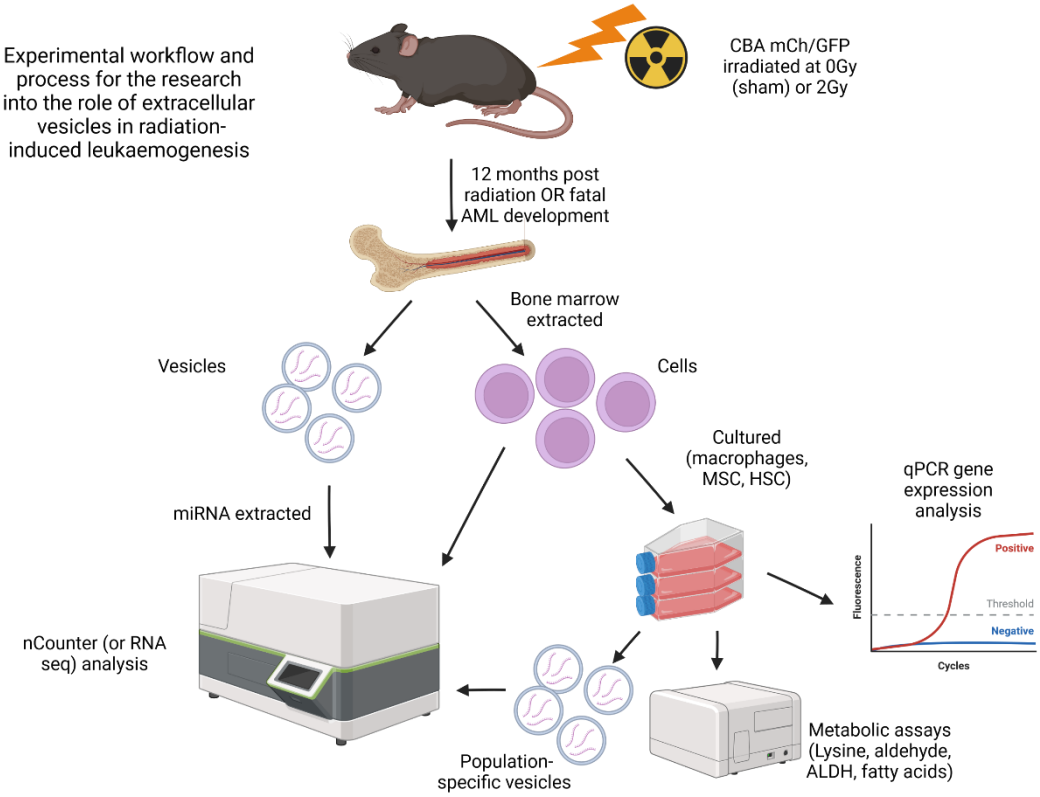


Figure 2.09: General experimental workflow. Cells and EVs taken from irradiated mice were processed as described, with EVs being directly analysed via nCounter. BM cells were cultured in 3 different ways; to isolate and purify macrophages, to generate MSCs, and to expand and purify HSCs within the BM. These were then subjected to another 3 assays: analysis of EV miRNA content, by nCounter or by RNA Sequencing; metabolic assays to assess lysine, aldehyde, and fatty acid levels as well as ALDH activity; and qPCR for gene expression of genes suspected to be targeted by significant miRNAs identified in the first assay.

3. Extracellular vesicle landscape of the bone marrow

The genesis of this research was the LEUTRACK project, an EU CONCERT funded research project. The goal of LEUTRACK was to perform a multiomic approach to EV content and its potential role in radiation exposure and post-exposure late effects such as AML. This consisted of three arms; the *in vivo* effect of EVs on AML development, performed by our collaborators in the National Public Health Center, Department of Radiobiology and Radiohygiene, in Budapest, Hungary; the protein content of EVs determined by mass spectrometry, performed by our collaborators in the Metabolomics and Proteomics Core, Helmhotz Zentrum, in Munich, Germany, and the miRNA content of EVs, performed by our research group, the Cancer Mechanisms and Biomarkers group at (then) PHE Harwell, now UKHSA.

3.01 Immediate post-radiation response; the miRNA landscape of CBA mice 24 hours post radiation insult

CBA mice, non-transgenic, were irradiated at 0.1 and 3Gy. 0.1Gy was chosen as this is the upper limit of what is considered low dose radiation, while 3Gy was chosen for both consistency with prior irradiations and because it is the optimal dose for leukaemia induction in these mice. The irradiations were performed using two X-ray sources; the first, located in Hungary, was a X-RAD 225/XLi X-ray source (Precision X-Ray, Madison, CT, USA) while the second, on site at UKHSA Harwell, was an AGO X-Ray Set (AGO, Reading, UK) running at 250V (constant potential) with a Cu/Al filter producing a beam of 1.2mm HVL Cu. Low dose (0.1Gy) exposure was performed at a rate of 4.9mGy/min at a sample to emitter distance of 91cm and a current of 0.2mA, while high dose (3Gy) exposure was performed at a rate of 0.5Gy/min at a distance of 60cm and a current of 13mA. and 24 hours later bone marrow was harvested on site in Hungary, EVs isolated, lysed and frozen in that lysis buffer, and shipped to us at UKHSA Harwell for miRNA extraction, performed as described in the previous chapter. This miRNA was then analysed using the nCounter murine miRNA expression panel.

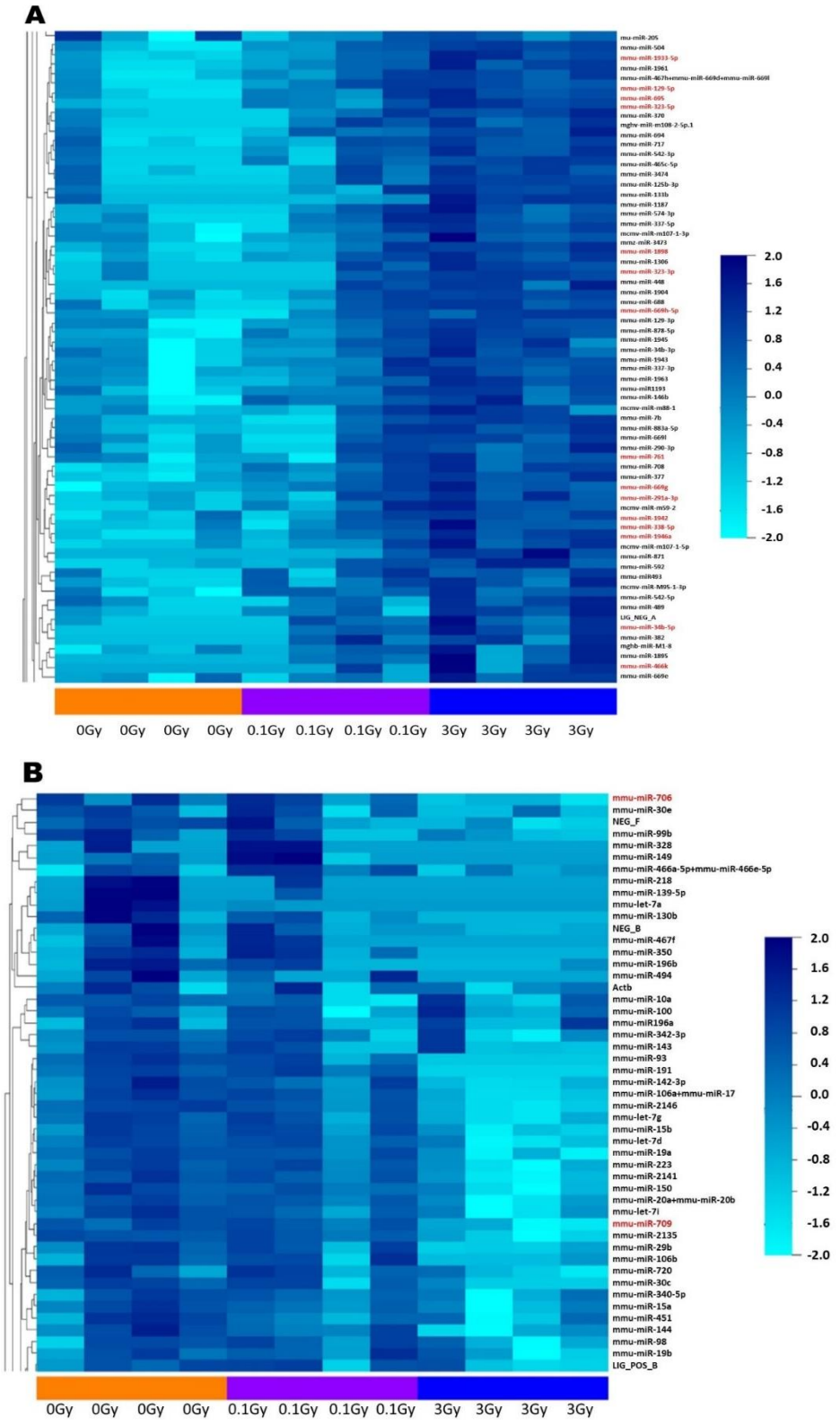


Figure 3.01: Heatmap graphical representation of murine miRNA, isolated from bone marrow, 24 hours post radiation exposure. All mice were WT-CBA, and represent a mixed gender pool. Each column **does not** represent an individual mouse, but rather circa 12 mice pooled together in a single sample. A: A cluster of upregulated miRNA and B: a cluster of downregulated miRNA. miRNA marked in **red** are miRNA flagged by DianaTools mirExTra 2.0 as significantly differentially regulated. Clustering performed by BRBArrayTools. Reproduced from Csordas & Rutten, *et al.,* 2023, International Journal of Molecular Science.

It is important to note that each column or lane of the heatmap shown in figure 14 does not represent an individual mouse, as seen in other heatmaps in following sections. Each column instead represents an aggregate of roughly 12 mice, meaning that the total sample set was circa 144 wildtype CBA mice.

As can be seen in figure 3.01, radiation, especially the high dose of 3Gy, induces a significantly different miRNA expression profile when compared to the control radiation dose at 0Gy. 0.1Gy shows more variation, with 2/4 sample sets showing a profile much more similar to 3Gy.

When assessing the statistical significance of miRNA across all three sample sets, the following miRNA were found:

Table 3.01: Dysregulated miRNA in 24 hours post IR WT-CBA mice. All miRNA were searched through miRbase; predicted biological interactions found via article search (as cited) and via predicted targets using the TargetScanMouse database, excluding low confidence or high FDR predictions.

miRNA	Predicted Biological Interactions
Mmu-miR-1933-5p	Unknown; most likely targets methyltransferases.
Mmu-miR-695	Appears to be involved in monocyte recruitment in liver regeneration, as well as in corneal senescence.
Mmu-miR-323-5p	Potential biomarker for gastric cancer.
Mmu-miR-1898	Unknown.
Mmu-miR-323-3p	Inhibits oxidative stress and apoptosis post myocardial infarction. Appears to be involved in heart development.
Mmu-miR-1904	Appears to be involved in immune response to viral infection, otherwise unknown.
Mmu-miR-688	Involved in colorectal and pancreatic cancer development.
Mmu-miR-669h-5p	Involved in an oxidative stress cluster.
Mmu-miR-129-5p	Suspected tumour suppressor (as part of the mmu-miR-129 cluster of miRNAs) in various carcinomas, osteogenic differentiation via Dkk3 repression.
Mmu-miR-878-5p	Expressed at high levels in rat pluripotent stem cells; otherwise direct role unknown.
Mmu-miR-761	Predicted to interact with acetyltransferase pathways via targeting N(alpha)-acetyltransferase 15 (Naa15), as well as many other genes e.g. Dolpp1, Snx12 (vesicle-mediated transfer), Cpsf4 (mRNA processing) etc. Otherwise relatively unknown. GO predicts miRNA silencing role.
Mmu-miR-669g	Predicted to target Naa15, Abca1 (transmembrane transport), Ywah (transmembrane transport) and Top2a (HSC cell differentiation).
Mmu-miR-291a-3p	Predicted to target Mgat5 (glycoprotein oligo synthesis), inhibits cellular senescence via TGF-beta.
Mmu-miR-1942	Unknown.
Mmu-miR-338-5p	The 3p variant suppresses cell proliferation and induces apoptosis in non-small-cell lung cancer; inhibits hepatocarcinoma cells; represses oligodendrocyte differentiation, involved in osteoblast differentiation via Runx2.
Mmu-miR-1946a	Modulates TGFbeta1 expression.
Mmu-miR-34b-5p	Notch/MAPK signalling, HSC lineage, fatty acid biosynthesis, lysine degradation, protein export.

Expanding the miRNA view past those flagged as significantly differentially regulated when compared to the control, an analysis was performed to determine which miRNA correlated to dose.

Table 3.02. MiRNAs correlating with the dose. Dose correlation analysis was performed with the BRB array tools. Correlations were considered at the nominal 0.001 level of the univariate test. Clustering performed by BRBArrayTools. Reproduced and modified from Csordas & Rutten, *et al.,* 2023, International Journal of Molecular Science.

Correlation coefficient	**Parametric p-value**	**miRNA name**
0.953	<1e-07	mmu-miR-323-5p
0.888	9.17e-05	mmu-miR-1933-5p
0.888	9.17e-05	mmu-miR-1961
0.888	9.17e-05	mmu-miR-338-5p
0.888	9.17e-05	mmu-miR-504
0.884	0.0001922	mcmv-miR-m107-1-5p
0.875	0.0003089	mmu-miR-290-5p
0.874	0.0003089	mmu-miR-708
0.857	0.0005971	mmu-miR-181c
-0.857	0.0005971	mmu-miR-2146
0.859	0.0005971	mmu-miR-467h+mmu-miR-669d+mmu-miR-669l
0.857	0.0005971	mmu-miR-669j
-0.843	0.0009695	mmu-miR-93

Of these, four **statistically significant miRNA** were conserved in both 0.1Gy and 3Gy, overlapping both data sets: mmu-miR-761, mmu-miR-129-5p, mmu-miR-669g, and mmu-miR-34b-5p.

Table 3.03: Overlapping miRNA across 0.1Gy and 3Gy-irradiated CBA mice 24 hours post radiation exposure. A dose effect appears to be present- an increased dose (0.1Gy to 3Gy) results in a non-linear increase in effect.

miRNA	Fold change at 0.1Gy	Fold change at 3Gy
mmu-miR-761	4.67	8.75
mmu-miR-129-5p	4.75	6.60
mmu-miR-669g	3.67	6.75
mmu-miR-34b-5p	4.50	11.33

As shown in table 3.01, the four conserved miRNA are predicted to play the following biological roles: suspected tumour suppression and osteogenic differentiation, acetyl metabolism, transmembrane transport, HSC cell differentiation, Notch & MAPK signalling, fatty acid biosynthesis, lysine degradation and protein export. While several other functions apply to these miRNA, these are the pathways active within the BM; pathways active in other tissues e.g. brain tissue, have been excluded. This combination of pathways suggests that immediately post-radiation, and in a seemingly dose-dependent matter, major signalling networks (Notch and MAPK) are affected, important metabolic functions are compromised (lysine degradation, acetyl synthesis, and fatty acid biosynthesis), cell differentiation (HSC and osteogenic) is impacted, and transmembrane transport especially regarding vesicles is somehow affected as well.

At 0.1Gy, all miRNA that were differentially regulated (miR-761, miR-129-5p, miR-669g and miR-34b-5p) were upregulated. At 3Gy, as shown in table 3, downregulated miRNA were also present, and actually constituted the bulk of involved pathways. As can be seen, many different pathways are predicted to be targeted by the dysregulated miRNA at 3Gy; of note

are several major regulatory pathways such as MAPK, Wnt, FoxO and Hippo, but also metabolic pathways such as lysine degradation, fatty acid biosynthesis, glutamine metabolism, among others. Combined with other pathways such as cell cycle dysfunction and actin cytoskeleton regulation, and the more explicitly labelled ‘pathways in cancer’, a collective reference to known pro-oncogenic pathways, this depicts the distinct possibility that miRNA in BM-derived EVs 24 hours post exposure act upon the BM tissue using similar pathways as found later on in cancer development, dysregulating metabolism, regulatory pathways, and cytoskeletal structure, with the same survival pathways being used to regenerate bone marrow later on used by cancers for maintenance and proliferation. It should however be noted that we lack direct evidence for a dose of 0.1Gy being sufficient to induce AML in WT-CBA, and without direct correlation of response at this timepoint and future AML induction this must be regarded with due consideration. It is indeed more likely that we are seeing a basic radiation wound response signal, with the extent of this response being dose-dependent, and that this should be considered normal tissue response.

The four conserved miRNA between both doses target a variety of pathways. It is important to note here the statistical methods and algorithms used to analyse the pathways the miRNAs are predicted to act upon. DIANATools miRPath benefits from four different algorithms; the simplest, and most often used, is genes union, a method which creates a UNION_SET from the input miRNA and from this generates a list of genes targeted by at least one miRNA in the UNION_SET. By contrast, genes intersection creates an INTERSECTION_SET which generates a list of pathways targeted by a set number of miRNA within the INTERSECTION_SET; at default, this specifies all of the miRNA, and at a value of 1, it works identically to genes union. Using this latter algorithm and setting the threshold value at 2, Sox2 is found to be targeted by both mmu-miR-34-5p and mmu-miR-129-5p, and is involved in Hippo signalling and stem cell pluripotency regulation.

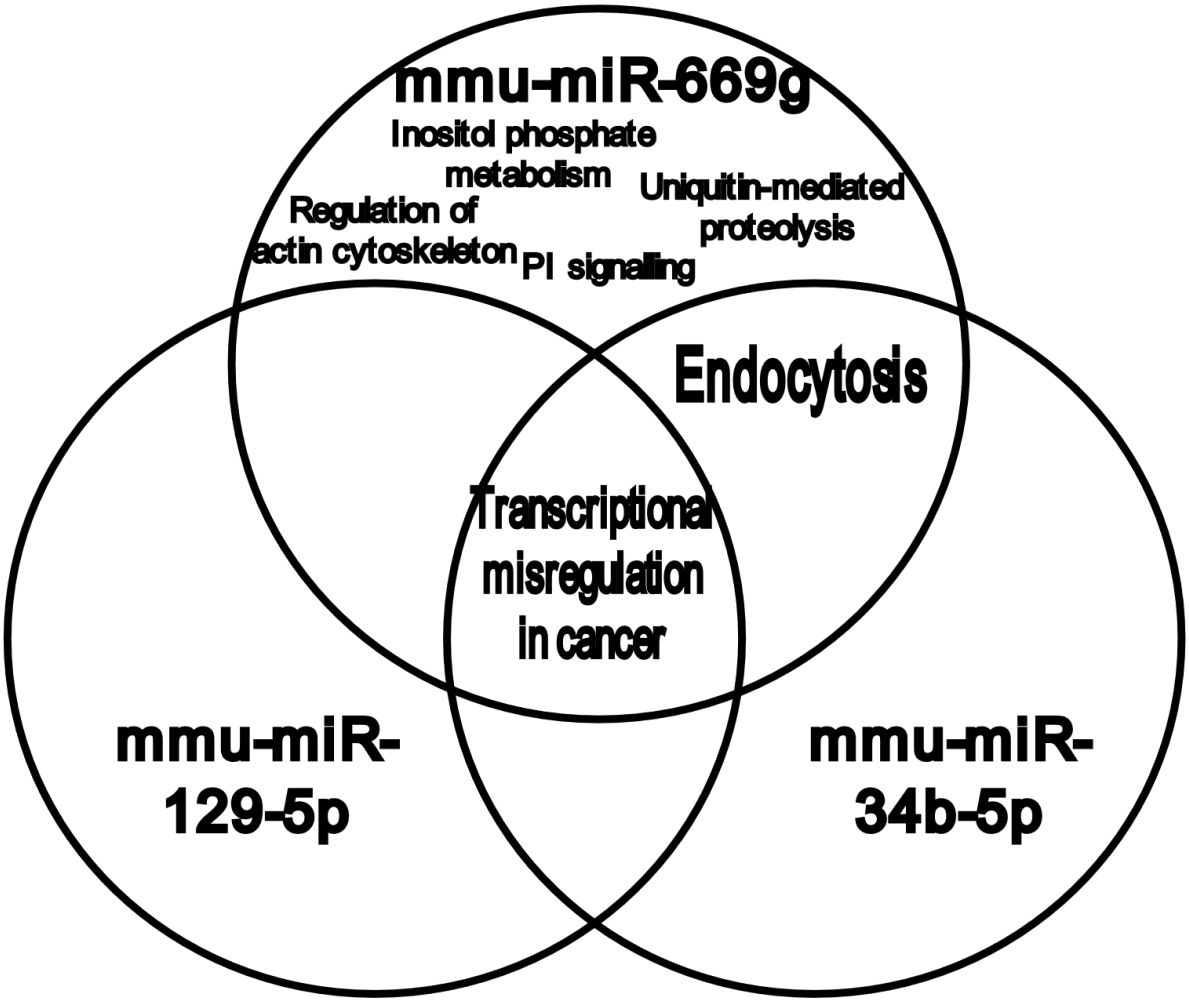


Figure 3.02: Venn diagram showing the involved pathways and intersections between the four conserved miRNAs at 0.1 and 3Gy. As seen, miR-669g is involved with all the pathways, with an overlap in endocytosis and transcriptional misregulation in cancer. This set was produced using miRPath v.3, and using the gene union clustering algorithm.

Table 3.04: Targeted pathways as predicted by KEGG in sham vs 3Gy WT CBA mice, 48 hours post radiation exposure.

Upregulated miRNA pathways (3Gy)	Downregulated miRNA pathways (3Gy)
Endocytosis	Adherens junction
Cell cycle	Leukocyte transendothelial migration
MAPK signalling	Regulation of actin cytoskeleton
Ubiquitin-mediated proteolysis	Fatty acid biosynthesis
Regulation of actin cytoskeleton	Proteoglycans in cancer
Phosphatidylinositol signalling system	Lysine degradation
D-glutamine and D-glutamate metabolism	N-Glycan biosynthesis
Inositol phosphate metabolism	Protein processing in ER
T cell receptor signalling pathway	Hippo signalling pathway
	Pathways in cancer
	mTOR signalling pathway
	Acute myeloid leukaemia
	Wnt signalling pathway
	Transcriptional misregulation in cancer
	FoxO signalling pathway

It is difficult to predict the precise impact that a miRNA might have on its associated pathway without *in vivo* or *in vitro* experimental data. A miRNA might silence a protein that has an inhibitory effect on a pathway, thus promoting the pathway, or it might instead silence an enzyme or receptor, thus inhibiting the pathway. As such, table 3.04 has “upregulated

miRNA" and "downregulated miRNA" to emphasize that it is the miRNA, and not the pathways themselves, that are differentially regulated in this fashion.

Protein-miRNA interactions were also explored as part of the LEUTRACK project; however, as this was performed by a collaborating group and not as a direct part of this project, the results will only be briefly summarized here for added contextualization and understanding of the potential role EV-shuttled miRNA may have in post radiation injury. All data is credited to our collaborators at the Metabolomics and Proteomics Core at the Helmholtz Zentrum München, and a full set of data can be found in Csordas & Rutten *et al.,* 2023, our manuscript on the results of the LEUTRACK project. The protein cargo of EVs was first analysed independently, using mass spectrometry, and then the KEGG-predicted pathways cross-referenced and associated with miRNA where overlap occurs.

Table 3.05. Common pathways between differentially expressed miRNAs from bone marrow-derived extracellular vesicles from mice irradiated with 3Gy and deregulated proteins in bone marrow cells treated with bone marrow-derived extracellular vesicles of mice irradiated with 3Gy. Reproduced from Csordas & Rutten *et al.,* 2023.

Common pathways between 3Gy EV miRNAs and BM+3Gy EV proteins		
Pathway Name	**KEGG pathway class**	**KEGG pathway subclass**
Lysine degradation	1. Metabolism	1.5 Amino acid metabolism
Protein processing in endoplasmic reticulum	2. Genetic information processing	2.3 Folding, sorting and degradation
Focal adhesion	4. Cellular Processes	4.3 Cellular community - eukaryotes
Adherens junction	4. Cellular Processes	4.3 Cellular community - eukaryotes
Cell cycle	4. Cellular Processes- Cell growth and death	4.2 Cell growth and death
Progesterone-mediated oocyte maturation	5. Organismal Systems	5.2 Endocrine system
Proteoglycans in cancer	6.Diseases-cancer	6.1 Cancer: overview
Prostate cancer	6.Diseases-cancer	6.2 Cancer: specific types
Colorectal cancer	6.Diseases-cancer	6.2 Cancer: specific types
Glioma	6.Diseases-cancer	6.2 Cancer: specific types
Chronic myeloid leukemia	6.Diseases-cancer	6.2 Cancer: specific types
Pathways in cancer	6.Diseases-cancer	6.1 Cancer: overview
Pancreatic cancer	6.Diseases-cancer	6.2 Cancer: specific types
Acute myeloid leukemia	6.Diseases-cancer	6.2 Cancer: specific types
Non-small cell lung cancer	6.Diseases-cancer	6.2 Cancer: specific types
Transcriptional misregulation in cancer	6.Diseases-cancer	6.1 Cancer: overview
Hepatitis B	6.Diseases-Infectious	6.3 Infectious disease: viral

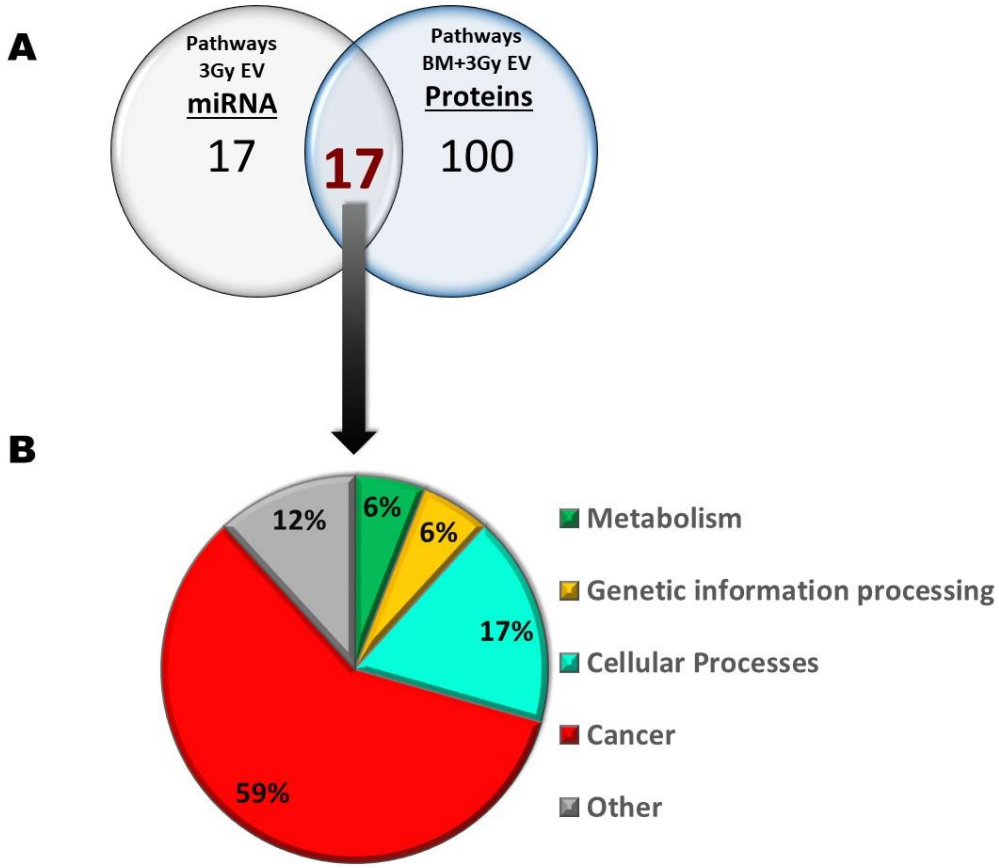


Figure 3.03. Common pathways between differentially expressed miRNAs from bone marrow-derived extracellular vesicles from mice irradiated with 3Gy and deregulated proteins in bone marrow cells treated with bone marrow-derived extracellular vesicles of mice irradiated with 3Gy. (A) Number of pathways; (B) Distribution of KEGG pathway classes. Reproduced from Csordas & Rutten *et al.,* 2023.

As can be seen, there is significant overlap between protein and miRNA-affected pathways at 3Gy; while proteins affect 100 different pathways, and miRNA affect only 17, all 17 of these are within the set of pathways affected by proteins. The majority of these pathways are explicitly associated with cancer, including two different types of leukaemia, chronic myeloid and acute myeloid. The rest can be grouped under metabolic and cellular processes and genetic information processing; altogether these are all heavily involved in cell behaviour regulation and homeostatic maintenance.

3.02 Late effects in transgenic mch/GFP CBA mice; the miRNA landscape in IR-induced AML

As described in sections 2.04 through to 2.08, CBA mCh/GFP mice were X-ray irradiated at 3Gy, on site at UKHSA Harwell, at a dose rate of 0.5Gy/min and subsequently monitored on a monthly basis 6 months post exposure up until 50% clonal expansion in the myeloid compartment or 12 months post exposure had been reached, upon which the mouse was culled. The 50% clonal expansion was chosen because of ethical concerns, with the project license stipulating that mice should be terminated before symptoms of AML became terminal. Through experience at the lab, we determined that mice at 50% would be ~24 hours from exhibiting severe systems and bone marrow collapse, in most cases. Mice were separated into four different categories: sham, i.e. 0Gy, as a control. No expansion, covering the cohort of mice that had been TBI at 3Gy but exhibited no clonal expansion by the 12-month end point. Low expansion, which was mice from between 5% to 30% clonal expansion. And finally high expansion, which was mice at any level above 30%. The aim was to derive a population of preleukaemic mice; in the case of mice that had an over 50% clonal expansion level, the argument could be made that these had developed into full blown leukaemia. The bone marrow of all mice was harvested and the EVs isolated, miRNA extracted, and then analysed using the same nCounter panel as in section 3.01.

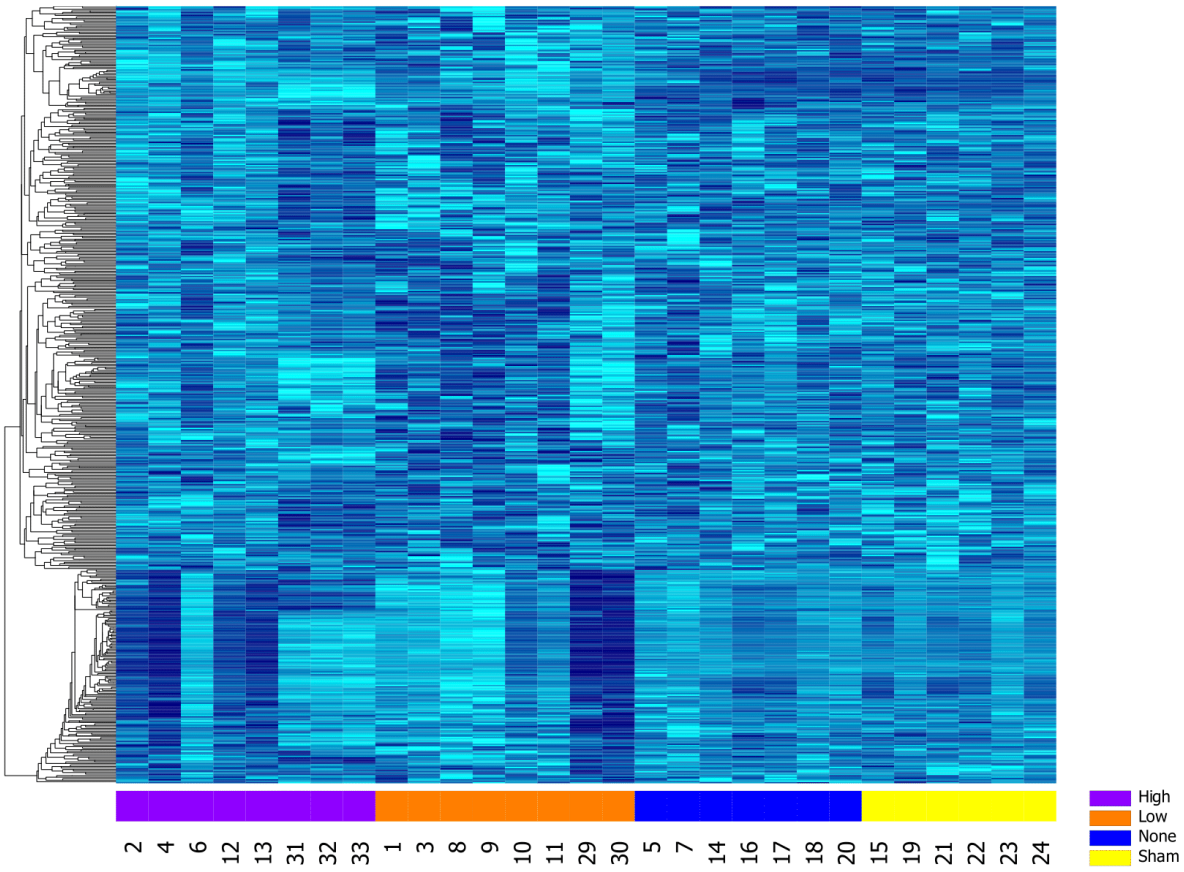


Figure 3.04: Heatmap showing the miRNA expression patterns in CBA mCh/GFP mice TBI at 3Gy. Numbers denote an individual mouse, i.e. 24 mice are represented in this table. Heat map and clustering created with BRBArraytools.

As can be seen in the heat map, a high degree of variability exists in mice with clonal expansion, with patterns of over and underexpression being variable between individual mice. However, in mice with no expansion, or mice that were never irradiated at all, the expression profiles are similar to each other. On the other hand, mice with clonal expansion, in particular high levels of expansion, demonstrate a pattern of high expression in the lower quadrant when compared to shams, with some samples, especially in the low expansion category, showing a pattern of downregulation versus the shams.

Using the DIANATOOLS miRExtra 2.0 tool and LIMMA statistical analysis, the following sets were compared: sham vs no expansion, sham vs low expansion, and sham vs high expansion. Predicted pathways were also provided using DIANATOOLS miRPath 3.0, as well as associated confidence levels. Once again, genes were first analysed using the

Genes Union setting, followed by Genes Intersection, with the parameters being modulated until a set of pathways targeted by multiple miRNA was identified, as well as which genes were targeted as a result.

At sham vs low expansion, the following miRNA were identified. However, it should be noted that the false discovery rate (FDR) of these is high, above the widely accepted cut-off point of 0.05; this indicates that these findings may not be “real” and rather false positives, indicating that it is quite likely that low expansion mice have a very similar miRNA profile to sham exposed mice in their BM EV cargo.

Table 3.06: List of differentially regulated miRNA in sham vs low clonal expansion (<30%) CBA mCh/GFP mice. It should be noted that due to the high FDR, these cannot be considered statistically sound or relevant. Unless otherwise noted, all predicted targets are sourced from miRPath3.0 and TargetScanVert using the mouse database. MirDB was used to screen for open access papers. Continues on pages 82-85.

Name	PValue	FDR	Predicted biological interactions
mmu-miR-1897-3p	1.8e-04	9.9e-02	Potential marker of ovarian toxicity (Furlong *et al.,* 2018, Journal of Applied Toxicology); predicted to target Erg (a proto-oncogene), Lonfr3, Zfp324, and Lifr (leukemia inhibitory factor receptor)
mmu-miR-2861	5.1e-04	1.2e-01	Targets HDAC5 and regulates osteoblast differentiation (Li *et al.,* 2009, Journal of Clinical Investigation)
mmu-miR-384-3p	6.7e-04	1.2e-01	Predicted to target Otub2 (ubiquitin aldehyde binding), Gp6mb (glycoprotein M6-B), which is associated with subleukaemic leukaemia and acute erythroid leukaemia,
mmu-miR-125b-1-3p	8.9e-04	1.2e-01	Predicted to target HIF1AN hypoxia inducible factor 1 subunit alpha, and Rab23, a member of the Ras oncogene family.
mmu-miR-470-5p	2.5e-03	2.2e-01	Predicted to target several predicted genes, IKAROS family zinc finger 1, Cacng4 (a calcium channel subunit), Gpr174 (G-protein receptor subunit) and ALDH1A1 (aldehyde dehydrogenase) among others.
mmu-miR-1928	2.8e-03	2.2e-01	Predicted to target Lifr and play a role in leukaemia progression (Kuchenbauer *et al.,* 2008, Genome Research).
mmu-miR-1941-5p	2.8e-03	2.2e-01	Believed to play a role in leukaemia progression (Kuchenbauer *et al.,* 2008, Genome Research).
mmu-miR-690	3.3e-03	2.2e-01	Found to be upregulated in murine radiation skin burn models (Islam *et al.,* 2015, PLoS One).
mmu-miR-582-5p	4.4e-03	2.4e-01	Predicted to target Hif1a, SNF2 histone linker PHD RING helicase, Tet3 (Tet methylcytosine dioxygenase 3); found upregulated in myocardium of Nrf2-KO mice (Quiles *et al.,* 2017, BMC Genomics).

mmu-miR-710	4.5e-03	2.4e-01	Predicted to target Tet3, known to be involved in horizontal transfer of exosomal miRNAs in apoptotic signal transduction (Guay *et al.,* 2015, Cell Communication and Signalling)
mmu-miR-125b-5p	4.9e-03	2.4e-01	Predicted to target HIF1AN; induces metastasis in breast cancer cells (Tang *et al.,* 2012, PLoS One), regulates p53 (Le *et al.,* 2011, PLoS Genetics), promotes endometrial carcinoma proliferation (Jiang *et al.,* 2011, BMC Cancer).
mmu-miR-877-5p	6.7e-03	3.0e-01	Predicted to target Ilrapl1 (interleukin 1 receptor accessory protein-like 1), Noxo1 (NADPH oxidase organizer 1), Gpx1 (glutathione peroxidase 1) associated with fatty acid biosynthesis.
mmu-miR-125a-3p	7.4e-03	3.1e-01	Involved in adipose tissue response to obesity (Diawara *et al.,* 2014, PLoS One), acute ischemic stroke (Liu *et al.,* 2017, International Journal of Molecular Medicine), angiogenesis (Che *et al.,* 2014, Aging Cell), neutrophil development (Qin *et al.,* 2017, PLoS Genetics).
mmu-miR-130b-3p	1.1e-02	4.0e-01	KEGG predicted involvement in lysine degradation, protein ER processing, FoxO, and multiple cancers (renal, prostate, non-small-cell lung).
mmu-miR-130a-3p	1.2e-02	4.0e-01	A member of the miR-130 family, with similar predicted biological roles and interactions.
mmu-miR-292a-3p	1.2e-02	4.0e-01	No KEGG predictions; part of a cluster involved in murine embryonic cell development (Yuan *et al.,* 2017, Cell & Bioscience).
mmu-miR-326-3p	1.2e-02	4.0e-01	No KEGG predictions; TargetScanMouse predictions include Zscan22, a zinc-finger domain.
mmu-miR-362-5p	1.4e-02	4.2e-01	KEGG-predicted involvement in lysine degradation, fatty acid biosynthesis, general transcriptional misregulation in cancers, and FoxO signalling.
mmu-miR-148b-3p	1.5e-02	4.2e-01	KEGG-predicted involvement in fatty acid metabolism, elongation and degradation; chemical carcinogenesis. Frequently downregulated in gastric cancer (Song *et al.,* 2011, Molecular Cancer).
mmu-miR-126a-5p	1.7e-02	4.2e-01	NO KEGG predictions; associated with 8;21 translocation leukaemias (both ALL and AML) (Ohyashiki *et al.,* 2010, BMC Research Notes).
mmu-miR-30a-5p	1.8e-02	4.2e-01	KEGG-predicted involvement in fatty acid biosynthesis & metabolism, N-glycan biosynthesis, proteoglycans in cancer, HIF-1 signalling, and Ras signalling. Acts as a tumour suppressor in multiple cancers (Liu *et al.,* 2017, Scientific Reports; Xie *et al.,* 2017, BMC Cancer).

mmu-miR-183-5p	1.8e-02	4.2e-01	KEGG-predicted involvement in ECM-receptor interactions, proteoglycans in cancer, and choline metabolism in cancer.
mmu-miR-301b-3p	1.8e-02	4.2e-01	KEGG-predicted involvement in lysine degradation, protein ER processing, N-glycan biosynthesis, TNF signalling, HIF-1 signalling, FoxO signalling, mTOR signalling, and TGF-beta signalling.
mmu-miR-216a-5p	2.0e-02	4.2e-01	No KEGG predictions; may be a biomarker of asthma (Paulene *et al.,* 2022, Respiratory Research), increased by TGF-beta in mouse models of diabetes (Shaffi *et al.,* 2018, International Journal of Molecular Sciences).
mmu-miR-382-5p	2.0e-02	4.2e-01	Targets Cdh1, involved in adherens junction, cell adhesion molecules and Hippo signalling (KEGG). Involved in multiple stress response pathways (GO) e.g. to ROS.
mmu-miR-369-3p	2.1e-02	4.2e-01	May be biomarkers of pulmonary tumourigenesis (Hao *et al.,* 2017, Biochemical and Biophysical Research Communications). Can reprogram colon cancer cells (Ogawa *et al.,* 2015, PLoS One).
mmu-miR-187-3p	2.2e-02	4.2e-01	Modulates oral carcinoma progression via BARX2 (Lin *et al.,* 2016, Oncotarget).
mmu-miR-3471	2.4e-02	4.2e-01	Predicted to target N(alpha)-acetyltransferase 11, a catalyctic subunit.
mmu-miR-466g	2.4e-02	4.2e-01	May be biomarkers of pulmonary tumourigenesis (Liang *et al.,* 2020, Journal of BUON). Predicted to target Map2k4, observed to be involved in several solid tumour cancers (Rajasegaran *et al.,* 2021, Biomedicines).
mmu-miR-2137	2.5e-02	4.2e-01	Unknown; predicted to target Pex26, involved in peroxisome biogenesis.
mmu-miR-876-3p	2.5e-02	4.2e-01	Unknown.
mmu-miR-384-5p	2.5e-02	4.2e-01	Predicted to target Stim2 (stromal interaction molecule 2), FoxG1 (Forkhead box G1), among others. Targets Gli2 and negatively regulates age-related osteogenic differentiation in BM MSCs (Li *et al.,* 2019, Stem Cells & Development).
mmu-miR-208a-3p	2.6e-02	4.2e-01	Predicted to be involved in thyroid hormone mediated signalling pathway, cell fate commitment (Gene Ontology), target Snrk (Serine/threonine-protein kinase), which is involved in sarcomas.

mmu-miR-1902	2.7e-02	4.2e-01	Involved in immune response to infections (lipoteichoic acid, sepsis, rabies virus) (Hsieh *et al.,* 2013, Journal of Biomedical Science; Wu *et al.,* 2013, PLoS One; Zhao *et al.,* 2012, Journal of Virology).
mmu-miR-320-3p	2.7e-02	4.2e-01	Suppresses colorectal cancer via Sox4, FoxM1, FoxQ1 (Vishnubalaji *et al.,* 2016, Oncotarget). Involved in embryonic development (Feng *et al.,* 2015, Scientific Reports). Present in cardiac-derived exosomes which reduce leukaemia mortality in rodents (Grigorian-Shamagian *et al.,* 2017, Oncotarget).
mmu-miR-138-5p	3.0e-02	4.4e-01	Involved in bladder cancer proliferation (Yang *et al.,* 2016, Molecular Cancer). Suppresses gallbladder carcinoma (Ma *et al.,* 2015, PLoS One). Regulated by p53 in humans but not in mice (Li *et al.,* 2016, Scientific Reports).
mmu-miR-875-3p	3.1e-02	4.5e-01	Predicted to target Kcnd2 (potassium-gated voltage channel), among others; otherwise unknown.
mmu-miR-3099-3p	3.2e-02	4.5e-01	Present in developing mouse brains, potential regulatory effects (Ling *et al.,* 2011, BMC Genomics).
mmu-miR-770-5p	3.4e-02	4.7e-01	Radition-inducible and sensitizes tumours to radiation (Lee *et al.,* 2017, Cell Death & Disease).
mmu-miR-376c-3p	3.5e-02	4.8e-01	Predicted to target Vldr (very low density lipoprotein receptor), Hif1a.
mmu-miR-195a-5p	3.7e-02	4.9e-01	Suppresses Hippo-YAP pathway in colorectal cancer (Sun *et al.,* 2017, Journal of Haematological Oncology). Circulates in murine breast cancer models (Waters *et al.,* 2012, PLoS One).
mmu-miR-802-5p	3.8e-02	4.9e-01	Inhibits fine particulate-induced carcinogenesis and metastasis (Li *et al.,* 2016, Oncotarget). Has anti-oncogenic effects in murine liver cancer (Tao *et al.,* 2015, Oncotarget).
mmu-miR-127-3p	4.0e-02	4.9e-01	Predominantly expressed in muscle tissue and regulates myogenic stem cell differentiation (Zhai *et al.,* 2017, Cell Death & Disease).
mmu-miR-483-5p	4.1e-02	4.9e-01	Regulated by O-linked N-acetylglucosamine transferase in liver cancer cells (Pepe *et al.,* 2017, Oncogenesis). Promotes adipogenesis via RhoA/ROCK1/ERK pathway (Chen *et al.,* 2015, Scientific Reports).
mmu-miR-714	4.1e-02	4.9e-01	Predicted to target Vamp2 (vesicle-associated membrane protein 2) and Map3k4.

mmu-miR-188-5p	4.4e-02	4.9e-01	Suppresses G1/S transition (Wu *et al.,* 2014, Cell Communication & Signalling).
mmu-miR-546	4.5e-02	4.9e-01	Predicted to target Lfrn4, most likely involved in postsynaptic density assembly.
mmu-miR-883a-5p	4.5e-02	4.9e-01	Predicted to target Sorbitol Dehydrogenase.
mmu-miR-324-3p	4.7e-02	4.9e-01	Suppresses HMGXB3 and WASF-2 in colorectal cancer (Sun *et al.,* 2017, Oncotarget).
mmu-miR-192-5p	4.7e-02	4.9e-01	Suppress lncRNA HOTTIP in hepatocellular carcinoma (Ge *et al.,* 2015, PLoS Genetics). Activated by p53 (Chen *et al.,* 2016, Scientific Reports).
mmu-miR-1193-3p	4.8e-02	4.9e-01	Unknown.
mmu-miR-709	4.9e-02	4.9e-01	No KEGG predictions; widely involved in multiple regulatory pathways throughout most body tissues, including injury and stress responses (Surendran *et al.,* 2016, Scientific Reports).
mmu-miR-615-3p	4.9e-02	4.9e-01	No KEGG predictions; regulates lipoapoptosis (Miyamoto *et al.,* 2014, PLoS One), involved in non-small cell lung cancer (Chen *et al.,* 2019, BMC Molecular Cancer).
mmu-miR-328-3p	4.9e-02	4.9e-01	KEGG-predicted involvement in unsaturated fatty acid biosynthesis, fatty acid metabolism, ECM-receptor interaction, among others.

While, as previously stated, the high FDR prevents these miRNAs from being statistically probable, it is nevertheless important to examine the roles of the suspected differentially regulated miRNAs, in order to get some modicum of insight into the organism's response to radiation. As can be seen in table 3.06, while very few miRNA are explicitly known to be associated with the development of rAML, several are linked with other cancers, especially solid cancers, and interact along similar pathways to those found in 24-hours post exposure WT-CBA mice, in particular targeting the Mapk family of genes as well as the Sox family of genes, and having heavy involvement in metabolic pathways.

The suspected pathways involved were also assessed in sham vs low clonal expansion, but as previously, it should be noted that this suffers from the high FDR problem, and as such is, at best, an indication of a potential trend rather than confirmation in any way of a definitive response or signature of either irradiation or cancer development in mice with low clonal expansion.

Table 3.07: KEGG-predicted targeted pathways in sham vs low clonal expansion mch/GFP CBA mice.

Upregulated miRNA pathways (Low clonal expansion)	Downregulated miRNA pathways (Low clonal expansion)
Fatty acid biosynthesis	N-Glycan biosynthesis
Fatty acid metabolism	Protein processing in ER
Proteoglycans in cancer	Proteoglycans in cancer
Protein processing in ER	Lysine degradation
FoxO signalling pathway	FoxO signalling pathway
Valine, leucine and isoleucine degradation	Central carbon metabolism in cancer
Endocytosis	Valine, leucine and isoleucine degradation
N-Glycan biosynthesis	ErbB signalling pathway
Fatty acid elongation	Hippo signalling pathway
Axon guidance	MAPK signalling pathway
FoxO signalling pathway	Adherens junction
Lysine degradation	TGF-beta signalling pathway
Fatty acid degradation	HIF-1 signalling pathway
p53 signalling pathway	AMPK signalling pathway
AMPK signalling pathway	mTOR signalling pathway
Ras signalling pathway	Acute myeloid leukemia
Rap1 signalling pathway	Pathways in cancer

High clonal expansion mice were also compared to sham, which resulted in a list of differentially regulated miRNA that satisfied both the p-value parameter and the FDR parameter, indicating that it is very likely these results are genuine, and the miRNA are indeed differentially regulated in mice with high clonal expansion vs mice that were sham irradiated.

Table 3.08: List of differentially regulated miRNA in sham vs high clonal expansion (>30%) CBA mCh/GFP mice. Unless otherwise noted, all predicted targets are sourced the KEGG database, the GO dataset, or from TargetScanVert using the mouse database. MiRBase and Pubmed were used to screen for relevant publications. Continues on pages 90 and 91.

Name	PValue	FDR	Predicted biological interactions
mmu-miR-540-3p	1.9e-06	1.0e-03	Predicted to target Hif1an, Tcl1b2 (involved in T cell leukaemia). Predicted to be involved in Hippo signalling (KEGG), involved in GO categories: myeloid leukocyte differentiation, regulation of clathrin-mediated endocytosis, among others.
mmu-miR-486a-5p	6.1e-06	1.6e-03	No KEGG or GO categories; involved in negative regulation of hepatocellular carcinoma (Fu *et al.,* 2017, Oncotarget), may be a diagnostic marker of cervical cancer (Li *et al.,* 2018, BMC Cancer), upregulated in metastatic prostate cancer (Watahiki *et al.,* 2011, PLoS One).
mmu-miR-710	5.3e-05	6.4e-03	No KEGG or GO categories. Predicted to target Tet3, known to be involved in horizontal transfer of exosomal miRNAs in apoptotic signal transduction (Guay *et al.,* 2015, Cell Communication and Signalling)
mmu-miR-139-5p	8.0e-05	6.4e-03	No KEGG or GO categories. Expresses tumour suppressor function in colorectal cancer via Notch1 (Zhang *et al.,* 2014, Molecular Cancer). Downregulates BCL2 thereby increasing radiosensitivity of colorectal cancer cells (Li *et al.,* 2016, Scientific Reports). Predicted to target Tet3 and TNF receptor 3.
mmu-miR-1983	9.5e-05	6.4e-03	No KEGG or GO categories. Biological significance unknown.
mmu-miR-128-3p	9.9e-05	6.4e-03	Involved in multiple KEGG pathways, including but not limited to fatty acid biosynthesis & metabolism, FoxO signalling, lysine degradation, protein processing in the ER, Wnt signalling, TGF-beta signalling, transcriptional misregulation in cancer. GO categories include intracellular, cell differentiation, cell death, and response to stress, among others. Inhibits lymphoid progenitors from developing into progenitor B cells (Yang *et al.,* 2016, Oncotarget).
mmu-miR-1897-3p	9.9e-05	6.4e-03	No KEGG or GO categories. Potential marker of ovarian toxicity (Furlong *et al.,* 2018, Journal of Applied Toxicology); predicted to target Erg (a proto-oncogene), Lonfr3, Zfp324, and Lifr (leukemia inhibitory factor receptor)
mmu-miR-423-5p	1.1e-04	6.4e-03	No KEGG or GO categories. Involved in HCN4 channel remodeling and sinus brachycardia (D'Souza *et al.,* 2017, Circulation Research). Found in white blood cells 48 hours post acute radiation injury (Li *et al.,* 2022, Dose Response).

mmu-miR-1224-5p	1.1e-04	6.4e-03	No KEGG or GO categories. Modulates osteogenesis via osteoblast/clast differentiation control by targeting ADCY2 (Hu *et al.,* 2022, Experimental & Molecular Medicine). Inhibits proliferation and invasion of ovarian cancer via SND1 (Wang *et al.,* 2020, Human Cell). Acts as a tumour suppressor for rectal cancer (Song *et al.,* 2020, IUBMB Life) as well as in several other cancers (Cui *et al.,* 2020, Pathology, Research & Practice; Jin *et al.,* 2020, OncoTargets & Therapy; Chen *et al.,* 2020, OncoTargets & Therapy).
mmu-miR-1902	1.2e-04	6.4e-03	No KEGG or GO categories. Biological function unknown.
mmu-miR-676-3p	1.5e-04	6.6e-03	Involved in colorectal cancer and pathways in cancer (KEGG); top 5 GO are intracellular, cell, establishment of Sertoli cell barrier, platelet alpha granule membrane, and regulation of establishment of protein localization to plasma membrane. Found in white blood cells 48 hours post acute radiation injury (Li *et al.,* 2022, Dose Response).
mmu-miR-370-3p	1.5e-04	6.6e-03	Involved in FoxO signalling (KEGG), top 5 GO are cell, secretory granule lumen, intracellular, poly(A) RNA binding, and focal adhesion assembly. Regulates adipogenesis via Mknk1 (Zhang *et al.,* 2021, Molecules).
mmu-miR-326-3p	2.3e-04	9.6e-03	No KEGG or GO categories. Predicted to target Zscan22, a zinc finger, predicted to be involved in DNA transcription.
mmu-miR-191-5p	3.1e-04	1.2e-02	Involved in multiple KEGG pathways, such as PI signalling, inositol phosphate metabolism, TGF-beta signalling, FoxO signalling, and lysine degradation. Top 5 GO categories are cell, intracellular, organelle, anatomical structure development, and cell differentiation. Involved in angiogenesis (Wu *et al.,* 2021, Neurology India) and B-cell development (Blume *et al.,* 2019, European Journal of Immunology).
mmu-miR-1949	3.3e-04	1.2e-02	No KEGG or GO categories. Potential inducer of bladder cancer in rats (Wang *et al.,* 2015, Molecular Medicine Reports).
mmu-miR-302c-3p	3.7e-04	1.2e-02	Involved in cell cycle and protein processing in the ER (KEGG); no GO category. Human equivalent (hsa-miR-302c) suppresses cervical and hepatocellular carcinoma (Ding *et al.,* 2021, Molecular Medicine Reports; Yang *et al.,* 2018, Journal of Cancer).
mmu-miR-1198-5p	4.0e-04	1.3e-02	KEGG pathways predict involvement with cell cycle and vasopressin-regulated water reabsorption; top 5 GO terms are positive regulation of chromosome segregation, nitric-oxid synthase regulator activity, regulation of mitotic metaphase/anaphase transition, cytomplasmic dynein complex, and negative regulation of phosphorylation.

mmu-miR-132-3p	4.3e-04	1.3e-02	Involved in multiple KEGG pathways, such as FoxO signalling, T cell receptor signalling, chronic myeloid leukaemia, pathways in cancer, lysine degradation, protein processing in the ER, and proteoglycans in cancer. Targets SOX4 in human breast cancer (Hanieh, 2015, Molecular Cancer). Involved in carcinogenesis of solid tumours (Rafat *et al.,* 2021, Human Cell).
mmu-miR-2861	5.5e-04	1.6e-02	Involved in viral carcinogenesis (KEGG); various muscoskeletal development pathways (GO). Regulates programmed necrosis in cardiomyocytes (Wang *et al.,* 2016, Free Radical Biology & Medicine).
mmu-miR-483-5p	6.3e-04	1.7e-02	Targets Gna13, involved in platelet activation (KEGG), and Skil, involved in positive regulation of intrinsic apoptotic signalling pathway in response to DNA damage (GO).
mmu-miR-345-5p	7.7e-04	2.0e-02	Involved in several different metabolic and biosynthesis pathways, e.g. Tryptophan, glycosaminoglycan, glyoxylate, and O-glycans (KEGG); predicted to be involved in histone deacetylation (GO).
mmu-miR-154-5p	8.2e-04	2.0e-02	Involved in lysine degradation and Hippo signalling (KEGG). Regulates osteogenic differentiation of adipose-derived MSCs via Wnt11 (Li *et al.,* 2015, Bone).
mmu-miR-497a-5p	1.4e-03	3.3e-02	No KEGG or GO categories. Suppresses angiogenesis and metastasis of hepatocellular carcinoma (Yan *et al.,* 2015, Oncotarget).
mmu-miR-181c-5p	1.6e-03	3.7e-02	Involved in multiple KEGG pathways, such as MAPK signalling, proteoglycans in cancer, FoxO signalling, and protein processing in the ER. Involved in multiple intracellular organization processes (GO). Related miR, miR-181a, targets Ras/MAPK in AML (Huang *et al.,* 2016, Oncotarget).
mmu-miR-382-5p	1.9e-03	4.1e-02	Targets Cdh1, involved in adherens junction, cell adhesion molecules and Hippo signalling (KEGG). Involved in multiple stress response pathways (GO) e.g. to ROS.
mmu-miR-138-5p	2.4e-03	5.0e-02	Involved in fatty acid biosynthesis & metabolism, ECM-receptor interaction, and glycan degradation (KEGG). Involved in cell differentiation and cytoskeletal development and organization (GO). Involved in multiple solid cancers (Yang *et al.,* 2016, Molecular Cancer; Ma *et al.,* 2015, PLoS One; Chen *et al.,* 2017, Journal of Experimental & Clinical Cancer Research).

The majority of significant miRNAs were upregulated vs sham at high levels of clonal expansion (>30%) in CBA mCh/GFP mice. Several pathways feature in both high clonal expansion mice and 24-hour post TBI mice, such as lysine degradation, fatty acid biosynthesis, MAPK signalling, FoxO signalling, among others, although while in TBI mice the miRNA associated with these pathways were downregulated, the miRNA in high clonal expansion mice were upregulated.

Table 3.09: KEGG-predicted pathways in sham vs high clonal expansion CBA mch/GFP mice. Table continued on page 94.

Upregulated miRNA pathways (High clonal expansion)	Downregulated miRNA pathways (High clonal expansion)
Fatty acid biosynthesis	Long-term depression
FoxO signalling pathway	FoxO signalling pathway
Protein processing in endoplasmic reticulum	Acute myeloid leukaemia
Hippo signalling pathway	
Proteoglycans in cancer	
Neurotrophin signalling pathway	
Thyroid hormone signalling pathway	
TGF-beta signalling pathway	
Adherens junction	
Axon guidance	
Gap junction	
GnRH signalling pathway	
ErbB signalling pathway	
PI3K-Akt signalling pathway	
AMPK signalling pathway	
Transcriptional misregulation in cancer	
Focal adhesion	
Osteoclast differentiation	
Chronic myeloid leukemia	
Ras signalling pathway	

TNF signalling pathway	
Ubiquitin mediated proteolysis	
Insulin signalling pathway	
MAPK signalling pathway	
ECM-receptor interaction	
Pathways in cancer	
mTOR signalling pathway	
Endocytosis	
T cell receptor signalling pathway	
Estrogen signalling pathway	
Wnt signalling pathway	
Cell cycle	
Prostate cancer	
Thyroid cancer	
Fatty acid metabolism	
Regulation of actin cytoskeleton	
Citrate cycle (TCA cycle)	
Lysine degradation	
RNA degradation	
Colorectal cancer	
Long-term potentiation	
Acute myeloid leukaemia	
HIF-1 signalling pathway	

AML is explicitly involved and targeted by the following miRNAs: miR-181c, miR-326, miR-128, miR-497a, miR-1224, miR-382, miR-138, miR-154, miR-486a, miR-710, miR-302c, miR-132, and miR-423. Of these, Pik3r1, Tcf712, Runx1t1, Braf and Sos1 are all targeted by 3 or more miRNAs, with Sos2, Pik3r3, Map2k1, Nras and Runx1 being targeted by 2 or more miRNAs. Furthermore, 6 of these miRNAs are also all involved in regulation of lysine degradation, a pathway which has appeared multiple times in different data sets.

Several other cancers, including chronic myeloid leukaemia, are involved. Moreover, several key metabolic pathways are predicted to be impacted, including but not limited to the citrate cycle, lysine degradation, fatty acid metabolism and biosynthesis, and protein processing in the endoplasmic reticulum. This indicates a consistent pattern of dysregulation in mice with high clonal expansion, precursor to a fully developed AML disease state. It is important to note that while certain pathways are found to be in common between both 24-hour TBI and 12 month TBI high clonal expansion CBA mch/GFP mice, no miRNA are carried over between the two sets.

Table 3.10: Gene targets of miRNA associated with AML development in the KEGG database.

miRNA	Genes targeted
miR-181c	Pik3r3 Tcf712 Rps6kb1 Braf Map2k1 Runx1
miR-326	Cebpa
miR-128	Pik3r1 Sos1 Grb2 Runx1 Runx1t1
miR-497	Sos2 Braf Pik3r1 Nras Map2k1
miR-1224	Runx1t1 Braf Sos1
miR-382	Tcf712 Braf
miR-138	Tcf7 Rela Braf Eif4ebp1
miR-154	Sos2
miR-486a	Pik3r1 Pim1
miR-710	Pik3r3 Tcf712 Nras
miR-302c	Sos1
miR-132	Runx1t1 Sos1
miR-423	Pml

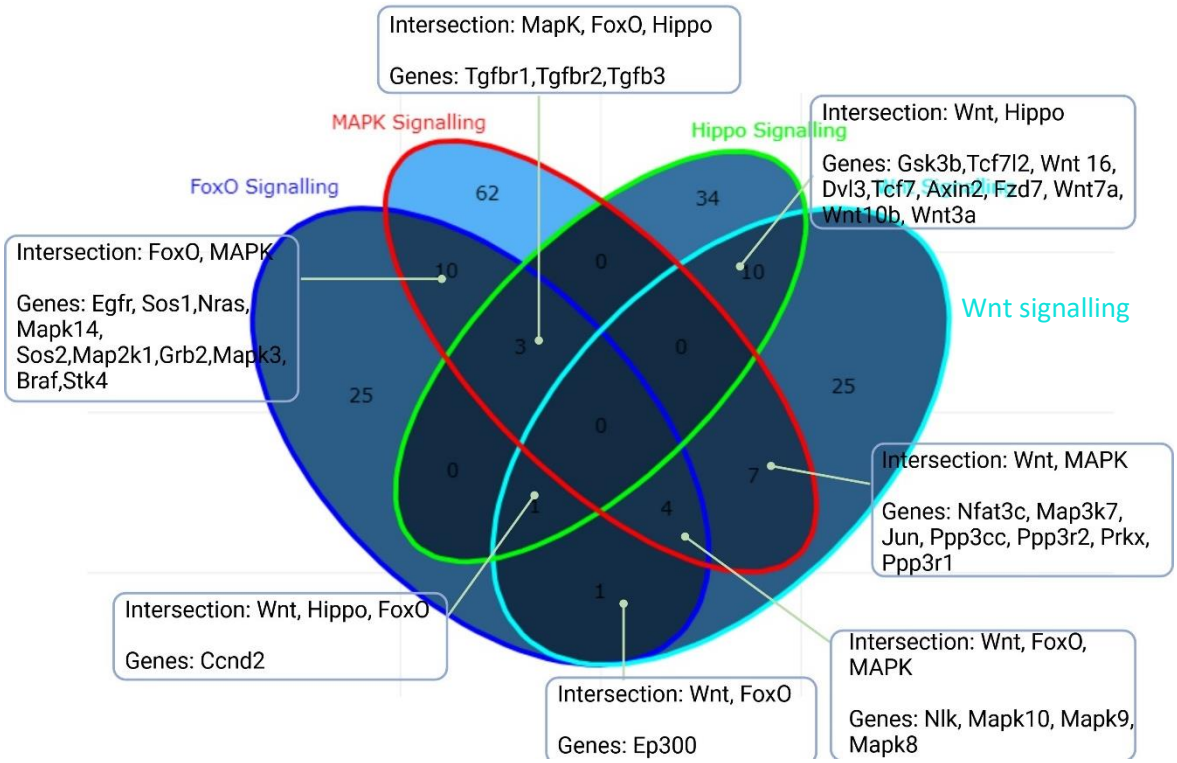


Figure 3.05: Gene target overlaps of the Wnt, Hippo, MAPK and FoxO signalling pathways in high clonal expansion mCh/GFP mice. Numbers in the Venn diagram are separate; the outer number describes genes not in the intersection, and the number in the intersection describes overlapping genes, for which the pathways are given.

As seen in figure 3.05, several genes overlapped between four signalling pathways represented as miRNA targets. Of these, no one gene target was present in all 4 pathways. Three intersections representing the junction of three signalling pathways were identified. MAPK, FoxO and Hippo had 3 genes in common: Tgfbr1, Tgbr2, and Tgfb3. Wnt, FoxO and MAPK had Nlk, Mapk10, Mapk9, and Mapk8 in common. Finally, the only conserved gene target of the significantly dysregulated miRNA in common between Wnt, Hippo and FoxO was Ccnd2. The largest single overlap between two signalling pathways was between FoxO and MAPK, with 10 genes in common that were targeted by miRNAs. Therefore, there is no single gene targeted at the junction of all signalling networks, but there are at junctions of 3 and less pathways.

The genes found at the intersection of 3 signalling pathways were analysed for all miRNA targeting them to determine if there was an overlap with a set of miRNA targeting all of these genes, or if such an overlap did not exist and miRNA were independent in each case.

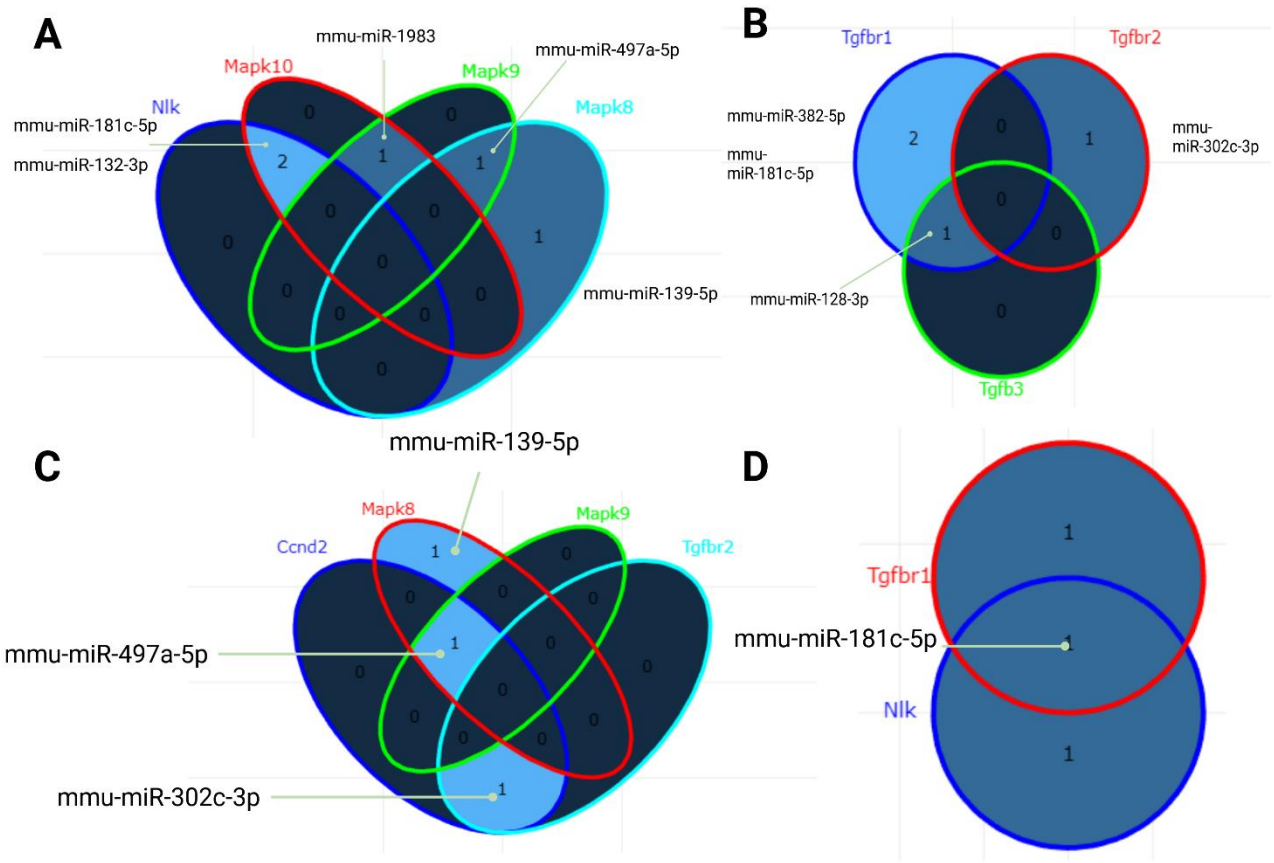


Figure 3.06: Overlaps in interacting miRNA between common genes. A: Genes found in the Wnt, FoxO, and MAPK intersection. B: Genes found in the MAPK, FoxO and Hippo junction. C: Overlap in miRNA between Mapk8, Mapk9, Ccnd2, and Tgfbr2. Ccnd2 was found at the Wnt, FoxO and Hippo intersection (see figure 3.05). D: Overlap in miRNA between Tgfbr1 and Nlk. Numbers in the Venn diagram are separate; the outer number describes genes not in the intersection, and the number in the intersection describes overlapping genes, for which the pathways are given.

As shown in figure 3.06, there was no one miRNA at the nexus of all gene targets, but genes did have miRNA in common. Nlk and Mapk10 had the most miRNA regulators in common at 2. When merging the intersections to analyse for miRNA overlap between discrete genes, it was discovered that multiple overlaps exist. Mmu-miR-302c-3p was found to regulate both Tgfbr2 and Ccnd2. By targeting both, this miRNA is thus directly involved in all 4 signalling networks via different gene targets. Another example of this is mmu-miR-497a-5p, found to target 3 genes: Ccnd2, Mapk8, and Mapk9. This miRNA is thus involved in all four signalling pathways: with MAPK, Wnt and FoxO via interaction with Mapk8 and Mapk9, and with Wnt, FoxO and Hippo via Ccnd2. Mmu-miR-181c-5p targets both Tgfbr1 and Nlk, thereby also targeting all 4 signalling pathways, with targeting of Wnt, FoxO and

MAPK via Nlk, and MAPK, FoxO and Hippo via Tgfbr1. These three miRNAs, mmu-miR-497a-5p, mmu-miR-302c-3p, and mmu-miR-181c-5p, can therefore be found as a set that targets Wnt, Hippo, FoxO, and MAPK signalling pathways but not always via the same gene target. It is likely other such miRNA exist, but with the parameters of this data analysis, analysing the set of genes directly represented in an intersection of at least 3 signalling pathways, these are the miRNA that are apparent. Therefore, these three miRNAs are hypothesized to be at the centre of signalling dysregulation in later stages of IR-induced AML.

While miR-497a, miR-302c and miR-181c are promising candidates for major control miRNA in later stage AML development, the involvement of the Son of Sevenless (Sos) family must be mentioned. While they do not find themselves at the intersection of more than two signalling pathways, they are present in FoxO/MAPK intersection and the Proteoglycans in Cancer pathway, meaning that miRNA targeting the Sos are also promising biomarkers and potential therapeutic targets. However, given their less central role (in terms of being found in all pathways at once), this research hypothesizes they should be used in conjunction with the three miRNAs listed previously.

miR-497a, miR-302c and miR-181c were all **upregulated** in high clonal expansion mCh/GFP CBA mice. Follow-up research to correlate level of upregulation with AML progression could confirm and establish the use of these three miRNAs as prognostic biomarkers and therapeutic targets for clinical intervention. These three miRNAs were not seen to be statistically significantly differentially regulated in low levels of clonal expansion ($p=0.41$, 0.20 and 0.10 respectively), however all showed slight upregulation vs control. It is possible that future work expanding this study and clarifying the statistics of low-level clonal expansion mCh/GFP mice could establish that at least 302c and 181c are upregulated at low levels in early AML development, but this is conjecture and must be considered with due scepticism.

BM cells were also retained and the miRNA within extracted and analysed using nCounter, to discern whether or not EVs were a reflection, or copy, of the cellular miRNA content, or if they differed. High clonal expansion EV samples were matched with BM cells, i.e. both coming from the same mouse, and then compared. As can be seen in figure 3.07, there is a clear difference in miRNA content between BM EVs and BM cells. Using miRextra, the following miRNA and pathways were found to be differentially expressed in EVs vs BM cells (see table 3.11).

It must be noted that EVs 1 represents a significant outlier vs EVs 2 and EVs 3, and tracing this sample to the mouse of origin did not reveal any evident reason as to why it is an outlier. Due to the limited size of the dataset, the data was included, but with further repeats and concrete demonstration it is the outlier, it may be excluded from this data set.

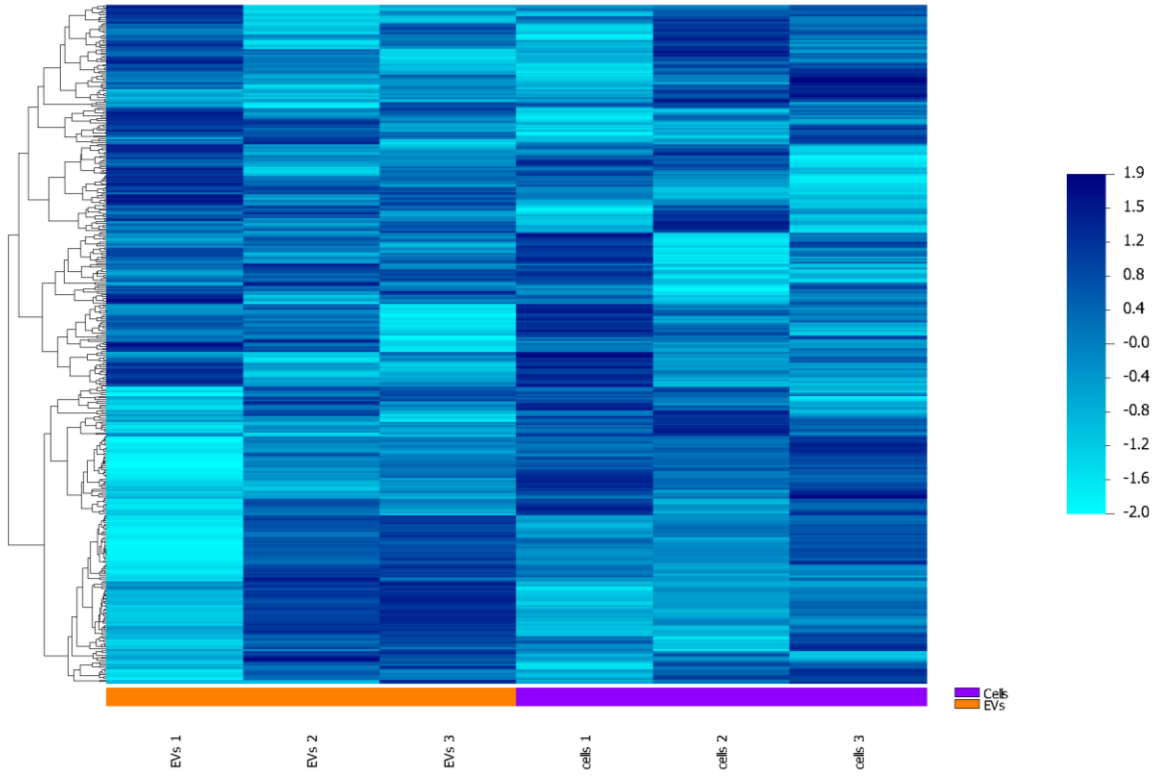


Figure 3.07: EV vs cellular miRNA. This heatmap shows miRNA expression in EV vs cellular miRNA. As can be seen, the two populations seem to be relatively distinct, particularly in the lower half of the heat map.

Table 3.11: KEGG-predicted pathways targeted by statistically relevant miRNA in EVs vs BM cells in irradiated CBA mCh/GFP with >30% clonal expansion in the myeloid compartment.

Pathways with upregulated miRNA	Pathways with downregulated miRNA
Fatty acid biosynthesis	Wnt signalling
Fatty acid metabolism	Hippo signalling pathway
Metabolic pathways	Proteoglycans in cancer
Lysine biosynthesis	Lysine degradation
	Protein processing in ER
	Pathways in cancer
	Transcriptional misregulation in cancer
	MAPK signalling pathway
	mTOR signalling pathway
	Various types of cancer (Prostate, lung, pancreatic, chronic myeloid leukaemia, etc)

Five miRNA were identified as satisfying both the p-value and FDR parameters, seen in table 3.12:

Table 3.12: Statistically relevant miRNA enriched in EVs and their predicted biological function.

Name	PValue	FDR	Predicted biological interactions
mmu-miR-34c-5p	1.8e-08	9.9e-06	Involved in fatty acid biosynthesis/metabolism, steroid biosynthesis, central carbon metabolism in cancer, and RNA degradation (KEGG).
mmu-miR-1931	3.7e-05	1.0e-02	No KEGG or GO categories.
mmu-miR-143-3p	1.2e-04	2.0e-02	Involved in steroid biosynthesis, fat digestion and absorption, the TCA cycle, and carbon metabolism (KEGG).
mmu-miR-145a-5p	3.9e-04	5.0e-02	No KEGG or GO categories.
Mmu-miR-199a-5p	4.2e-4	5.0e-02	Involved in renal cell carcinoma, central carbon metabolism in cancer, and thyroid hormone signalling, via Hif1a (KEGG).

The five miRNAs identified were miR-34c-5p, miR-1931, miR-143-3p, miR-145a-5p, and miR-199a-5p, all upregulated in preleukaemic EVs compared to bone marrow cells of origin. mmu-miR-34c-5p was massively upregulated in extracellular vesicles vs BM cells, with a fold change of 634. The miRNA identified were not found in the miRNA significantly differentially regulated when comparing non-leukaemic EVs to leukaemic EVs. This indicates that miRNAs are most likely specifically packaged into EVs for transport out of the cell, and that cargo sorting into EVs is not random, as was previously thought; however, in

the absence of a data set with non-leukaemic cells compared to non-leukaemic EVs, it is impossible to determine whether or not these miRNAs are specifically enriched in preleukaemic EVs, or if these EVs are upregulated in all EVs when compared to their baseline cells.

While it has been established that there is a conserved targeting of signalling pathways during clonal expansion, there is also a conserved targeting of metabolic pathways, namely lysine degradation, fatty acid biosynthesis, and fatty acid metabolism. This is an interesting set of pathways to study due to their potential for non-invasive clinical intervention. Targeting of miRNA that directly target and regulate major signalling pathways, e.g. miR-302c, must be carefully considered due to their potential to disrupt major signalling cascades and cause significant off-target effects. Levels of metabolites, on the other hand, are much more easily controlled via diet and supplementation, and can present a potential for prophylactic care to minimise a) risk of radiation-induced damage and b) risk of said damage leading to long-term stochastic effects. Coupled with targeting of signal-disrupting miRNAs in AML, they could form the core of a highly effective two-prong approach to combating AML development.

To further study this, the genes along the lysine degradation, fatty acid biosynthesis and fatty acid metabolism pathways were grouped and compared to look for significant overlaps, along with proteoglycans in cancer, to monitor which genes have KEGG-predicted oncogenic involvement. This was done to test if there was a singular miRNA, or a set thereof, constitutively targeting these metabolic pathways and thus serving as valuable biomarkers, akin to the signalling ‘core’ of miR-302c, miR-181c, and miR-497a.

As seen in figure 3.08, once again there is no single gene shared by all metabolic networks, nor is there any gene target overlap with the proteoglycans in cancer pathway, indicating discrete gene targets. However, much as with signalling networks, extrapolating from these gene targets and analysing for their miRNA overlap reveals a single miRNA present at the

junction of lysine degradation, fatty acid biosynthesis and fatty acid metabolism: mmu-miR-128-3p.

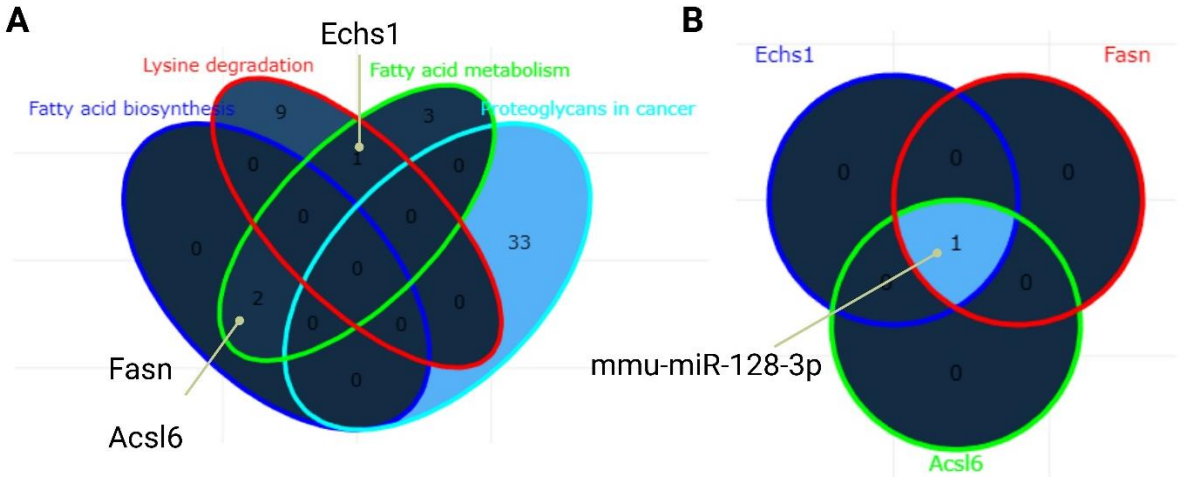


Figure 3.08: Genetic and miRNA overlap between metabolic pathways. A: Genetic target overlap between lysine degradation, fatty acid biosynthesis, fatty acid metabolism and proteoglycans in cancer. B: miRNA overlap between Echs1, Fasn and Acsl6. Numbers in the Venn diagram are separate; the outer number describes genes not in the intersection, and the number in the intersection describes overlapping genes, for which the pathways are given.

miR-128-3p interacts with lysine degradation via regulating most of the genes active in that pathway, including but not limited to Kmt2c, Nsd1, Aldh3a2, Setd7 and Echs1. Echs1 is a common pathway with fatty acid metabolism. No common gene targets exist between lysine degradation and fatty acid biosynthesis, while Fasn and Acsl6 are common between the latter pathway and fatty acid metabolism. Both genes are also regulated by miR-128. As such, via multiple gene targets, miR-128-3p regulates all three metabolic networks. It should also be noted that miR-128 also regulates Tgfbr1 and Tgfb3, genes found in FoxO, MAPK and Hippo, demonstrating that miR-128 has multi-spectrum involvement at both the signalling level and the metabolism control level.

Given this, this renders the metabolic study of miR-128 even more important; as it seemingly has two modes of action in later stage AML development, it therefore has two intervention routes. By understanding the metabolic effects miR-128 and associated

miRNAs have, as well as its signalling effect, it is possible to robustly control its effects via two separate approaches (metabolic and signalling).

Much as with miR-302c, miR-181c and miR-497a, miR-128 is not found to be statistically different at low clonal expansion, p=0.25 and a slight upregulation vs control. miR-128 is upregulated in high clonal expansion mCh/GFP CBA mice, and to a higher extent, although with the dubious statistics present in the low clonal expansion data set this cannot be said to be significant. Nevertheless, this research hypothesizes that a profile of consistent upregulation in miR-302c, miR-181c, miR-497a and miR-128 is a predictive factor for AML development and could serve as biomarkers thereof as well as clinical targets for treatment. These are not the only important miRNA but serve as a potent core for the development of a biomarker panel. Genetic level biomarkers would consist of their overlapping gene targets: Echs1, Fasn, Acsl6, Ccnd2, Mapk8, Nlk, Mapk9, Tgfbr2, Tgbr1, and Tgb3. Treatment may consist of targeted blocking with oligonucleotides complimentary to the mature miRNA target (Lima *et al.,* 2018, RNA Biology) to protect signalling function, or via action on the metabolic dysregulation caused by miRNA.

3.03 Comparison of irradiated mice to preleukaemic, non-irradiated mice

CBA SPM mice, as described in chapter 2.04, possess a single point mutation which renders them especially susceptible to AML development, both after IR exposure and *de novo.* This mutation means that they are in a unique state wherein *all* CBA SPM mice exist in a preleukaemic state, especially older individuals, with unirradiated CBA SPM mice developing AML at similar rates and timepoints when compared to IR-exposed CBA mCh/GFPs.

As such, SPM mice offer a valuable source of “natural” leukaemias. The word natural is contentious, and could be disagreed with, given the transgenic nature of the model, but relative to irradiated mCh/GFP mice, these have never suffered a radiation insult. To determine whether the irradiated preleukaemic GFP/mCh CBA mice were somehow distinct

from a preleukaemic state arising in a non-irradiated SPM mouse, the two BM EV populations were compared to one another, to determine if there were any significant differences in miRNA expression, as seen in the heat map in figure 3.06.

Due to the COVID pandemic, plans to add more SPM samples for direct comparison were curtailed, as such only two were present, making statistical analysis between the two groups (high clonal expansion mCh/GFP vs age matched unirradiated SPM mice) difficult. Indeed, the FDR of all miRNA that satisfy the p-value parameter exceeds 0.3, with the exception of mmu-mi540-3p, with an FDR of 0.07 and p-value of 3.0e-4, being upregulated by a factor of 8.5 in SPM samples when compared to high clonal expansion mCh/GFP cells. miR-540-3p was also identified as being upregulated in high clonal expansion EVs when compared to sham EVs in mCh/GFP mice. This miRNA is predicted to play a role in cancer pathways (table 3.08), is involved in Hippo signalling and myeloid leukocyte differentiation, and targets Hif1an and Tcl1b2, among others. miR-540-3p was also the most significant result in high clonal expansion vs sham.

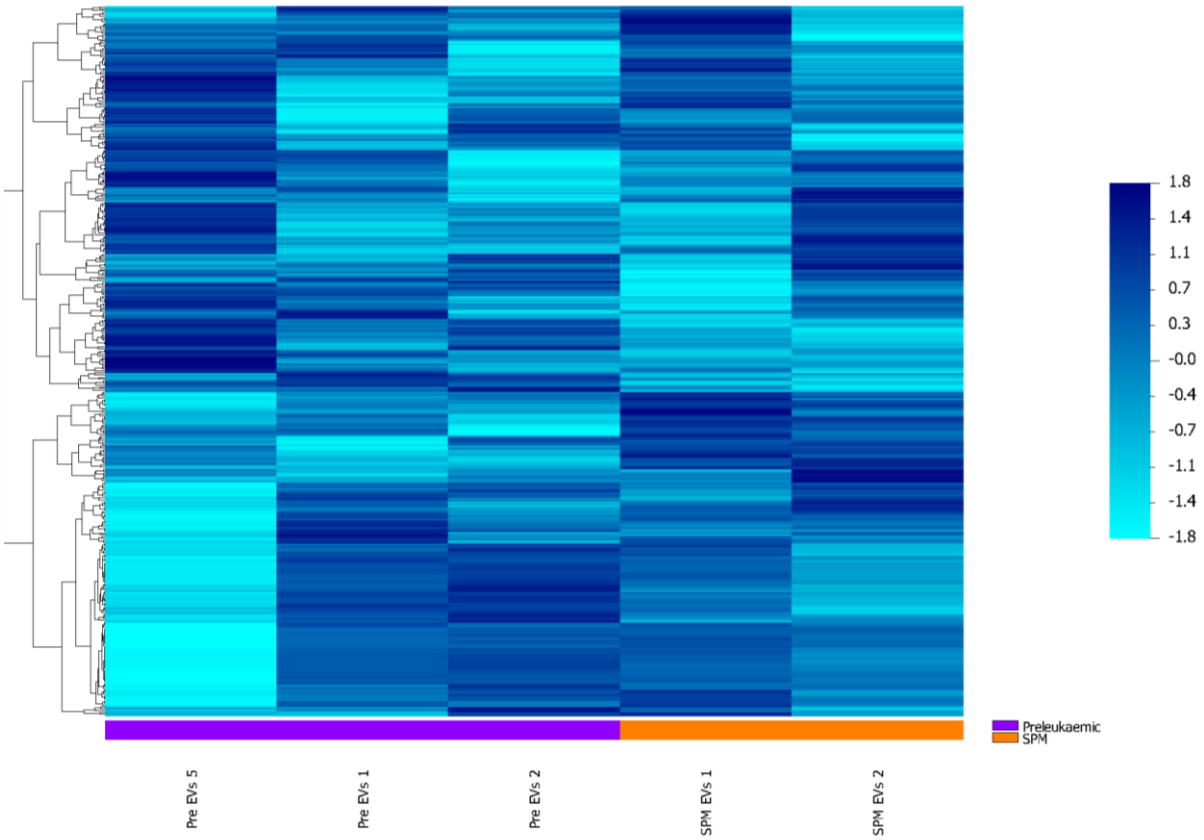


Figure 3.09: Heat map of preleukaemic EVs vs SPM-derived EVs. Preleukaemic EVs were high clonal expansion mice, specifically those with <30% clonal expansion. Generated with BRBArrayTools.

3.04 Strain Dependent Variation on Radiation Signature and Potential Dose Dependent Responses

Murine strains differ from one another in characteristics and biology; C57 mice, for example, are resistant to the spontaneous development of leukaemias, with an extremely low incidence rate *de novo*, and a low susceptibility to tumours overall, especially when compared to CBA mice. The opportunity to determine whether the miRNA signatures seen in sections 3.01 and 3.02 were strain-specific arose when a collaborating group performed a large-scale pilot study, involving the irradiation of C57BL/6J Ldlr KO (Ldlr-/-) mice. These mice were TBI irradiated at 4 doses: 0Gy (sham), 0.5Gy, 2Gy, and a very high dose of 4Gy, all on site at UKHSA Harwell and using the dose rates described. These were culled 6 months post exposure, and their femurs and tibia harvested and EVs isolated in the same manner as used in CBA mCh/GFP mice. Unlike the CBA mCh/GFP mice, which were mixed gender, all mice in this cohort were male.

2 mice were excluded from this analysis, due to QC flags and aberrant data; with the exception of a handful of miRNAs, all counts were 80 on these two samples, indicating poor hybridization and improper fixation to the glass cartridge for counting.

Table 3.13: Statisfically significant miRNA, determined by both p-value and FDR being sub 0.05, when comparing different doses of irradiation to sham controls in C57BL/6J Ldlr KO mice. *Both miRNA satisfy p-value but fail to satisfy FDR (FDR=0.10).

Class Comparison	**Statistically significant miRNA**
Sham vs 0.5Gy	Mmu-let-7a-5p
Sham vs 2Gy	Mmu-let-7a-5p
Sham vs 4Gy	*Mmu-miR-540-3p and mmu-miR-384-5p**

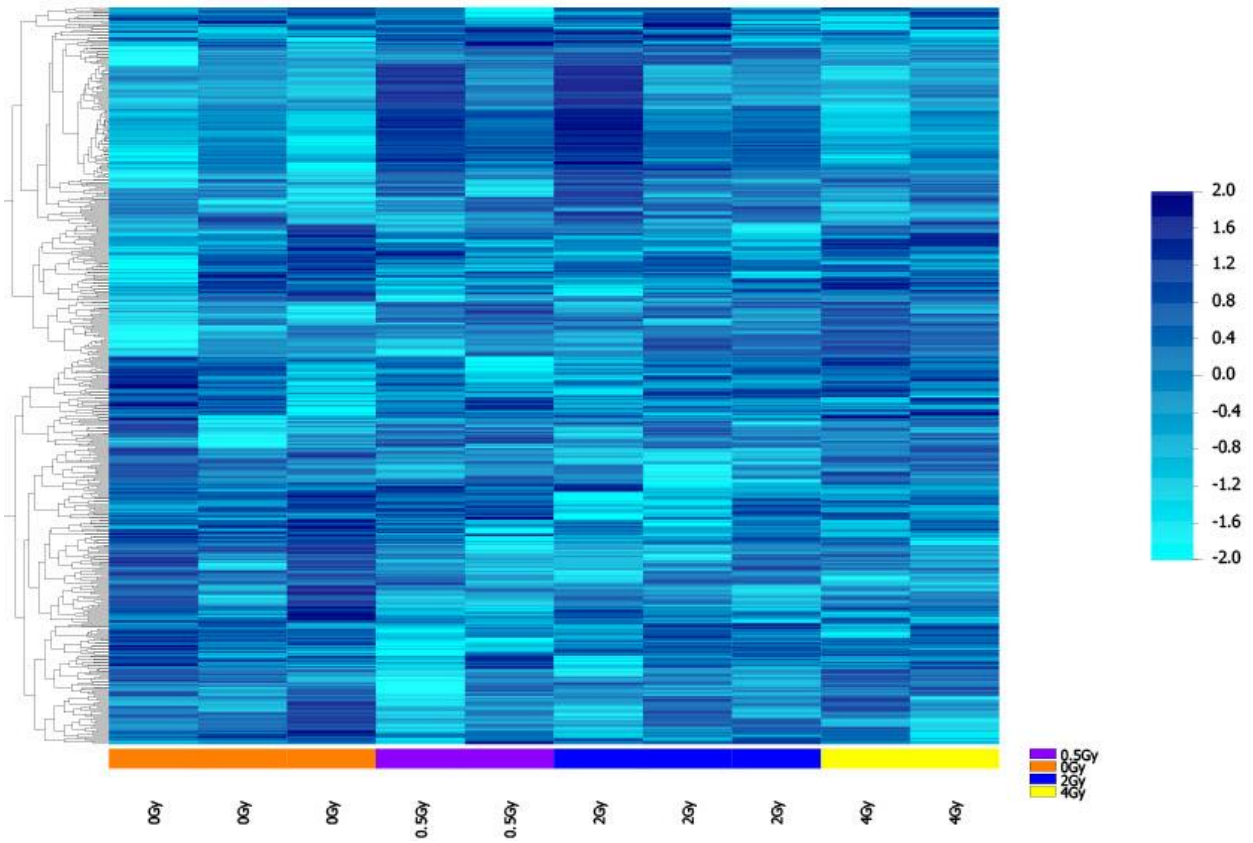


Figure 3.10: Heat map of BM-derived EVs from 0Gy, 0.5Gy, 2Gy, and 4Gy TBI irradiated C57BL6/J Ldlr -/- mice, 6 months post exposure. EVs are derived from femur and tibia, and do not include the spine. Generated with BRBArrayTools.

One miRNA was identified as being statistically relevant, with two more missing the FDR threshold: let-7a-5p, miR-540-3p, and miR-384-5p. Of these, let-7a was not found in any previous data set, miR-540 was found in high clonal expansion CBA mCh/GFP mice, and miR-384 was tentatively identified in low clonal expansion CBA mCh/GFP mice in both its variants, 3p and 5p. let-7a is technically a miRNA precursor rather than a full miRNA. In human cells, the let-7 family is a direct regulator of the Ras oncogene family (Johnson *et al.,* 2005, Cell). The KEGG database furthermore associates let7a-5p with regulation of lysine degradation, MAPK signalling, fatty acid metabolism, FoxO signalling, and proteoglycans in cancer, all pathways identified in 48 hours post irradiation WT CBA mice and high clonal expansion 12-month post exposure CBA mCh/GFP mice. Further pathways

it targets include the p53 signalling pathway and involvement in known chronic myeloid leukaemia pathways.

miR-540-3p is predicted to be involved in the regulation of myeloid differentiation, while miR-384-5p, tentatively identified in low clonal expansion mice, is involved with osteogenic differentiation regulation in BM MSCs, as well as injury recovery (Zhou *et al.,* 2020, Neuroscience Letters; Ye *et al.,* 2020, Neurological Research).

It is difficult to interpret whether CBA mice have a strain specific response; the tentative miRNAs at 4Gy are shared with 3Gy WT CBA mice, while the positively identified let-7a is not, but does target pathways that are conserved between both strains with regards to radiation condition. Furthermore, the time point is different, with these mice being only 6 months post exposure. It is possible that, given the nature of C57 being resistant to radiation-induced malignancies, these miRNAs are lingering signs of radiation injury as opposed to a pre-oncogenic state, and the pathways they then target results in an increased risk of oncogenic development as a late effect of TBI exposure, even at low doses. This would then mean that regarding a miRNA screen of post-exposure individuals, the pathways targeted, rather than the explicit miRNAs themselves, is the critical aspect to look for when evaluating susceptibility to late effects.

3.05 Chromosomal locations of differentially regulated miRNAs

To see whether there was a relationship between differentially regulated miRNAs either post IR exposure or in a preleukaemic state and their location on the murine genome, the miRbase database was used to establish the location of each miRNA on the chromosome, separated by IR condition and strain. For this analysis, only miRNA that satisfied both the p-parameter and FDR threshold were used.

Table 3.14: Genomic locations of differentially regulated miRNA across murine data sets, sourced from miRDB. HCE: High Clonal Expansion.

miRNA	Location on chromosome
48 hours post IR WT CBA	
Mmu-miR-1933-5p	chr11: 21344588-21344675
Mmu-miR-695	chr2: 155356817-155356925
Mmu-miR-323-5p	chr12: 109712508-109712593
Mmu-miR-1898	chr15: 12171492-12171574
Mmu-miR-323-3p	chr12: 109712508-109712593
Mmu-miR-1904	chr13: 109903809-109903888
Mmu-miR-688	chr15: 102671792-102671866
Mmu-miR-669h-5p	chr2: 10518155-10518279
Mmu-miR-129-5p	chr6: 29022619-29022691
Mmu-miR-878-5p	chrX: 66801508-66801585
Mmu-miR-761	chr4: 109017655-109017730
Mmu-miR-669g	chr2: 10477150-10477272
Mmu-miR-291a-3p	chr7: 3218919-3219000
Mmu-miR-1942	chr15: 76215611-76215673
Mmu-miR-338-5p	chr11: 120014765-120014862
Mmu-miR-1946a	chr16: 32267450-32267583
Mmu-miR-34b-5p	chr9: 51103562-51103645
HCE CBA mCh/GFP 12 months post IR	
mmu-miR-540-3p	chr12: 109586080-109586146
mmu-miR-486a-5p	chr8: 23142555-23142682
mmu-miR-710	chr8: 64514332-64514441
mmu-miR-139-5p	chr7: 101475376-101475443
mmu-miR-1983	chr13: 21896918-21897049
mmu-miR-128-3p	chr1: 128202361-128202430
mmu-miR-1897-3p	chr3: 34638464-34638542
mmu-miR-423-5p	chr11: 77078064-77078172
mmu-miR-1224-5p	chr16: 20604452-20604536
mmu-miR-1902	chr2: 104428861-104428940
mmu-miR-676-3p	chrX: 100381097-100381185
mmu-miR-370-3p	chr12: 109618258-109618336
mmu-miR-326-3p	chr7: 99552269-99552363
mmu-miR-191-5p	chr9: 108568319-108568392
mmu-miR-1949	chr18: 35554567-35554636
mmu-miR-302c-3p	chr3: 127545363-127545430
mmu-miR-1198-5p	chrX: 7807101-7807221
mmu-miR-132-3p	chr11: 75173682-75173747
mmu-miR-2861	chr2: 32712807-32712888
mmu-miR-483-5p	chr7: 142654924-142654996
mmu-miR-345-5p	chr12: 108836973-108837068
mmu-miR-154-5p	chr12: 109738433-109738498
mmu-miR-497a-5p	chr11: 70234717-70234800
mmu-miR-181c-5p	chr8: 84178873-84178961
mmu-miR-382-5p	chr12: 109733771-109733846
mmu-miR-138-5p	chr8: 94324311-94324381
6 month post IR C57BL/6J	
mmu-let7a-5p	chr13: 48538179-48538272

In WT CBA mice 48 hours post TBI exposure at a dose of 3Gy, 2 miRNA are found on chromosome 11, 3 miRNA are found on chromosome 2, 2 miRNA are found on chromosome 12, 3 miRNA are found on chromosome 15, 1 miRNA on chromosome 13, 1 miRNA on chromosome 6, 1 miRNA on chromosome X, 1 miRNA on chromosome 4, 1 miRNA on chromosome 7, and 1 miRNA on chromosome 9.

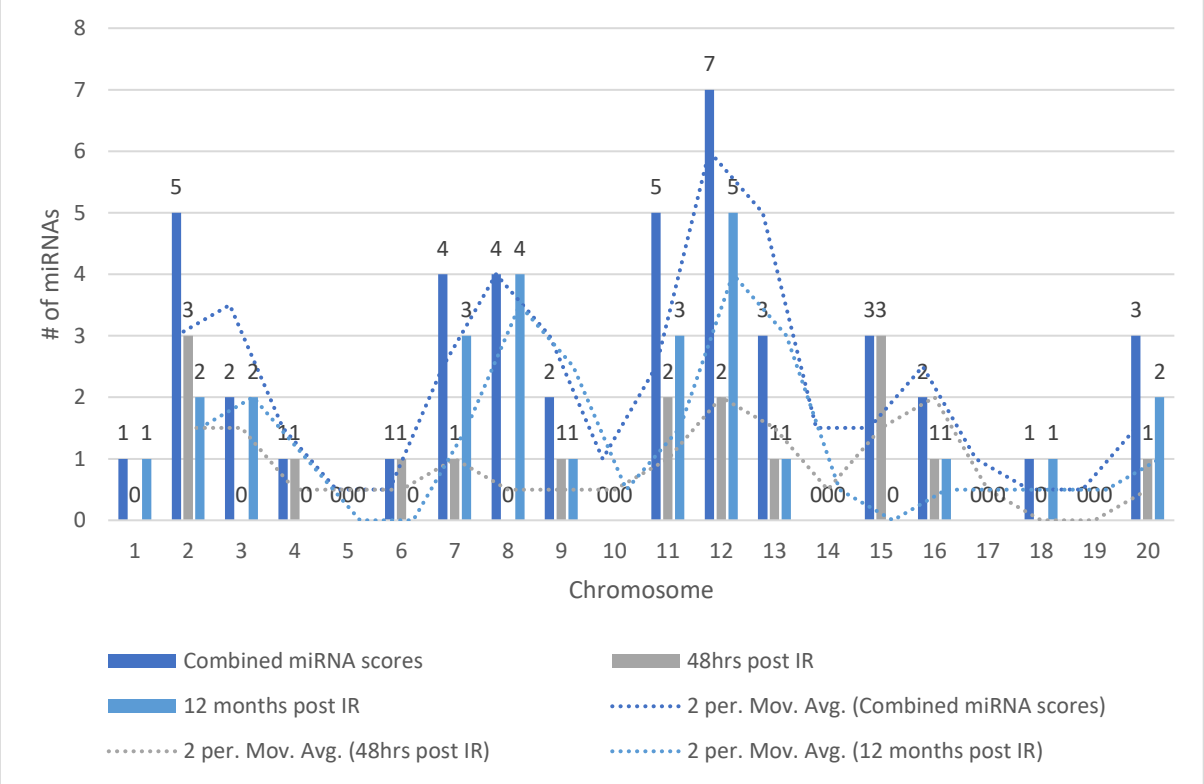


Figure 3.11: Number of miRNAs per chromosome as combined score, 48 hours post IR in WT CBA mice, and 12 months post IR in high clonal expansion CBA mCh/GFP mice. Chromosome 20=X chromosome.

The highest number of miRNAs per chromosome in a combined score occur in chromosomes 2, 7, 8, 11, 12, 15 and 20. In 48 hours post exposure WT CBA mice, the highest scores are on chromosomes 2, 11, 12, and 15. In 12 months post TBI CBA mCh/GFP mice, the highest scores occur at chromosomes 7, 8, 11, and 12. Chromosomes 11 and 12 overlap in both instances, and along with chromosome 2 represent the 3 peaks in terms of miRNA localization to the chromosome. It is difficult to determine whether any

kind of chromosome clustering occurs in terms of radiation damage or activated miRNAs; it is important to note that miRNA chromosomal localizations in both data sets follow the same peak trend for the most part, with similar chromosomes being affected in many cases.

3.06 Discussion

IR at both 0.1Gy and 3Gy causes a clear and identifiable response at 48 hours post exposure in WT CBA mice, as demonstrated by the data from the genotypical CBA mice irradiated by our collaborators in Hungary. Four miRNA were identified as being shared between 0.1Gy and 3Gy: miR-761, miR-129-5p, miR-669g, and miR-34b-5p. These miRNA were upregulated vs the control in a dose-dependent manner, with 3Gy showing a higher upregulation than 0.1Gy. 3Gy also showed an expanded response to radiation, with more miRNA being significantly differentially regulated. The involved pathways heavily involved metabolic regulation, including but not limited to lysine degradation and fatty acid biosynthesis, suggesting that these metabolic pathways are important in post-radiation injury response. Other involved pathways are major signalling networks, such as MAPK, and known oncogenic pathways, clearly demonstrating a conserved miRNA response activating survival pathways during IR wound healing that are later on used by cancer, and this is visible at the miRNA level only 24 hours post exposure, and possibly sooner, although shorter time period experiments were not carried out.

12-month post exposure transgenic CBA mCh/GFP mice, exposed to 3Gy of radiation on site at UKHSA Harwell, were segregated based on their irradiation status and clonal expansion level. While they exhibited a response distinct from 24 hours post exposure WT CBA mice at the individual miRNA level, at the pathway level they demonstrated a marked similarity, with involvement of metabolic pathways such as lysine degradation and fatty acid biosynthesis, major signalling networks, and oncogenic pathways. A comparison of high clonal expansion murine cellular miRNA content to EV miRNA content revealed a specific exclusion and inclusion packaging strategy, with EVs having upregulated levels of miRNA interacting with fatty acid and lysine metabolic pathways, and lower levels of signalling

network-interacting miRNAs e.g. Wnt, Hippo, and MAPK. While it is difficult to establish functional effect without appropriate assays, it is possible that this profile represents a pro-oncogenic response at the systemic level with inhibition of major signalling networks being reduced via miRNA exclusion, thereby promoting oncogenic behaviour. However, gene target analysis, as shown below, demonstrates a mixed relationship, with both pro- and anti-oncogenic behaviour being identified.

By comparing Wnt, Hippo, MAPK and FoxO, a set of gene overlaps that are targets of dataset-represented miRNA was established, although no one gene was present in all four signalling networks. A set of genes was found with involvement in at least three of the four signalling pathways: Ccnd2, Mapk8, Mapk9, Mapk10, Nlk, Tgfbr1, Tgfbr2, and Tgbf3. miRNA targeting these were then analysed, with a set of three miRNA found: mmu-miR-302c, mmu-miR-497a, and mmu-miR-181c.

Ccnd2 codes for cyclin D2, which is involved in the regulation of G1 to S phase transition during cell cycling (Turner *et al.,* 2016, Prostate Cancer). Inactivation of cyclin D2 has been found in gastric cancer (Yu & Leung, 2006, Handbook of Immunohistochemistry and *in situ* Hybridization of Human Carcinomas) as well as in breast and prostate cancer (Turner *et al.,* 2016, Prostate Cancer). Mutations are also often found in adult AML patients (t(8;21)(q22;q22) (Eisfeld *et al.,* 2017, Leukemia), and Ccnd2 has been identified to be highly expressed in AML (Chen *et al.,* 2012, Blood). Of the set of 3 miRNA identified, it is regulated by mmu-miR-302c and mmu-miR-497a. The DIANATools database lacks experimentally validated evidence of how mmu-miR-497a and mmu-miR-302c affect Ccnd2 expression, but given previous literature evidence in other cancers, we hypothesize that these miRNAs are post-transcriptional repressors of Ccnd2, thereby having a proliferation-suppressive effect.

Mapk8, Mapk9 and Mapk10 are active in the JNK pathway, which in turn is a regulator of transcription (via c-Jun, JunB, JunD and Fos) as well as control of the cell cycle, survival, cell death, migration, and invasion. JNKs inhibit p53 activity, but also promote apoptosis,

serving a dual role in pro- and anti-oncogenic functions. Knockout of Mapk8 in wild-type mice led to an increased rate of skin cancer development, although knockout of Mapk9 led to the inverse, indicating a mixed effect. JNK activity is reported variably in AML, with the JNK pathway being constitutively active in AML cells and important for AML survival (Hartman *et al.,* 2006, Hematological Malignancies) or extremely important for sensitizing AML cells to drug treatment, causing cell death (Wang *et al.,* 2018, Journal of Steroid Biochemistry and Molecular Biology). An earlier paper reported constitutive activation of JNK was important for leukaemic transformation (Elsässer *et al.,* 2003, Oncogene).

The miR-181 family, namely miR-181a and miR-181b, are inhibitors of Mapk10 (Chi *et al.,* 2009, Nature). While direct evidence for miR-181c doing the same is not available, it is likely that it may serve the same function as its related miRNA. miR-181 family miRNAs were found to be downregulated in patients with an aggressive leukaemia phenotype, while upregulation thereof caused progression of myelodysplastic syndromes to AML. High levels of miR-181 was associated with better AML prognosis (Indieri *et al.,* 2020, International Journal of Molecular Sciences). As such, we hypothesize that miR-181c inhibits Mapk10, and more broadly JNK function, during the majority of leukaemogenesis. In more aggressive forms of AML, miR-181c expression then falls, causing, most likely with other collaborating factors, the overexpression of JNK, facilitating AML survival.

Thus, miR-181c is potentially extremely important as a progress indication miRNA: increasing levels may indicate systemic stress to repress JNK to normal levels, with an as-of-yet unknown event in aggressive AMLs causing a switch and decrease in miR-181c, allowing for JNK overexpression and AML survival. By tracking expression, and monitoring for this ‘switch’ event, we hypothesize that it would be possible to determine a turning point in AML establishment and progression and effective prognosis for the aggressiveness of the cancer. Alternatively, another hypothesis would be that high levels of miR-181c indicates a less aggressive AML with lower JNK activity, while low levels of miR-181 indicate a developing aggressive AML. To confirm or refute these hypotheses, a time

course experiment following a cohort of mCh/GFP CBA mice post-IR must be performed, with analysis of miR-181c levels relative to control mice at different time points, separated based on rate of progression and aggressiveness of any resultant AMLs, thereby confirming whether or not this miR-181c 'switch' event exists.

Nemo-like kinase (Nlk) is a mitogen-activated protein kinase-related kinase (Wu *et al.,* 2021, Gene Reports) that has, in recent years, been implicated in the regulation of tumorigenesis in various cancers. Nlk is a regulator of the Wnt pathway, and has, via E-cadherin expression repression, been demonstrated to prevent the migration of non-small lung cancer cells. It plays a role in the control of cell proliferation, migration, apoptosis, and invasion, and has been identified variably as an oncogene or tumour suppressor depending on the cancer type (Daams and Massoumi, 2020, International Journal of Molecular Sciences). Nlk is a known target of the miR-181 family in natural killer (NK) cells and is suppressed by miR-181 (Cichoki *et al.,* 2011, Journal of Immunology). Via repression of Nlk, miR-181 promotes differentiation into NK cells. Nlk is hyperactivated in erythroid progenitors, and inhibition of its activity promotes erythroid expansion (Wilkes *et al.,* 2020, Experimental Hematology).

Upregulated miR-181c as seen in high clonal expansion mCh/GFP CBA mice represses Nlk activity, leading to enhanced NK cell and erythroid expansion, as well as repressing JNK activity, representing a hypothetical route for its established tumour suppressor function in AML via negative regulation of Nlk and Mapk10. This makes miR-181 a potent tracker of development, a prognostic marker, and a therapeutic target for treatment of AML.

Tgfbr1 and Tgfbr2 encode for transforming growth factor beta receptor types I and II, respectively, while Tgbf3 codes for transforming growth factor beta 3. Together, these proteins function in the TGF-β pathway, regulating proliferation, migration, differentiation and apoptosis (Ark *et al.,* 2018, Cellular Signalling). The TGF-β pathway plays an interesting role in normal vs cancerous tissue, with it serving a tumour-suppressing function in normal tissue, but a tumour-promoting one in cancerous cells. This seeming contradiction

can be explained by cancer cells disabling tumour-suppressant elements of the pathway while leaving growth, invasion and immune evasion promoting components intact, via dysregulation of core elements of the pathway, such as the TGF-β receptors, i.e. Tgfbr1 and Tgfbr2 in this case (Massagué, 2008, Cell).

Abrogation of Tgfbr2 expression resulted in impaired AML engraftment to the BM niche (Hamilton *et al.,* 2014, Blood). Additionally, Tgfbr2 deletion in mice resulted in slower growing tumours and increased anti-tumourigenic immune function in macrophages and T cells (Novitskiy *et al.,* 2012, Journal of Leukocyte Biology). Tgfbr2 expression is inhibited by miR-302c (Chen *et al.,* 2022, Journal of Cell Communication and Signalling) and miR-302c is found to be downregulated in human AML patient T lymphocytes (Rouas *et al.,* 2015, Blood).

Therefore, miR-302c upregulation in high clonal expansion mCh/GFP mice may appear to be aberrant, as it has a seemingly oncosuppressive effect by inhibition of Tgfbr2, but several explanations for this pattern of regulation exist. Firstly, this may signify that the developing AML will not have a high level of TGF-β function, allowing for an approximation of its aggressiveness and behaviour. Secondly, this may in fact be systemic response to increasing TGF-β activity and an attempt to return it to normal levels. In the latter case, TGF-β activity may be upregulated via other means not seen within this line of research. A third explanation may be, as hypothesized with miR-181c, that a ‘switch’ event may occur, a secondary mutation event knocking down miR-302c expression that has not yet occurred within this cohort of mice. Regardless of the mechanism behind it, a first step for future research would be to measure levels of Tgfbr2 expression in BM cells via qPCR, paired with measuring miR-302c expression up until natural AML death, i.e. without a culling event.

The culling of high clonal expansion mice was performed due to the ethics requirements of the animal licence used for this research, but in light of this data, a scientific justification could be made to follow animals to end of life. A culling event ultimately makes an assumption of remaining lifetime, one that may not be necessarily reflective of the actual

biology and that must be reassessed. In any scenario, miR-302c represents an important biomarker and target for clinical intervention, representing yet another EV-mediated route of regulation of AML development.

Echs1 (short-chain enoyl-CoA-hydratase) catalyses the second step in the β-oxidation of mitochondrial fatty acid (Janssen *et al.,* 1997, Genomics). It has been observed to trigger lipid biosynthesis and maintain stemness in cancer stem cells (Sahoo *et al.,* 2022, Frontiers in Oncology). miR-128 is predicted to target Echs1, although experimentally validated regulation is currently unknown. miR-128 has been indicated to be a discriminator between ALL and AML, with higher levels being reported in ALL (Mi *et al.,* 2007, PNAS) with no significant difference in the PBMC compartment in AML patients vs healthy donors (Li *et al.,* 2013, Experimental Cell Research). However, more recent research has shown that miR-128 is found *overexpressed* in AML cells compared to non-cancerous precursor cells, preventing AML differentiation, and maintaining progenitor-like nature (De Luca *et al.,* 2017, Cell Death & Disease). Given the AML phenotype of high clonal expansion CBA mCh/GFP mice, it is thus likely that miR-128 is a positive regulator of AML development, potentially via upregulation of Echs1, although this must be experimentally validated.

miR-128 further targets Tgfbr1 and Tgfb3. Inhibition of Tgfb3 upregulates haematopoiesis in Fanconi anemia, a major risk factor for future AML development (Rodriguez *et al.,* 2021, Experimental Hematology). Within prostate cancer cells, miR-128 inhibits Tgfbr1, with inhibition of the tumour-suppressant part of the pathway rendering haematologic neoplasms TGF-β resistant (Dong & Blobe, 2006, Blood). We hypothesize that miR-128 is a positive regulator of acute myeloid leukaemogenesis via upregulation of Echs1 and downregulation of Tgfbr1, with unknown interactions with Tgfb3 that requires more data before a hypothesis can be made.

Acsl6 codes for Acyl-CoA Synthetase long chain family member 6, catalysing the formation of acyl-CoA from fatty acids, ATP, and CoA, with Mg2+ as a cofactor (GeneCards). Involvement in AML has only been recently reported, with a rare cytogenetic abnormality

being observed with an ETV6;ACSL6 translocation in relapsed AML patients (Baldazzi *et al.,* 2021, Cancer Genetics) which promotes leukaemogenesis (Wang *et al.,* 2023, Current Oncology). Without sequencing of the gene in high clonal expansion transgenic CBAs, it is difficult to determine if a similar mutation has occurred. Acsl6 is also regulated by miR-128. Modified function of Acsl6 should be expected from the ETV6;ACSL6 translocation; while a direct interaction has not been reported, post-transcriptional regulation of Acsl6 by miR-128 could achieve a similar effect, promoting leukaemogenesis and AML establishment. Similar to Echs1, Acsl6 also requires a magnesium ion cofactor for its reaction. Alternatively, post-transcriptional miR-128 may be repressing the tumour-promoting activity of a dysregulated Acsl6. Identification of miR-128 as a mutual regulator suggests a two-prong approach via direct modulation of miR-128 combined with depletion of Mg2+, thus allowing for comprehensive control of oncogenic fatty acid biogenesis activity. More research must be performed into the expression of Acsl6 and its function in leukaemogenesis.

Fasn (fatty acid synthase) is highly expressed in cancer cells, with Fasn mRNA significantly higher in AML patients (Humbert *et al.,* 2021, Cell Death and Differentiation). In normal tissue, Fasn is downregulated by miR-128-2 (Adlakha *et al.,* 2013, Cell Death & Disease), but a direct regulatory relationship between these two has not been reported in cancers. Reduction of Fasn has been demonstrated to sensitize AMLs to differentiation therapy (Humbert *et al.,* 2021, Cell Death and Differentiation). Thus it is likely that miR-128, in this pathway, is part of a systemic stress response to downregulate Fasn expression, although given the complexities of metabolic network regulation and miRNA interactions, further study must be done. In chapter 5 of this thesis, a preliminary study on Fasn expression post-radiation, as well as other metabolism-involved genes, was conducted in an effort to better understand the state of metabolism immediately after radiation insult. However, the state of metabolism at a genetic and metabolite level has not been studied in high clonal expansion mice, necessitating future research.

Further analysis of chromosomal locations of the DE miRNA revealed no specific genomic clustering or co-location, but did show that chromosomes 5, 10, 14, 17, and 19 did not have any DE miRNA located on them in either 48 hours post exposure or 12 months post exposure, suggesting that radiation-activated or cancer-regulating miRNA are not located on these chromosomes, although this is not to say that targeted genes are not located on these chromosomes (and as discussed in chapter 6, they in fact are).

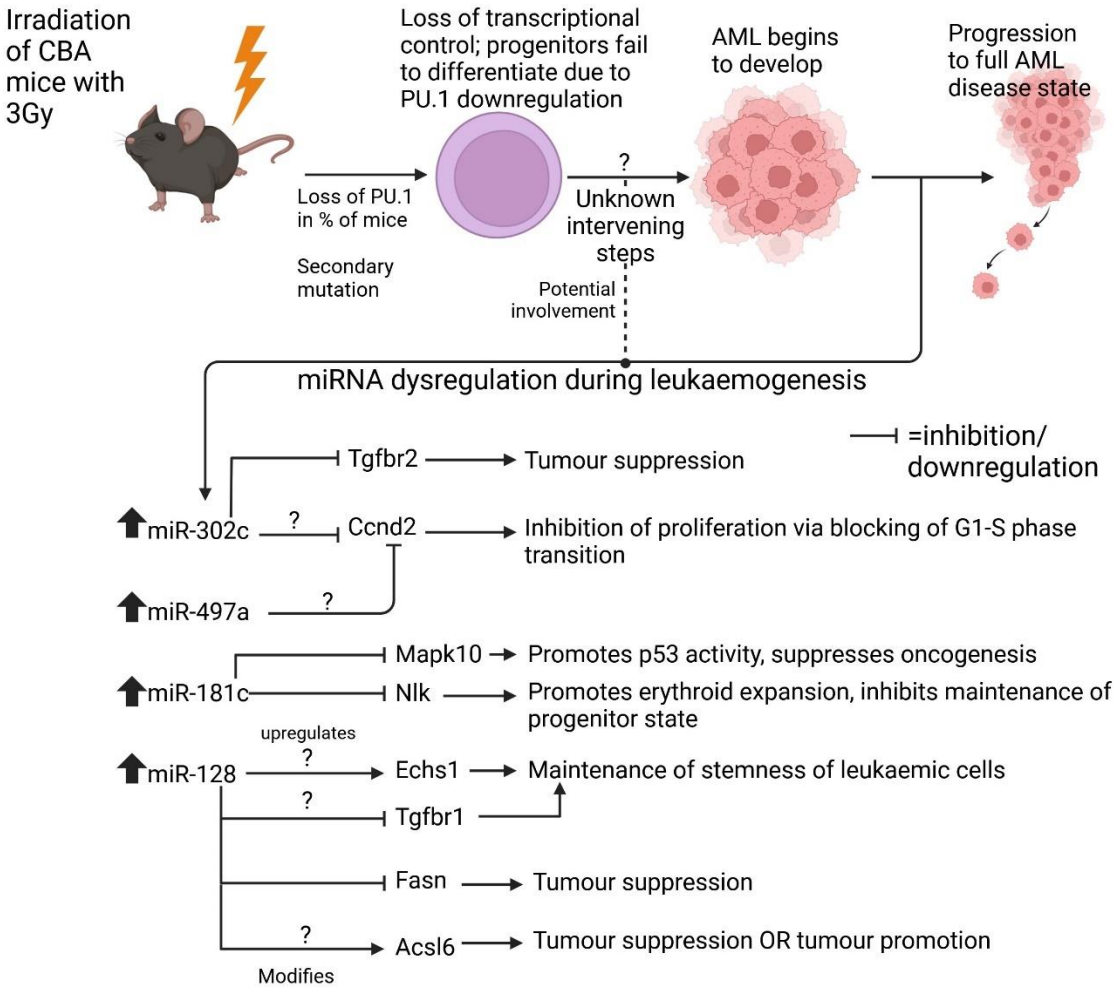


Figure 3.12: Hypothetical interaction pathway for miR-302c, miR-497a, miR-181c and miR-128 during AML progression after initial IR insult. Created with Biorender.com.

Overall, these results demonstrate a clear and significant difference in EV miRNA between irradiated and non-irradiated states, a set of dose dependent miRNA, and the importance of analysing miRNA not at an individual level but rather at a pathway level to identify

similarities between radiation exposure and subsequent late stochastic effect cancer development. When analysed at a pathway level and subsequent gene targets, it becomes possible to identify a set of highly interactive miRNA targeting several key networks.

In high clonal expansion mCh/GFP CBA mice, a set of four miRNA, miR-128, miR-181c, miR-302c, and miR-497a was identified targeting all 4 signalling networks with miR-128 also playing a central role in targeting lysine degradation, fatty acid metabolism and fatty acid biosynthesis. We hypothesize that this set, and their pattern of regulation, are a key biomarker for AML development and provide a precise insight into the developmental stage. Given their major regulatory role, we also hypothesize that they can be further used as a prognostic factor and in the future as therapeutic targets, with e.g. upregulation of miR-181c having a tumour supressing role in AML, thereby providing an endogenous method of boosting systemic response to AML. Given their effect on metabolic systems, we also later investigated the direct impact of EVs on metabolite levels, providing insight into and allowing for the development of a future treatment regime that is non-invasive and could be preventative in nature. Together, this provides a two-pronged approach to regulating miRNAs and their effects, first via direct modulation of the miRNAs themselves and secondly via modulation of their metabolic effects by dietary control. Combined with their ability to serve as biomarkers, this data serves as a core for a ‘theranostic’ (therapeutic + diagnostic) approach to AML treatment via miR-128, miR-181c, miR-302c and miR-497a, presenting a significant finding that urgently merits further research. Married with targeted treatment of metabolic effects, e.g. via diet, a comprehensive therapy plan addressing multiple pathways of action is possible. Prior to this, however, it must be established if this miRNA are causative or correlative to AML development.

Our primary hypothesis is that this set of four miRNAs, transported via EVs, act via independent routes and exert sometimes contrary effects, most likely due to the heterogeneous nature of BM, with a wide variety of cells being represented, explaining the discrepancy in activity. These four miRNAs likely serve a tumour-suppressing role in

normal, healthy cells, while serving a tumour-promoting function in AML cells. Given constitutive upregulation of these miRNA with tumour-suppressant function, we are likely capturing a systemic stress response aimed to combat AML development. This gives a clear, defined set of biomarkers for tracking of AML development, the system's state of stress, the prognosis of said AML via miRNA levels, predicted phenotype of the AML, and a set of clinical targets for boosting of an endogenous stress response signal, allowing for suppression of AML development. Combined with modulation of metabolism, this allows for a prophylactic treatment regimen to minimize chance of AML development in both pre- and post-radiation therapy and radiation exposure patients.

This represents a significant finding reporting and, to this writer's knowledge, the first time this set of four miRNA has been observed as a central control regulator in both signalling and metabolic pathways, presenting a cross-pathway control nexus that must be further studied. With the lack of statistically significant results in low clonal expansion mice, it is unknown how these four miRNAs are regulated during the initial latency period between post-PU.1 two-hit event and low levels of AML development. To further study this, and to resolve the heterogeneity of BM and attempt to subdivide and characterize cell-type specific IR response, early-stage post-IR cells were studied in the following chapter, namely macrophages and mesenchymal stem cells. Future work must perform wider scale experiments with low clonal expansion mCh/GFP CBA mice to statistically validate the data set and further elucidate the progression of AML in the early stage.

4. Cell-type specific miRNA responses to radiation: Breaking down the larger picture

4.01 BM-derived macrophage response to ionising radiation

As described in section 2.1, murine macrophages were derived from murine BM. EVs were collected from cells irradiated at 0Gy and at 2Gy (with a dose rate of 0.5Gy/min), as a dose of 3Gy resulted in almost total tissue death within less than 24 hours. These were then shipped to ArrayStar for analysis by RNA sequencing. As such, the data presented here will be in a different format to the data presented in chapter 3, with different statistical analyses used by ArrayStar. Where relevant this will be explained, and later discussed to identify whether any discrepancies might arise as a result of differing methodologies. Moreover, due to small sample sizes compared to the dataset in chapter 3, FDR could not be reliably calculated for this dataset: FDR calculations are not performed when only a single replicate set exists, i.e. 1 triplicate of both variable and control as opposed to 2 or 3.

Table 4.01: Differentially regulated miRNAs in 2Gy vs 0Gy BM-derived macrophages, and their suspected or confirmed biological interactions. Targeted genes are listed at a cut-off threshold of target score 95, as provided by TargetScan. miRNAs marked with * are miRNAs flagged as NOT being high confidence miRNAs. Confidence in this case refers to an miRBase annotation criteria: in short, mapped reads must exceed 10 across the database to both arms of a mature miRNA. If this criterion is not met, the miRNA is not flagged as high confidence. The confidence criterion is as such a measure of how likely a miRNA is to be 'real'. However, there are well-known and well-conserved miRNA (e.g. MiR-184) that fail to meet this criterion, and it is not a definitive predictor of the authenticity of a given miRNA. Continued on pages 125 and 126.

Name	PValue	FDR	Predicted biological interactions
mmu-miR-222-5p	1.6e-02	N/A	Involved in murine melanoma (Dahmke *et al.,* 2013, PLoS One), necessary in cardiac growth (Liu *et al.,* 2015, Cell Metabolism), upregulated in B-cell chronic lymphoblastic leukaemia (Dehkordi *et al.,* 2016, Indian Journal of hematology and blood transfusion), 3p arm involved in proliferation of AML via Wnt pathway (Liu *et al.,* 2022, Biochemical and Biophysical Research Communications), overexpressed in AML (Rommer *et al.,* 2013, BMC Cancer).
mmu-miR-1960-5p*	4.3e-02	N/A	Targets Hf2afy. Biological activity unknown. KEGG predicts involvement in endocytosis, RNA degradation, ErbB signalling and viral myocarditis, via targeting of Arf3, Hspa9, and Abl2, Abl2 being involved in the latter 2 pathways.
mmu-miR-98-3p	3.5e-02	N/A	Downregulated in mouse embryonic stem cells exposed to benzene (Aoki *et al.,* 2020, Toxicology and Applied Pharmacology). Acts as a tumour suppressor in hepatocellular carcinoma (Zhou *et al.,* 2016, Oncotarget). High expression of human equivalent (hsa-miR-98) is a good prognostic factor in AML patients treated with chemotherapy (Hu *et al.,* 2019, Journal of Cancer).
mmu-miR-1843a-3p	3.5e-02	N/A	5p arm identified in serum exosomal miRNA post acute radiation exposure, shared between all applied doses of radiation (2Gy, 6.5Gy and 8Gy) (Zhang *et al.,* 2020, Dose Response).
mmu-miR-582-5p	2.2e-02	N/A	Predicted to target Hif1a, SNF2 histone linker PHD RING helicase, Tet3 (Tet methylcytosine dioxygenase 3); found upregulated in myocardium of Nrf2-KO mice (Quiles *et al.,* 2017, BMC Genomics).
mmu-miR-148b-5p	3.3e-02	N/A	Targets Rrp36. Underexpressed in human AML patients, along with other members of the miR-148 family (Wang *et al.,* 2017, Medical Science Monitor), with high levels of miR-148b being associated with lower risk and higher remission rates in AML patients.
mmu-miR-223-3p	5.5e-03	N/A	Targets Fbxw7. hsa-miR-223-3p is upregulated in human AML, and mmu-miR-223-3p regulates granulopoeisis in mice (Pandita *et al.,* 2019, PLoS One); however low serum expression is associated with poor prognosis in AML patients (Yu *et al.,* 2020, Journal of Clinical Laboratory Analysis). Decreases cell proliferation and increases apoptosis in AML via Fbxw7 (Xiao *et al.,* 2016, Oncology Letters).

mmu-miR-150-5p	3.6e-02	N/A	Human equivalent induces myeloid differentiation of AML and progenitor cells (Morris *et al.,* 2013, PLoS One); expression is decreased in CML and AML vs normal BM. Correlates with delivered dose in thoracic radiation therapy for non-small cell lung cancer, decreasing with delivered dose (Dinh *et al.,* 2016, Radiation Oncology).
mmu-miR-142a-5p*	3.1e-02	N/A	Very commonly mutated in CML and AML (Galka-Marciniak *et al.,* 2022, Nature Scientific Reports), with high levels of miR-142 associated with increased patient survival (Dahlhaus *et al.,* 2013, Neoplasma). Mutations in AML decrease miR-142 function which promotes leukaemogenesis (Trissal *et al.,* 2018, Cancer Research).
mmu-miR-1298-5p	2.1e-02	N/A	Human equivalent upregulated in a subpopulation of innate lymphoid cells (ILC), regulatory ILCs (ILCReg) in AML patients (Yu *et al.,* 2019, Cancer Management and Research).
mmu-miR-291b-3p	4.3e-02	N/A	Upregulated in undifferentiated embryonic stem cells, with rapid downregulation during differentiation, promotes G1/S transition (Mens & Ghanbari, 2018, Stem Cell Reviews & Reports).
mmu-miR-3473g-5p*	3.4e-02	N/A	Unknown; predicted to target Ppm1e, Ubr5, Stim2, Myt11, Camk2d, Adgrb3, Ube2q2, Cadm2, Arhgap12, Dmrta1, Csmd3, Trim2, Zfxh4, B4galt6, Esp31, and others.
mmu-miR-433a-3p*	3.9e-02	N/A	Mediates ERR-gamma suppression of osteoblast differentiation via targeting of RUNX2 (Kim *et al.,* 2013, Life Sciences). Targets CREB directly, increasing chemosensitivity in human glioma (Sun *et al.,* 2016, Oncotarget).
mmu-miR-465d-5p	2.2e-02	N/A	Unknown, no predicted KEGG targets. Predicted to target Pank3, Kitl, Gabra6, Dpyd, Avl9 etc.
mmu-miR-5100-5p*	1.2e-02	N/A	Regulates apoptosis and autophagy in gastric cancer cells, interacting with mTOR (Zhang *et al.,* 2022, International Journal of Molecular Sciences). Human equivalent overexpressed in lung, gastric, pancreatic, and oral squamous cell carcinomas (Zhang & Hu, 2022, Cancers).
mmu-miR-5106-5p*	1.9e-02	N/A	Highly expressed in M2-polarized macrophage-derived exosomes, inducing BM MSC osteogenic differentiation via salt-induced kinase 2 and 3 targeting (Zhang *et al.,* 2021, Frontiers in Oncology).
mmu-miR-5108-5p*	1.9e-02	N/A	Present within mitochondria of murine heart cells, may play a role in senescent-cell mediated chronic low-grade inflammation (Giuliani *et al.,* 2017, Mediators of Inflammation); otherwise unknown.
mmu-miR-5110-5p*	3.2e-04	N/A	Regulates pigmentation via targeting of melanophilin and Wnt-1 (Yang *et al*, 2018, The FASEB Journal); regulates eumelanin production in *Vicugna pacos* melanocytes (Liu *et al.,* 2019, BMC Genomics).
mmu-miR-5112-5p*	2.6e-02	N/A	Increased in adipocytes in human breast cancer tissue, predicted to target Cpeb1 (Lee *et al.,* 2017, PLoS One). Increasing miR-5112 resulted in a pro-inflammatory, pro-oncogenic proliferation effect in cancer cells.

mmu-miR-7051-5p	2.9e-02	N/A	Upregulated in bleomycin-induced pulmonary fibrosis (Chen *et al.,* 2022, Biomed Research International), otherwise biological function unknown. Predicted to target Crocc2 and Mapre2, among others.
mmu-miR-764-3p	3.0e-02	N/A	May be a biomarker of hepatocellular carcinoma (Chen *et al.,* 2015, Medical Science Monitor). Regulates 17beta-estradiol synthesis of mouse ovarian granulosa cells via steroidogenic factor-1 (Wang *et al.,* 2015, In Vitro Cellular & Developmental Biology-Animal).5p arm promotes osteoblast differentiation (Guo *et al.,* 2012, Journal of Bone and Mineral Research), with the 3p arm inhibiting it.
mmu-miR-7648-3p*	3.9e-02	N/A	Highly upregulated in breast cancer in a PyMT murine model of the disease (Nogales-Cadenas *et al.,* 2016, Breast Cancer Research).
mmu-miR-7655-3p*	2.0e-02	N/A	Unknown.

A total of 23 miRNA transcripts were identified as being significantly differentially regulated in 2Gy vs 0Gy macrophages: miR-222, miR-1960, miR-98, miR-1843, miR-582, miR-148b, miR-223, miR-150, miR-142a, miR-1298, miR-291b, miR-3473g, miR-433a, miR-465d, miR-5100, miR-5106, miR-5108, miR-5110, miR-5112, miR-7051, miR-764, miR-7648, and miR-7655, which satisfied the p-value cutoff at 0.05. Of these, miR-222, miR-1960, miR-98-3p, miR-1843a, miR-582, miR-148b, miR-223, miR-150, and miR-142a were upregulated when compared to the control 0Gy group. miR-1298, miR-291b, miR-3473g, miR-433a, miR-465d, miR-5100, miR-5106, miR-5108, miR-5110, miR-5112, miR-7051, miR-764-3p, miR-7648 and miR-7655 were downregulated in 2Gy compared to the control group.

Several of these miRNAs are not flagged as high confidence, as seen in table 4.01. One advantage of RNASequencing is the sequencing of all miRNAs within a given sample, and the ability to identify novel miRNA, as opposed to dealing with a predetermined panel of miRNAs (as with the nCounter panel), which might lead to certain miRNAs being omitted. However, as a result of this, the main miRNA database, miRBase, has been flooded with thousands of novel miRNA reads. Depending on the level of annotation confidence, this

may result in misidentified miRNA e.g. poorly defined hairpins, degraded mRNA, or artifacts being submitted as mature miRNA. The High Confidence annotation is a remedial measure to this problem, but as explained in table 4.01 it is not foolproof, with well-studied and oft-reported miRNA failing to meet the criteria necessary for High Confidence. Nevertheless, it must be noted that these miRNA have a risk of not being genuine, and should be regarded with due scepticism.

Multiple miRNAs are known from literature to explicitly play a role in AML. miR-222 and miR-1298 are found to be overexpressed in many human AML cases, while high levels of miR-98 and miR-148b are associated with a good prognosis for AML patients. miR-223, miR-150, and miR-142 are all underexpressed in human AMLs, with low expression levels being correlated to a poor disease prognosis.

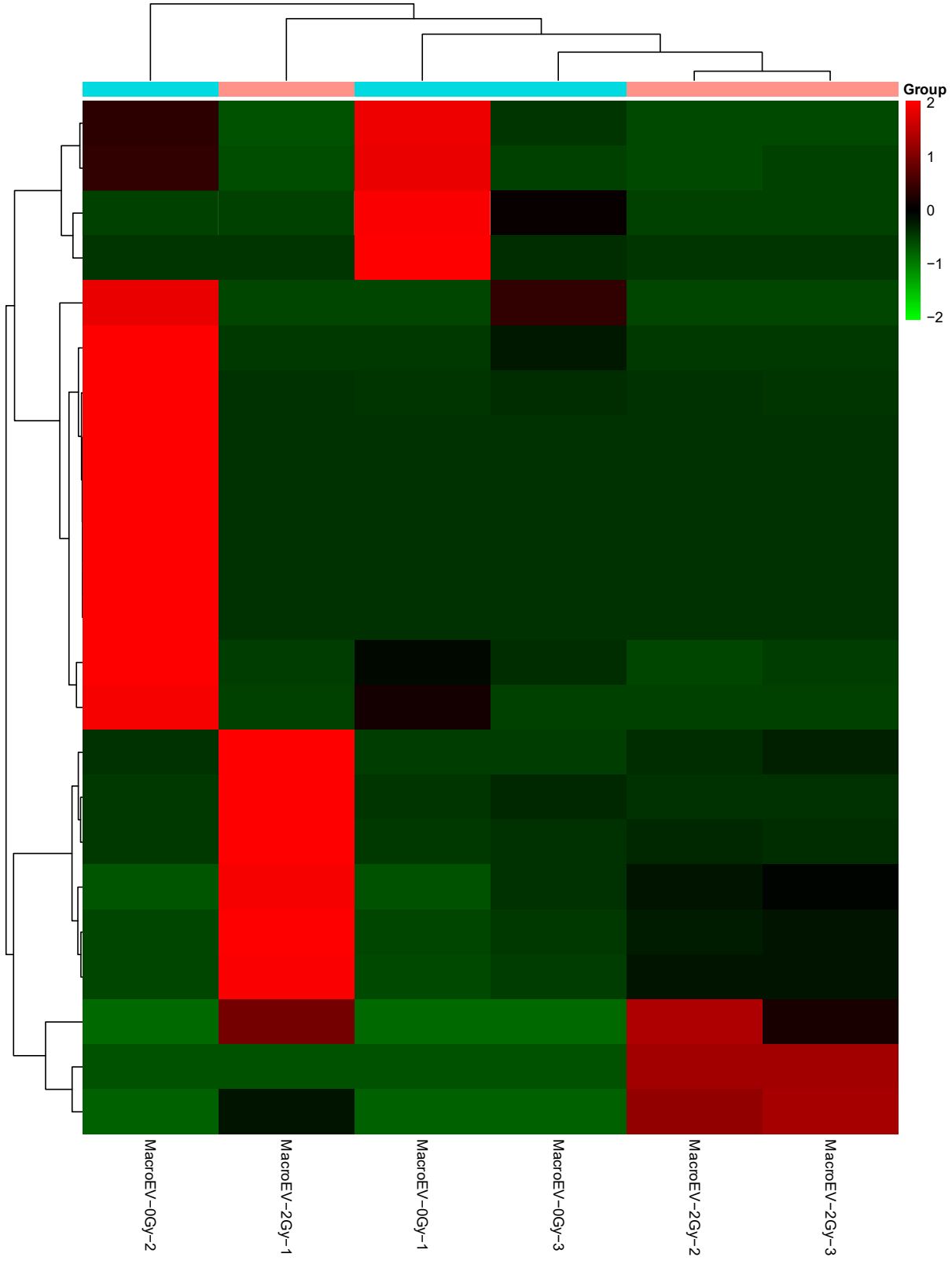


Figure 4.01: Irradiated and unirradiated murine BM-derived macrophage EV miRNA. As can be seen, there is intra-category variation with regards to this dataset, with differences being seen between samples of the same type.

miR-582-5p was tentatively identified in low clonal expansion mice vs sham exposed mice, reported in chapter 3. The 3p arm of miR-148b was also identified in this dataset. The rest of the miRNA are unique to this dataset, but as previously mentioned in chapter 3, miRNA overlap is not as important as targeted pathway overlap. As seen in the KEGG predicted pathways in figure 4.02, several pathways are found to be in common with both 48 hours-post exposure WT CBA mice and 12 months post exposure mice, in particular mice with high clonal expansion.

A common motif in 48 hours post exposure WT CBA mice, 12 months post exposure mCh/GFP mice, and finally BM-derived macrophages is the dysregulation of fatty acid biosynthesis and metabolism, with multiple pathways relating to fatty acids being affected, and lysine degradation. Multiple genes are targeted in lysine degradation: Phykpl, Aldh9a1, Kmt2c, Nsd1, Setd2, Dlst, Whsc11, Aldh3a2, Kmt2b, Plod2, Setd7, Suv420h1, Ehmt1, Aldh1b1, and Bbox1. Acute myeloid leukaemia is also predicted as a target pathway, with various genes being targeted (table 4.02). Of these, Jup is targeted by 2 miRNA, Sos1 by 3miRNA, and Nras by 2 miRNA. The Ribosomal protein S6 kinases (Rps6kb) are also targeted, as is the Sos family. The Rps6kb family is involved in the MAPK/ERK pathway, while Sos (Son of sevenless) interacts with Ras proteins for GDP to GTP phosphorylation. Rps6kb, Sos, Map2k, Runx, and the Pik gene family were all also targets of DE miRNA identified in high clonal expansion CBA mCh/GFP mice.

Table 4.02: miRNA-gene interactions in the KEGG database acute myeloid leukaemia pathway.

miRNA	Genes targeted
miR-7648-3p	Pml Rps6kb2
miR-582-5p	Runx1t1 Zbtb16
miR-465d-5p	Kras
miR-98-3p	Tcf712 Jup
miR-433-3p	Jup
miR-222-5p	Sos2 Map2k1 Runx1
miR-142a-5p	Kit
miR-7051-5p	Nras Sos1 Bad
miR-7655-3p	Runx1t1 Nras Sos1
miR-291b-3p	Stat3 Sos1
miR-764-3p	Pik3r5
miR-1298-5p	Rps6kb1 Pik3cb
miR-223-3p	Rps6kb1

Table 4.03: KEGG-predicted pathways associated with differentially expressed miRNA in 2Gy vs 0Gy BM-derived murine macrophages. Created using DIANATools miRPath v.3.

Pathways with upregulated miRNA	Pathways with downregulated miRNA
Axon guidance	ECM-receptor interaction
Signalling pathways (stem cell pluripotency)	GABAergic synapse
Transcriptional misregulation in cancer	Endocytosis
Thyroid hormone synthesis	N-glycan biosynthesis
Cytokine-cytokine receptor interaction	Proteoglycans in cancer
TGF-beta signalling pathway	Other types of O-glycan biosynthesis
Regulation of actin cytoskeleton	Glutamatergic synapse
Pathways in cancer	Glycosaminoglycan biosynthesis - chondroitin sulfate / dermatan sulfate
Lysine degradation	Hematopoietic cell lineage
ECM-receptor interaction	Axon guidance
FoxO signalling pathway	Pathways in cancer
Ras signalling pathway	cGMP-PKG signalling pathway
Chronic myeloid leukaemia	Apelin-signalling pathway
Acute myeloid leukaemia	Melanogenesis
MAPK signalling	FoxO signalling pathway
	Chronic myeloid leukaemia
	Acute myeloid leukaemia

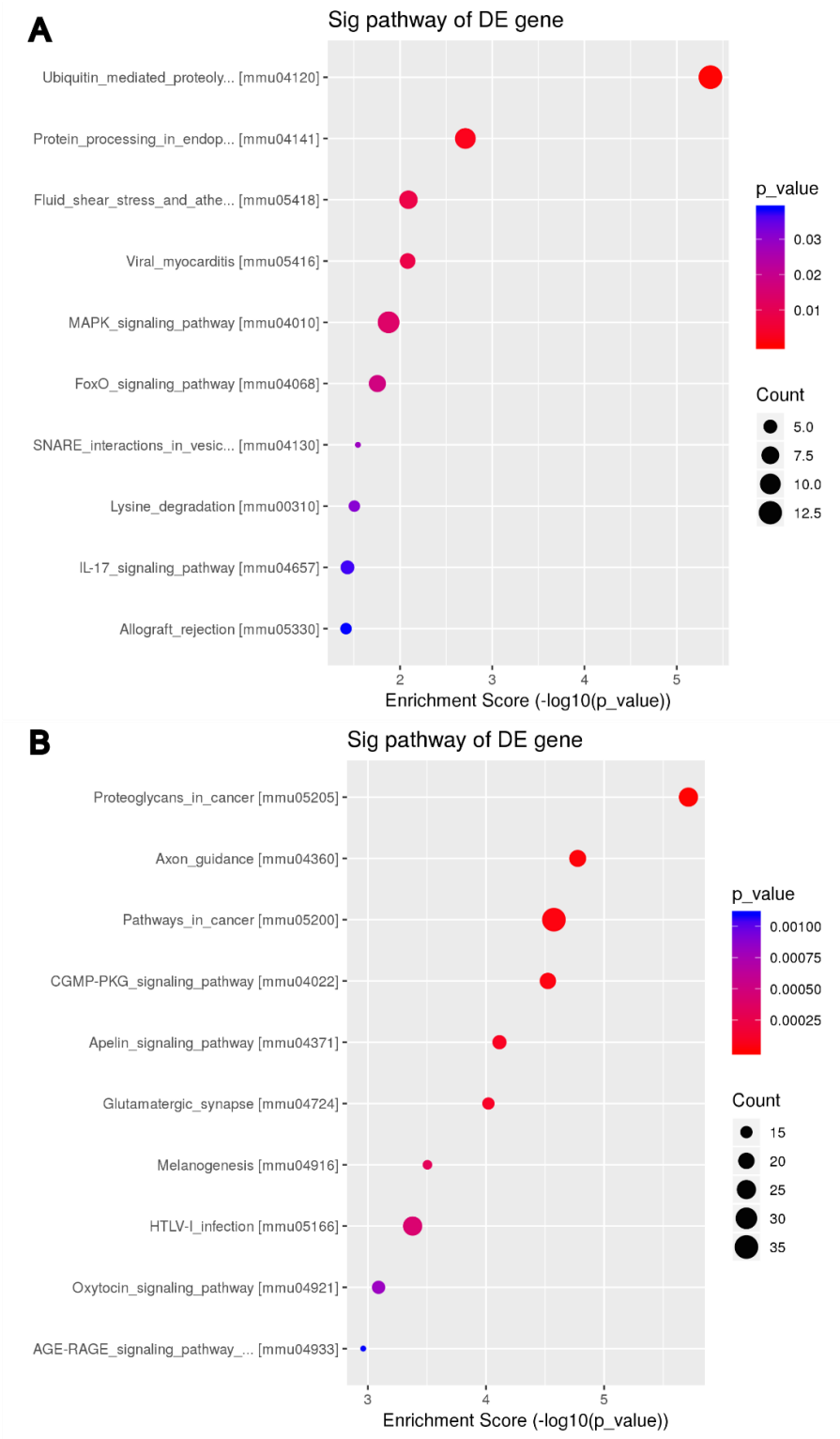


Figure 4.02: Significant pathways of differentially expressed genes (DE) in BM-derived macrophages. A: Pathways associated with gene targets of upregulated miRNA vs 0Gy control. B: Pathways associated with gene targets of donwregulated miRNA vs 0Gy control. Dot size indicates amount of targeted genes, not involved miRNAs.

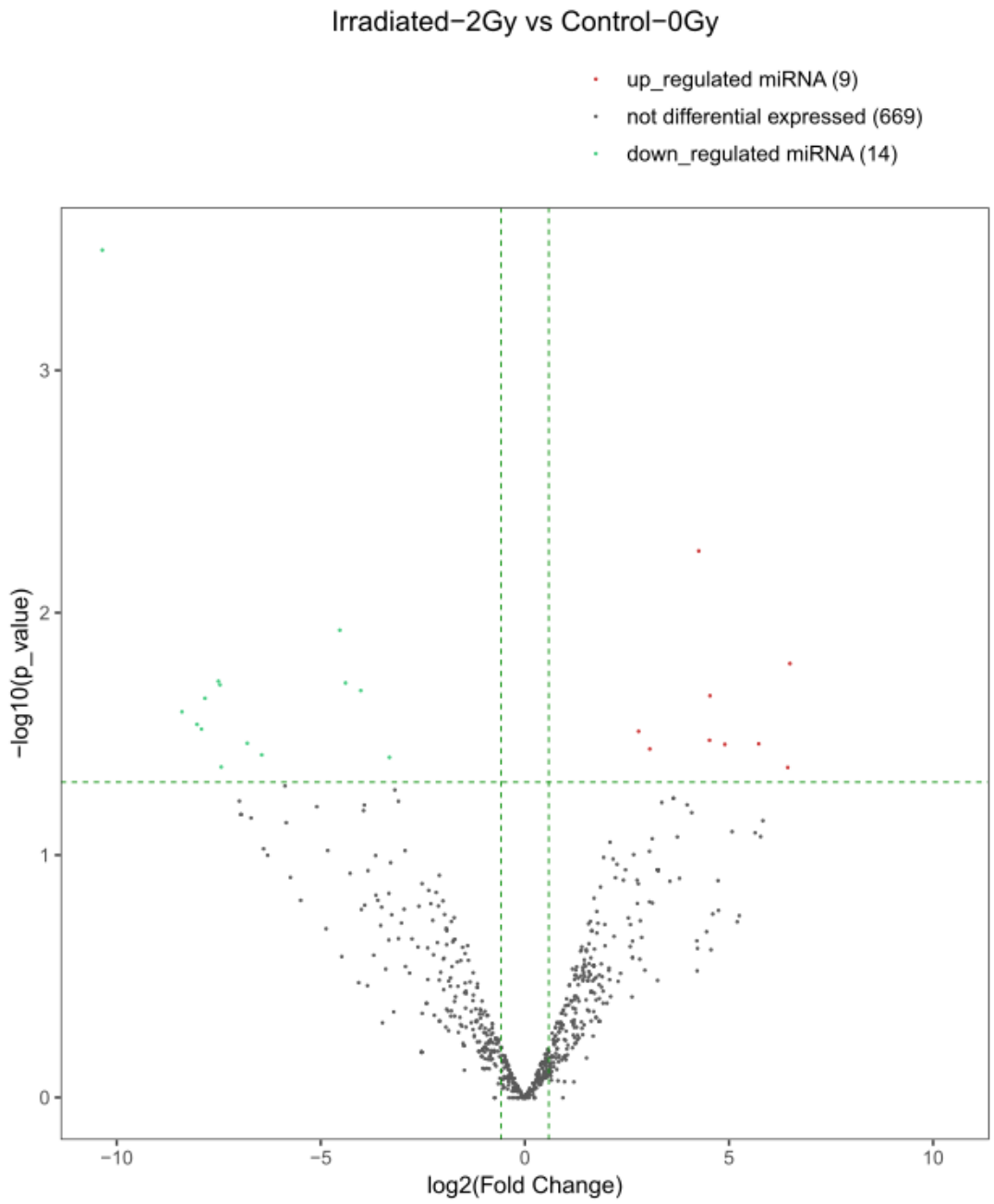


Figure 4.03: Volcano plot showing statistically significant DE miRNA and their fold changes with respect to 0Gy control in BM-derived macrophages.

In addition, over a hundred novel miRNA were found; however, pending experimental validation, and with their biological functions unknown, these remain the topic of focus for future work.

In summary, macrophages respond to radiation in a similar manner to mice with high clonal expansion and 48 hours post radiation exposure. The significant miRNA involved differ between both, but several key pathways are affected in all instances. These include, but are not limited to, ubiquitin-mediated proteolysis, protein processing in the ER, MAPK and FoxO signalling, fatty acid metabolism and biosynthesis dysregulation, and lysine degradation. Some of the most significant and highly involved pathways (table 4.02) were explicitly associated with cancers, such as MAPK signalling, FoxO signalling, proteoglycans in cancer, and pathways in cancer.

FoxO was found to be targeted by both up- and downregulated miRNAs, warranting further study to elucidate the gene targets involved. An overlap of 15 genes was identified when comparing predicted genetic target involvements in the up- and downregulated miRNA sets, as seen in figure 4.06. While regulatory interactions have not been experimentally validated in the downregulated miRNAs, 3 main points of interest are identified: mmu-miR-142a-5p, mmu-miR-291b-3p, and Sos1, which encodes for the guanidine nucleotide exchange factor Son of Sevenless 1 (Pierre *et al.,* 2011, Biochemical Pharmacology) and is a Ras protein interactor. Mmu-miR-142a is flagged due to its wide host of (experimentally validated) interactions, being a post-transcriptional inhibitor of 5/15 of the shared gene targets. Mmu-miR-291b does not have experimentally validated interactions, but also regulates a significant share of the shared genes (6/15). Sos1 is interesting due to the amount of predicted regulatory interactions it has, with a total of 5 regulatory interactions. Inhibition of Sos1 has been demonstrated to block Ras signalling activation (Hillig *et al.,* 2019, PNAS). Ras signalling has been demonstrated to increase radiation resistance (McKenna *et al.,* 2003, Oncogene). Ras signalling regulates normal tissue proliferation, survival, migration and differentiation via molecular switching, switching from an inactive state to an active state (GDP to GTP) (Weber & Caroll, 2021, American Journal of Pathology). While the regulatory interactions between mmu-miR-291b and its downregulated predicted coregulators, mmu-miR-7051, mmu-miR-3473g, and mmu-miR-7655 are unknown, we

hypothesize that these are all inhibition regulators that suppress the expression of Sos1 in normal tissue. Within normal tissue, macrophages regulate surrounding cell expression via export of Sos1-suppressing miRNA. Upon radiation injury, macrophages modify their EV-mediated intercellular signalling, now downregulating the Sos1-suppressor, thereby increasing Sos1 expression. Sos1 in turn activates Ras signalling, which promotes proliferation and plays a role in damage repair of the radiation injury. Given the high dose administered to the tissue (2Gy) and the significant level of apoptosis induced, it is likely that this response is dose dependent and we predict based on detection of cell death, prompting Ras-mediated proliferation to replace lost tissue.

Thus macrophages likely promote Sos1 expression post-radiation injury by minimizing their normal Sos1-suppressing EV signal. To experimentally validate this, the interplay of mmu-miR-291b and its coregulators and Sos1 should be examined, with rates of cell proliferation after injury being monitored vs induction of higher miR-291b (and coregulator) expression. It is possible that in a percentage of such cells, Sos1-mediated Ras activation may enhance the risk of Ras oncogene mutations or activate the Ras pathway in cells with DNA damage from the initial IR event, thus over time leading to the accumulation of cells with constitutive Ras-activation and leukaemogenesis. In the majority of cells, however, this is predicted to be a normal tissue response to repair radiation damage.

miR-142a inhibits five gene targets: S1pr1, Igf1, Tgfbr2, Ccng2 and Sgk1. Of these, Tgfbr2 was observed to be targeted in high clonal expansion mCh/GFP CBA mice, coding for TGF-β receptor II. Within the context of homeostatic bone marrow function, the TGF-β pathway plays an important role in lineage specification, especially in mesenchymal stem cells, stimulating osteoprogenitor proliferation and inhibiting terminal differentiation (Krambs *et al.,* 2020, PLoS One). The effect of TGF-β activation on both MSCs and HSCs remains controversial, with inhibition and promotion effects on progenitor population being observed, with one explanation for such a contradiction being a dose-dependent, biphasic regulatory effect (Farias *et al.,* 2018, Cytokine and Growth Factor Reviews). Macrophages

upregulate inhibition of Tgfbr2 post IR injury in their EV release profile. We hypothesize that *in vivo* these EVs are meant to be messengers to proximal MSCs and HSCs within the BM niche, given the role macrophages play in HSC and MSC regulation, especially in maintaining quiescence to prevent pool depletion (Sinder *et al.,* 2015, Journal of Bone and Mineral Research; Kaur *et al.,* 2017, Seminars in Cell & Developmental Biology). As part of radiation injury response, macrophages lower their suppression of TGF-β activation, allowing for increased MSC and HSC proliferation to replace dead and damaged bone tissue following radiation injury. The extent of TGF-β activation is likely dose dependent, and future experiments should repeat the same procedure used at a variety of different doses lower than 2Gy. Co-cultures of macrophages and HSCs/MSCs would also yield interesting information in terms of confirming macrophage/progenitor EV-mediated crosstalk. The proliferation-promoting function is supported by inhibition of Ccng2 (cyclin G2), an inhibitor of cell division (Huang *et al.,* 2019, Frontiers in Immunology), thereby strengthening the idea that macrophages respond to radiation injury by easing suppression of progenitor proliferation.

S1pr1 codes for sphingosine-1-phosphate receptor 1, necessary for the migration of immature B cells from BM into blood (Allende *et al.,* 2010, Journal of Experimental Medicine). Its targeting protein, sphingosine-1-phosphate (S1p) promotes osteoblast differentiation (Grewe *et al.,* 2022, Bone Research). A well-known and relatively common late effect of radiation treatment is bone fractures (Jeffrey Wiley Lab; Bartelstein *et al.,* 2021, Sarcoma; Ishikawa *et al.,* 2021, Japanese Journal of Radiology). Macrophages, as part of the short term IR damage response, appear to inhibit osteoblast differentiation in favour of promoting progenitor expansion. The duration of such suppression must be characterized, for it is possible that macrophages commence and mediate bone tissue remodelling by reallocation of resources from mineralized bone formation to prioritizing the functionality of the haematopoietic compartment. An extended duration of such remodelling may potentially explain fractures years later.

This hypothesis is supported by the inhibition of Igf-1 (insulin-like growth factor 1) by miR-142a-5p, abrogation of which decreases bone regeneration and formation (Wang *et al.,* 2023, PNAS).

The involvement of Sgk1 (serum and glucocortoid-regulated kinase 1) is more contentious, with research still elucidating its function with homeostatic maintenance of the bone marrow microenvironment. Current research focuses on Sgk1 dysregulation in a variety of disease states, rather than in normal, healthy tissue. Sgk1 is a significant regulatory protein, catalysing the phosphorylation of several proteins e.g. Foxo3a, β-catenin, Ndrg1, etc (Jang *et al.,* 2022, Frontiers in Pharmacology). Via phosphorylation of Foxo3a, Sgk1 is suggested to be an inhibitor of Foxo3a-induced apoptosis (*idem*). Given this, and macrophages upregulating the inhibition of Sgk1 translation in target cells post-IR, it is likely that macrophages post-IR inhibit antiapoptic function, thus indirectly promoting the completion of apoptosis to clear radiation-damaged cells, afterwards clearing the apoptosed cells.

In lysine degradation, a total of 7 miRNAs that were upregulated in EVs post-IR were identified, with only two genes being targeted by more than one miRNA: Kmt2c, targeted by miR-223-3p and miR-98-3p, and Setd2, targeted by miR-142a-5p and miR-148b-5p. While other metabolic pathways were involved, given the later direction of this research and a focus on fatty acid regulation and lysine degradation, this pathway was focused on. Setd2, a lysine methylase, is downregulated by miR-142a-5p according to Tarbase 7.0, although its regulation by miR-148b is unknown. Deletion of Setd2 in MSCs decreased osteoblast differentiation in favour of adipocyte differentiation (Wang *et al.,* 2018, PLoS Biology). Given the inhibition of S1pr1, Igf-1, and Setd2, therefore, it appears that macrophages post-IR reduce osteoblast differentiation in favour of adipocyte and progenitor expansion. Given the mode of action of Setd2 with lysine methylation, this provides a metabolic function link, with levels of free lysine as well as levels of Setd2 protein regulating functionality and promotion of osteoblast differentiation.

Direct regulation of Kmt2c by miR-223 and miR-98 is unknown, although miR-223 is a widely studied miRNA in a haematopoietic context (Favero *et al.,* 2021, Wiley Interdisciplinary Reviews). miR-223 is found to reduce pyroptosis in irradiated macrophages (Zhang *et al.,* 2023, International Immunopharmacology), reducing tissue inflammation following radiation. Kmt2c, a histone lysine methyltransferase (Reis *et al.,* 2023, Genes) is considered a myeloid tumour suppressor, with deletions thereof frequently found in AML and myelodysplastic syndrome. Deletions confer a competitive advantage to HSCs, enhancing murine stem cell self-renewal activity (Chen *et al.,* 2021, Cell Reports). Kmt2c is not deleted in the context of normal tissue reaction to IR injury, but is most likely downregulated by miR-223 and miR-98, promoting stem cell renewal.

miRNA regulate complex networks, with multiple gene targets that can vary depending on tissue-specific pathway expression. Based on this data, we hypothesize that macrophages communicate with MSCs and HSCs post-IR, with EV-shuttled miRNA sending signals that upregulate progenitor self-renewal and expansion while inhibiting osteoblast differentiation, prioritizing regeneration of the progenitor niche over osteoblast repair. Among other miRNAs, important miRNA for this regulation are miR-142a, which downregulates S1pr1, Igf1, Tgfbr2, Ccng2 and Sgk1 activity, in conjunction with miR-223 and miR-98, which are hypothesized to downregulate Kmt2c. Sos1 activation is hypothesized to be activated by a reduction in miRNA downregulation, triggering radiation repair pathways to be activated.

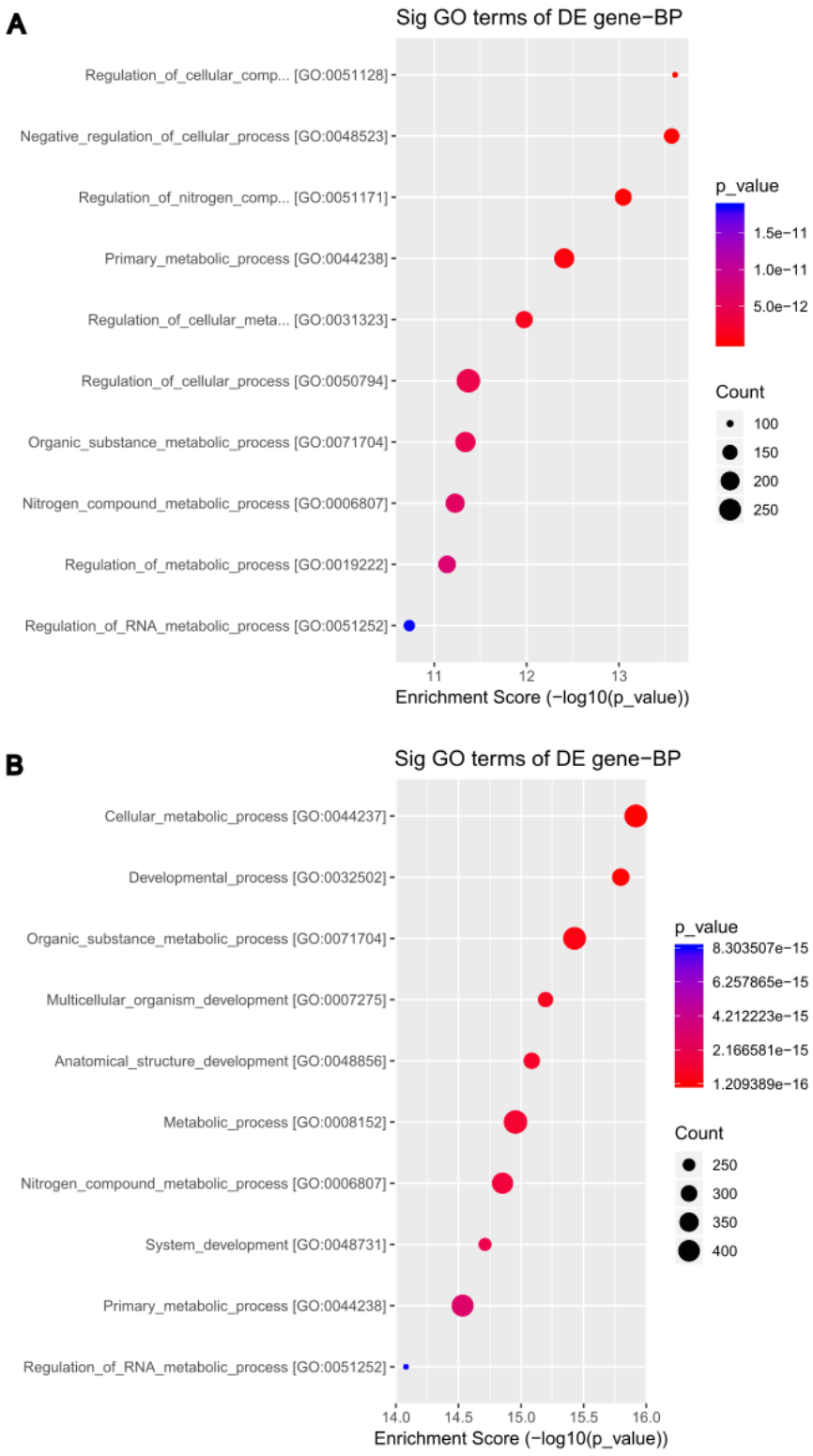


Figure 4.04: Significant pathways of differentially expressed genes (DE) in BM-derived Macrophages. A: Pathways associated with gene targets of upregulated miRNA vs 0Gy control. B: Pathways associated with gene targets of donwregulated miRNA vs 0Gy control. Dot size indicates amount of targeted genes, not involved miRNAs.

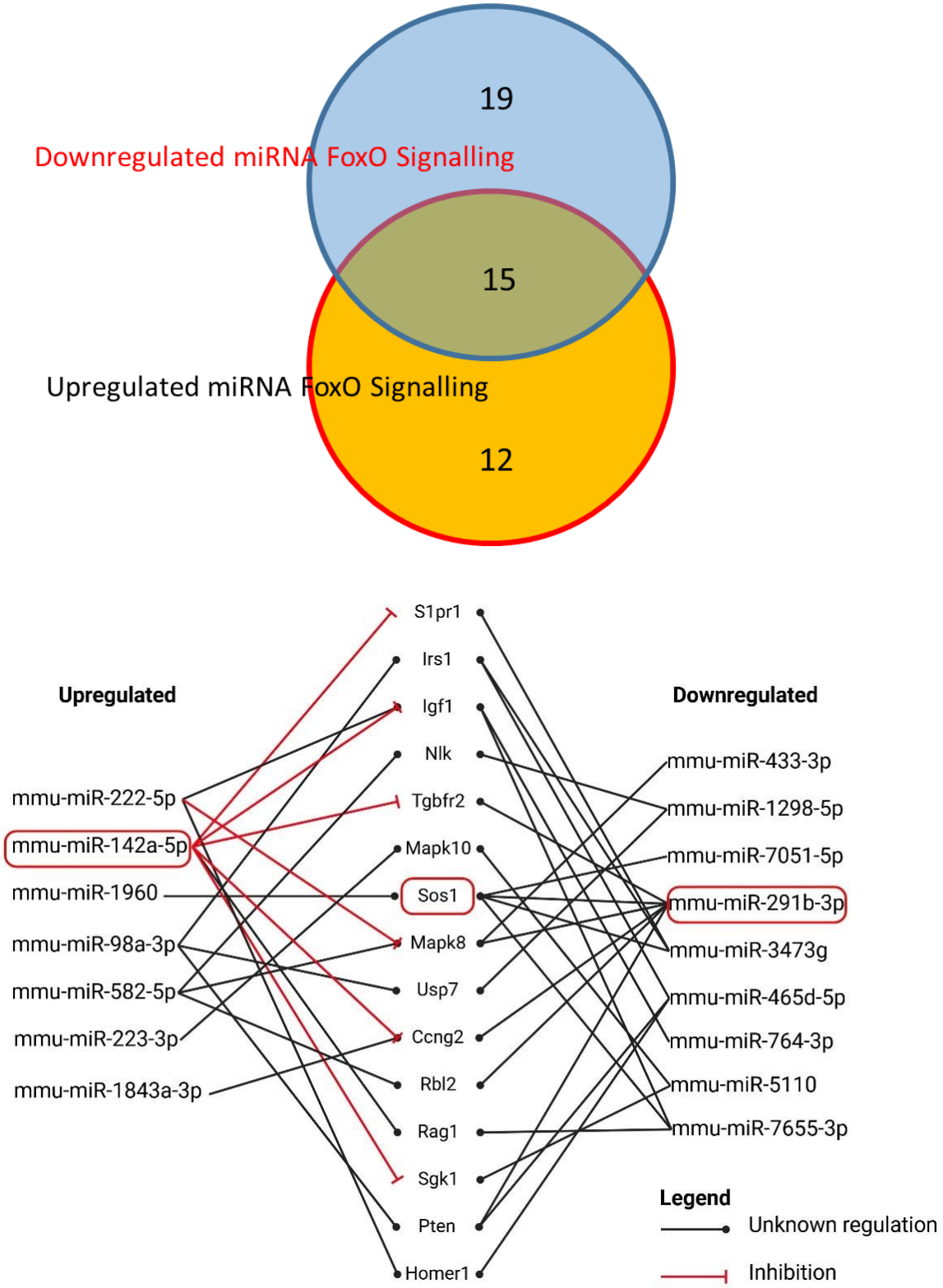


Figure 4.05: Gene target overlap between up- and downregulated miRNA gene targets of the FoxO pathway in BM-derived macrophages. Red boxes identify key points of interest due to the highest number of interactions. Numbers in the Venn diagram are separate; the outer number describes genes not in the intersection, and the number in the intersection describes overlapping genes, for which the pathways are given.

4.02 BM-derived mesenchymal stem cell (MSC) response to ionising radiation

Macrophages play an important role within the bone marrow, but are not a progenitor cell. To further elucidate the role of EV-shuttled miRNAs within the bone marrow in a radiation context, studying precursor cells was a necessary next step. The first of these precursor cells to be studied were MSCs, cultured directly from bone marrow, using the same CBA mCh/GFP colony as used for macrophages and later haematopoietic stem cells (HSCs). These were processed in an indentical fashion to macrophages, being irradiated at 2Gy and a control dose of 0Gy, EVs harvested, and then shipped to ArrayStar for further analysis. Just as before, FDR could not be calculated due to there only being one group per variable. Further repeats would allow for the calculation of a reliable FDR and further clarification of the data.

Table 4.04: Differentially regulated miRNAs in 2Gy vs 0Gy MSCs, and their suspected or confirmed biological interactions. Targeted genes are listed at a cut-off threshold of target score 95, as provided by TargetScan. miRNAs marked with * are miRNAs flagged as NOT being high confidence miRNAs.

Name	PValue	FDR	Predicted biological interactions
mmu-miR-128-3p	1.2e-02	N/A	Involved in multiple KEGG pathways, including but not limited to fatty acid biosynthesis & metabolism, FoxO signalling, lysine degradation, protein processing in the ER, Wnt signalling, TGF-beta signalling, transcriptional misregulation in cancer. GO categories include intracellular, cell differentiation, cell death, and response to stress, among others. Inhibits lymphoid progenitors from developing into progenitor B cells (Yang *et al.,* 2016, Oncotarget). Has significant potential as a blood-based liquid biopsy biomarker for childhood ALL (Rzepiel *et al.,* 2023, Molecular and Cellular Probes), as well as lung cancer (Pan *et al.,* 2018, Scientific Reports), overall found in multiple human malignancies (Budi *et al.,* 2022, Frontiers in Oncology).
mmu-miR-34a-5p	2.4e-02	N/A	Is one of the most well-characterized tumour suppressor miRNAs (Wang *et al.,* 2020, Journal of Cancer). Promotes DNA damage repair after ionising radiation (Zeng *et al.,* 2019, FASEB). Mediates drug resistance in AMLs and other cancers (Gabra & Salmena, 2017, Frontiers in Oncology; Bhise *et al.,* 2019, Genes).
mmu-miR-652-3p	2.4e-02	N/A	Upregulated in non-small cell lung cancer, promoting metastasis via Lgl1 targeting (Yang *et al.,* 2016, Oncotarget). High expression of this correlates with increased prostate recurrence (Nam *et al.,* 2018, Oncotarget). Expression is negatively correlated to pediatric ALL (Buhagiar *et al.,* 2020, Non-coding RNA Research).
mmu-miR-345-3p	3.6e-02	N/A	Involved in several different metabolic and biosynthesis pathways, e.g. Tryptophan, glycosaminoglycan, glyoxylate, and O-glycans (KEGG); predicted to be involved in histone deacetylation (GO). 5p arm regulates proliferation, cell cycle and apoptosis behaviour of AML cells via AKT2 (Ying *et al.,* 2019, Journal of Cellular Biochemistry). Upregulated in post-remission AML patients (Agha *et al.,* 2020, International Journal of Molecular Sciences).
mmu-miR-484*	3.7e-02	N/A	Targets various genes that have roles in inflammation, apoptosis and mitochondrial functions e.g. SMAD7, BCL2L13, and oncogenes e.g. VEGFB, MAP2, HNF1A, is frequently observed to have differential expression in cancers (Jia *et al.,* 2022, Frontiers in Oncology), downregulated by ionising radiation (Chaudhry *et al.,* 2013, Journal of Radiation Research).
mmu-miR-412-5p	3.9e-02	N/A	Identified as dysregulated in brain tissue in mice after proton irradiation (Khan *et al.,* 2013, Molecular and Cellular Biochemistry). Targets Xpo1 in angiogenesis in haemorrhoidal tissue (Wang *et al.,* 2019, Gene).
mmu-miR-339-5p	4.3e-02	N/A	Directly targets SOX4, inhibiting the proliferation of AML cells (Sun *et al.,* 2018, Molecular Medicine Reports). 3p arm significantly decreased in AML (Liu *et al.,* 2019, Journal of Hematology & Oncology). Increases radiosensitivity of lung cancer cells via targeting Cdc25A (Luo *et al.,* 2019, Oncogene). Is inducible by IR (Wang *et al.,* 2018, Medical Science Monitor).
mmu-miR-23a-5p	4.7e-02	N/A	Stromal cells downregulate miR-23a-5p to activate protective autophagy in AML (Ganesan *et al.,* 2019, Nature Cell Death & Disease).

A total of 8 miRNAs were identified as differentially expressed in MSCs. miR-345-3p, miR-412-5p, miR-339-5p, and miR-128-3p were upregulated. miR-23a-5p, miR-34a-5p, miR-484 and miR-652-3p are downregulated. Of these, 2 miRNA were found in other datasets: miR-128-3p was found in high clonal expansion CBA mCh/GFP mice, while the 5p arm of miR-345 was identified in the same. Unlike macrophages, the distinction between 0Gy and 2Gy-irradiated murine BM-derived MSCs (figure 4.03) was fairly clear-cut, with a clear difference in differential expression that was consistent within a sample type group.

While not explicitly mentioned as part of the KEGG-predicted pathways, multiple miRNAs have been found in the literature to be explicitly associated with carcinogenesis or AML specifically, such as miR-34a, miR-345, miR-23a, and miR-339, as seen in table 4.04. Multiple pathways within the KEGG predictions were also found in common with other datasets, such as lysine degradation, FoxO signalling, Rap1 signalling, proteoglycans in cancer, MAPK signalling, and fatty acid biosynthesis and metabolism. Various carcinomas are also present; as seen in table 4.04, several of these miRNAs play a wide-ranging role in various different cancers and tissues.

In the common pathway lysine degradation, the following genes are targeted: Hadha, Kmt2c, Nsd1, Setd2, Colgalt1, Whsc1, Suv39h1, Aass, Whsc11, Aldh3a2, Ehhadh, Setd7, Colgalt2, and Dot11. Kmt2c was also targeted in macrophages and high clonal expansion CBA mCh/GFP mice, while Aldh3a2 family members Aldh9a1 and Aldh3a1 were similarly targeted. Within fatty acid biosynthesis, a more limited number of genes are affected, with Fasn, Oxsm and Acs11 being targeted by miRNAs. In particular, miR-484 seems to be an important regulator of multiple different fatty acid pathways, being at the nexus of fatty acid biosynthesis and metabolism, steroid biosynthesis, bile acid biosynthesis, and fatty acid degradation.

The proteoglycans in cancer pathway also features a plethora of genes, being directly targeted by 5 out of 8 miRNA (table 4.05).

Table 4.05: miRNA-gene interactions in the KEGG database proteoglycans in cancer pathway.

miRNA	Genes targeted		
miR-128-3p	Mapk14 Pik3r1 Pdpk1 Ank2 Hbegf	Ank3 Sos1 Itgb1 Ddx5 Grb2	Wnt3a Met Ppp1cc Itga5 Egfr
miR-345-3p	Pdpk1		Itgav
miR-484	Pik3r1 Flnb Igfl Itpr2	Ppp1r12c Fn1 Erbb3 Ctsl	Hcls1 Sdc4 Fzd5
miR-339-5p	Ddx5 Erbb4		Tfap4 Sos1
miR-34a-5p	Map2k1 4930544G11Rik		Met Rras

Some of these genes are found in common with the acute myeloid leukaemia pathway, such as the Pik3r family of genes as well as Sos1. Also of note is the presence of Rras, an oncogene similar to Kras, that has also previously been associated with the development of acute myeloid leukaemia (Flex *et al.,* 2014, Human Molecular Genetics).

Several of the pathways associated with downregulated DE miRNA in BM MSCs were all cancer-related (table 4.06): Rap1 signalling which is known to be active in many cancers (Looi *et al.,* 2020, Biomedicines), MAPK signalling, and Ras signalling. This was repeated in downregulated DE miRNA. PI3k-Akt signalling which is often observed as being aberrant in almost all human cancers (Yang *et al.,* 2019, BMC Molecular Cancer), choline metabolism in cancer, and the Ras and Rap1 signalling pathways once more. These pathways not only were highly significant, but also had multiple genes being targeted within that pathway. This, similar to WT CBA, demonstrates that radiation injury healing and cancer survival share similar pathways and survival strategies.

As with macrophages, novel miRNA were identified, with 544 novel miRNA being identified during sequencing. However, as no biological functional data is available for this, they will not be discussed until further functional assays can be performed, or their existence can be validated.

To further study the gene targeting and EV-mediated miRNA regulation response post IR in BM MSCs, known gene involvement was compared in signalling networks targeted by upregulated miRNA as well as downregulated miRNA. In downregulated miRNA, the Notch signalling network did not have any gene targets in common with any other signalling pathway (see Appendix figure 4.01A). Gene targets found to be central to two or more signalling pathways in both conditions were then compared for intersections as well, to determine if any genes were targeted by both up- and downregulated miRNA.

Among upregulated miRNA, only one miRNA was predicted to have statistically significant gene targets among signalling pathways. Graphing the two signalling pathways as well as haematopoietic cell lineage (to verify if the same gene target controlled lineage commitment), a single gene target common to GnRH and FoxO was identified, Sos1.

Downregulated miRNA exhibited a much more complex network of gene targets and involved pathways. The intersections between MAPK, Rap1, FoxO, GnRH, and Ras were graphed. A total of 14 genes were found to be common to 3 or more signalling pathways, and of these, Sos1 was found to be commonly regulated by both up- and downregulated miRNA. Of these 14, 12 were regulated by only two miRNA, miR-34a-5p and miR-128-3p, regulating 4 and 8 gene targets respectively. Of these, miR-128-3p had the most experimentally validated regulatory interactions, downregulating Mapk14, Egfr, Grb2, Pik3r1, Insr, and Sos1, and has unknown interactions with Fgl4 and Rap1b. Unlike in macrophages, where every common gene target was regulated by at least two miRNAs, all gene targets were regulated by only 1 miRNA with the exception of Sos1.

When comparing intersection genes found in macrophages to intersection genes identified in mesenchymal stem cells, only one gene was found in common, Sos1, suggesting that post-IR response in both macrophage and mesenchymal stem cell signalling has a conserved element of Sos1 regulation.

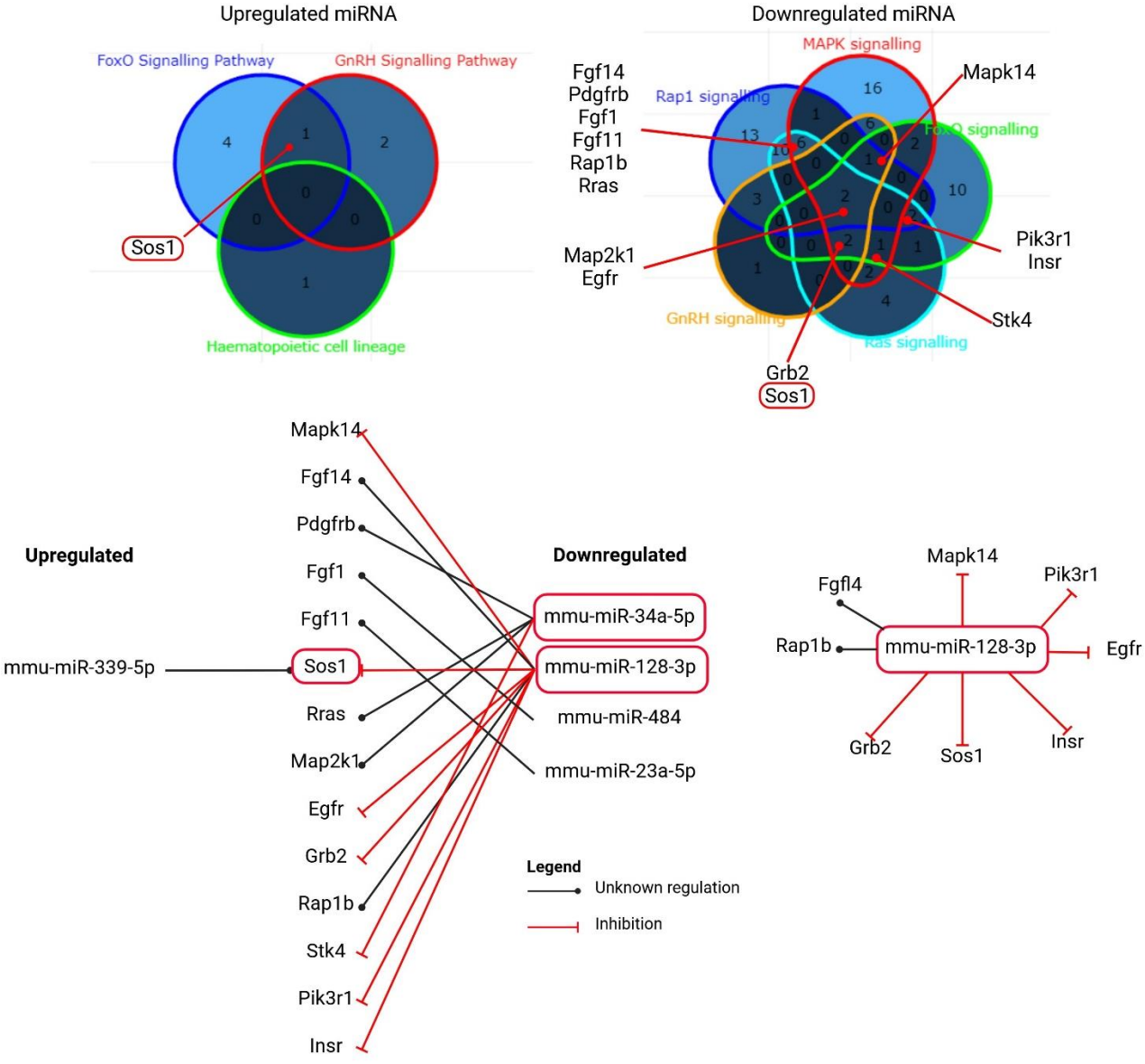


Figure 4.06: BM mesenchymal stem cell signalling network gene target overlap and regulating miRNA. Numbers in the Venn diagram are separate; the outer number describes genes not in the intersection, and the number in the intersection describes overlapping genes, for which the pathways are given.

All other gene targets were different in these conserved, commonly targeted genes. The approach of selecting only commonly represented genes was chosen to filter for targets most likely to be present *in vivo* as an interactor, based on their common representation in

multiple networks, and their importance as nexus coordinators operating along more than one pathway, making them the most interesting subjects for study.

The main difference between MSC and macrophage post-IR response in the conserved Sos1 element appears to be extent and robustness of activation. miR-128-3p is downregulated, thereby allowing for more Sos1 transcript translation to occur- likely balanced by miR-339-5p regulation. In macrophages however, no less than four miRNA regulators are downregulated and only one is upregulated, with their activity hypothesized to be post-transcriptionally inhibiting Sos1 expression. Macrophages are likely to be the main source of Sos1 activity suppression in the bone marrow microenvironment, with MSC lifting of inhibition via miR-128-3p downregulation post-IR being a complementary, but not driving contribution to the tissue-wide activation of Sos1.

Other targets of miR-128-3p include Mapk14, Pik3r1, Egfr, Insr, Grb2, Rap1b, and Fgf14.

Mapk14 is also known as p38α and has been demonstrated to be critical in erythropoiesis (Geest & Coffer, 2009, Journal of Leukocyte Biology) as well as stimulating BM adipogenesis in MSCs (Wang *et al.,* 2022, Stem Cells). Inhibition of the p38MAPK pathway was also found to enhance neutrophil development. *In vivo,* MSCs regulate HSC homeostasis via direct cell contact (Crippa *et al.,* 2021, Frontiers in Cell Development Biology) and exhibit cross-talk with macrophages, mainly via cell-cell contact but also by EV secretion (Lu *et al.,* 2021, Frontiers in Cell Development Biology). By downregulating a significant Mapk14 inhibitor, MSCs are promoting erythropoietic and adipogenic expansion in HSCs. In macrophages, MAPK14 regulates M1 polarization and ferroptosis, with downregulation of MAPK14 attenuating ferroptotic activity and inflammatory cytokine levels. MSCs likely signal for the activation of inflammatory activity and an increase in ferroptosis mediated by their macrophage targets via activation of MAPK14, mediated by downregulation of miR-128-3p.

Deletion of Egfr in mice resulted in a bone marrow phenotype with less mesenchymal stem cells and other progenitor types, along with a reduction in osteoblast number (Zhang *et al.,* 2011, Journal of Bone and Mineral Research). Downregulation of Egfr inhibition may thus contribute to MSC and HSC maintenance, as well as promote osteoblast differentiation. This latter signal is opposite to that exhibited by macrophages, which send anti-osteoblastic differentiation signals after IR exposure. This pro-maintenance signal secreted by MSCs is further supported by the activation of Grb2. Grb2 is found to be expressed in HSCs and (to a lesser extent) other progenitors, and while not modulating quiescence, was found to play a major role in proliferation and cycling of progenitors (Frelin *et al.,* 2017, Biochimica et Biophysica Acta), with negative effects of Grb2 being seen immediately in short-term, highly proliferative progenitor cells vs long term quiescent ones. MSCs may thus contribute to the maintenance and proliferation of HSCs and progenitors, along with macrophages which secrete the same signal post-IR.

Unlike macrophages, MSCs also downregulate miRNA that regulate the Notch signalling pathway. Of the four downregulated miRNA, three are predicted to target the Notch pathway: miR-34a, miR-484, and miR-128, demonstrating miR-34a and miR-128's central role in signalling pathway control considering their involvement in multiple signalling pathways. miR-128-3p and miR-34a downregulate Notch1 expression. By downregulating Notch1 inhibitors, MSCs shift their EV secretion profile post-IR to favour the activation of Notch signalling, which is important for mesenchymal stem cell maintenance by suppression of osteoblast differentiation (Hilton *et al.,* 2008, Nature).

MSCs therefore shift their post-IR EV profile from one that inhibits the expression of Sos1, promoting progenitor proliferation and damage repair, and also serve to polarize macrophages, promoting M1 polarization and a pro-inflammatory profile as well as promoting ferroptosis. Maintenance of progenitors mediated by EVs also signal for a reduction in osteoblast differentiation, although unlike macrophages EVs lifting of Egfr inhibition promotes osteoblast differentiation, suggesting a minor counterbalancing signal.

Unlike macrophages, MSCs trigger the Notch pathway, most likely signalling to other proximal MSCs to encourage their own self renewal and proliferation. Overall, both cell types upregulate progenitor proliferation and maintenance as part of post-IR response.

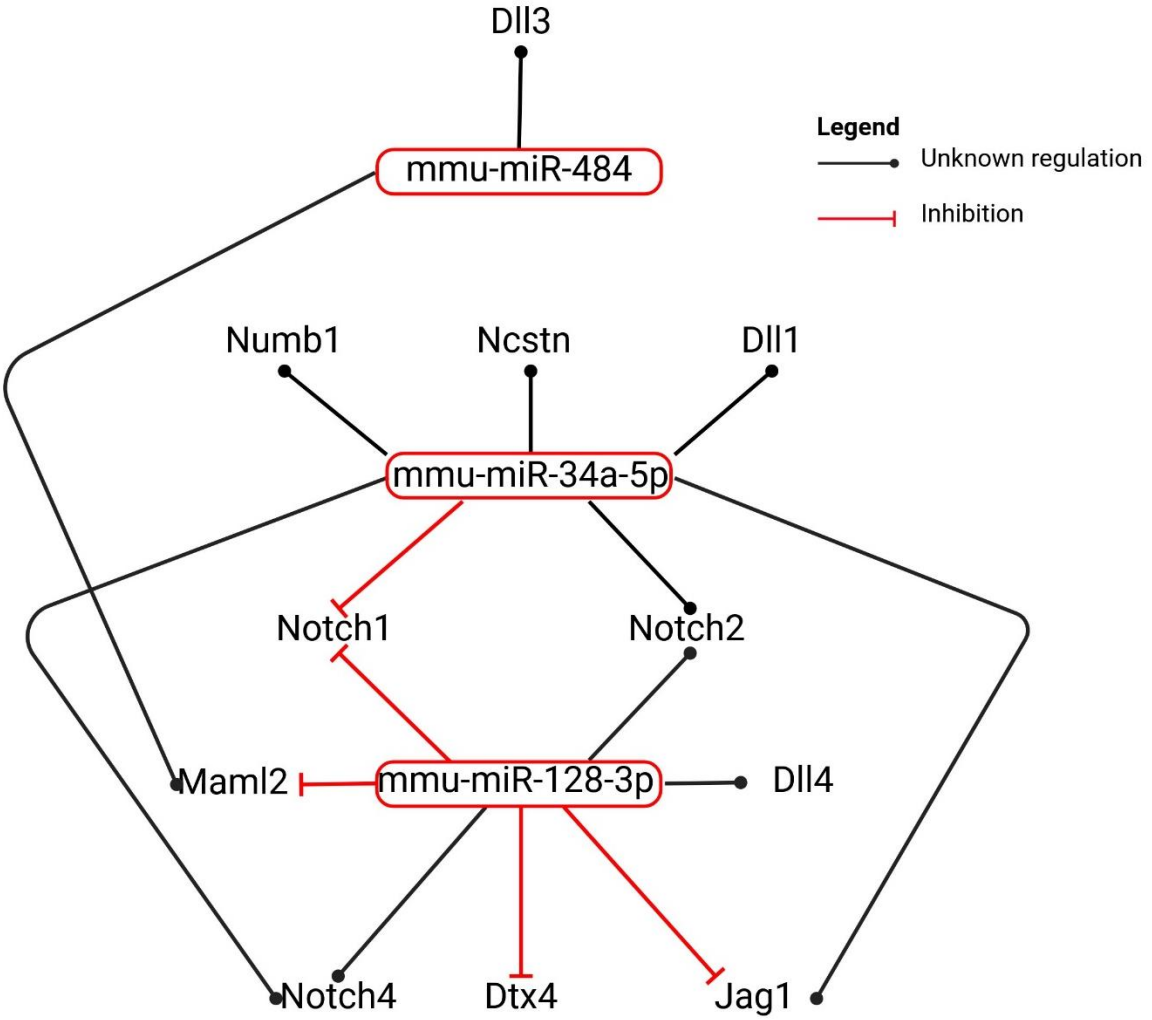


Figure 4.07: Notch signalling pathway interactome with downregulated miRNA in BM-derived mesenchymal stem cells. Created with Biorender.com.

On a metabolic pathway level, genetic targets on the lysine pathway were targeted by downregulated miRNA transcripts, suggesting an activation signal unlike in macrophages. Kmt2c is inhibited by miR-128-3p, and unlike in macrophages, where the inhibiting miRNA is upregulated, it is downregulated in MSCs, suggesting that MSCs secrete a pro-Kmt2c activation signal. Kmt2c downregulation promotes stem cell self-renewal, thereby making MSCs counter macrophage signalling in this regard, likely to balance out pro-self-renewal signalling and apply a level of negative control to prevent unchecked proliferation. Setd2 is

also inhibited by miR-128-3p, suggesting activation of Setd2 contrary to downregulation in macrophages. Setd2 upregulation promotes osteoblast formation, again demonstrating a balancing signal profile that partially counters, rather than reinforcing, signals secreted by macrophages.

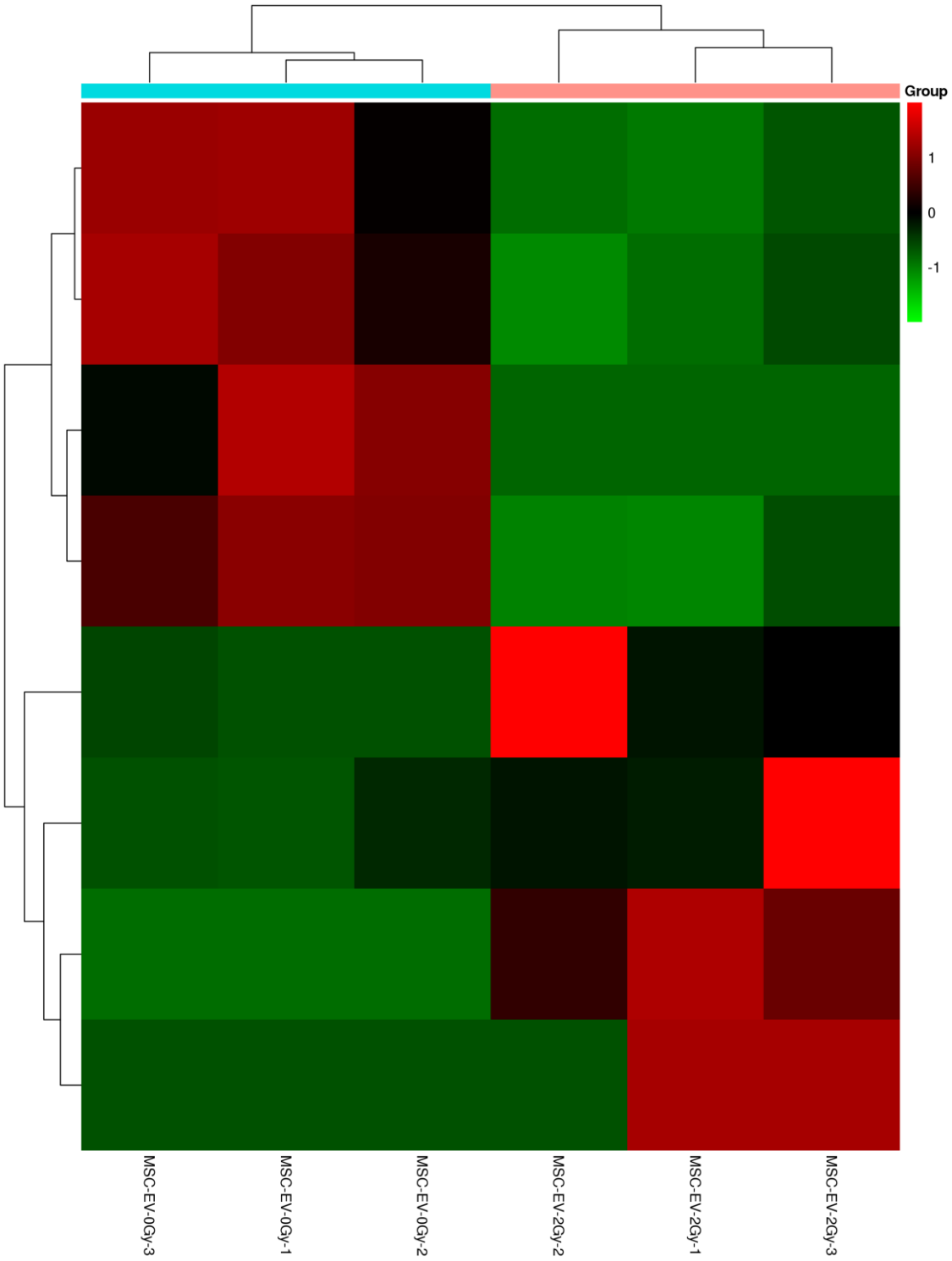


Figure 4.07: Irradiated and unirradiated BM-derived MSC EV miRNA. As can be seen, the two sets are clearly distinct from one another.

Table 4.06: KEGG-predicted pathways associated with differentially expressed miRNA in 2Gy vs 0Gy BM-derived murine mesenchymal stem cells. Created using DIANATools miRPath v.3.

Pathways with upregulated miRNA	Pathways with downregulated miRNA
Glycosaminoglycan degradation	Other types of O-glycan biosynthesis
Fatty acid elongation	Rap1 signalling pathway
Fatty acid metabolism	Lysine degradation
FoxO signalling pathway	Fatty acid elongation
Chronic myeloid leukaemia	Phosphatidyl inositol signalling system
Alanine, aspartate and glutamine metabolism	Thyroid hormone signalling pathway
Spliceosome	MAPK signalling pathway
GnRH signalling pathway	FoxO signalling pathway
Cell adhesion molecules	Pathways in cancer
Renal cell carcinoma	Vitamin B6 metabolism
Fatty acid degradation	Ras signalling pathway
Haematopoietic cell lineage	Notch signalling pathway
Renal cell carcinoma	GnRH signalling pathway
	Choline metabolism in cancer

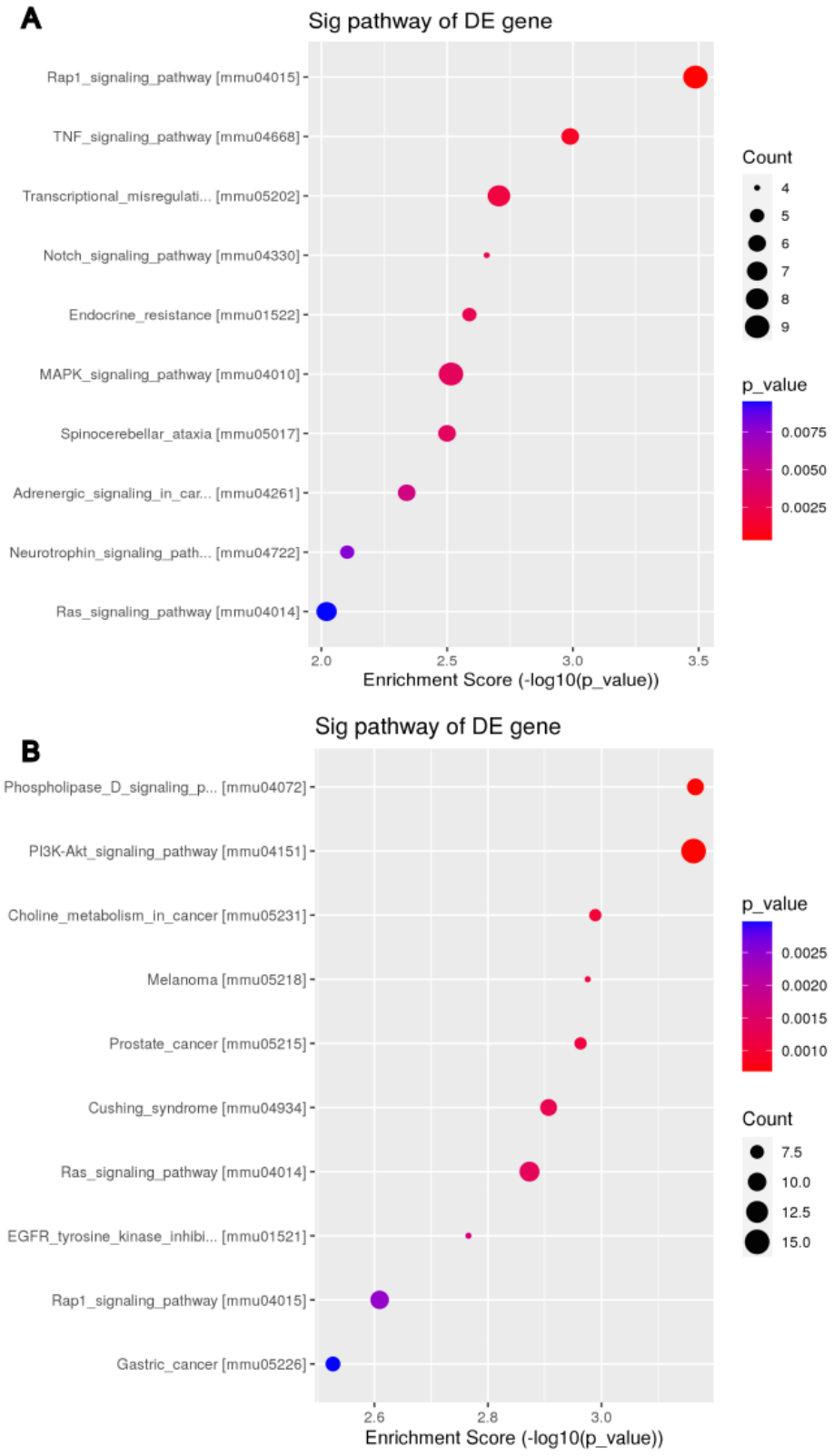


Figure 4.07: Significant pathways of differentially expressed genes (DE) in BM-derived MSCs. A: Pathways associated with gene targets of upregulated miRNA vs 0Gy control. B: Pathways associated with gene targets of donwregulated miRNA vs 0Gy control.

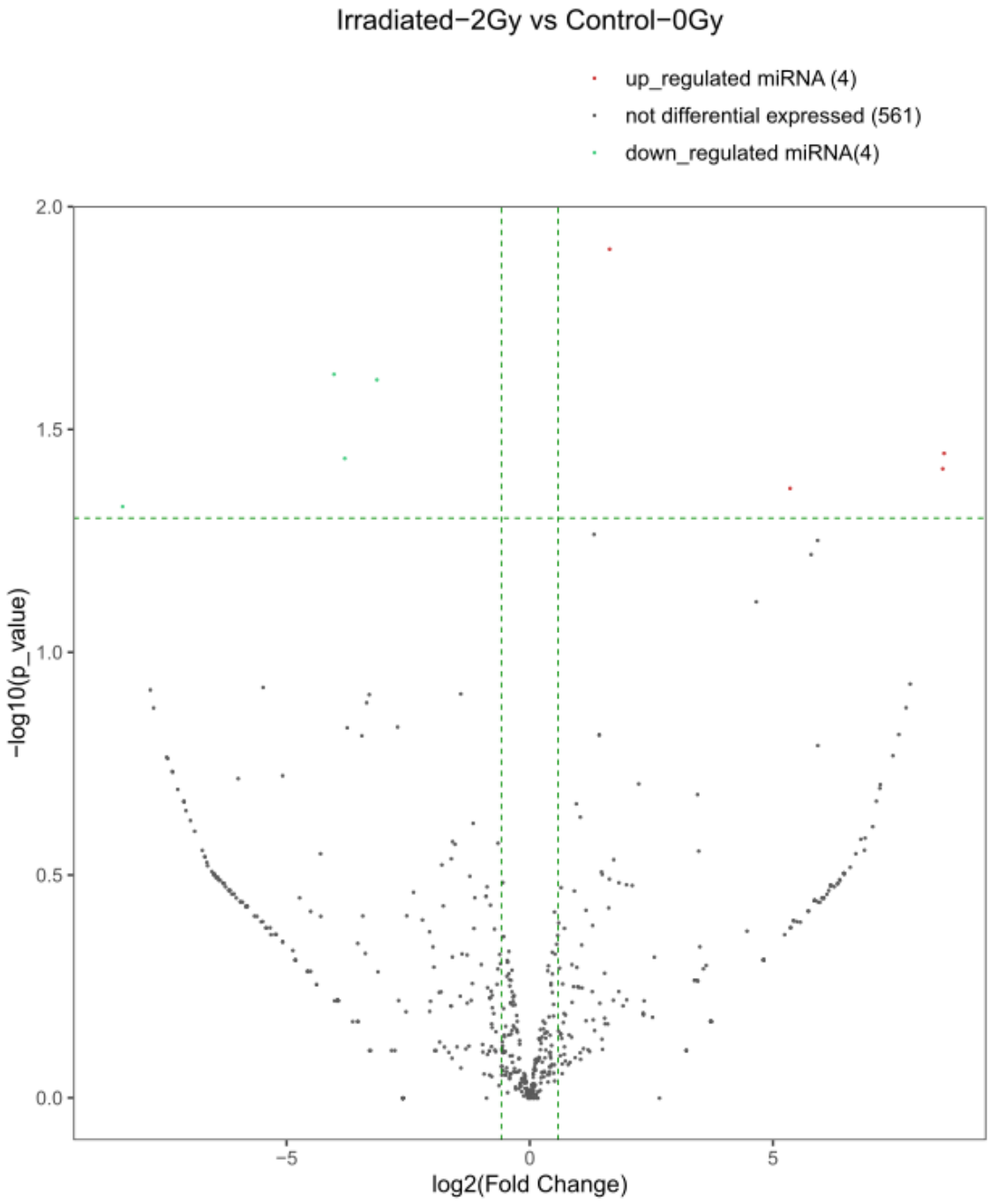


Figure 4.08: Volcano plot showing statistically significant DE miRNA and their fold changes with respect to 0Gy control in BM-derived macrophages.

In addition to KEGG-predicted pathways, Gene Ontology (GO) is a useful way to break down and analyze where the majority of pathways are categorized, facilitating cursorial analysis by demonstrating what biological functions are most impacted.

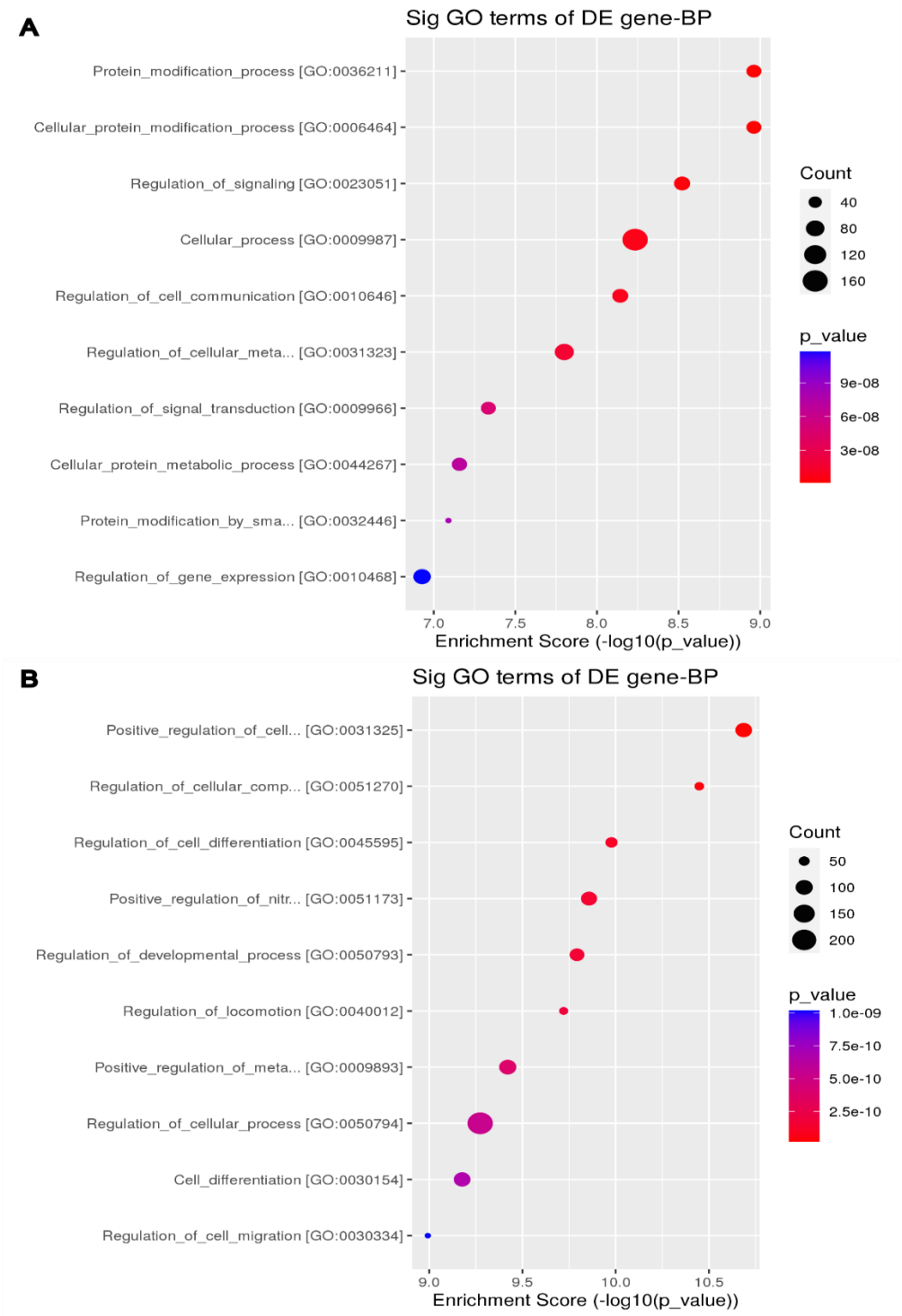


Figure 4.09: Gene Ontology (GO) terms for DE miRNA gene targets in MSCs. A: Pathways associated with upregulated miRNA. B: Pathways associated with downregulated miRNA. In A, GO:0031323 is regulation of cellular metabolic processes, GO:0032446 is protein modification by small protein conjugation e.g ubiquitination. In B, GO:0031325 is positive regulation of cellular metabolic processes, GO:0051173 is positive regulation of nitrogen compound metabolic process, and GO:0009893 is positive regulation of metabolic process.

Within the set of GO pathways targeted by upregulated DE miRNA, the majority of them impact signalling/communication and protein modification and metabolism by the cell. With downregulated DE miRNA, instead there appears to be mostly metabolic pathway involvement, with some cell migration and differentiation being represented as well. The GO categories therefore suggest that the upregulated DE miRNA and downregulated DE miRNA target and are involved in relatively distinct cellular processes, rather than having significant overlap; as seen with the KEGG pathways which do suggest overlap, this may mean that different parts of the same pathway, which are inherently more closely associated with certain functions over others, are targeted.

4.03 Chromosomal distributions of DE miRNA in BM macrophages and MSCs

As was done with BM-EVs, we attempted to discern whether there was clustering behaviour in DE miRNAs or if they were more closely associated with certain chromosomes over others, which would suggest a radiosusceptibility of these chromosomal regions.

Table 4.07: Genomic locations of differentially regulated miRNA across murine data sets, sourced from miRBase

miRNA	Location on chromosome
48 hours post IR macrophages	
mmu-miR-222-5p	chrX: 19146893-19146971
mmu-miR-1960-5p	chr5: 30170739-30170816
mmu-miR-98-3p	chrX: 151913214-151913321
mmu-miR-1843a-3p	chr12: 80391613-80391677
mmu-miR-582-5p	chr13: 109324744-109324824
mmu-miR-148b-5p	chr15: 103285125-103285221
mmu-miR-223-3p	chrX: 96242817-96242926
mmu-miR-150-5p	chr7: 45121757-45121821
mmu-miR-142a-5p	chr11: 87756864-87756927
mmu-miR-1298-5p	chrX: 147064905-147065002
mmu-miR-291b-3p	chr7: 3219482-3219560
mmu-miR-3473g-5p	chr2: 126902250-126902385
mmu-miR-433a-3p	chr1: 23272269-23272339
mmu-miR-465d-5p	chrX: 66822656-66822713
mmu-miR-5100-5p	chr11: 60728663-60728726
mmu-miR-5106-5p	chr4: 44221195-44221267
mmu-miR-5108-5p	chr10: 61774737-61774821
mmu-miR-5110-5p	chr11: 85760616-85760702
mmu-miR-5112-5p	chr18: 82720281-82720340
mmu-miR-7051-5p	chr7: 43457497-43457569
mmu-miR-764-3p	chrX: 147002259-147002366
mmu-miR-7648-3p	chr15: 90224360-90224412
mmu-miR-7655-3p	chr2: 18057846-18057903
48 hours post IR MSCs	
mmu-miR-128-3p	chr1: 128202361-128202430
mmu-miR-34a-5p	chr4: 150068454-150068555
mmu-miR-652-3p	chrX: 142739000-142739097
mmu-miR-345-3p	chr12: 108836973-108837068
mmu-miR-484	chr16: 14159626-14159692
mmu-miR-412-5p	chr12: 109743289-109743368
mmu-miR-339-5p	chr5: 139369650-139369745
mmu-miR-23a-5p	chr8: 84208518-84208592

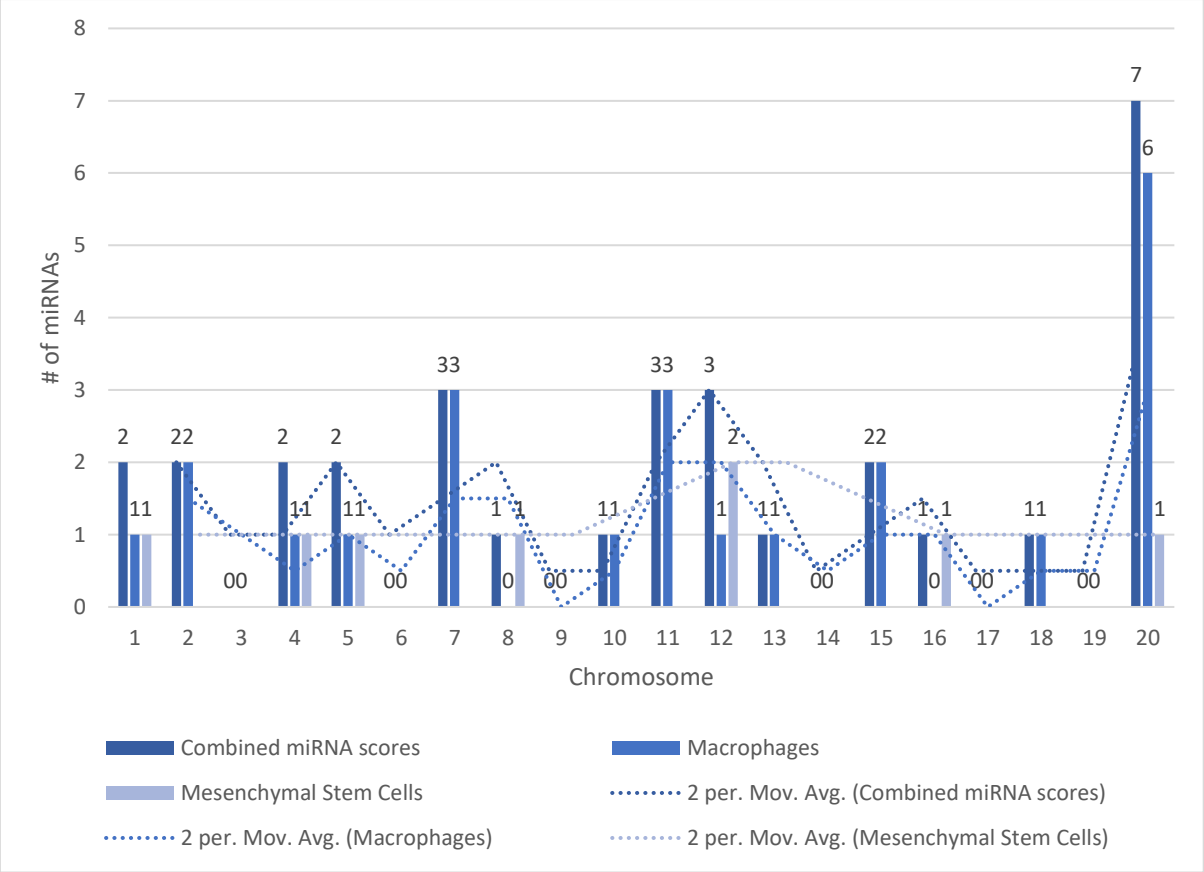


Figure 4.10: Number of miRNAs per chromosome as combined score, in macrophages, and mesenchymal stem cells. Chromosome 20=X chromosome.

Due to the small number of DE miRNA in BM MSCs, it is difficult to discern whether or not a significant clustering occurs. In macrophages, however, the majority of DE miRNA can be found on chromosome X. Chromosomes 14, 17 and 19 were not affected in this dataset or total murine BM, whether it be 12 months post IR or 48 hours post IR, suggesting that the miRNA loci located on these chromosomes are either not involved in radiation response, or somehow radioresistant and are not differentially regulated or induced by IR.

In macrophages, miR-1298 and miR-764, both differentially regulated, are found in regions of chromosome X that are in close proximity. Other examples in macrophages of proximal miRNAs are miR-150 and miR-7051 on chromosome 7, and miR-142a and mirR-5110 on chromosome 11. Within mesenchymal stem cells, miR-345 and miR-412 are also in close proximity to one another.

4.04 Discussion and implications

Macrophages and BM-derived MSCs demonstrated a wealth of miRNA information. Multiple miRNAs in both datasets were found to be explicitly associated with AML or closely related conditions; e.g. miR-222, miR-98, miR-148b, miR-223, miR-150 and others were found in the literature to be involved in AML disease progression or establishment, while in MSCs miR-34a, miR-339, and miR-23a were explicitly established to be involved in AML, with another miRNA, miR-128, potentially being a potent biomarker for childhood ALL. Children tend to develop ALL rather than AML, meaning that miR-128 still has potential to play an important role in AML development.

In the majority of miRNA, these were unique to both datasets; however, miR-128 and the alternate variant of miR-345 were identified in high clonal expansion mice, suggesting that these two miRNAs may play a long-lasting role in AML development, persisting, or that they appear in an initial early damage event such as with 48 hours post radiation, with a recurrence as the disease establishes itself.

The KEGG-predicted pathways were found to be quite similar between MSCs, macrophages, and total bone marrow, with a heavy involvement in multiple metabolic pathways, such as lysine degradation and fatty acid metabolism. The direct impact of these, given the recurrence of these pathways and multiple genes within them being repeatedly targeted, was tested in the following chapter. Of note as well is the involvement of multiple signalling pathways, e.g. Ras, Rap1, Notch, TNF and MAPK. These pathways are known to play roles in AML development. Notch is a pathway crucial in early fetal development but may also play a role in leukaemia stem cell development and AML establishment and recurrence (Lainez-Gonzalez *et al.,* 2022, Cancers). A large proportion of human AMLs exhibit mutations in Ras or associated genes (Pomeroy & Eckfeldt, 2020, Small GTPases). TNF-α is upregulated in the sera of human AML patients (Tian *et al.,* 2014, Stem Cell Investigation) and TNF signalling promotes *in vitro* growth of AML cells (Volk *et al.,* 2013, Blood). The MAPK pathway is also closely tied to the Ras signalling pathway and is

dysregulated in AML with mutations in RUNX1 being associated with poor prognosis (He *et al.,* 2022, Expert Review of Hematology).

Closer analysis of the most highly represented genetic targets in macrophages revealed an EV secretion profile that substantially activated pro-proliferation and stem cell maintenance pathways via proposed downregulation of proliferation and maintenance pathway inhibitors. It is hypothesized that macrophages during normal tissue homeostasis partially suppress proliferation and maintenance pathways, and after IR exposure reduce this level of negative control. Macrophage support of progenitor proliferation and renewal is accompanied by a reprogramming of differentiation fate, with a downregulation of pro-osteoblastic differentiation in favour of progenitor maintenance and adipocytic differentiation. These signals are hypothesized to be destined for macrophage:progenitor communication, given the known regulatory functions of macrophages in the bone marrow microenvironment *in vivo.* Contrary to MSC EV signalling, macrophages exhibit a complex profile of up-and-downregulated miRNA that mutually regulate gene targets, suggesting a complex push-pull relation with regulation.

Mesenchymal stem cells largely recapitulate this signalling profile to a lesser degree, with pro-proliferation and maintenance pathways being activated via downregulation of negative control miRNA. Unlike macrophages, MSCs promote activation of Kmt2c and Setd2, promoting osteoblastic differentiation and inhibiting stem cell renewal, likely as a balancing signal to progenitor cells to prevent unchecked proliferation. MSCs further promote the polarization of macrophages to M1 state, triggering pro-inflammatory activity and upregulating ferroptosis.

Within macrophages, the driving miRNA with the highest level of gene targets are miR-142a-5p (upregulated) and miR-291b-3p (downregulated). We suggest that the best two miRNA targets for tracking macrophage response over time and for lab validation of function are miR-142a-5p, given its wide variety of gene targets, and miR-291b-3p, for the same reason, with their respective regulation providing deep insights into macrophage response

over time and dose to IR. Partner miRNAs in the regulation of Sos1, miR-7051-5p, miR-3473g, and miR-7655-3p would also be useful miRNA to study, especially given that their actual regulatory interaction with Sos1 is unknown, and elucidation of function would be vital in confirmation of the proposed hypotheses regarding macrophage response post-IR.

In MSCs, we propose that the most important miRNA to monitor are the downregulated miR-34a-5p and miR-128-3p, given their involvement in a wide array of signalling networks as well as involvement in metabolic regulation via the lysine degradation pathway. Particular interest should be paid to miR-128-3p's ability to inhibit associated pathways, to give further clarification on the potency of its control network and how differential regulation may affect entire signalling networks.

Chromosomal location analysis did not reveal any clustering shared between both cells in the significantly differentially expressed miRNA, although macrophages showed a preponderance of miRNA originating from the X chromosome. Chromosomes 14, 17 and 19 were not affected in this or any of the previous data sets, which suggests a lack of radiation response genes being located on these chromosomes, or a certain resistance to stimulation by radiation in these regions.

In macrophages, lysine degradation-involved miRNA were involved to be upregulated, with two genes being modulated by more than one miRNA, Kmt2c and Setd2, which are important developmental regulators and play a part in the anti-osteoblastic, pro-progenitor proliferation signal secreted by macrophages. Kmt2c and Setd2 are major elements of the metabolic chain converting a protein-lysine complex to a protein-N-trimethyllysine. Other genes targeted in the lysine degradation pathway, however, are responsible for direct metabolism of a lysine intermediate, with Phykp1, one of the other genes targeted (by miR-223-3p) responsible for the conversion of 5-phosphooxy-L-lysine to L-2-aminoadipate-6-semialdehyde (KEGG). Downregulated miRNA elements were also involved in N-glycan biosynthesis, with several genes (Tusc3, Alg14, Man1b1, Alg13 etc) being targeted. While the direct regulation is unknown, it is hypothesized that this downregulation of miRNA

constitutes an activation of N-glycan biosynthesis, crucial for post-translational modifications (Esmail & Manolson, 2021, European Journal of Cell Biology).

In mesenchymal stem cells, in another difference in post-IR response vs macrophages, fatty acid metabolism was targeted, with upregulated miR-339 targeting Hadha (with unknown regulation pressure), which is responsible for the interconversion of hexadecanoyl-CoA to Acetyl-CoA (KEGG pathways). Hadha also plays a role in the lysine degradation pathway, converting Crotonoyl Co-A, itself an output of the L-lysine to glutaryl-CoA and L-lysine to L-3-aminobutyrl -CoA pathways, to S-3-hydroxybutanoyl-CoA, which ultimately feeds into the citrate cycle after further conversion into Acetyl-CoA. Fatty acid elongation reactors were also downregulated, via Hadha, Elovl4 and Elovl7, the latter two responsible for Malonyl-CoA formation (KEGG pathways). This suggests that MSCs both up-and-down regulate Hadha expression in nearby cells, affecting Acetyl-CoA generation via fatty acid and lysine intermediates, post-IR.

While the majority of targeted genes play regulatory roles in the methylation of lysine residues, a significant metabolic signature is still seen in both macrophages and mesenchymal stem cells, especially the latter. It is unknown how significant the interaction between miRNA regulators and directly metabolism involved genes is. Signalling networks within the context of IR and cancer development are increasingly researched, but the metabolic involvement in signalling function, whether direct or indirect, does not receive nearly as much attention. We hypothesize that miRNA differential regulation in both macrophages and mesenchymal stem cells has effects on both signalling pathway expression and on metabolic function, with metabolic function supporting and influencing the effectiveness of signalling pathways. Metabolism is inherently interesting to study in the wider context of radiation exposure due to its targetability. While signalling networks can be targeted, this requires targeted peptides and/or drugs to knockdown or upregulate specific, discrete and distinct elements. Metabolism, on the other hand, can be much more readily addressed via dietary changes, e.g. a diet either rich or poor in lysine to mitigate post-IR

damage effects. Dedicated study of how EV-shuttled miRNAs affect bystander cells post-IR is absolutely warranted, however within the scope of this research we decided to further study the currently relatively poorly characterized metabolic impact of IR and EV regulation in bystander tissues, focusing on progenitor cells. We hypothesize that better understanding of metabolic dysregulation will open further avenues for research into prophylactic care to minimize IR damage and offer insights into miRNA biomarkers or therapeutic targets that can be used in combination with dietary control to mitigate IR-induced damage and lessen the risk of late effect development. In particular, the metabolism of fatty acids (mediated mostly by fatty acid synthase, Fasn) has been demonstrated to affect survival in irradiated cancers (De Martino *et al.,* 2023, Cancer Letters; Rae *et al.,* 2020, Advances in Radiation Oncology; Jin *et al.,* 2021, FEBSPress) and low-dose IR has the potential to induce metabolic dysregulation, e.g. in serum L-lysine levels, in radiation workers (Guo *et al.,* 2022, Journal of Pharmaceutical and Biomedical Analysis). However, much of this has been studied in an explicit disease context (metabolic function within tumours) or in low-dose, long-term exposure. To better understand the mechanisms behind metabolic response to acute IR, as we used in our study, and relate this to future potential late effects, we chose to use 2Gy radiation as previously on *in vitro* MSCs and HSCs.

Much remains to be elucidated, with functional assays on the actual metabolic effect of 2Gy EVs being necessary. Chapter 5 is a first step, with further long-term experiments being required to establish if 2Gy EVs have a protective or deleterious effect, as this is extremely difficult to predict based on cargo and content alone.

A limitation that must be stated is the lack of experimental validation of direct targeting by several miRNA to their predicted gene targets. However, given the overlap in miRNA targeting a single gene or pathway, it is statistically likely that the gene is in fact targeted by a set, if perhaps not all, of the represented miRNA, strengthening this association and reducing some uncertainty. Furthermore the presence of a single miRNA in a wide variety

of pathways, especially with a preponderance of experimental validation data, further solidifies the reliability of the bioinformatic prediction. However, validation *in vitro* of direct regulation of miRNA with their predicted gene target would be beneficial for the robustness of this data set and the subsequent findings.

Another limitation is the difference in techniques used to analyse miRNA, potentially hindering the ability to cross-compare data sets between *in vitro* cultured cells and *in vivo* irradiated mice. Of the represented miRNA, most are present in the nCounter Nanostring panel, except for: miR-1843a, miR-1298, miR-7051, miR-5110 and miR-7655. Of these, none were identified as key miRNA for further study, nor were any of these miRNAs heavily involved with multiple targets with the potential exceptions of miR-7655 and miR-7051 as predicted co-regulators of Sos1. Therefore, the key DE miRNA in MSCs and macrophages were adequately represented in the Nanostring nCounter miRNA panel, rendering comparison between the two data sets possible. However, approximately 2300 miRNAs are predicted to exist in the mammalian genome (Alles *et al.,* 2019, Nucleic Acids Research), and due consideration must be given to the size disparity of ~2300 miRNA vs ~800 miRNAs in the nCounter Nanostring panel.

5. Metabolic effects and gene dysregulation in progenitor cells

5.01 Lysine dysregulation in progenitor cells

Lysine degradation is a pathway involved in every dataset so far, being found in 48-hour post exposure WT CBA mice, 12-month post exposure high clonal expansion mCh/GFP CBA mice, C57BL6/J Ldlr-/- mice, and BM-derived murine macrophages and MSCs. As of this writing, data return is still pending for RNA sequencing of EVs derived from HSCs isolated and expanded from murine BM; however, given the prevalence of this pathway, it was decided to use both MSCs and HSCs, as two major progenitor cell populations, to test the direct and indirect effects radiation has on lysine levels within the cell. Future work would expand on this by incorporating other cell types, e.g. macrophages and osteoblasts, and assaying how their lysine levels are impacted and if this differs in any way, as well as other metabolite levels, using the same timepoint of 48 hours post exposure.

A major caveat which needs to be mentioned prior to interpreting this data is an issue with control groups. The control group for both MSC and HSC assays is 0Gy, unirradiated cells with no added EVs; however, an additional control would have been ideal, consisting of unirradiated cells with EVs from unirradiated cells added to them. This control was initially excluded due to sample and culture number availability, but in a repetition of this experiment would be required to remove any ambiguity in the results. However, given the differentially regulated miRNA and their suspected involvement seen in past results chapters, it is still highly possible that irradiated cell derived EVs have an effect distinct to a general, ubiquitous EV population, regardless of the radiation status of their cell of origin.

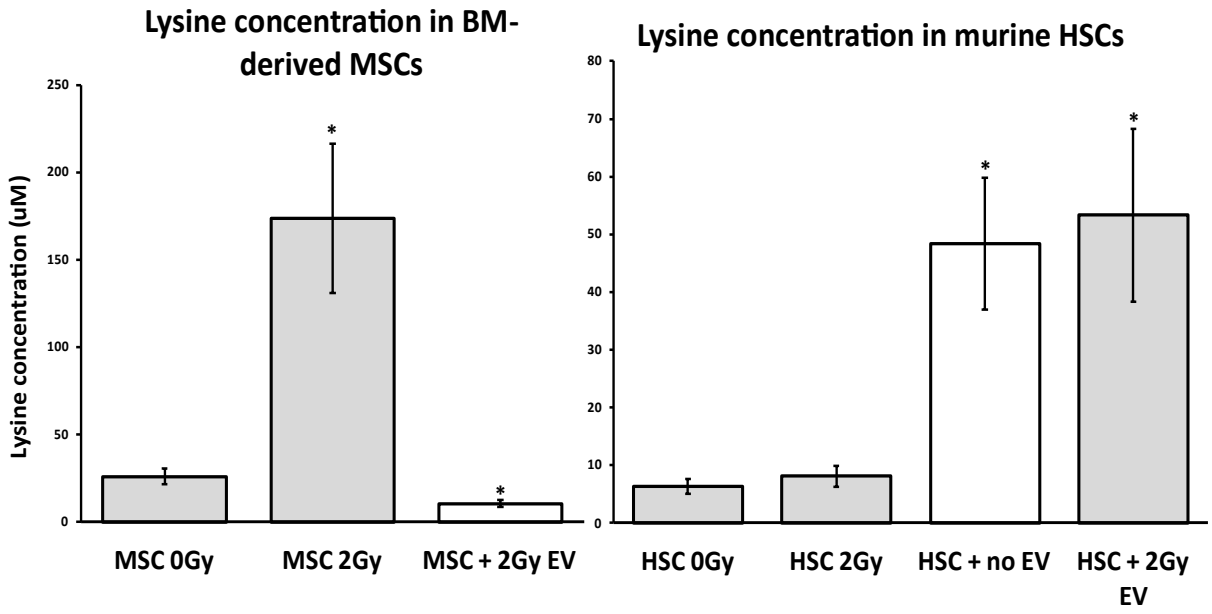


Figure 5.01 Lysine concentration in BM-derived MSCs and HSCs. The * symbol denotes statistical significance when compared to the control 0Gy condition. An equal amount of cells (n=1E06) was processed for each condition to avoid variation occurring due to amount of starting material. p=0.05

As seen in figure 5.01, radiation at 2Gy massively dysregulates the lysine level in mesenchymal stem cells, which sees a rise from an average 25.81µM to 173.57uM, a fold change of 6.72 versus the baseline. However, the addition of 2Gy derived EVs to radiation-naïve cells sees a fall to an average of 10.36 uM, a fold change of 0.4 i.e. a 60% reduction in the lysine level vs baseline. This suggests that within MSCs, EVs have an opposing effect to radiation, presenting the opposite phenotype in terms of how the lysine concentration is affected.

However, this effect was not replicated in murine HSCs. There was no statistically significant difference found between the lysine concentrations of HSC 0Gy (6.26) and HSC 2Gy (8.1), p=0.15. However, both HSC + no EV, a sample consisting of radiation-naïve HSCs fed with fresh media, and HSC + 2Gy EV, consisting of 2Gy EVs added to radiation-naïve HSCs with *no* fresh media, both had significantly higher lysine levels when compared to baseline (no EV: 48.35uM, 2Gy EV: 53.31uM), p=0.0003 and p=0.0007 respectively.

These two did not differ significantly when compared to one another. 2Gy EVs were resuspended in the same media already found within the radiation naïve HSCs, with a small volume (circa 100ul) being taken to resuspend the isolated EVs in. Nevertheless, even without the addition of fresh media, the addition of extra EVs had an impact comparable to the refreshment of nutrient-rich media on the HSC population, with a fold change of circa 8.5 over the control baseline. This behaviour, the opposite of what was observed in MSCs, suggests that cell types, or at the very least progenitor cell types, interact in different ways with EVs and that EV-cell response is not universally conserved or consistent.

5.02 Effect of radiation on aldehyde and fatty acid concentrations

The aldehyde dehydrogenases, namely Aldh9a1, 7a1 and 3a1, were also commonly found across the data sets. Of these, two were assayed due to time constraints. Combined with qPCR assaying of the direct impact on gene expression, the level of their most commonly associated metabolite, aldehydes, was also assessed, with Aldh9a1 catalyzing the conversion of gamma-aminobutyraldehyde to GABA (Marchitti *et al.,* 2008, Expert Opinion on Drug Metabolism and Toxicology), with Aldh7a1 also being involved in aldehyde conversion as well as lysine degradation (NCBI).

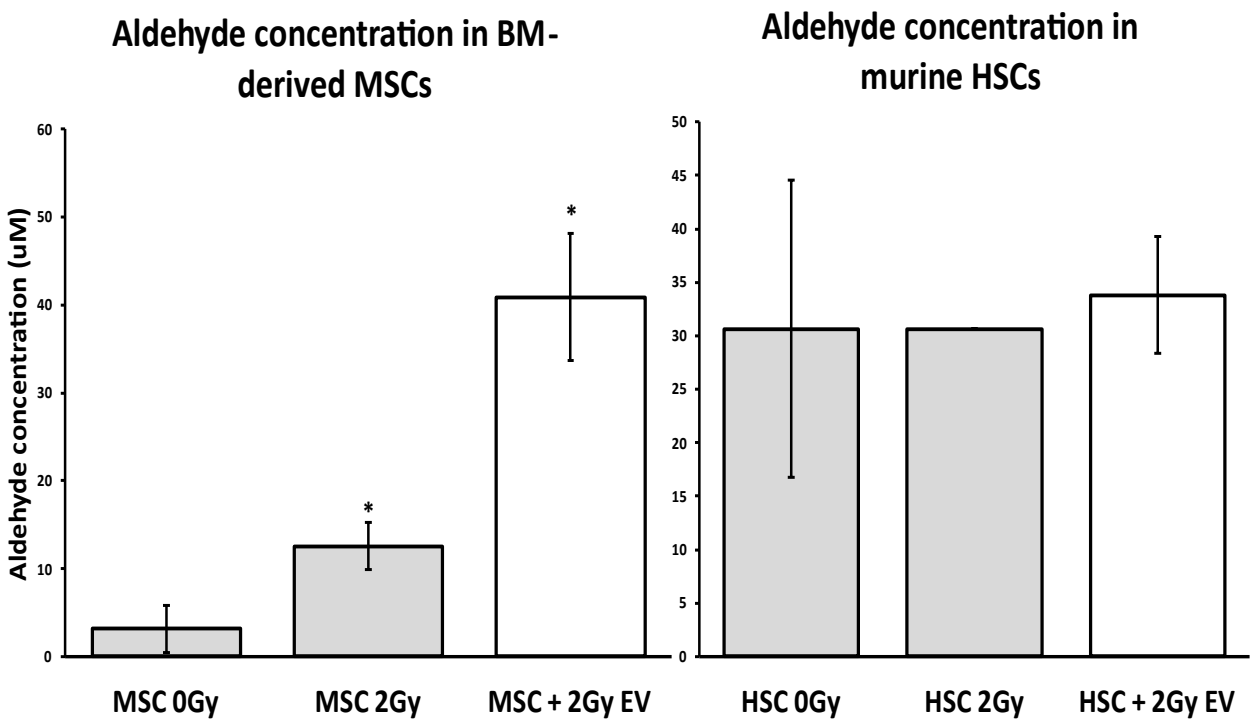


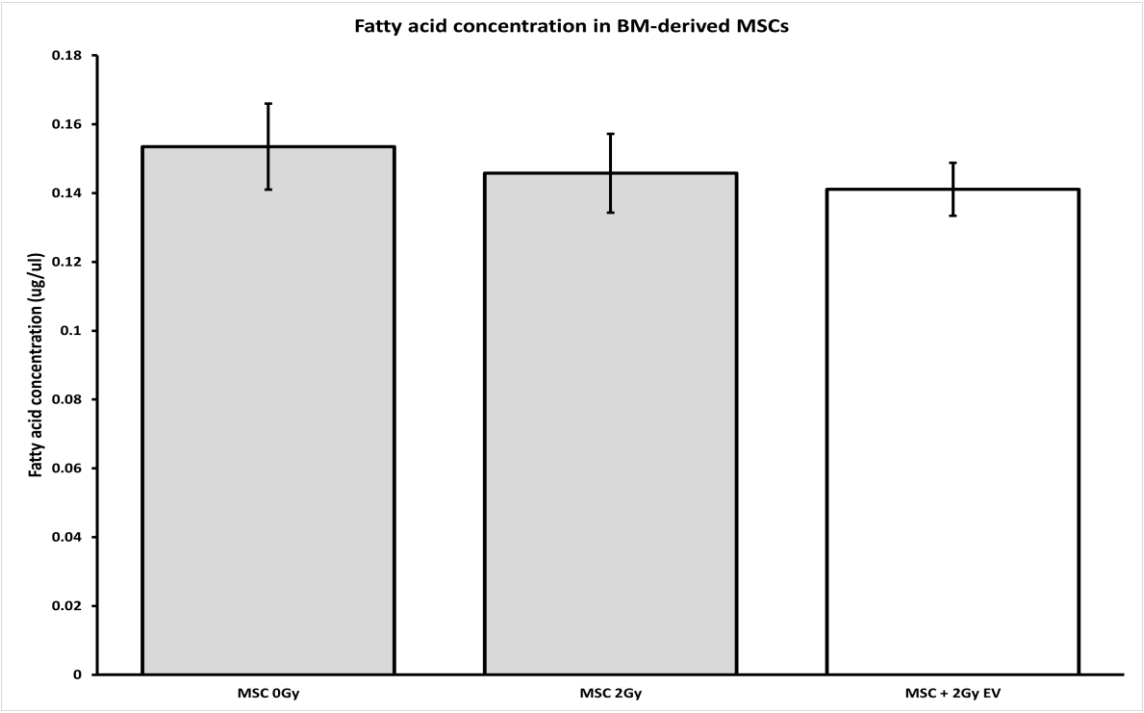
Figure 5.02 Aldehyde concentration in BM-derived MSCs and murine HSCs. The * symbol denotes statistical significance when compared to the control 0Gy. An equal amount of cells (n=1E06) was processed for each condition to avoid variation occurring due to amount of starting material. In this case, MSC + 2Gy EV and MSC 2Gy were statistically distinct from one another as well (p=0.003). p=0.05

As seen in figure 5.02, radiation dysregulates the aldehyde concentration within mesenchymal cells, with the addition of irradiated cell derived EVs raising this even higher when compared to both baseline and irradiated conditions. Direct radiation increases the aldehyde concentration by 4-fold vs the baseline, while the indirect effect of radiation, adding bystander EVs, increases this by 13-fold vs the baseline. This is in stark opposition to the effect seen in lysine, where bystander EVs had the opposite effect of radiation in MSCs. Aldehydes are known to be geno- and cytotoxic (Xie *et al.,* 2016, Mutation Research), which suggests that in the irradiated and bystander cases the cell is under significantly more stress than baseline, even independently of an actual radiation event.

Aldehyde generation can be a result of oxidative stress, e.g. lipid perodixation among other causes (Chan *et al.,* 2011, Chemicobiological Interactions). This suggests that the bystander effect could potentially cause *more* oxidative stress than direct radiation.

HSCs differ from MSCs in their response to radiation. Radiation did not significantly alter the level of aldehydes within the cellular population, nor did adding bystander EVs. It should also be noted that HSCs appear to endogenously have much higher natural levels of aldehydes when compared to MSCs, once again suggesting a difference in the internal environment and regulatory mechanisms of these two progenitor cell types.

Another frequently found gene was Fasn, fatty acid synthase, with an important role of this enzyme being fatty acid biosynthesis, which was ubiquitously found across all data sets. The cell media was sampled for differential levels of fatty acids, with the hypothesis being that a dysregulation in fatty acid biosynthesis would be reflected in export of material via EVs into the extracellular space. However, despite miRNAs targeting this gene being found to be differentially regulated, the fatty acid levels in the extracellular space were not significantly different across all experimental conditions, although a necessary secondary step would be to assay whether this is the same within the cell itself.



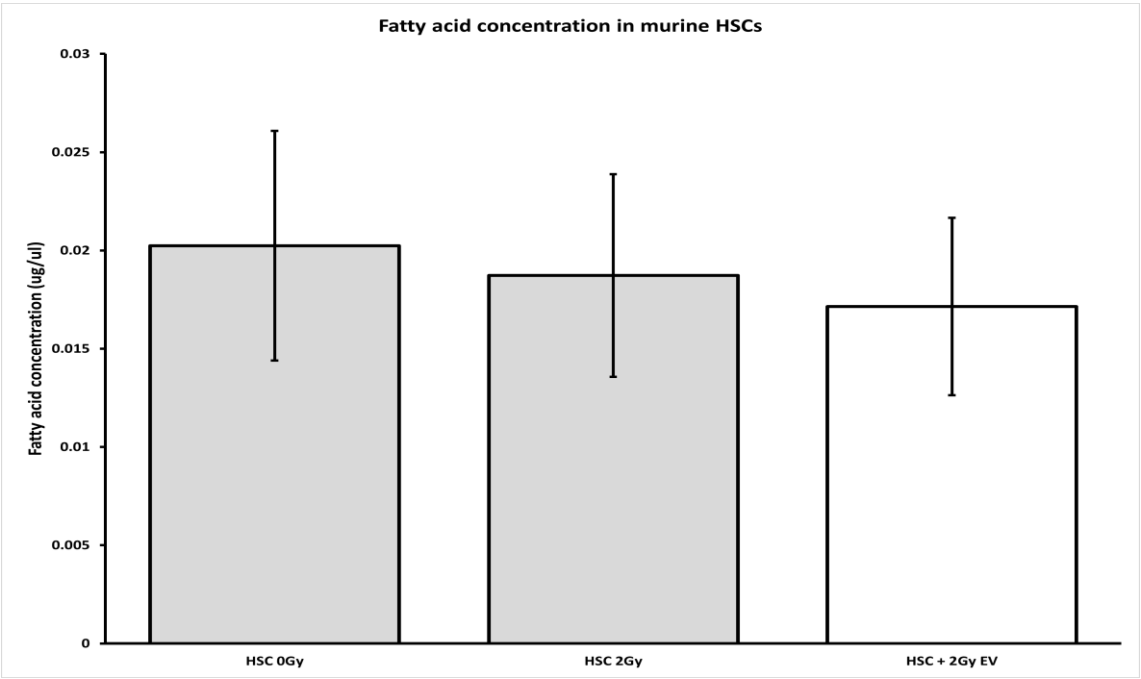


Figure 5.03 Fatty acid concentration in conditioned media. Media was filtered for cells, leaving EVs and other extracellular factors within it and then assayed for its fatty acid content. No significant differences were found. Media from the same amount of cells, and the same volume of media, was used for all assays. p=0.05

5.03 Differential expression of miRNA-targeted genes in progenitor cells

Following on from the metabolic tests, the other aspect we wanted to investigate was the impact of both radiation and radiation-induced EVs on the expression of the proteins that play a major role in these metabolic pathways.

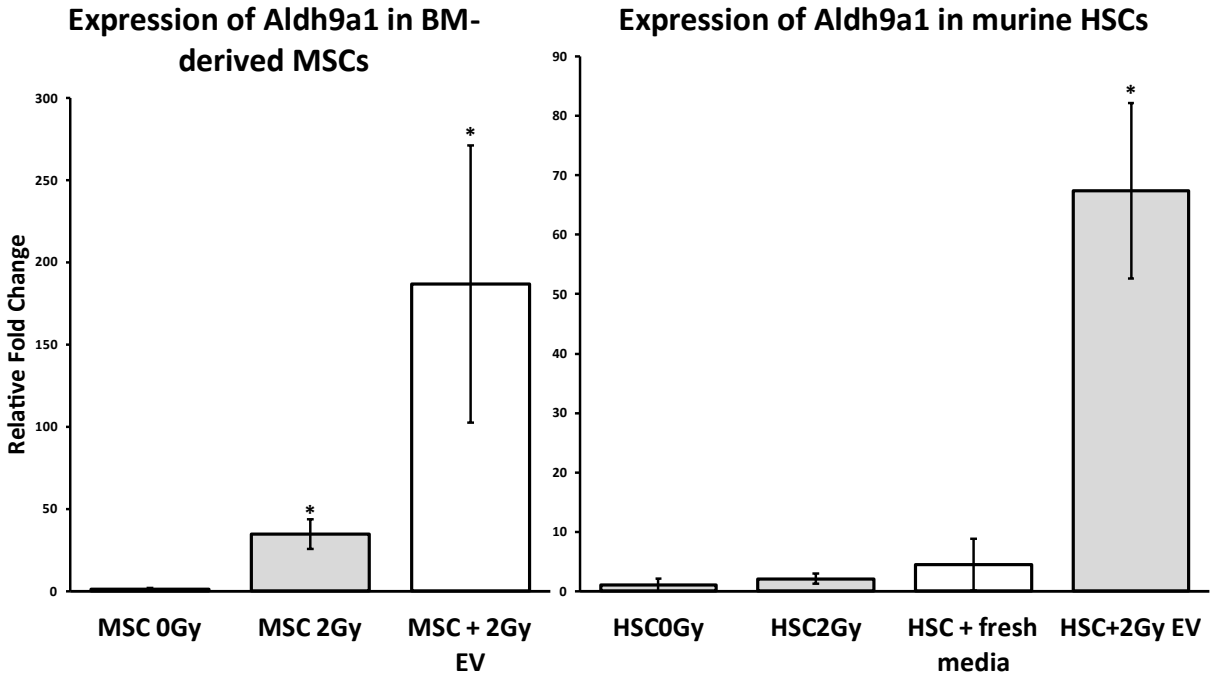


Figure 5.04 Aldh9a1 expression in BM-derived MSCs and HSCs. mRNA (converted to cDNA) from MSCs in 3 conditions was assayed using qPCR. * denotes significance below the threshold value of p=0.05. MSC2Gy and MSC+2Gy EV were significantly different from one another as well as compared to baseline. p=0.05

The expression of Aldh9a1, which as previously mentioned is an aldehyde dehydrogenase responsible for the dehydrogenation of gamma-aminobutyraldehyde to GABA, rises in BM-derived MSCs in the irradiated condition versus baseline, and to a much higher degree in the bystander condition, as seen in figure 5.04. This is somewhat surprising, as the level of aldehyde in MSCs also increases following the same pattern. This may indicate several possibilities: one would be that Aldh9a1 is upregulated in response to the increase in aldehyde level brought on both by radiation and by radiation-induced EVs, and as such is a response to stress stimuli and not something directly mediated by EV cargo. The second

possibility would be that Aldh9a1 is upregulated by EV cargo, but it is not sufficiently upregulated to compensate for the aldehyde increase. The third possibility is that the aldehydes that are increased within MSCs have only a minority portion that is gamma-aminobutyraldehyde, meaning that Aldh9a1 cannot catalyse its conversion.

Murine HSCs, despite not seeing an increase or decrease in aldehyde levels otherwise, do demonstrate an extremely significant response to radiation-induced EVs. HSC 0Gy, HSC 2Gy, and HSC + fresh media all do not demonstrate any significant change in Aldh9a1 expression throughout. Adding 2Gy EVs, resuspended in conditioned media, does demonstrate a massive increase in Aldh9a1 expression.

This could potentially suggest that, at least within these two classes of progenitor cells, an increase in Aldh9a1 expression is either a conserved response to stimuli from EVs, and may be radiation-independent, or it is a conserved response to the miRNA cargo these EVs contain, which, given that these are differentially regulated between radiation and radiation-naïve cells as demonstrated throughout chapters 3 and 4, would be a likely sign that these miRNA have a consistent response along this particular target pathway, even though the ultimate outcome re: metabolite levels may differ.

Aldh7a1 expression does not follow an identical pattern under the same conditions in MSCs. While both direct radiation and exposure to radiation derived EVs causes an increase in the expression of Aldh7a1 when compared to baseline, radiation derived EVs cause a fold change lower than that of direct radiation, as seen in figure 5.05. This is despite aldehyde levels being much higher in bystander EVs than in direct radiation, seen in figure 5.02. This could suggest that the cellular response to bystander radiation in terms of damage protection is much more inefficient versus an indirect challenge, despite the commensurate level of oxidative stress potentially being higher.

HSCs demonstrate an interesting difference in response with regards to bystander EVs. Radiation severely downregulates the level of available Aldh7a1 within the cell, suggesting

a compromised damage response and an inability to deal with aldehyde related oxidative stress. However, bystander EVs cause a massive upregulation, a starkly opposite effect, in Aldh7a1 expression, suggesting a much more pronounced protective response in HSCs, once again demonstrating a difference in cellular reactions and stress-related processes between MSCs and HSCs. This can also be seen by the immediate, and opposing, reactions in terms of Aldh7a1 expression after radiation.

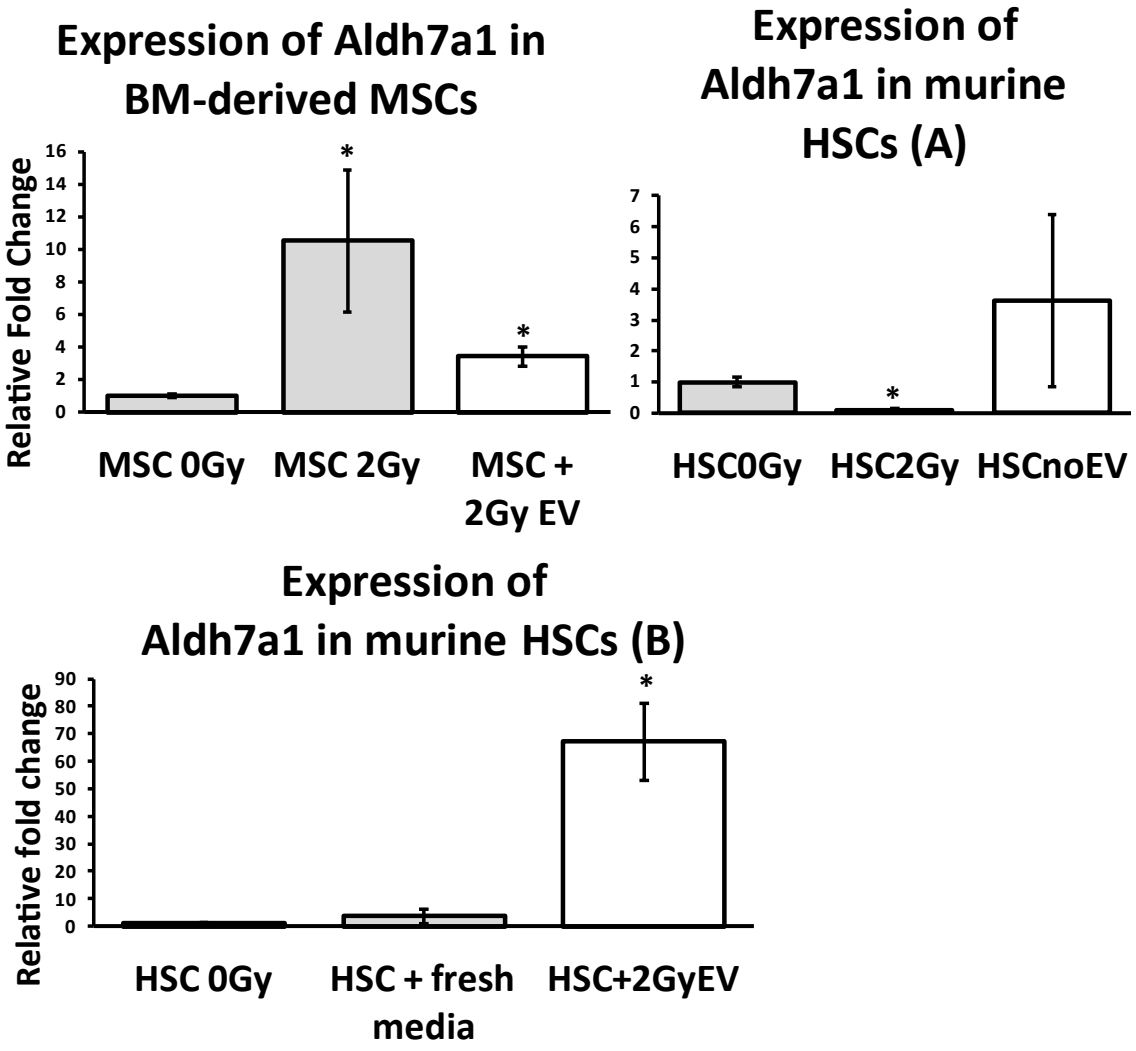


Figure 5.05 Aldh7a1 expression in BM-derived MSCs and in HSCs. * denotes statistical significance vs 0Gy; HSC 2Gy and HSC + 2Gy EV are also significantly different when compared to each other. A and B represent the same data set, but are split due to differences in magnitude of relative fold change vs control. p=0.05

Finally, Fasn also demonstrates a difference in response behaviour between the two progenitor cell types. In BM-derived MSCs, Fasn's expression is increased, with a fold change of circa 10 versus the baseline. Addition of irradiated cell derived EVs accomplishes the same effect, with the two-fold changes being statistically near identical (p=0.94). This demonstrates that within murine BM MSCs, it appears that EVs can recapitulate the effect of radiation on Fasn expression independently of actual ionising radiation. However, HSCs once again show the opposite effect. Radiation sharply depresses the expression of Fasn in murine HSCs, while 2Gy-derived EVs strongly upregulates Fasn expression.

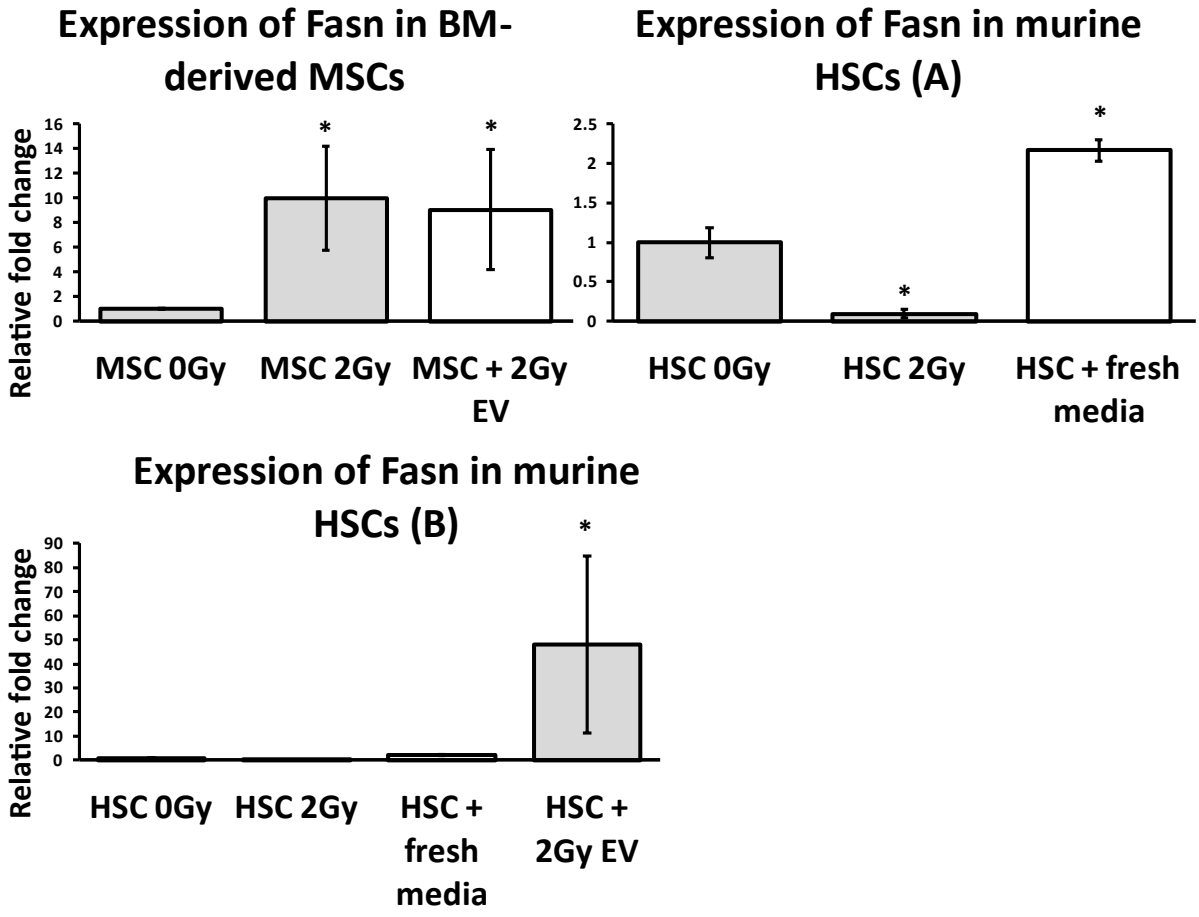
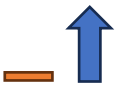
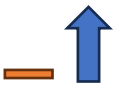


Figure 5.06 Fasn expression in BM-derived MSCs and HSCs. * denotes significance ($p<0.05$) when compared to baseline 0Gy. MSC 2Gy and MSC + 2Gy EV do not significantly differ. Graphs A and B depict the same data, but have been split for the sake of clarity so that HSC 2Gy is visible. All samples are significantly different from one another, including HSC + 2Gy EV despite its high degree of variability. p=0.05

5.04 Discussion and potential implications

To briefly summarize the findings, please see figure 5.07 below.

Figure 5.07: Pictorial summary of metabolic data. Orange arrows represent direct radiation with 2Gy. Blue arrows represent EVs isolated from 2Gy-irradiated cells and incubated with non-irradiation cells of the matching type. Arrow size represents relative response but is not to scale with response, i.e. a larger blue arrow pointing up vs a smaller orange arrow pointing represents EVs upregulating to a higher level than direct radiation. Up= upregulation, down=downregulation. Flat bars indicate no change vs control.

Cell type	**Changes in level VS 0Gy Control**					
	Lysine	Aldehyde	Fatty acid	Aldh9a1	Aldh7a1	Fasn
MSC						
HSC						

This data suggests that MSC and HSC have different, unique response mechanisms to radiation-induced stress and radiation bystander-induced stress. EVs as such *do not* have a universal effect nor do they elicit a universal, conserved response. While confirmation of such a statement would require further repeats and assays of different cell types and other tissues, it would appear that response to EV stimuli differs between cell types, most likely dependent on their function and active genome makeup.

Overall, in MSCs it seems that EVs (except for their impact on lysine levels) serve to propagate whatever stress response was initiated versus a radiation insult. In all three genes, Aldh9a1, Aldh7a1, and Fasn, EVs either upregulated to a greater, lesser, or equal to extent when compared to the effect of direct ionising radiation. There are two potential implications of this: MSCs could be particularly radiation susceptible, with MSC EVs initiating damaging stress response cascades in unirradiated neighbouring cells, thus propagating damage. Alternatively, the opposite might also be true. This initiation of a strong response past direct radiation could in fact be protecting and preparing unirradiated cells to deal with other bystander particles, such as free radicals or other signals.

With HSCs, the relationship between EVs and radiation is somewhat more complex. Immediately, on a metabolic level HSCs appear more resilient to change influenced by radiation; lysine content is unchanged by 2Gy radiation, and both aldehyde and fatty acid content is unchanged. However, EVs upregulate lysine content sharply, suggesting an interference in the lysine catabolism process within the cell, which would be congruent with the amount of miRNAs identified in the BM dataset that target the lysine degradation process. On a genetic level, the trend is to incur the opposite effect that radiation did. While Aldh9a1 is unaffected by radiation, it is upregulated in the bystander scenario; Aldh7a1 and Fasn are both downregulated by radiation, but sharply upregulated by EVs. One possible explanation for this is that, while HSCs are strongly affected by radiation on a genetic level (as found in previous literature, with HSCs being one of the most radiosensitive cell types) HSC EVs promote a strong response to mitigate radiation damage. However, given how strong this response is versus the baseline, it is possible that this is an overcorrection, and this stress response could cascade and cause more damage, thus indirectly propagating radiation damage past the initial population via a malfunctioning repair response.

Of course, this is all predicated on a single time point of 48 hours. Future experiments would focus on both earlier and later timepoints, as it may be possible that the interplay between radiation and bystander EV function changes dramatically as the timeline evolves.

One limitation that must be noted is that a high dose radiation of 2Gy induces significant cell apoptosis. Rates of apoptosis post-radiation were not measured as part of this experiment, so it is likely that apoptotic bodies were co-precipitated and analysed. Given that apoptotic bodies may still play a role in intercellular signalling and fall under the broader ‘extracellular vesicle’ classification, this changes the significance of the results only insofar as the potential drivers for metabolic changes are not only microvesicles and exosomes, but apoptotic bodies as well.

6. Discussion

6.1 Summary of key findings and context within the research

The research question, and driving inquiry behind this research, has been “what is the role of extracellular vesicles in radiation-induced acute myeloid leukaemia?” To answer this question, a variety of approaches have been used, summarized below:

1) The BM miRNA content of mouse EVs 24 hours post IR insult, sourced from the whole BM, has been characterized.
2) The BM miRNA content of mouse EVs in non-irradiated, irradiated but non-leukaemic, irradiated and pre-leukaemic with low clonal expansion, and irradiated and pre-leukaemic with high clonal expansion has been characterized.
3) The miRNA content of discrete, BM-derived cell populations, these being macrophages and mesenchymal stem cells, has been characterized 48 hours post-IR insult.
4) The direct impact of radiation and radiation derived EVs on certain key metabolites, these being lysine, fatty acids, and aldehydes, in BM-derived cell populations (mesenchymal stem cells and HSPCs) has been measured.
5) The mRNA levels and therefore gene expression of certain genes (Aldh9a1, Aldh7a1, and Fasn) in MSCs and HSPCs exposed to EVs as above have been measured.

Together, these research lines give an insight into what the miRNA cargo of EVs is in different cell contexts and scenarios, and how these EVs impact cells with respect to the pathways studied, in particular the relation between miRNAs and their targeted mRNAs in affecting gene expression.

Before these results can be combined, a brief summary of the key findings of each of these experiments is necessary.

For point 1), wildtype CBA mice were irradiated at 0.1Gy or 3Gy using an X-ray source, with a sham radiation at 0Gy being the control. These were then culled, BM extracted and EVs purified, pooled according to radiation condition, and then assayed for miRNA content using the nCounter panel system. 0.1Gy showed heavy intrasample variability, but nevertheless showed a small set of miRNAs which were statistically significant and differentially regulated versus the control, these being mmu-miR-761, mmu-miR-129-5p, mmu-miR-669g, and mmu-miR-34b-5p. 3Gy showed a more consistent intrasample response to radiation, and an expanded miRNA response, as seen in table 3.1, with the four miRNA identified at 0.1Gy being present as well, and seemingly regulated in a dose-dependent manner. The pathways these miRNAs were predicted to target included several major signalling pathways, such as MAPK, Hippo and mTOR, and metabolic pathways, such as fatty acid biosynthesis, lysine degradation, actin cytoskeleton remodelling, and finally key cancer pathways, with explicitly acute myeloid leukaemia being involved. Taken together, this implies a wide range of targets involved in radiation response, with many key regulatory and homeostatic processes being targeted, providing a route for radiation-induced damage to accumulate and be propagated to secondary cells via EV-mediated miRNA transfer.

Point 2) was an expansion and alternate perspective on the experiment from point 1). Using transgenic mCh/GFP CBA mice, mice were tracked throughout lifespan (6-12 months depending) post 3Gy X-ray radiation insult, with EVs being harvested from the BM at endpoint and segregated according to radiation and leukaemia development status. It was found that irradiated mice showing no clonal expansion were statistically not significantly different from control mice that had not been irradiated at all, suggesting that a radiation signal is not persistent over a 12 month period, and thus mice can be considered to have returned to baseline without any lasting damage visible in the EV miRNA landscape (although genetic analysis e.g. via cytogenetics may reveal lasting radiation ‘scars’). Mice with low clonal expansion showed some tenuous differences in miRNA expression when

compared to control: of the 54 miRNA identified that show differences in expression that satisfy the p-value cutoff of 0.05, only one miRNA satisfies both the p-value and FDR cutoffs, this being mmu-miR-1897-3p. miR-1897-3p is predicted to target Erg and Lifr, the former being a proto-oncogene, the latter being Leukaemia Inhibitory Factor Receptor, suggesting the possibility that this could be the beginning of a leukaemia development, with Erg and Lifr playing roles in very early initiation of clonal expansion, but this claim must be approached with due scepticism. Mice with high clonal expansion showed 26 miRNA which satisfied both the p-value and FDR cutoffs, including mmu-miR-1897-3p, previously identified in low clonal expansion mice. These miRNAs were involved in a variety of gene targets and pathways, including, as found in 24 hours post exposure mice, fatty acid biosynthesis, MAPK signalling, lysine degradation, acute myeloid leukaemia, Hippo, and several others. No miRNA overlap was identified between late effect, high clonal expansion mch/GFP mice and 24 hours post exposure WT-CBA mice; however, multiple common pathways were identified, suggesting that while the interacting element may change as disease progresses, the affected pathways remain constant, suggesting a major involvement of these pathways in the initiation, then sustaining and subsequent progression of radiation-induced AML.

Comparison of extracellular vesicle to BM cellular miRNA confirmed a pattern of specific packaging and enrichment of miRNA, with perhaps the exclusion of certain miRNA being noteworthy as well, such as the downregulation of miRNA governing important signalling pathways such as Wnt, Hippo, MAPK and mTOR, as well as explicit cancer development pathways and proteoglycans in cancer. A noteworthy finding is that enriched miRNA in EVs specifically target various metabolic pathways, including the oft-recurring fatty acid biosynthesis and lysine degradation pathways. A further study compared a transgenic C57Bl/6j derived mouse population, with various irradiation conditions, 6 months post exposure; 3 miRNA were found, with one satisfying both FDR and p-value thresholds, mmu-let-7a-5p, and two others which failed to satisfy FDR, mmu-miR-540-3p and mmu-miR-384-

5p. let-7a-5p was identified in both sham vs 0.5Gy and 2Gy, with the latter two identified at 4Gy. Let-7a is a regulator of the Ras oncogene family, further being associated with the regulation of lysine degradation, MAPK signalling, fatty acid metabolism, FoxO signalling, and proteoglycans in cancer; again, while individual miRNA signal did not persist between experimental groups, targeted outcome pathways did. Finally, mapping of statistically significant miRNA to their chromosomal locations did not reveal any specific clustering of damage on a set of chromosomes, although some chromosomes seemed to have more prevalence in terms of represented miRNA e.g. chromosomes 2, 12, and X.

Consequently, from this broad-spectrum view of the bone marrow, the bone marrow was then broken down into constituent cell populations, with two of them being marked as being especially relevant in the miRNA environment, macrophages and mesenchymal stem cells. A third cell population, haematopoetic stem cells, was also studied, but the data has not been provided by a third-party research centre as of this writing. In EVs from macrophages, a total of 23 miRNA transcripts were identified as being statistically significant and differentially regulated in the experimental group (macrophages 48 hours post exposure to 2Gy X-rays) vs the control (a sham radiation at 0Gy). Of these, multiple are known from prior research to be explicitly implicated in the development of AML in humans, such as miR-222, and miR-1298, which were found to be overexpressed in human AML cases. Of these, miR-222 was found upregulated in irradiated macrophages while miR-1298 was downregulated. Further miRNA found were also implicated in human AML; miR-98 and miR-148b were upregulated in irradiated macrophages, and high levels of these indicate a good prognosis in human cases. miR-223, miR-150, and miR-142 are all associated with poor prognosis when low levels are present, however all of these were upregulated in irradiated macrophages. This suggests that, while part of the signal may be similar to future AML pathways, the behaviour is not identical, with radiation wound healing occurring along different pathways than AML expansion and radiation resistance.

Within mesenchymal stem cell EVs, a smaller set of 8 miRNA were identified 48 hours post radiation exposure, under the same conditions as macrophages. Unlike macrophages, these miRNA actually exhibited an overlap with another data set, with two being present in high clonal expansion of mch/GFP CBA mice; miR-128-3p and the 5p splice variant of miR-345 (the 3p being present in this data set), demonstrating an overlap in radiation wound healing and AML proliferation, giving insights into the behaviour of proliferating leukaemic cells. Once again, fatty acid biosynthesis and lysine degradation are targeted, alongside several signalling pathways such as FoxO, MAPK and Ras. Of the upregulated miRNA, miR-128 has promise as a biomarker in ALL, miR-345 is found upregulated in post-remission AML patients, and miR-339 inhibits AML proliferation via Sox4. It is possible, as indicated later on in section 6.5, that in a small percentage of cells in a small percentage of post-IR cases, this miRNA signal causes constitutive signalling, explaining its involvement in later AML; more likely hypotheses are explained in section 6.5.

As previously done with whole BM, miRNAs were mapped to their respective chromosomal locations. In macrophages, the majority of differentially expressed miRNA were found on chromosome X. In neither this dataset nor the earlier whole BM dataset were chromosomes 14, 17 and 19 affected. Some miRNA e.g. miR-142a and miR-5110 were found in close proximity to one another. These findings suggest a sex factor in radiation response; we have observed higher rates of leukaemia incidence post-exposure in male CBA mice, suggesting this could indeed be the case, with female mice being able to better cope with post-IR repair. The exclusion of chromosomes 14, 17 and 19 suggest that miRNA loci located on these chromosomes are not involved in radiation response or could be resistant to activation by radiation stress stimuli.

To gain some understanding of what the actual biological outcome and effect of these EVs are, a small study based on metabolite levels (lysine, fatty acids and free aldehydes) was performed alongside qPCR to determine actual impact on targeted gene expression. This was performed in two progenitor cell populations, mesenchymal stem cells and

haematopoetic stem cells. The former study revealed some surprising results. Irradiated MSCs exhibited vastly increased lysine levels when compared to the control sham populations. However, exposure to radiation derived EVs had the opposite effect, with a decrease in lysine level relative to both the control and the irradiated population. HSCs showed a starkly different response, with radiation having no statistically significant effect on lysine level, but bystander EVs massively increasing lysine levels, on a level akin to feeding completely fresh media to the population. Free fatty acid concentrations in the extracellular serum did not vary across conditions in MSCs or HSCs; due to sample availability cellular levels were not tested. Aldehydes did not vary due to radiation or bystander effects in HSCs, but did in MSCs, with both radiation and bystander EVs upregulating aldehyde levels within the cell, the latter upregulating it to a higher extent than radiation alone. This suggests that EV impact on recipient cell depends on cell type, with no universal response being present. An interesting experiment to perform would be to cross the bystander EVs, that is to say expose HSC to MSC-derived bystander EVs and vice versa, to see if the effect is due to recipient response or donor cell response reflected in its EV emissions.

The qPCR study focused on three genes found to be regularly targeted across data sets: Aldh9a1, Aldh7a1 and Fasn. Aldh9a1 followed a similar pattern to aldehyde levels in MSCs, with radiation increasing Aldh9a1 levels and bystander EVs increasing them even further. HSCs showed a dramatic difference, with Aldh9a1 levels remaining identical in control, irradiated, and fresh media conditions, but experiencing a dramatic spike in bystander EVs. Aldh7a1 in MSCs showed the inverse effect as with Aldh9a1, with both bystander and irradiated increasing gene expression, but the former to a lesser extent than the latter. In HSCs, radiation instead decreased Aldh7a1 expression, and bystander massively increased it. Finally, Fasn expression was increased in MSCs following both radiation and bystander to similar extents, and in HSCs it followed the same pattern as Aldh7a1, with a stark decrease in expression after radiation but an increase in expression in the bystander

condition. Once again this implies a cell-type specific response to radiation; furthermore, it may demonstrate a compensatory damage response mechanism in HSCs, with an overwhelming opposite response in Aldh7a1 and Fasn in bystander EVs, suggesting a course correction to compensate for lower levels caused by direct radiation damage. This could mean that irradiated HSCs may signal to other nearby HSCs to protect themselves from damage, thus preventing a spread of the effect. However, given that this effect results in gene expression many times higher than baseline, this could be causing damage, with an overzealous damage response resulting in haywire metabolic pathways.

6.2 Extracellular Role in the Radiation Damage Response and Oncogenesis

One factor immediately apparent would be the lack of overlap in miRNA among distinct data sets, even when using identical or similar stressors in the form of radiation dose, type, or time point. However, it is important to note that despite this lack of conserved miRNA, there is a significantly conserved miRNA *response* found amongst all data sets, with certain pathways being identified as being involved in every single instance, such as key signalling pathways (e.g. FoxO, Wnt, MAPK) and key metabolic pathways, chiefly lysine degradation and fatty acid biosynthesis.

It is important to properly contextualize and separate the results based on conditions. While it is tempting to draw immediate parallels and similarities between, for example, mice 24 hours post exposure and those 12 months post exposure, based on their similarly affected pathways, they must nevertheless be separated. In the former case, we are discussing the *direct* and nigh immediate effects of radiation exposure in cells. 24 hours later, in the case of the subcultured homogenous cell populations, we are again discussing a later point in the normal tissue damage response pathway. By the time of the 12 months post exposure mice, we are no longer discussing a radiation response at all, as evidenced by the fact that irradiated mice without clonal expansion had no significant differences when compared to control, unirradiated mice. We are, instead, discussing an early cancer response or

development signal. This is not to say that the two are necessarily discrete and separate but should not be conflated as identical.

This progression through time after radiation stress may be one explanation for this lack of conservation of miRNA signal. As time goes on, different genes are activated in response to detected cell damage or signals received from other cells, causing an evolving response landscape. However, what is particularly interesting is that despite this evolution at the miRNA level, the targeted pathways scarcely change, suggesting that these pathways play key roles no matter the stage of cancer development or radiation response, and that radiation repair and cancer development share similar strategies. As demonstrated in section 6.5, upregulation of maintenance of stemness and resistance to terminal differentiation, with one explanation being the failure of damaged, pre-leukaemic cells to stop responding to proliferation signals and become insensitive to quiescence regulation.

The relationship between the signalling pathways (MAPK, FoxO, Ras, Wnt, and PI3K) and radiation is well known. FoxO3a is activated by radiation (Yang *et al.,* 2006, International Journal of Oncology), and levels of FoxO transcriptional activity is correlated with favourable response to chemoradiation courses in patients with esophageal adenocarcinomas (Creemers *et al.,* 2022, Journal of Translational Medicine). MAPK is known to be involved in post-radiation cell survival and repopulation, via the classical ERK pathway and others, e.g. the P38 pathway (Dent *et al.,* 2003, Oncogene). The Ras pathway of the MAPK family is a key target of interest mediating tumour survival in radiotherapy (Toulany, 2023, Clinical and Translational Radiation Oncology); Wnt is also a mediator of tumour survival and radiation resistance (Yang *et al.,* 2019, Journal of Cancer Research and Therapeutics). In colorectal cancer, PI3k/Akt promotes the formation of ‘cancer stem cells’ via SOX2 upregulation following radiation (Park *et al.,* 2021, Cells).

Their importance in cancer development and maintenance, beside the aforementioned radiation response pathways and involvement, has also been noted. Highly phosphorylated FoxO3a is a negative prognosis factor for AMLs (Kornblau *et al.,* 2010, Clinical Cancer

Research,). Dysregulated MAPK signalling has also been identified in acute myeloid leukaemias, albeit with RUNX1 mutations (He *et al.,* 2022, Expert Review of Hematology). Inhibitors of MAPK have been demonstrated to impair growth and lower survival of acute myeloid leukaemias in cell line research (Milella *et al.,* 2001, The Journal of Clinical Investigation). Ras oncogene mutations occur in as much as 27% of AML patients (Neubauer *et al.,* 2008, Journal of Clinical Oncology), with a variety of (and hence overall inconclusive) prognostic outcomes (Liu *et al.,* 2018 Clinica Chimica Acta). Wnt signalling is observed to be upregulated in AMLs (Gruszka *et al.,* 2019, Cells). Finally, the PI3K/Akt/mTOR pathway is also upregulated in AML, with this particular pathway appearing to be of particular importance to leukaemogenesis (Nepstad *et al.,* 2020, International Journal of Molecular Sciences).

In other words, the representation of these pathways is consistent with knowledge about radiation response and leukaemogenesis, and many of these pathways are represented in a variety of cancers; they are key responders and players within a cell's signalling hierarchy, which means this result is no surprise. What this does indicate is the definite involvement and non-trivial nature of EVs in the context of leukaemogenesis, via modulation and interaction with these pathways. EVs interact with and modulate significant pro-oncogenic signalling networks, in early leukaemia scenarios, with similar pathways being activated (for different purposes) during normal tissue wound response but do so via different miRNA interactors. The extent of this EV involvement in signalling networks is currently unknown and was not the later focus of this research- but the fact of their involvement remains. This suggests that at least part of these EV responses is along classical post-radiation and oncogenic pathways, respectively.

The reason why this is important is because another significant part of the EV response involves certain conserved metabolic pathways, including the oft-mentioned lysine degradation and fatty acid biosynthesis pathways. The specific effects of these pathways

have, to this writer's knowledge, not been studied in the context of radiation or leukaemogenesis, making these novel pathways in both mechanisms.

A 1936 work by Carl Voegtlin and J.W. Thompson, published in Public Health Reports, measured the effect of a lysine-deficient diet, based on heated powdered milk which denatured the amino acid, on the growth rate of neoplasms- to this writer's knowledge, it is the earliest such instance of this line of research. Besides demonstrating that lysine deficiency slowed the rate of growth of small tumours, which were all comprised of mammary carcinomas, they then went on to show that reintroduction of lysine into the diet, even in small amounts, rapidly accelerated tumour growth. They posited that due to the high growth rate of malignant cancerous cells, a high degree of essential amino acids was required.

This research has since been built on, with a variety of strategies targeting essential amino acids being employed. Of these amino acids, lysine finds itself a frequent subject of interest for therapeutic restrictive diets for the attenuation or prevention of cancers. In 2021, Hsu *et al.* demonstrated that lysine deprivation could overcome tyrosine kinase inhibitor resistance in non-small cell lung cancer (Hsu *et al.,* 2021, Cancers), suggesting a potential therapeutic route via lysine deprivation in order to sensitize or overcome drug resistance. Lysine was found to promote dissemination of oestrogen receptor positive breast cancer cells, and that it was the most utilized essential amino acid by these breast cancer cells (Rodriguez *et al.,* 2020, Frontiers in Oncology). Deamination of lysine via L-lysine a-oxidase was also shown to have anti-cancer effects via the production of cytotoxic H_2O_2 and ammonia, which reduced tumour growth (Lukasheva *et al.,* 2021, Pharmaceuticals). Most research focuses, logically, on the therapeutic possibilities of decreasing lysine concentrations: lowering lysine concentrations inhibits cancer cell growth. The referred 1936 study indicates that the opposite may also be true. Therefore, a sharp increase in levels of l-lysine within a cell creates a potently pro-oncogenic environment, which is rich in vital amino acids required for cancer proliferation. While lysine elevation alone is most likely not sufficient to cause

cancer, it nevertheless means that should one arise, the cellular cytoplasm contains cancer-friendly levels of nutrients. More likely, however, lysine levels could be used as a proxy for metabolic rate, their use as a biomarker of high metabolism cells flagging a cell population for further investigation as being potentially cancerous.

With regards to ionising radiation, their impact on levels of free l-lysine appears to be cell-type specific, at least amongst differing progenitor cell types. In mesenchymal stem cells, this radiation causes a sharp spike and increase in lysine levels, suggesting that direct radiation severely dysregulates lysine catabolism and breakdown, resulting in high intracellular lysine levels. However, surprisingly, EVs derived from these cells have the opposite effect on their recipients, decreasing lysine levels. This implies that the direct damage arising from radiation is sufficient to dysregulate lysine regulation in MSCs, but the cellular response is protective and antagonistic to radiation-induced dysregulation, communicating to other cells to *increase* rates of lysine degradation. This might indicate that in MSCs, a protective stress response to ionising radiation exists and is executed via EV signalling- a method that does not salvage the donor cell or any directly irradiated cells but serves to spare surrounding bystander cells.

In HSCs, this response operates differently. Direct radiation damage does not change lysine levels when compared to unirradiated controls, indicating that HSCs are more robust than MSCs in this regard, potentially as a result of their increased need for control and maintenance in their pluripotent state (being a less derived stem cell type than MSCs). Alternatively, HSC regulation may rely more heavily on apoptosis rather than restoration of homeostasis, which would explain the high rate of HSC die-off post IR, with signalling being part EV, part apoptotic body in an attempt to spare non-directly damaged HSCs and promote proliferation, regenerating the HSC population. Bystander EVs dramatically increase lysine levels in neighbouring cells. This could indicate that the relative importance of direct vs indirect effects is cell-type dependent within the context of metabolic regulation, with the direct effect being more important in MSCs and the indirect effect being more

important in HSCs, in fact being the only damage pathway that causes a dysregulation of lysine within HSCs. Further research in different cell types e.g., macrophages, osteoclasts, osteoblasts etc must be performed to find if every cell type has its unique response, or if one response (i.e. protective EVs vs damaging EVs) is more prevalent. It must also be determined whether the response is EV or recipient dependent, i.e. whether it is the EV content that mediates the lysine metabolism response or the specific configuration of receptor pathways within the recipient. The former is more likely, given the miRNA cargo (among others, such as mRNA, lipids, and proteins), but the latter cannot yet be discarded as a possibility.

HSCs once again demonstrate a surprising metabolic robustness versus radiation insult when it comes to levels of free aldehyde in the cell, a result surprising due to the otherwise extremely radiosensitive nature of these cells. As before, this may be due to a different regulatory strategy which must be investigated by measuring rate of apoptosis, with cell death being the preferred strategy to cope with a sudden influx of ROS-induced stress. This has been seen in many cases of severe radiation poisoning e.g. in 1945, at the first Los Alamos 'demon core' incident, which led to acute radiation syndrome with a haematopoietic focus for physicist Haroutune Krikor Daghlian Jr., and the much later death of Robert J. Hemmerly, a special engineer detachment guard, of acute myeloid leukaemia 33 years after the incident. The former was estimated to have received a dose of 2Gy of neutron and 1.1Gy of gamma radiation, and the latter sustained a radiation insult of 0.08Gy of neutron radiation and 0.001Gy of gamma radiation (McLaughlin *et al.,* 2000, Los Alamos National Laboratory).

Neither direct nor indirect effects caused a significant fluctuation in aldehyde levels. On the other hand, direct and indirect effects increased aldehyde levels present in MSCs. Reactive aldehydes are known to be genotoxic (Wang *et al.,* 2022, Blood), being considered a ROS-many types of aldehyde dehydrogenases have evolved in order to metabolize and neutralize their oxidative stress ability (Singh *et al.,* 2013, Free Radical Biology and

Medicine). Aldehydes are divided into many different chemical subgroups, but the assay used in this research does not discriminate between these.

The elevated level of aldehyde seen after radiation in MSCs is therefore a classic sign of radiation-induced oxidative stress, with high levels of ROS being generated, as seen in figure 5.02, a level roughly triple that of the control. More significantly, bystander EVs increase this even further, to a level almost ten times higher than the control baseline. There is precedent for the involvement of EVs in oxidative stress management, with healthy cells secreting antioxidant EVs under normal physiological circumstances, and EVs also serve a function as ROS scavengers (e.g. endothelial microvesicles). EVs may also contain enzymes or other factors which serve to promote ROS production via interfering in antioxidant pathways (Chiaradia *et al.,* 2021, Cells; Bodega *et al.,* 2019, Journal of Extracellular Vesicles). As such, this provides evidence that in MSCs, the indirect effect of radiation is more severe, and unlike with lysine, secreted EVs are not protective of radiation damage. This may seem initially contradictory with the qPCR gene expression of Aldh7a1 and Aldh9a1, both aldehyde dehydrogenases essential in detoxifying reactive aldehydes. The levels of both aldehyde dehydrogenases increase after radiation and bystander EV exposure, which is beneficial to the cell. It is likely however that this is a cellular response to elevated aldehyde levels, and not due to EVs specifically- any cause of increased ROS levels within the cell would likely exhibit the same upregulation behaviour.

The expression levels of Aldh9a1 and Aldh7a1 in HSCs adds more weight to this argument. Levels of Aldh9a1 remained identical post-radiation but were massively increased in bystander EVs. Aldh7a1 decreased after radiation, and bystander response increased it. Taken together, this implies that HSCs have an alternative mechanism (perhaps another member of the aldehyde dehydrogenase protein family) for scavenging and neutralizing aldehydes that is notably more efficient than the mechanisms employed by MSCs.

Three possibilities exist for why the expression of both genes is increased by bystander EVs: the first is that the EVs possess an oxidative, aldehyde-formation promoting effect, as

seen in MSCs, leading to this gene upregulation to combat it, resulting in an efficient return to baseline levels. The second is that HSC-derived EVs possess antioxidant effects, expressed via the upregulation of these genes. The third possibility is that the reason aldehyde levels are normal even after radiation is due to EV action, exporting ROS via physical encapsulation and jettisoning, akin to the old 'garbage bin' paradigm. Upon absorbing this waste, cells must then upregulate dehydrogenases to cope with this sudden influx of reactive aldehydes. The half-life of reactive aldehydes varies heavily, between 1 second to 2 minutes, making it difficult to estimate whether these aldehydes have become inactive by the time they entered the bystander cells (Fritz & Petersen, 2013, Free Radical Biology and Medicine).To resolve this, further work must be carried out, chiefly via the isolation of these EVs and testing them for levels of aldehyde, and subsequently for anti-oxidant effect promoting mRNAs, miRNAs or proteins; in short, a further characterisation of their complete cargo rather than just the miRNA view we have taken so far.

Thus, it is likely that EVs are oxidative when released as a result of radiation/oxidative stress, but the efficiency of neutralizing these effects varies by cell type, with MSCs being less efficient at coping with EV-induced oxidative stress, and HSCs managing to completely mitigate their oxidative effects via reactive anti-oxidation mechanisms. As stated before, this is a somewhat surprising result given the known radiosusceptibility of HSCs. However, it is possible that this was due to the dose, dose rate, or time point, or an alternate regulation mechanism relying on apoptosis. A time course series may reveal a delayed response with rapid deterioration, although this is speculative and remains to be seen.

There has been an increased interest in the role of fatty acid synthase, Fasn, in recent years, particularly since 2020, with regards to its role in radiation resistance and in subsequent carcinogenesis. Fasn has been observed to be upregulated in multiple human cancers, with high expression levels being correlated with a poor patient prognosis (Yang *et al.,* 2011, International Journal of Biochemistry and Molecular Biology; Rae *et al.,* 2020, Advances in Radiation Oncology), with a reduction in Fasn expression resulting in

sensitization of tumours to radio- and chemotherapy. Fasn is believed to be a crucial mediator of cancer development as, like with lysine, cancers require a lot of material, whether it be in the form of amino acids for protein production or fatty acids for cell membrane production and vesicle secretion. While extracellular fatty acid remained unchanged, this merely means that active export of fatty acids into the extracellular space is not occurring in MSCs or HSCs.

In MSCs, Fasn was upregulated following both radiation and bystander EV exposure, indicating a deleterious upregulation which, again, favours cancer development should the prerequisite mutations occur, essentially creating ideal conditions. However, HSCs demonstrate an antagonistic response, with a downregulation of Fasn when irradiated, potentially indicating a stress pathway being activated to counteract the effect of radiation. However, bystander EVs upregulated Fasn in recipient cells; given the pathology and function of Fasn in many cancers, it is therefore likely that HSC EVs upregulate Fasn expression, possibly via silencing of Fasn antagonists. As with aldehyde regulation, it is thus highly likely that radiation derived EVs are in this case communicating a deleterious signal to unirradiated cells which provides an evolutionary advantage to any damaged, highly proliferative cells that may later become cancerous. Within the context of normal tissue response, however, Fasn upregulation is most likely stopped and downregulated to homeostatic levels later on, with healthy cells returning to baseline level once cell cycling activity returns to normal and IR injury is healed.

With regards to metabolic behaviour, therefore, one possibility is that EVs communicate pro-damage, harmful behaviour to recipient cells after a radiation insult, as seen by increasing the level of lysine, inducing oxidative stress via aldehyde generation, and upregulating Fasn. The effectiveness of the antagonistic response to mitigate this damage is dependent on cell type, with HSCs exhibiting a more robust, efficient response to EV-mediated stresses than MSCs, although the reason for this is unknown. An alternate hypothesis, and the one we believe is further supported by the data, is that the upregulation

of metabolic enzyme activity is indicative of heightened wound response triggered in healthy cells to replenish the damaged bone marrow niche. This will be further expanded upon in section 6.5.

One of the driving factors behind the activation and modulation of these metabolic pathways, along with the significant amount of signalling network involvement is the miRNA cargo of EVs- the first experiment to be performed, but perhaps most appropriately discussed last. As noted throughout this research, miRNA varies from condition to condition, with little to no overlap of individual miRNA transcripts between them. The conditions vary quite radically, from 24 hours post irradiation to 12 months, their leukaemic condition varies, as does cell type and dose. A single miRNA persisting throughout the entire response cycle and oncogenesis would be highly unlikely. Before we venture into discussing the ramifications of certain miRNA, and their potential significance, this must first be addressed, because what is remarkable is the persistence not of individual, discrete miRNA, but their targeted pathways. Despite the varied conditions and different doses, major radiation and carcinogenic pathways are represented in the form of the previously discussed signalling mechanisms, and metabolism remains disrupted during all conditions shortly after radiation insult, as well as during early leukaemia clonal expansion.

Radiation damage is stochastic in nature; while certain loci may be more prone to damage due to structural or genetic makeup, ultimately electron tracks cross DNA at random junctures, and ROS attacks the double helix at random places as well. Despite this, a consistent response, randomly distributed throughout the genome and across chromosomes, exists. This may indicate that 1) these miRNA are not directly ‘activated’ by radiation, but rather as a response to radiation damage, 2) this damage response has multiple redundancies and many different ways for it be activated, and 3) this could indicate the presence of a widespread, flexible, basic stress response mechanism mediated by miRNA and EVs that does not necessarily rely on classical signalling or immune cell recruitment.

Even though individual miRNA vary so heavily, the representation of these transcripts nevertheless presents extremely interesting implications. In 24 hour post irradiation WT-CBA mice, we see several miRNA being differentially expressed, but two are particularly notable: miR-34b-5p and miR-129-5p. These are notable for two reasons, the first being their function. miR-34b-5p is part of the miR-34 family, which are suspected to be tumour suppressors working synergistically with p53 (Zhang *et al.,* 2019, Journal of Experimental & Clinical Cancer Research). miR-129-5p is also a suspected tumour suppressor. The second reason they are notable is the fact that they are represented at both 0.1Gy and 3Gy, and upregulated to different levels at each dose, with a higher expression at a higher dose (implying some level of dose dependency). Their tumour suppressive function would imply that radiation-induced EVs confer a short-term protective effect in this regard (and at this timepoint) via the export of tumour suppressant miRNA.

Moving further along the post exposure timeline to 48 hours, macrophages and mesenchymal stem cells showed a distinct miRNA response but similar pathways being affected. It is unknown whether this miRNA variation is due to the different time point, or due to the homogeneous cell population makeup as opposed to the heterogeneous cell makeup of total bone marrow.

Macrophages play a critical role in the maintenance and regulation of the bone marrow microenvironment, especially with regards to progenitor cell populations. Macrophages play an important part in maintaining progenitor quiescence (Winkler *et al.,* 2010, Blood), with osteal macrophages supporting osteoblast formation (Sinder *et al.,* 2016, Journal of Bone and Mineral Research). It is here important to note that it is not a single macrophage subset that performs these functions, but two: osteal macrophages and so-called HSC niche macrophages. Macrophages are also found to participate in cross-talk with MSCs (Fan *et al.,* 2023, Frontiers in Cell Development Biology) during cross-talk, regulating MSC regeneration and macrophage inflammation and polarization. It is unknown if this represents a third subset of MSC niche macrophages, but we hypothesize, given the EV

secretion profile we identified, that a common pool of macrophages regulates both HSC and MSCs. The normal tissue function of BM-resident macrophages can be described as a maintenance function, regulating progenitor quiescence, and directing novel bone formation via upregulating osteoblast differentiation. Post-IR, this function changes: macrophages downregulate quiescence maintenance miRNA and activate pro-proliferation and self-renewal pathways, expanding the progenitor cell population, while simultaneously downregulating osteoblast differentiation in favour of adipogenesis in the bone marrow. This indicates a post-IR profile of reallocation of priorities to expansion and maintenance of the vulnerable progenitor niche, which is most likely to be damaged due to IR, and the regeneration of the bone marrow over the formation of novel bone. The duration of such a signal is unknown, but a possibility exists for this reallocation of resources and differentiation reprogramming to have long term consequences resulting in lowered bone density over time, contributing to fractures which are a well-documented and relatively common late effect after radiation treatment. We hypothesize that once the BM microenvironment progenitor population has been replenished, macrophages restore their pro-quiescence EV secretion profile.

We further hypothesize that in, a small percentage of cases, progenitor cells that have been stimulated to proliferate by macrophage signalling carry concurrent direct IR or ROS-induced genetic damage, resulting in a signalling cascade that results in self-reinforcing proliferation and expansion over time and fail to return to quiescence or undergo apoptosis. This process is slow, with a slow accumulation over time of genetic damage and pathway dysregulation. In cells where damage to PU.1 has occurred, this may lead to a deletion event due to high levels of cycling and replication- replication activity strain on the surviving PU.1 allele then mutates it (with cells bearing a double PU.1 deletion as a result suspected to undergo cell death). This double-hit event, as described previously, then gives rise to a clonal population which may become AML.

In macrophages, many miRNA bear explicit ties to AML development, such as miR-222 (albeit the 5p splice variant, as opposed to the 3p variant seen here), miR-98, miR-148b, miR-223, miR-150, miR-142a, and miR-1298. Of these, miR-98, miR-148b, miR-223 and miR-142a are prognostic markers for radiotherapy patients, with high levels of these miRNA correlating with better patient survival and recovery. miR-223, miR-98, miR-148b, and miR-142a are all upregulated in radiation-induced macrophage EVs, with miR-150 also being upregulated- miR-150 is typically seen to be downregulated in the BM of AML patients vs healthy controls. miR-1298, which is upregulated in human AML patients, is downregulated here. This demonstrates that macrophage modulation of the bone marrow niche post-IR injury does not operate along the same pathways and principles as AML proliferation does, with different miRNA pathways being used in each case to stimulate proliferation and cell cycling.

Mesenchymal stem cells also have several important miRNAs, these being miR-128, miR-34a, miR-652, miR-345, miR-339 and miR-23a. Of these, miR-34a, miR-345, miR-339 and miR-23a are tumour and cancer suppressant, especially miR-34a, exhibiting known anti-tumour functions and/or being correlated with good patient prognosis, including high expression levels post-remission, or low levels being associated with poor clinical outcomes. miR-345 and miR-339 are both upregulated, but miR-34a is downregulated in MSC EVs. miR-128 is upregulated as well, a miRNA which is known to be heavily associated with AML and worse patient outcomes (Seca *et al.,* 2014, Current Pharmaceutical Biotechnology). miR-652 and miR-23a are both downregulated in radiation-induced MSC EVs; a high level of miR-652 expression correlates with a higher risk of prostate cancer recurrence and is negatively correlated with patient outcomes in paediatric ALL. miR-23a is downregulated by stromal cells in AML, conferring drug resistance to the cancer cells via activation of protective autophagy. Thus a lower export of miR-23a is pro-proliferative, and indicates an overlap in proliferation upregulation in both healthy MSCs and in AML cells. As expanded upon in section 6.5, MSCs largely recapitulate the

proliferation, anti-differentiation repair response secreted by macrophages, but bear several key differences, namely the activation of the Notch pathway and exhibiting cross-talk with macrophages, triggering inflammation.

Given the mixture of responses in MSCs and to a lesser extent macrophages, it therefore appears as if these EVs are not the result of a homogeneous signalling effort. Instead, it is more likely that multiple independent response pathways have been activated within the cell, each with their own level of influence over the miRNA packaging or exclusion process into EVs- thereby, a cell is able to simultaneously produce protective signals, while also behaving in a pro-oncogenic way. This suggests a lack of central control over miRNA packaging and instead multiple independent routes existing.

Pre-leukaemic mice show a different EV miRNA landscape. There is no miRNA overlap, but, as previously explained, this is not surprising. Multiple miRNA are explicitly and heavily involved with important signalling networks, such as miR-540 being involved in Hippo signalling, miR-128 in FoxO, Wnt, and TGF-B, but also in fatty acid biosynthesis and lysine degradation, miR-370 (FoxO), and others. Of these miRNA, a few stand out due to their known modulation of carcinogenic or cancer-related processes: miR-540, miR-486a, miR-139, miR-128, miR-1897, miR-1224, miR-1949, miR-302c, miR-132, miR-345, miR-497, miR-181c, and miR-138. These can be subdivided into pro- or anti-oncogenic or unknown, as seen in table 1 below:

Table 6.1: Subdivision of miRNAs into known pro-oncogenic, anti-oncogenic or unknown categories. miRNA marked with an asterisk * either have contradictory reports in literature or behave differently dependent on patient population and type of cancer.

Pro-oncogenic	**Anti-oncogenic**	**Unknown**
miR-486a*	miR-486a*	miR-540
miR-1897	miR-139	
miR-1949	miR-128	
miR-181c*	miR-1224	
	miR-302c	
	miR-132	
	miR-345	
	miR-497	
	miR-181c*	
	miR-138	

Of the pro-oncogenic miRNA, miR-486a and miR-181c were upregulated (although it serves a dual purpose with known anti-oncogenic properties), along with miR-1949. miR-1897 was downregulated. Of the anti-oncogenic miRNAs, miR-139, miR-128, miR-302c, miR-132, miR-345, miR-497 and miR-138 were upregulated, with miR-1224 being downregulated. As such, only one explicitly pro-oncogenic miRNA was upregulated, and all but one known tumour suppressant miRNAs were upregulated, with one known pro-oncogenic miRNA being downregulated. Overall, it would appear that based on the regulation of the known cancer-implicated miRNA represented in the EV dataset, EVs are in fact exerting an anti-cancer effect, although there is a minor pro-oncogenic element of this response. This could be attributed to the fact we are sampling a heterogeneous mixture of cancerous and non-cancerous cells, although the possibility that EVs are part of a

lingering anti-cancer response still active even in leukaemic cells is also possible. Note that these miRNAs have not been found to have explicit roles in AML but have been found in multiple other cancers.

Without functional assessment of the oncogenic role of the other miRNA represented in this dataset, however, it is difficult to tell whether this hypothesis is likely to be true, but given the behaviour seen during short term post exposure radiation, this lends more weight to this line of thought.

Each miRNA targets multiple gene targets, but some notable targets are listed in table 6.2.

Table 6.2: Gene targets of select miRNA. Data sourced from either ENSEMBL where not stated, otherwise from cited literature.

miRNA	Genes targeted		
miR-181c	Rps6kb1 Map2k1	Braf Runx1	Tcf712
miR-540	Lats1 Thoc2	Tcerg1 Fanc1	
miR-139	Unknown; interacts with Wnt/TGF-B,	MAPK (Krishnan *et al.,* 2013, RNA)	
miR-128	Fasn Mapk14 Sos2	Pik3r1 FoxO1 Tgfbr1	Egfr Sos1 Smad3
miR-1224	Runx1t1 Braf		Sos1
miR-1897	Unknown		
miR-138	Tcf7 Braf		Rela Eif4ebp1
miR-1224	TNS4 (Shi *et al.,* 2020, Cell Death & Disease,)		
miR-1949	Unknown		
miR-345	Aldh2		
miR-302c	Sos1		
miR-132	Runx1t1 Sos1		
miR-486a	Cadm1		

Of these genes, Sos1 is targeted by multiple miRNA. The Mapk family of genes is also frequently targeted; Fasn and Smad are also seen. The importance of Fasn has been previously discussed, as has the importance of Mapk dysregulation, although its reoccurrence as a target (with different genes being targeted) hints at its vital nature. Sos1 (Son of Sevenless 1) is a well-studied mechanism for Ras activation, the latter of which constitutes the most frequently found mutation in human cancers (Tanizaki *et al.,* 2008), International Journal of Hematology). Smad proteins are responsible for signal transduction from activated TGF-beta (Witkowska *et al.,* 2017, Tumour Biology), with higher levels being found in chronic myeloid leukaemia patients, and high levels of Smad3 and Smad7 (the former of which is targeted here, by miR-128) predict poor prognosis for AML patients (Zhang *et al.,* 2019, Cancer Gene Therapy).

From this it becomes apparent that there is a high degree of targeting and modulation of known oncogenic genes, either via direct modulation of the pathway e.g Map2k1 or indirect modulation e.g. Sos1/Sos2 and Smad3. EVs that are present in high-clonal expansion, early leukaemic development are likely to be anti-leukaemic: they overexpress a host of anti-cancer miRNAs and have few known pro-oncogenic transcripts. Their presence is the result of targeting done by miRNAs that are known to have anti-tumour effects. This cannot be definitively said without further functional assays, but given the data found during this project there is weight to this hypothesis of protective, anti-cancer EVs being part of a wider response to attempt to combat AML development. Given that AML is irreversible once it has reached such a high level of clonal expansion, however, this response is clearly insufficient by itself, being perhaps the remnants of an early higher-level response, which could perhaps have been missed, or a last-ditch effort by the organism to combat AML development. It is nevertheless quite remarkable that most of the miRNA signal (at least, among those miRNAs previously characterized in the literature to be associated with cancer development) in a pre-leukaemic mouse is in fact anti-cancer. The source of this response must be isolated before further conclusions are drawn, as it is possible that they are

produced by highly active healthy cells, e.g. macrophages, or that they are still being produced by cancerous cells as a non-immune-dependent signalling mechanism that is still intact despite mutation and carcinogenic development.

There are some caveats to this conclusion with regards to certain miRNA, e.g. miR-181c. miR-181 is variably reported as being associated with good patient survival, but paradoxically also poor patient survival, both at high expression. A meta-analysis carried out in 2017 by Guo *et al.* found that while in American patients miR-181 expression was a diagnostic marker for high survival, the inverse was seen in a population of Chinese patients. The actual anti-tumour action of this particular miRNA is unknown within mice.

miRNAs that are activated in response to radiation appear to be evenly distributed throughout the genome, with little to no clustering seen along specific chromosomes or chromosomal loci. There are three exceptions to this: of the significantly dysregulated miRNAs, none were expressed on chromosomes 14, 17 and 19 of the murine genome, implying that these chromosomes do not contain genes coding for miRNAs involved with radiation response, or those they do have are silenced.

Five major DNA damage response pathways exist: base excision repair, nucleotide excision repair, mismatch repair, homologous recombination and non-homologous recombination (Chatterjee & Walker, 2017, Environmental and Molecular Mutagenesis). Of the genes involved in base excision repair, two are present on these chromosomes: NTHL1 is present on chromosome 17, and NEIL2 is present on chromosome 14 (Ensembl). In nucleotide excision repair, DDB1 and MMS19 are both located on chromosome 19, with ERCC6 being located on chromosome 14 (Ensembl). This demonstrates that while miRNA located on these chromosomes are not activated by IR, this does not mean that these chromosomes are not involved with the response at all, the response instead occurring at the protein expression level.

Chromosome X is also somewhat frequently seen with multiple miRNA being expressed, suggesting a sex-linked element in terms of radiation response, with females having more inbuilt redundancy and resistance to complete loss-of-function than males (as evidenced by male mice being more susceptible to radiation-induced tumours).

The purpose of radiation-induced EVs, and later EVs in a radiation-induced AML environment, are thus unclear, but several novel findings may hint at their role and offer avenues for further research. Firstly, radiation-induced EVs appear to induce oxidative stress in recipient cells via dysregulation of Aldehyde dehydrogenases, with the effectiveness of the cell's response to this stress varying by cell type. Radiation-induced EVs also increase lysine levels in recipient cells; current research focuses on the effects of restricting lysine on cancer rates and development, with very few studies working on the inverse effect of increasing lysine. The 1936 work by Carl Voegtlin and J.W. Thompson demonstrated that increasing lysine levels increased neoplasm development, but this was performed on an already-existing cancer as opposed to an organism yet to develop a cancer. Given the evidence, however, it would appear likely that increasing levels of lysine in the cell may not induce a cancer *de novo but* will increase the odds for a cancerous cell to survive and proliferate, stacking the deck in favour of leukaemia, so to speak. A third prong of EV function is the upregulating of Fasn in recipient cells, an important central protein regulator for fatty acid biosynthesis and, like the availability of lysine, essential for cell proliferation.

When a leukaemia begins developing, at higher (over 30%) levels of clonal expansion, the EV response shifts to combat leukaemogenic expansion, with several tumour-suppressant miRNA being exported which target known genes that have heavy involvement in AML development and carcinogenesis in general. Given that this response does not exist in low-clonal expansion mice, it would appear as if it is only activated under conditions of higher systemic stress due to AML, and as such may be a 'last ditch' effort to suppress a leukaemia, which often appears to be unsuccessful on its own, as mice past 30% clonal

expansion seldom experience remission without outside intervention (Zuber *et al.,* 2009, Genes & Development). Capitalizing and expanding on this response, however, perhaps boosting it via artificial injection or upregulation of these tumour-suppressant miRNA could tip the scales the other way and allow AML expansion to be overcome; alternatively, inducing this response at earlier stages of clonal expansion could allow for the suppression of AML development.

In early post-IR damage response, miRNA have a significant regulatory role in the activation of proliferation pathways and the regeneration of the progenitor niche, as demonstrated in 6.5 with a hypothetical mode of action and pathway.

In an established rAML, EVs cannot be said to have a purely pro-oncogenic or anti-oncogenic role. This diversity of behaviours implies that multiple simultaneous responses are activated upon radiation insult, with each response to some level governing miRNA packaging and export into secreted EVs. Two potential processes that may explain this are presented in figure 6.01.

There is still much unknown about EV sorting processes and the selective loading of miRNA, but it is known that this is not a passive process. It would in fact appear that individual miRNA have different sorting processes depending on different proteins. hnRNPA2B1 is an RNA binding protein that appears to be heavily involved in the packaging of certain miRNA via miRNA motif recognition, e.g levels of exosomal miR-503, miR-198, miR-601, and miR-93 are all tied to hnRNPA2B1 expression and sumoylation. SYNCRIP, another RNA binding protein, is also responsible for miRNA export, binding miR-3470a and miR-194, again via motif/domain interaction and recognition. Further export mechanisms exist, e.g. the Argonaute 2/RISC complex, which may sort miRNAs into EVs via the KRAS-MEK-ERK pathway, and others, such as Y-box binding protein 1, MEX3C, Major Vault Protein, and La Protein- and all of these under normal physiological conditions, without involving a disease state (all of the above sourced from Groot & Lee, 2020, Cells).

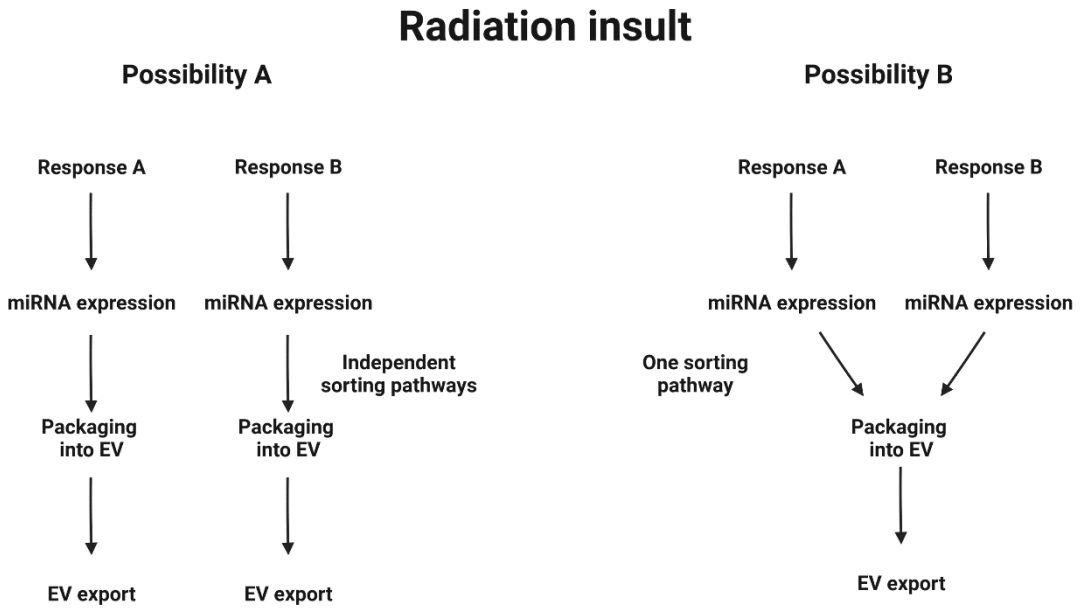


Figure 6.01: Possible pathways for EV export and miRNA profile composition. Image created using BioRender.

This therefore makes Possibility A more likely, with after radiation insult each response operating along its complimentary sorting pathway and packing its own miRNA into EVs, which leads to this diverse response with simultaneous protective and deleterious elements.

EVs thus play an important role in early radiation response, and in mid-stage AML are most likely secreted by healthy cells, containing cancer-repressing miRNA, in an attempt to suppress cancer development, with concurrent release of miRNA by cancerous cells in an attempt to compete with healthy tissue, and a potential ‘paradoxical’ effect (as seen with TGF-β) where activation of the pathway suppresses tumourigenesis in healthy cells while increasing it in cancerous ones. This research does not account for protein, mRNA, mtDNA, lipid or any other EV cargo, which may further nuance just how EVs interact with their recipients. Further research is necessary, but nevertheless several important factors have been elucidated in this project, chiefly the ability of EVs to induce oxidative stress, dysregulate lysine catabolism, and multiple instances of protective anti-tumour function in

rAML, as opposed to an overwhelming pro-oncogenic, leukaemic-transformation inducing secretion of miRNA.

6.3 Limitations of the study

There are a number of limitations within this body of work that must be acknowledged and should be accounted for and built upon in any future work deriving from this research.

The first would be limitations in terms of animal models. CBA GFP/mCh transgenic mice are incredibly powerful models that have the potential to offer a deep insight into different stages of radiation injury and AML development; however, it is not the model itself that is in question, but the handling thereof. As acknowledged earlier in this text, an observable sex difference exists in terms of a mouse's reaction to radiation exposure, with male mice being more susceptible to tumours. This study, in the interest of achieving enough power, used a mixed gender cohort of both males and females, without segregating and with insufficient power to conduct a male vs female study. As such variability within a single condition may have been introduced due to sex differences, which might obfuscate the significance of certain data or mask sex-specific miRNA signatures. Any future work would do well to attempt to expand the numbers and thus make a study of sex-based response and reactions possible.

Another limitation would be with the purification and treatment of the EVs themselves. In the interest of keeping data consistent with previous EU-funded research, LEUTRACK, under the CONCERT umbrella, ExoQuick was used to purify extracellular vesicles. However, this is not a widely accepted method for EV isolation, with the gold standard being and remaining an ultracentrifuge process, to which the lab did not have access. A comparison of ExoQuick-derived samples and ultracentrifuge-derived samples would be useful to determine how much of an impact, if any, this purification process might have had. Furthermore, it was not verified that the miRNAs identified by nCounter were indeed packaged within the EVs, rather than external via co-precipitation or binding to the outside

membrane, the latter of which is still a question in EV research to this day as to the precise localization of cargo miRNAs. Finally, the very term “extracellular vesicle” indicates another limitation, as it demonstrates that the sample is a mixture of exosomes and microvesicles. As technology advances and more size or marker segregation techniques become standard operating procedure, it may be possible to separate these into populations of purely exosomes or purely microvesicles, allowing for more in-depth studies to discern whether there is a difference in function between these two vesicle populations.

An assumption was made, given prior literature and radiation-specific differences seen in BM-derived EVs, that only radiation derived EVs would exert a specific effect on recipient cells in the context of the metabolic studies performed, these being lysine levels, free fatty acids and aldehyde levels, as well as gene expression of Fasn, Aldh7a1 and Aldh9a1. A more appropriate control would have been the use of non-irradiated derived EVs, to conclusively demonstrate whether or not the effect seen was radiation-induced or occurred in the presence of EVs regardless of radiation status. Due to the lack of this control, it is difficult to make completely confident assertions based on this data, and inclusion of this control would strengthen the argument and fidelity of the findings.

Much of the research done in this study was done at high dose radiation (2Gy and 3Gy) rather than low dose, and was mostly done as an acute, high dose rate exposure rather than low dose rate exposure over long periods. While we hypothesize that the extent of certain pathway activation (e.g. Sos1 in macrophages and MSCs post IR) is dose dependent, it is nevertheless critical to remember that low dose dynamics are substantially different, with much less apoptosis directly conferred on tissue and a greater representation of indirect vs direct damage. As seen in figure 6.02, a total dose of 50 rad (0.5Gy) results in an rAML induction rate of less than 5%. Therefore, there is direct evidence that low dose can induce rAML in CBA, but at a much lower rate than higher dose. Hypotheses as to the dose response of certain pathways must be confirmed by *in vitro* low dose exposures, with subsequent experiments testing the effect of dose rate. The extrapolation of high dose to

low dose cannot be done trivially and must be considered with due scepticism and validated with experimental evidence.

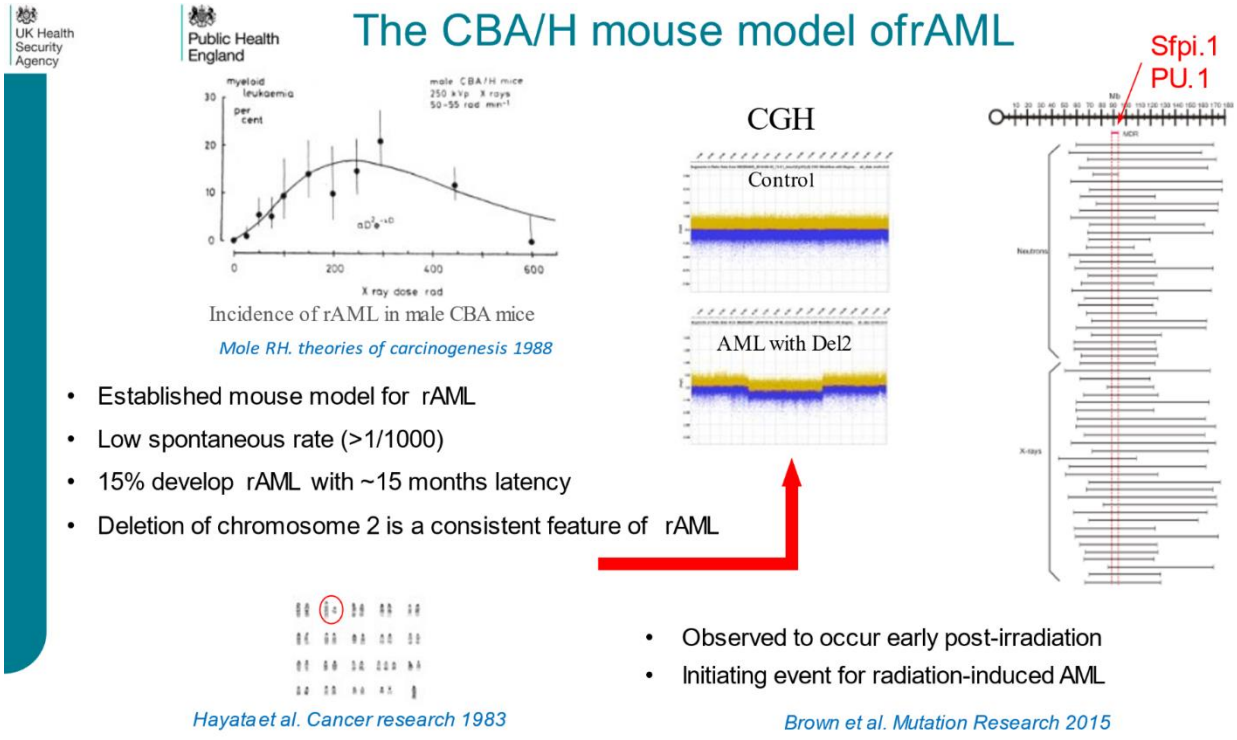


Figure 6.02: Induction of AML in CBA mice vs applied dose. Provided by Dr Christophe Badie (Internal communication).

Co-precipitated factors, i.e. small apoptotic bodies or extracellular RNA not packaged with EVs were most likely included in the samples used in this research. However, we do not believe these to constitute confounding factors to the data. Extracellular RNA and apoptotic bodies are also part of the bone marrow microenvironment signalling network, and whether miRNA uptake into a cell is mediated by an EV or not, it nevertheless exerts an affect. It may nuance the interpretation of the data insofar as the actual responsible extracellular mechanism is concerned or may demonstrate that multiple extracellular bodies and factors act in tandem to exert regulatory effects. Better resolution of the actual composition of the analytes would be useful in biological classification and clarification but does not lessen the significance of the data and the role of extracellular factors in post-IR and late-stage BM tissue response.

6.4 Future research and implications

A planned experiment that could not be carried out due to the Coronavirus pandemic was injecting EVs from pre-leukaemic CBA mCh/GFP mice into radiation-naïve CBA SPM mice, transgenic models especially susceptible to developing AML but more importantly with a very well-known and defined latency of AML development. It is this latter feature we were hoping to exploit, and what makes this model ideal for one of the first future projects which should be done. Injections of EVs isolated from the BM of irradiated CBA mCh/GFP mice, both leukaemic and non-leukaemic, as well as EVs from non-irradiated CBA mCh/GFP mice, would be performed via tail vein injections. There would then be two conditions. First, the SPM mice would then be irradiated at a total body dose of 3Gy. The reason for this is that when irradiated, the latency of AML development is an extremely consistent 3 months, with only +/- 2 weeks in variance. Any significant change to this latency period could thus be ascribed to the effect of the injected EVs. The second condition would be not irradiating the SPM mice at all. Due to their engineered mutations, these mice will develop AML regardless of radiation status within 12 months, but this has a higher variance of +/- 3 months. Any significant change, whether it be a shortening or lengthening of onset, could again be due to EVs and studied. This would allow for an *in vivo* quantification of how large an impact EVs have on AML development, and whether the presence of pre-existing AML EVs have the potential to vastly accelerate disease progression, or indeed perhaps retard it.

The ability of EVs to have direct effects on recipient cells has been demonstrated; however, it has not been explored whether individual miRNA have this ability as well. To establish the relative importance and impact of specific miRNA, further study is required. One possible method for tackling this would be the creation of artificial nanovesicles, a simple lipid bi-membrane, which is then filled with a single miRNA of interest, e.g. miR-1897-3p. Assays to determine if concentration is a limiting factor, or if combinations of miRNA rather than single transcripts are necessary, would need to be performed. This packaged miRNA

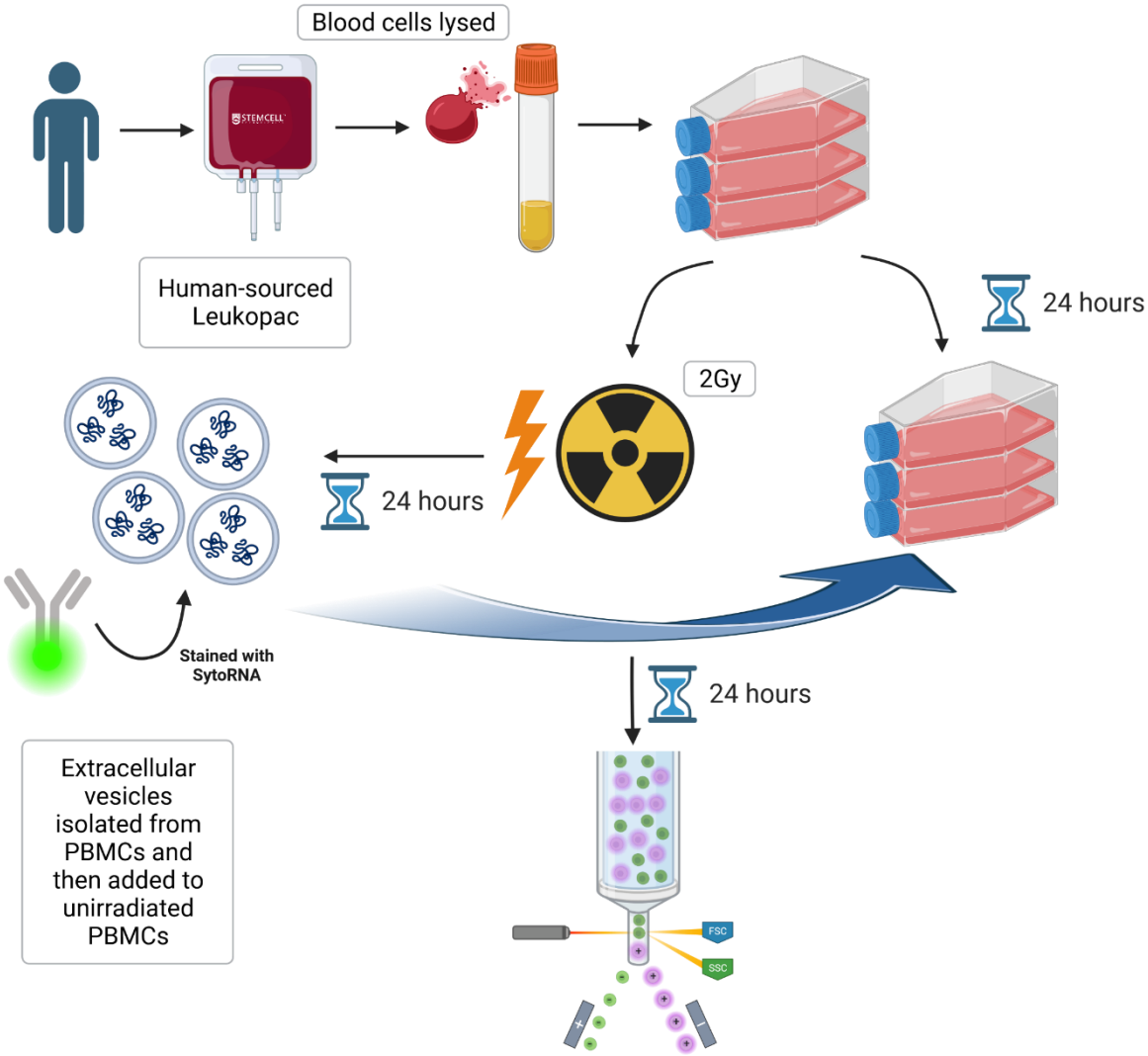
would then be exposed to a recipient cell of choice and the effect observed. In this example, qPCR could be performed to see how the gene expression of its targets Erg and Lifr is affected within the cell. Other studies such as colony formation assays could also be performed to see how cell behaviour is affected. A further step would be to test combinations of packaged miRNA to identify which have the most deleterious impact, with a final step being to then introduce anti-sense miRNA and observe whether this prevents or rescues the miRNA-caused cell phenotype- if this is the case, this presents a whole new avenue of potential clinical studies in terms of miRNA interference and silencing to prevent spread of radiation damage.

Work was performed towards the development of a novel method for analysing EV-mediated chromosomal damage during this research, but ultimately did not bear fruit- an outcome which does not preclude the eventuality it might. Briefly, human Leukopacs sourced from healthy human donors had their PBMCs isolated and purified. This was then split into three groups, recipient and donor, with a third group acting as control. Donors were further split into two groups: both were stained using an intercalating RNA dye, and then one of the groups was irradiated at 2Gy using X-rays. After 12 hours, EVs were isolated from the donors and then added to fresh medium into recipient PBMCs. This was then left a further 12 hours before FACS. The control group had fresh media containing an equivalent volume of PBS as EVs added, and underwent the same FACS procedure, which separated based on fluorescence level of the dye fluor, with the cut-off being established by an unstained PBMC control.

The protocol up until FACS has been well established, but more work must be done to optimize post-FACS culture and then cytogenetic analysis. The core question behind this particular arm of research was whether radiation derived EVs could cause *de novo* chromosomal aberrations within a recipient cell. Complications and difficulties with post FACS culture, leading to total loss of culture on more than one occasion, have precluded the generation of any significant results. Experimenting with different media, culture timings,

and perhaps FACS settings could work towards solving this issue and allowing for an in-depth, specific look at how EV-absorbing cells behave and if they are more prone to DNA damage. This would allow for (to this writer's knowledge and as of this writing) the first insight into the *specific* effects of EVs on recipient cells in terms of chromosomal damage, with the assurance that these cells have indeed absorbed EVs and not another component of the more usually used indiscriminate, non-segregated conditioned media from irradiated cultures.

Figure 6.03: Flowchart showing the experimental process for FACS-assisted determination of EV-induced chromosomal damage in human PBMCs. A 1/4 Leukopac, sourced from BioIVT, had its erythrocytes lysed and the remaining cells placed in culture. Half of these were irradiated at 2Gy or sham at 0Gy, the other half unirradiated. EVs were stained with SytoRNA and added to the unirradiated cells. After 24 hours this was sorted by FACS based on presence of fluorescence. Created with Biorender.com.



To establish whether EVs are the determining factor for chromosomal damage, a human model based on PBMCs was established. As seen in figure 13, a fresh ¼ size Leukopac (BioIVT) was procured. Upon arrival, the bag was sterilized with 70% ethanol and then the insert tube cut with a sterile pair of scissors. The blood was then allowed to drain by gravity into a sterile container containing 15% by volume acid citrose dextrose (ACD) solution, an anticoagulant which had been chosen over heparin due to heparin's ability to interfere with downstream analysis processes. While anticoagulant is not stated to be necessary in processing a Leukopac, it is nevertheless highly recommended to use due to the tendency for the blood to clot rapidly upon exposure to air, resulting in extremely high loss rates and poor recovery of the PBMCs.

The bag was then flushed with 20ml of RPMI1640 containing antibiotics to collect leftover cells. The container was then dispensed into 50ml Falcons, rinsed once more, and the Falcons gently spun at 1200 RPMI to pellet the cells. The supernatant was removed, leaving 5ml above the cell pellet so as not to disturb it, and then resuspended in 45 ml of RPMI1640. This was then spun down once more, and the wash repeated once again in order to wash off all the anticoagulant. 2ml red blood cell lysis buffer was then added and the pellet incubated for 2-3 minutes, and the tube filled with 45ml PBS and spun down to wash off the lysis buffer. This was repeated once more if a significant erythrocyte population as still present, as determined by a red pigmentation. Once this was finished, the cells were counted using an Incucyte and then resuspended at $5x10^6$ per ml in complete RPMI1640 with 10% FBS and antibiotics and incubated at 37C, 5% CO_2.

This population was split into two halves. One population was to be the recipient population. The other population was to be the donor population. The donor population was further split into two; one half irradiated at 2Gy using an X-ray source, and the other half sham irradiated at 0Gy. Both were then stained using SytoRNA Green according to manufacturer's instructions, a synthetic fluor designed to bind to RNA, which would then be packaged into EVs. These cultures were then returned to the incubator, and both donor and recipient

populations left for 24 hrs. The next day, the media from the stained donor groups was carefully spun down and filtered for cells, and then EVs were concentrated using the spin filter method described in a previous section. This was then added to a recipient culture, mixed thoroughly, and then put back into the incubator for another 24 hours. The following day, this was then sorted using a FACS machine, based on live/dead stain and the presence or absence of FITC fluorescence, which we gated based on an unstained control never exposed to stained EVs. This separated the population into ones with significant EV intake and those without. These cells were then assayed for yH2AX and dicentric breaks (using the CHO method) by our collaborating Cytogenetics department.

Other methodologies for this process were also tested prior to this workflow. To generate stained EVs, we initially used a human leukaemic cell line, and tested three; CESS, MLP3, and THP1. Of these, CESS proved the most promising in terms of growth rate and overall EV yield. Initially, we relied on volunteer blood donations to provide a source of PBMCs, but due to low volumes as specified by regulations and loss rates due to FACS, this ultimately provided too few cells to be analysed by cytogenetic assays. As such we switched to Leukopacs, still using CESS as a donor source. However, due to not owning a bioreactor or having access to one, it was impossible to grow CESS to the numbers necessary to match the Leukopac-extracted PBMCs 1:1. Furthermore, it seemed as if, no matter the ratio of donor:recipient cells, CESS-derived EVs were not preferentially absorbed by PBMCs, and in fact seemed to be excluded. As such a modification to the protocol was performed, yielding the above.

So far, all research has been done using X-rays. However, an ongoing evolution in the field of radiotherapy has led to the rise of alternative sources and types of radiation, for example neutron particles and carbon ions. It is currently unknown whether the radiation type or quality affects EV response, or even perhaps if some radiation types might spare a radiation EV response and thus minimize any deleterious effects this may have. An interesting future line of study would be a repeat of several experiments done during this research, e.g.

macrophage, MSC, and HSC cultures, but using alpha-particles rather than X-rays, and other radiation types and sources if available, and using the same methodologies described throughout this work, thus establish how and if radiation type plays into EV response. Given the different molecular effects of different radiation types, with different types of damage occurring (e.g. concentrated damage in neutron beams vs more scattered damage with gamma or X-rays) it is highly likely that we would see a rather different EV response and miRNA landscape represented. The impact of dose-rate differences, e.g. in FLASH irradiation, would also need to be investigated.

As seen throughout this research, metabolism regulation plays an important role both in normal tissue response to radiation injury and in AML establishment, with an unclear through-line linking both events in those cases where IR causes an AML. IR exposure does not mean a certain development of AML, only causing the disease in a percentage of cases (circa 35% for the mCh/GFP mice used). A mechanistic explanation linking early radiation response to AML development in this 35% cohort must be established. Within the context of metabolism, this is especially important due to the potential for non-invasive intervention and for diet to lessen AML development risk, e.g. a lysine-deficient diet reducing 35% AML induction to a 20% induction rate. To further study metabolism, a variety of techniques can be used to elucidate a clear and detailed image of the cellular metabolome.

Basic techniques for metabolism study include some of the molecular techniques used in this research e.g. the lysine, fatty acid and aldehyde assays, but also include protocols such as ELISA, FACS, immunoprecipitation, and the ChIP assay. Broader spectrum techniques to capture the entire metabolic state of a cell would be the next step, thereby expanding view and establishing what other effects, past the studied targets, IR and potential AML development have on homeostatic metabolism regulation within normal BM tissue. Techniques to perform this include LC-MS, capillary electrophoresis (CE) MS, and NMR. More advanced techniques still would be protocols such as the Seahorse assay,

calorimetry, ATP luciferase assays, and cycling assays. Please note that this list is not exhaustive.

A combination of these techniques could then be fed into a computational model for temporal trajectory analysis. For future work, a large-scale animal study using irradiated mCh/GFP CBA mice could be used. Some proposed time points for metabolic analysis would be immediately post radiation (15 minutes) if possible, followed by 24, 48, and 72 hours, to capture the immediate to short-term post radiation tissue response. Subsequent proposed time points of interest would be one week, two weeks, and then one month, with testing occurring monthly until AML development. This should be combined with blood testing at these monthly time points to correlate the metabolic flux of collected murine BM with clonal expansion. This approach would resolve the currently unknown gap in metabolic activity post short-term radiation and AML development, thereby establishing exactly how metabolism evolves over time in a) restoration to normal tissue homeostasis post IR without late effects and b) failure to restore normal tissue homeostasis and the development of AML. Furthermore, blood samples could be pyrosequenced to further segregate into types of AML. We would also suggest not removing ALL mice from the dataset and instead typifying them. This would allow for discovery of whether or not metabolic state and change over time could be used to discriminate between ALL and AML development.

Using this approach, this would then lay subsequent groundwork for dietary interventions based on metabolic flux data and analysing the impact thereof on rates of leukaemia induction post-IR.

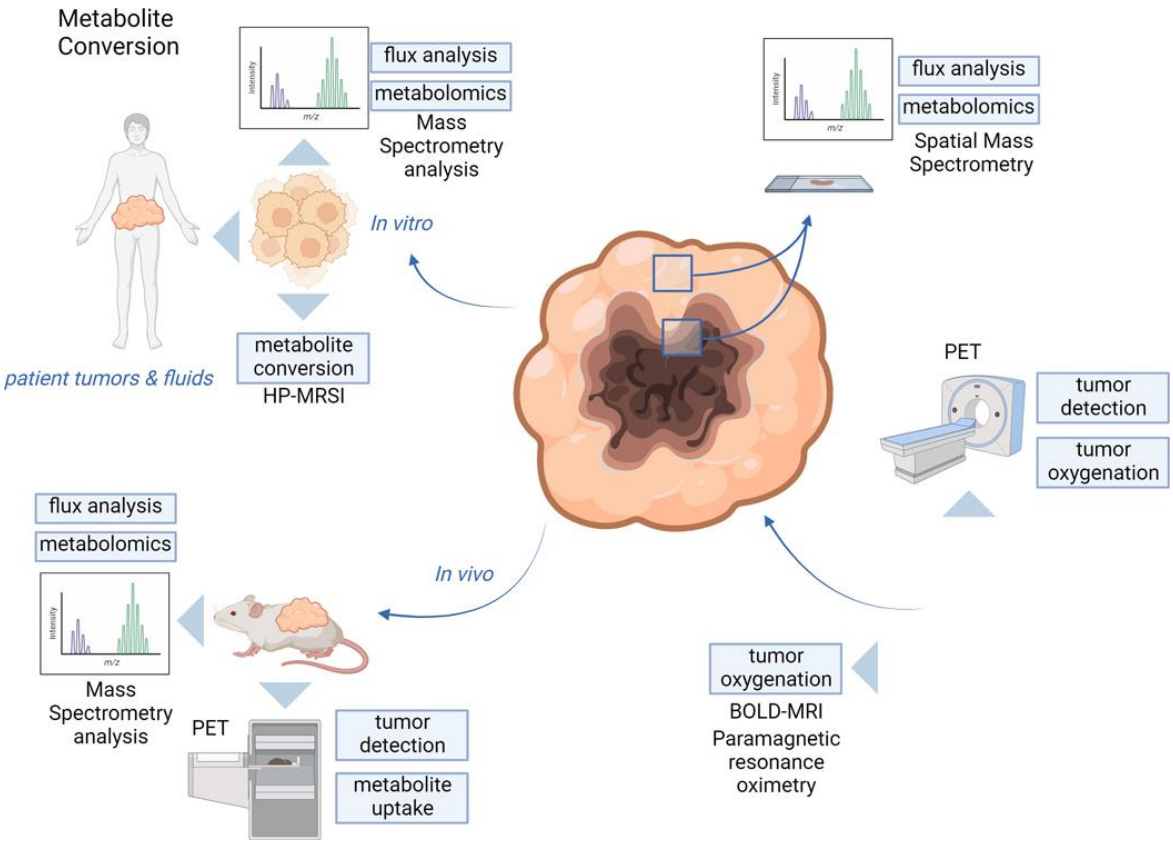


Figure 6.03: List of different techniques which can be used to study cancer cell metabolism. Reproduced from Read *et al.,* 2022, Molecular Carcinogenesis.

6.5 Hypotheses and Conclusions

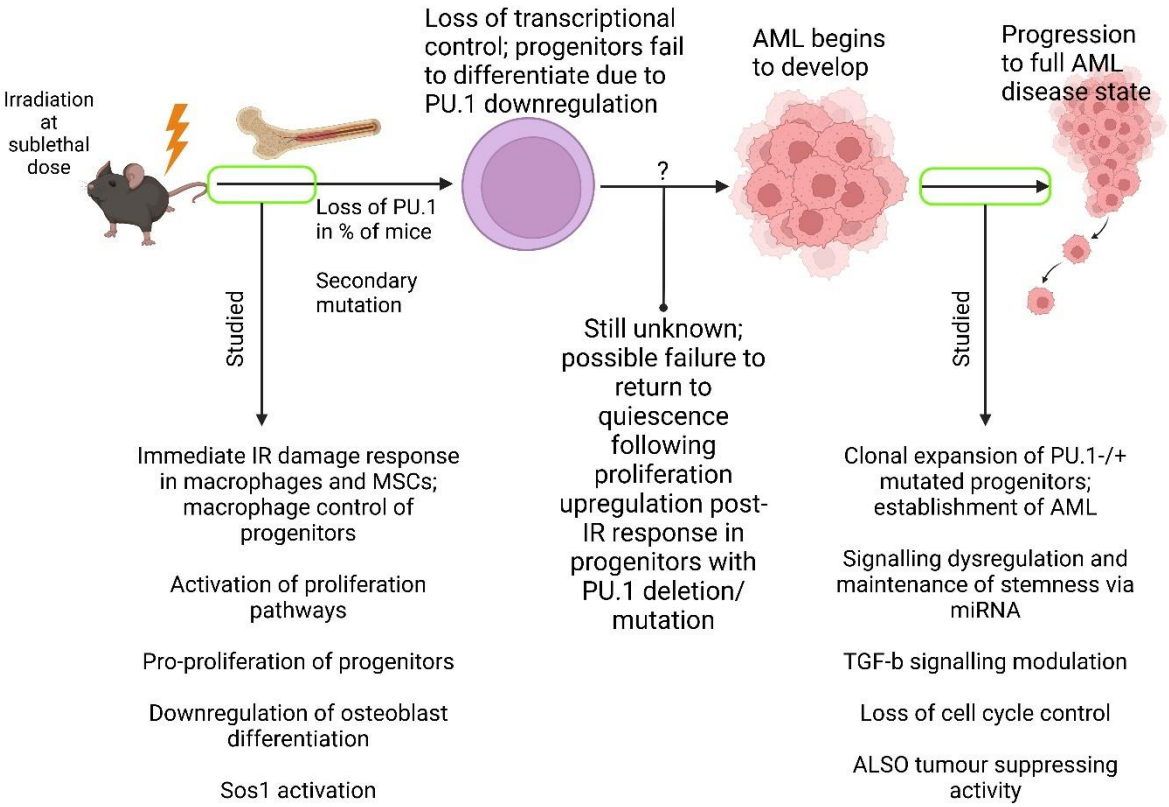


Figure 6.04: Overview of processes in rAML development and which sections of the process have been studied. Green boxes indicate the parts of the process that have been studied in the scope of this research. As seen, the middle section is still poorly understood and has not been studied in the present body of work. Created with Biorender.com.

The overall progression of rAML leukaemogenesis is shown in figure 6.04. The hypothesis behind this research is illustrated in figure 6.04. This study focussed on the sections of the leukaemogenic process marked in green. The middle section is still poorly understood, and was not directly studied as part of this present body of work. The hypotheses formulated as a result of this research are presented in figures 6.05 and 6.06. This research has served to elucidate EV-mediated miRNA regulation in the short term post IR, demonstrating how macrophages promote progenitor cell replenishment and shift differentiation profile to adipocytic from osteoblastic, as well as how MSCs contribute to and counter-balance this signalling, thus in-tandem regulating the healing of the radiation-damaged bone marrow niche. This study has further clarified the later stages of pre-leukaemic development, as clonal leukaemia cells are just beginning to establish themselves as the majority population

in the bone marrow microenvironment. To this writer's knowledge, this is the first time such a comprehensive study of EV-mediated regulation post-IR and pre-AML has been carried out, furthering the field by deepening understanding of these two ends of the pathway and unveiling important prognostic biomarkers and potential therapeutic targets. While the middle section of AML development, the progression from IR insult to potential AML development was not directly studied during this project, a hypothetical pathway has been constructed (figure 6.06) to explain how these two events are linked, providing a potential explanation.

To summarise, this research has substantially contributed to the understanding of bone marrow-resident macrophage and progenitor response to IR damage, with evidence that MSCs contribute to the immune activation of macrophages in stimulating inflammatory M1 polarization and induction of ferroptosis. It has also demonstrated the direct and indirect metabolic effects of radiation, to this writer's knowledge the first such attempt to do so with respect to lysine metabolism, an underreported and undervalued pathway of suspected high importance. Furthermore, this research has contributed to the understanding of late stage cancer development, demonstrating the existence of a tissue-level anti-tumour miRNA expression profile that is potentially context-dependent, with variable regulation of the TGF-β pathway resulting in both anti-tumour and pro-tumour action depending on cell status. A hypothetical link connecting both events, with macrophage-MSC axis pro-proliferation signalling combined with IR-event damaged progenitors increasing likelihood of PU.1 deletion and subsequent point mutation, serves as a valuable model for understanding rAML progression and extracellular communication regulation. Experimental validation or refutation of this hypothesis will provide extremely valuable insights into how normal tissue IR healing response may go wrong, leading to rAML in a minority of cases. The clearly demonstrated direct and indirect effects on progenitor cell metabolism provide further avenues of study and therapeutic targets, allowing for a multi-pronged therapeutic approach, and potentially provide further biomarkers in the form of metabolite levels.

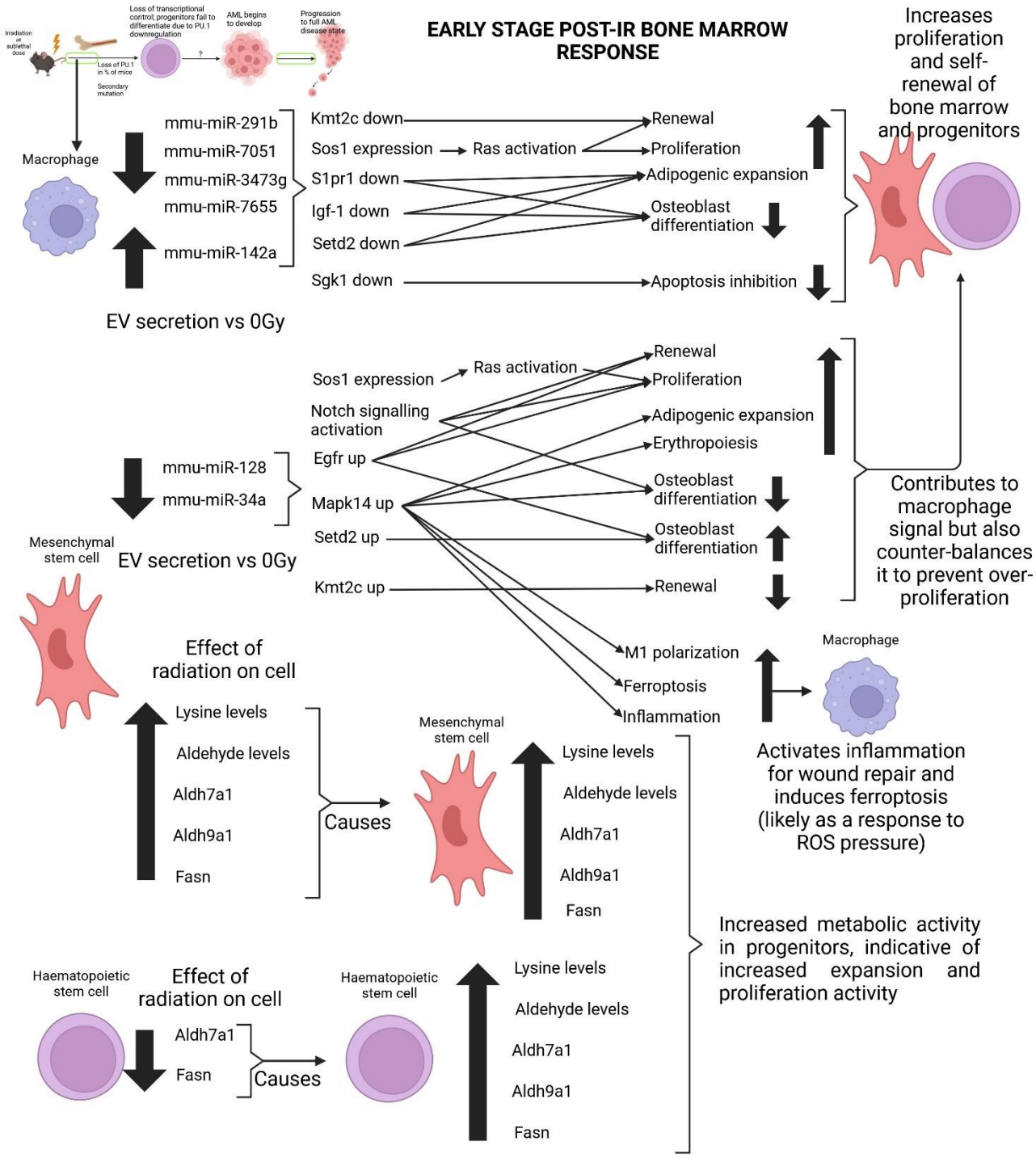


Figure 6.05: Hypothetical regulatory interaction network in early-stage post-IR response within the bone marrow. Created with Biorender.com.

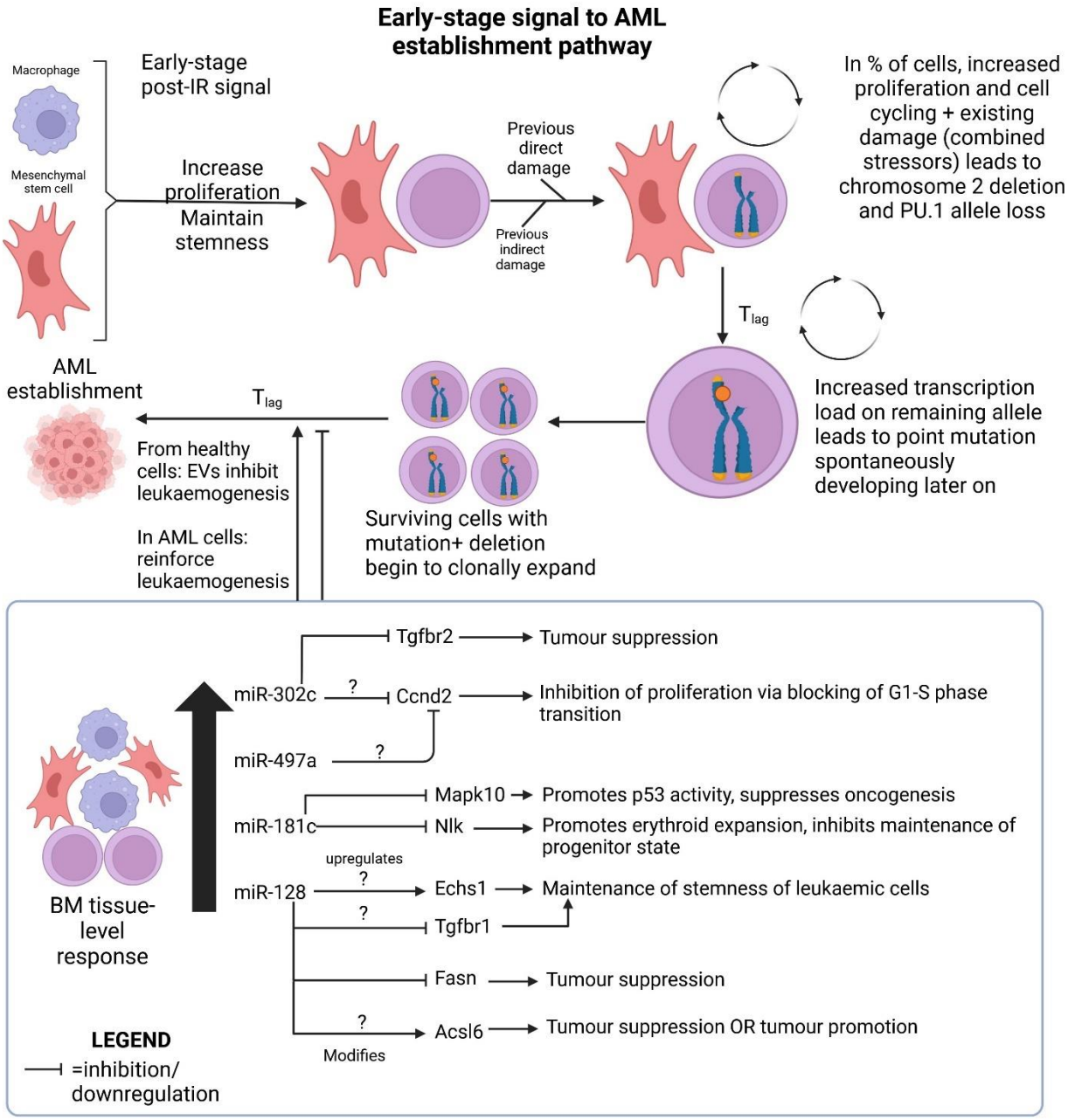


Figure 6.06: Hypothetical pathway for the development of AML over time. Initial early-stage post-IR signal, mediated by macrophages, MSCs and (likely) HSCs trigger a pro-proliferation, stem maintenance response in BM-resident progenitors. In progenitors with damage (either from the IR event or ROS), cell cycling pressures cause accumulation of mutations leading to chromosome 2 partial deletion and copy loss of PU.1. Increased transcription assay on remaining allele leads to spontaneous mutation, leading to PU.1 loss of function and failure for progenitors to differentiate. Clonal expansion of this population is partially inhibited by BM tissue EV secretion, although portion of activity e.g. via miR-128 inhibition of Tgfbr1 and regulation of Echs1 may contribute to leukaemic cell maintenance and resistance to differentiation, indicating a contextual response to signalling. Created with Biorender.com.

The implications of these findings are significant. Firstly, a biomarker panel for experimental validation is established. Short-term post IR, analysis of miR-128, miR-34a, miR-291b, miR-7051, miR-3473g, miR-7655 and miR-142a expression will demonstrate how different cell populations react to IR-induced stress and damage, with downregulation of all but miR-142a being a clear sign of IR-induced healing response being triggered. Further experimentation with dose may indicate if this is dose-dependent or independent, thereby providing a robust and clearly defined biomarker for either radiation exposure or allowing for determination of radiation exposure dose. Future research must test the expression of these miRNA firstly across dose, and then across time. Validation of such a robust biomarker panel will have far-reaching consequences for high-throughput screening in the case of radiation exposure events, allowing for more efficient triage of patients. Furthermore, these miRNAs provide insights into potentials for short-term post-IR interventions, with modulation of these miRNA allowing for tight control of post-IR tissue regeneration and amelioration of late effects. Especially, one significant discovery is the reprogramming of differentiation by macrophages, shifting from a pro-osteoblastic to a pro-adipocytic profile. This reprogramming may explain loss in bone density often seen in radiation therapy patients, and treatment of the symptoms by prescription of supplements or clinical intervention to boost osteoblastic differentiation may improve patient quality of life by reducing the possibility of long-term fractures.

Secondly, a clear and significant direct and indirect effect of IR on metabolism has been demonstrated in two progenitor populations, MSCs and HSCs. This has extremely significant implications and must be further studied. It is hypothesized that, in MSCs, IR exposure promotes a pro-proliferative response and cell cycling for DNA repair to occur, with an increase in rate of metabolic activity and upregulation of ROS scavenging enzymes (Aldh7a1 and Aldh9a1) to do so. Direct IR instead causes a downregulation in Fasn and ROS scavenging in HSCs, indicating that direct response to IR may be preferentially apoptosis while simultaneously releasing signals indicating to surviving HSCs to proliferate

and replenish the HSC pool. Depending on dose and dose rate, this metabolic program shift into a proliferative state may increase the chances for genetic instability to occur, be conserved, and pass down. Dietary interventions *prior to* radiation therapy, e.g. via a lysine and long chain fatty acid-deficient diet, will decrease the available metabolite pool for progenitor proliferation. This, then, in turn is hypothesized to trigger a fasting response, with increased monitoring and apoptosis of quasi-senescent and damaged cells, therefore preferentially ensuring proliferation of non-damaged, healthy progenitors. Thus, deeper understanding of metabolic activity post-IR allows for mitigation of late effects by early intervention. Furthermore, the interplay of several target genes seen throughout this research (e.g. Kmt2c) in metabolic-related pathways and regulatory pathways allows for even more comprehensive intervention strategies, by modulating both direct activity via modulation of miRNA expression, and indirect activity by modulating metabolite pool availability. To summarize, this body of research demonstrates the clear and significant involvement of metabolism which demands further study. A series of techniques and timepoints have been described in section 6.4, but the importance of potential prophylactic care given to radiation therapy patients pre, during and post-therapy as well as to radiation exposure patients cannot be understated. From an economic perspective, a simple measure such as diet control and micronutrient supply modulation to reduce long-term disease risk is of utmost importance.

Finally, a substantially tumour suppressant miRNA regulation profile has been demonstrated in late-stage AML, indicating that systemic response to oncogenesis stress does exist and has not been completely abrogated even in high levels of clonal occupation of the BM niche. This miRNA profile offers several benefits: first, its immediate use as a biomarker of systemic stress, thus indicating the development of a malignant neoplasm. This is incredibly useful for triage and early detection, allowing for characterization of the developing neoplasm. Furthermore, we strongly believe that these miRNAs are of significant prognostic value, indicating which pathways are likely to be constitutively active

with the developing leukaemia. This allows for oncologists to adjust treatment plans depending on, for example, TGF-β pathway repression within the developing cancer. By analysing miRNA expression, the aggressiveness and nature of the cancer can be predicted. Furthermore, we believe that the miRNA has strong use for predicting developmental stage; we predict that in extremely aggressive and well-established AML, with a shift in upregulation to downregulation of miR-181c and miR-302c marking the activation of p53-inhibiting JNK signalling, thus conferring further evolutionary advantages to leukaemia cells. Combining these beneficial aspects, we also propose that these miRNAs represent extremely valuable clinical targets, with artificial boosting of miRNAs (e.g. miR-181c) enhancing their tumour-suppressive capability and increasing the body's own ability to repress and combat a latent AML. Administration of such a therapy alongside chemotherapy and radiotherapy has dramatic potential for improving patient outcomes by chemo- and radio-sensitizing cancerous cells. We would extend this to propose use of such miRNA alongside radiotherapy for other cancers to mitigate the risk of secondary cancers, with such miRNA therapies being delivered months to years after treatment.

A complete summary of the hypothetical post-IR tissue response and subsequent development of leukaemic cells (in a small percentage of cases) is presented in figures 6.05 and 6.06, as well as hypothetical modes of action. A summarized overview of some of the major hypotheses is found in figure 6.07.

In summary, this body of research demonstrates early post-IR damage response in normal BM tissue, proposes a hypothetical model for progression from wound response to PU.1 deletion, mutation, and subsequent clonal expansion, and a pathway for clonal expansion to AML establishment alongside healthy tissue repression response. Taken together, a clear set of biomarkers that can be used to identify and quantify post-IR damage response has been identified, as well as a clear and distinct metabolic signature, that both provide significant clinical intervention targets for enhancing patient recovery from IR damage. Likewise, a set of biomarkers, prognostic factors, and clinical targets has been established

for an established clonally expanding leukaemic cell population, allowing for the tracking of AML progression and significantly, a major target for boosting of endogenous tumour suppression to improve patient outcomes. Coupled with dietary control to control metabolite availability for key targeted gene functions, e.g. Kmt2c, this demonstrates a powerful multi-pronged treatment approach to controlling and mitigating long-term stochastic risk and helping to improve patient response to chemo- and radiotherapy. This work has significantly advanced current understanding of early IR response and late AML development, and further research to validate the proposed hypothetical AML progression model will significantly advance the field's understanding of rAML leukaemogenesis.

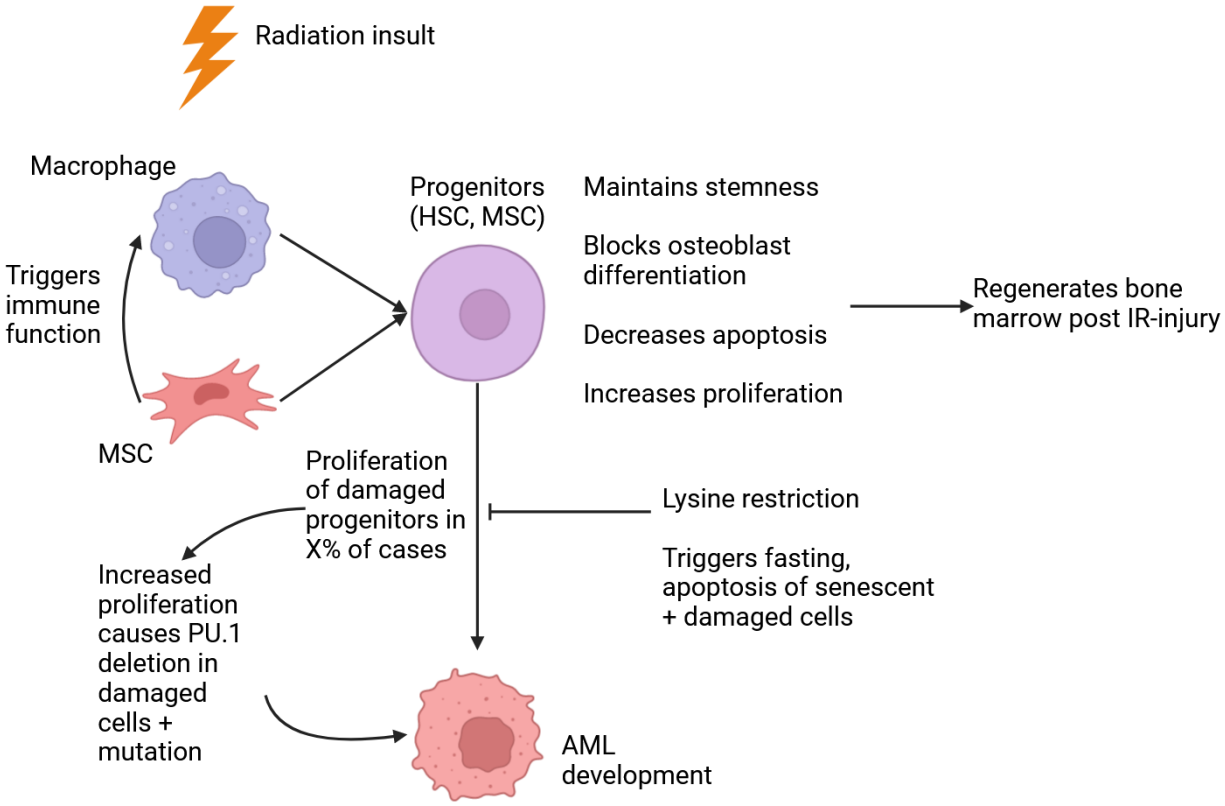


Figure 6.07: Simplified overview of some of the hypotheses generated during this research. We predict that a restriction in lysine would trigger more selective proliferation, scavenging damaged and senescent cells and reducing the likelihood of the regeneration of BM post-IR inadvertently causing the proliferation of damaged, pre-cancerous cells. Created with Biorender.com.

7. References Cited

1. Abels ER, Breakefield XO. Introduction to extracellular vesicles: biogenesis, RNA cargo selection, content, release, and uptake. *Cellular and Molecular Neurobiology* 2016;**36**:301–12.
2. Abrams HL. *Health Risks from Exposure to Low Levels of Ionising Radiation*., 2006.
3. Account - GeneCards Suite.
4. Agha DM, Rouas R, Najar M *et al.* Identification of acute myeloid leukemia bone marrow circulating MicroRNAs. *International Journal of Molecular Sciences* 2020;**21**:7065.
5. Akers J, Gonda D, Kim R *et al.* Biogenesis of extracellular vesicles (EV): exosomes, microvesicles, retrovirus-like vesicles, and apoptotic bodies. *Journal of Neuro-oncology* 2013;**113**:1–11.
6. Akkari Y, Baughn LB, Dubuc AM *et al.* Guiding the global evolution of cytogenetic testing for hematologic malignancies. *Blood* 2022;**139**:2273–84.
7. Akram S, Chowdhury Y S. Radiation Exposure Of Medical Imaging. *StatPearls* 2022.
8. ALDH7A1 aldehyde dehydrogenase 7 family member A1 [Homo sapiens (human)] - Gene - NCBI.
9. Allende ML, Tuymetova G, Lee BG *et al.* S1P1 receptor directs the release of immature B cells from bone marrow into blood. *The Journal of Experimental Medicine,* 2010;**207**:1113–24.
10. Alles J, Fehlmann T, Fischer U *et al.* An estimate of the total number of true human miRNAs. *Nucleic Acids Research* 2019;**47**:3353–64.

11. Aoki H, Tani H, Nakamura K *et al.* MicroRNA biomarkers for chemical hazard screening identified by RNA deep sequencing analysis in mouse embryonic stem cells. *Toxicology and Applied Pharmacology* 2020;**392**:114929.
12. Ark AV, Cao J, Li X. TGF-β receptors: In and beyond TGF-β signaling. *Cellular Signalling* 2018;**52**:112–20.
13. Ashrafi-Dehkordi K, Chaleshtori MH, Sharifi M *et al.* Inhibition of MicroRNA miR-222 with LNA Inhibitor Can Reduce Cell Proliferation in B Chronic Lymphoblastic Leukemia. *Indian Journal of Hematology and Blood Transfusion* 2016;**33**:327–32.
14. Azzam EI, Jay-Gerin J-P, Pain D. Ionizing radiation-induced metabolic oxidative stress and prolonged cell injury. *Cancer Letters* 2012;**327**:48–60.
15. Barzegar M, Farsani MA, Amiri V *et al.* AML-derived extracellular vesicles confer de novo chemoresistance to leukemic myeloblast cells by promoting drug export genes expression and ROS inhibition. *Deleted Journal* 2021;**20**:384–97.
16. Bentham Science Publishers. Effect of MIR-128 in DNA damage of HL-60 acute myeloid leukemia C...: Ingenta Connect.
17. Bhise N, Elsayed AH, Cao X *et al.* MicroRNAs mediated regulation of expression of nucleoside analog pathway genes in acute myeloid leukemia. *Genes* 2019;**10**:319.
18. Blume J, Ziętara N, Witzlau K *et al.* miR-191 modulates B-cell development and targets transcription factors E2A, Foxp1, and Egr1. *European Journal of Immunology* 2018;**49**:121–32.
19. Bodega G, Alique M, Puebla L *et al.* Microvesicles: ROS scavengers and ROS producers. *Journal of Extracellular Vesicles* 2019;**8**:1626654.

20. Boopathi E, Den RB, Thangavel C. Innate immune system in the context of radiation therapy for cancer. *Cancers* 2023;**15**:3972.
21. Budi HS, Younus LA, Lafta MH *et al.* The role of miR-128 in cancer development, prevention, drug resistance, and immunotherapy. *Frontiers in Oncology* 2023;**12**, DOI: 10.3389/fonc.2022.1067974.
22. Buhagiar A, Borg J, Ayers D. Overview of current microRNA biomarker signatures as potential diagnostic tools for leukaemic conditions. *Non-coding RNA Research* 2020;**5**:22–6.
23. Buss LG, De Oliveira Pessoa D, Snider JM *et al.* Metabolomics analysis of pathways underlying radiation-induced salivary gland dysfunction stages. *PloS One* 2023;**18**:e0294355.
24. Butler JT, Abdelhamed S, Kurre P. Extracellular vesicles in the hematopoietic microenvironment. *Haematologica* 2018;**103**:382–94.
25. Camacho V, McClearn V, Patel S *et al.* Regulation of normal and leukemic stem cells through cytokine signalling and the microenvironment. *International Journal of Hematology* 2017;**105**:566–77.
26. Cancer Research UK. Cancer statistics for the UK. *Cancer Research UK* 2023.
27. Caroti CM, Ahn HH, Salazar HF *et al.* A Novel Technique for Accelerated Culture of Murine Mesenchymal Stem Cells that Allows for Sustained Multipotency. *Scientific Reports* 2017;**7**, DOI: 10.1038/s41598-017-13477-y.
28. Cay P, Singer CA, Ba MA. Gene network analysis for identification of microRNA biomarkers for asthma. *Respiratory Research* 2022;**23**, DOI: 10.1186/s12931-022-02304-2.
29. Chan CM, Wong J, Wong CSM *et al.* Human antiquitin: Structural and functional studies. *Chemico-Biological Interactions* 2011;**191**:165–70.

30. Chatterjee N, Walker GC. Mechanisms of DNA damage, repair, and mutagenesis. *Environmental and Molecular Mutagenesis* 2017;**58**:235–63.
31. Chaudhry MA, Omaruddin RA, Brumbaugh CD *et al.* Identification of radiation-induced microRNA transcriptome by next-generation massively parallel sequencing. *Journal of Radiation Research* 2013;**54**:808–22.
32. Che P, Li J, Zhang S *et al.* miR-125a-5p impairs endothelial cell angiogenesis in aging mice via RTEF -1 downregulation. *Aging Cell* 2014;**13**:926–34.
33. Chen BB, Glasser JR, Coon TA *et al.* F-box protein FBXL2 targets cyclin D2 for ubiquitination and degradation to inhibit leukemic cell proliferation. *Blood* 2012;**119**:3132–41.
34. Chen H, Xiao Q, Hu Y *et al.* ANGPTL1 attenuates colorectal cancer metastasis by up-regulating microRNA-138. *Journal of Experimental & Clinical Cancer Research* 2017;**36**, DOI: 10.1186/s13046-017-0548-7.
35. Chen J, Wang J, Li H *et al.* p53 activates miR-192-5p to mediate vancomycin induced AKI. *Scientific Reports* 2016;**6**, DOI: 10.1038/srep38868.
36. Chen K, He H, Xie Y *et al.* miR-125a-3p and miR-483-5p promote adipogenesis via suppressing the RhoA/ROCK1/ERK1/2 pathway in multiple symmetric lipomatosis. *Scientific Reports* 2015a;**5**, DOI: 10.1038/srep11909.
37. Chen L, Nan A, Zhang N *et al.* Circular RNA 100146 functions as an oncogene through direct binding to miR-361-3p and miR-615-5p in non-small cell lung cancer. *Molecular Cancer* 2019;**18**, DOI: 10.1186/s12943-019-0943-0.
38. Chen L, Shi Z, Deng L *et al.* Construction of MicroRNA-mRNA regulatory network in the molecular mechanisms of Bleomycin-Induced pulmonary fibrosis. *BioMed Research International* 2022;**2022**:1–12.

39. Chen W, Yu Z, Huang W *et al.* LncRNA LINC00665 Promotes Prostate Cancer Progression via miR-1224-5p/SND1 Axis *OncoTargets and Therapy* 2020;**Volume 13**:2527–35.
40. Chen Y, Chen Y, Wang W *et al.* The miR-302c/transforming growth factor-β receptor type-2 axis modulates interleukin-1β-induced degenerative changes in osteoarthritic chondrocytes. *Journal of Cell Communication and Signaling* 2021;**16**:93–102.
41. Chen Y, Cui J, Liu Y *et al.* Plasma MIR-15B-5P, MIR-338-5P, and MIR-764 as biomarkers for hepatocellular carcinoma. *Medical Science Monitor* 2015b;**21**:1864–71.
42. Chi SW, Zang JB, Mele A *et al.* Argonaute HITS-CLIP decodes microRNA–mRNA interaction maps. *Nature* 2009;**460**:479–86.
43. Chiaradia E, Tancini B, Emiliani C *et al.* Extracellular Vesicles under Oxidative Stress Conditions: Biological Properties and Physiological Roles. *Cells* 2021;**10**:1763.
44. Creemers A, Van Der Zalm AP, Van De Stolpe A *et al.* FOXO transcriptional activity is associated with response to chemoradiation in EAC. *Journal of Translational Medicine* 2022;**20**, DOI: 10.1186/s12967-022-03376-w.
45. Crippa S, Santi L, Berti M *et al.* Role of ex vivo Expanded Mesenchymal Stromal Cells in Determining Hematopoietic Stem Cell Transplantation Outcome. *Frontiers in Cell and Developmental Biology* 2021;**9**, DOI: 10.3389/fcell.2021.663316.
46. Csordás IB, Rutten EA, Szatmári T *et al.* The MIRNA content of bone Marrow-Derived extracellular vesicles contributes to protein pathway alterations involved in ionising Radiation-Induced bystander responses. *International Journal of Molecular Sciences* 2023;**24**:8607.

47. Cui Y, Zhang C, Lian H *et al.* LncRNA linc00460 sponges miR-1224-5p to promote esophageal cancer metastatic potential and epithelial-mesenchymal transition. *Pathology Research and Practice* 2020;**216**:153026.
48. D'Souza A, Pearman CM, Wang Y *et al.* Targeting MIR-423-5P reverses Exercise Training–Induced HCN4 channel remodeling and sinus bradycardia. *Circulation Research* 2017;**121**:1058–68.
49. Daams R, Massoumi R. Nemo-Like Kinase in Development and Diseases: Insights from Mouse Studies. *International Journal of Molecular Sciences* 2020;**21**:9203.
50. Daguenet E, Louati S, Wozny A-S *et al.* Radiation-induced bystander and abscopal effects: important lessons from preclinical models. *British Journal of Cancer* 2020;**123**:339–48.
51. Dahlhaus M, Roolf C, Ruck S *et al.* Expression and prognostic significance of hsa-miR-142-3p in acute leukemias. *Neoplasma* 2013;**60**:432–8.
52. Dahmke IN, Backes C, Rudzitis-Auth J *et al.* Curcumin Intake Affects miRNA Signature in Murine Melanoma with mmu-miR-205-5p Most Significantly Altered. *PLOS ONE* 2013;**8**:e81122.
53. Dai S, Wen Y, Luo P *et al.* Therapeutic implications of exosomes in the treatment of radiation injury. *Burns and Trauma* 2022;**10**, DOI: 10.1093/burnst/tkab043.
54. De Groot M, Lee H. Sorting Mechanisms for MicroRNAs into Extracellular Vesicles and Their Associated Diseases. *Cells* 2020;**9**:1044.
55. De Martino M, Daviaud C, Hajjar E *et al.* Fatty acid metabolism and radiation-induced anti-tumor immunity. *International Review of Cell and Molecular Biology*. 2023, 121–41.

56. De Santis MC, Porporato PE, Martini M *et al.* Signaling pathways regulating redox balance in cancer metabolism. *Frontiers in Oncology* 2018;**8**, DOI: 10.3389/fonc.2018.00126.

57. Deficient Regulatory Innate Lymphoid Cells and Differential Expression of miRNAs in Acute Myeloid Leukemia Quantified by Next Generation Sequence. *Cancer Management and Research* 2020b, DOI: 10.2147/cmar.s234327.

58. Dent P, Yacoub A, Fisher PB *et al.* MAPK pathways in radiation responses. *Oncogene* 2003;**22**:5885–96.

59. Desouky OS, Ding N, Zhou G. Targeted and non-targeted effects of ionising radiation. *Journal of Radiation Research and Applied Sciences* 2015;**8**:247–54.

60. Diawara MR, Hue C, Wilder SP *et al.* Adaptive expression of MicroRNA-125A in adipose tissue in response to obesity in mice and men. *PLOS ONE* 2014;**9**:e91375.

61. Diez-Roux G, Lang RA. Macrophages induce apoptosis in normal cells in vivo. *Development* 1997;**124**:3633–8.

62. Ding H, Zhang H, Wang J *et al.* miR-302c-3p and miR-520a-3p suppress the proliferation of cervical carcinoma cells by targeting CXCL8. *Molecular Medicine Reports* 2021;**23**, DOI: 10.3892/mmr.2021.11961.

63. Dinh T-KT, Fendler W, Chałubińska-Fendler J *et al.* Circulating miR-29a and miR-150 correlate with delivered dose during thoracic radiation therapy for non-small cell lung cancer. *Radiation Oncology* 2016;**11**, DOI: 10.1186/s13014-016-0636-4.

64. Dong M, Blobe GC. Role of transforming growth factor-β in hematologic malignancies. *Blood* 2006;**107**:4589–96.

65. Duma MN, Oszfolk NI, Boeckh-Behrens T *et al.* Positive correlation between blood glucose and radiotherapy doses to the central gustatory system in

Glioblastoma Multiforme patients. *Radiation Oncology* 2019;**14**, DOI: 10.1186/s13014-019-1311-3.

66. Durante M, Formenti SC. Radiation-Induced chromosomal aberrations and immunotherapy: micronuclei, cytosolic DNA, and Interferon-Production pathway. *Frontiers in Oncology* 2018;**8**, DOI: 10.3389/fonc.2018.00192.
67. Eisfeld A, Kohlschmidt J, Schwind S *et al.* Mutations in the CCND1 and CCND2 genes are frequent events in adult patients with t(8;21)(q22;q22) acute myeloid leukemia. *Leukemia* 2016;**31**:1278–85.
68. Elsässer A, Franzen M, Kohlmann A *et al.* The fusion protein AML1-ETO in acute myeloid leukemia with translocation t(8;21) induces c-jun protein expression via the proximal AP-1 site of the c-jun promoter in an indirect, JNK-dependent manner. *Oncogene* 2003;**22**:5646–57.
69. Ensembl genome browser 110. *Ensembl*.
70. Eske K, Breitbach K, Köhler J *et al.* Generation of murine bone marrow derived macrophages in a standardised serum-free cell culture system. *Journal of Immunological Methods* 2009;**342**:13–9.
71. Esmail S, Manolson MF. Advances in understanding N-glycosylation structure, function, and regulation in health and disease. *European Journal of Cell Biology* 2021;**100**:151186.
72. Favero A, Segatto I, Perin T *et al.* The many facets of miR-223 in cancer: Oncosuppressor, oncogenic driver, therapeutic target, and biomarker of response. *Wiley Interdisciplinary Reviews RNA* 2021;**12**, DOI: 10.1002/wrna.1659.
73. Feng R, Sang Q, Zhu Y *et al.* MiRNA-320 in the human follicular fluid is associated with embryo quality in vivo and affects mouse embryonic development in vitro. *Scientific Reports* 2015;**5**, DOI: 10.1038/srep08689.

74. Flex E, Jaiswal M, Pantaleoni F *et al.* Activating mutations in RRAS underlie a phenotype within the RASopathy spectrum and contribute to leukaemogenesis. *Human Molecular Genetics* 2014;**23**:4315–27.

75. Frelin C, Ofran Y, Ruston J *et al.* Grb2 regulates the proliferation of hematopoietic stem and progenitors cells. *Biochimica Et Biophysica Acta Molecular Cell Research* 2017;**1864**:2449–59.

76. Fritz KS, Petersen DR. An overview of the chemistry and biology of reactive aldehydes. *Free Radical Biology and Medicine* 2013;**59**:85–91.

77. Fu S, Chen J, Ji F *et al.* MiR-486-5p negatively regulates oncogenic NEK2 in hepatocellular carcinoma. *Oncotarget* 2017;**8**:52948–59.

78. Furlong H, Stämpfli MR, Gannon AM *et al.* Identification of microRNAs as potential markers of ovarian toxicity. *Journal of Applied Toxicology* 2018a;**38**:744–52.

79. Furlong H, Stämpfli MR, Gannon AM *et al.* Identification of microRNAs as potential markers of ovarian toxicity. *Journal of Applied Toxicology* 2018b;3**8**:744–52.

80. Gabra M, Salmena L. MicroRNAs and Acute Myeloid Leukemia Chemoresistance: A Mechanistic Overview. *Frontiers in Oncology* 2017;**7**, DOI: 10.3389/fonc.2017.00255.

81. Ganesan S, Palani HK, Lakshmanan V *et al.* Stromal cells downregulate miR-23a-5p to activate protective autophagy in acute myeloid leukemia. *Cell Death and Disease* 2019;**10**, DOI: 10.1038/s41419-019-1964-8.

82. Gao C, Dusa A (2024). _ggVennDiagram: A 'ggplot2' Implement of Venn Diagram_. R package version 1.5.2, <https://CRAN.R-project.org/package=ggVennDiagram>.

83. Ge Y, Yan X, Jin Y *et al.* FMIRNA-192 and mIRNA-204 directly suppress LNCRNA HOTTIP and interrupt GLS1-Mediated glutaminolysis in hepatocellular carcinoma. *PLOS Genetics* 2015;**11**:e1005726.
84. Geest CR, Coffer PJ. MAPK signaling pathways in the regulation of hematopoiesis. *Journal of Leukocyte Biology* 2009;**86**:237–50.
85. Giuliani A, Prattichizzo F, Micolucci L *et al.* Mitochondrial (DYS) function in inflammaging: Do MItOMIRs influence the energetic, oxidative, and inflammatory status of senescent cells? *Mediators of Inflammation* 2017;**2017**:1–11.
86. Goldie BJ, Dun MD, Lin M *et al.* Activity-associated miRNA are packaged in Map1b-enriched exosomes released from depolarized neurons. *Nucleic Acids Research* 2014;**42**:9195–208.
87. Grewe JM, Knapstein P-R, Donat A *et al.* The role of sphingosine-1-phosphate in bone remodeling and osteoporosis. *Bone Research* 2022;**10**, DOI: 10.1038/s41413-022-00205-0.
88. Grigorian-Shamagian L, Fereydooni S, Liu W *et al.* Harnessing the heart's resistance to malignant tumors: cardiac-derived extracellular vesicles decrease fibrosarcoma growth and leukemia-related mortality in rodents. *Oncotarget* 2017;**8**:99624–36.
89. Gruszka-Westwood AM, Valli D, Alcalay M. WNT signalling in acute myeloid leukaemia. *Cells* 2019;**8**:1403.
90. Guay C, Menoud V, Rome S *et al.* Horizontal transfer of exosomal microRNAs transduce apoptotic signals between pancreatic beta-cells. *Cell Communication and Signalling* 2015;**13**, DOI: 10.1186/s12964-015-0097-7.

91. Guo J, Ren F, Wang Y *et al.* miR-764-5p promotes osteoblast differentiation through inhibition of CHIP/STUB1 expression. *Journal of Bone and Mineral Research* 2012;**27**:1607–18.
92. Guo L, Wu B, Wang X *et al.* Long-term low-dose ionizing radiation induced chromosome-aberration-specific metabolic phenotype changes in radiation workers. *Journal of Pharmaceutical and Biomedical Analysis* 2022;**214**:114718.
93. Hall J, Jeggo PA, West CML *et al.* Ionising radiation biomarkers in epidemiological studies – An update. *Mutation Research-reviews in Mutation Research* 2017;**771**:59–84.
94. Hamilton A, Foster K, Bonnet D. Impairment of AML engraftment to the bone marrow niche following inhibition of TGF-Beta signaling. *Blood* 2014;**124**:4372.
95. Hanieh H. Aryl hydrocarbon receptor-microRNA-212/132 axis in human breast cancer suppresses metastasis by targeting SOX4. *Molecular Cancer* 2015;**14**, DOI: 10.1186/s12943-015-0443-9.
96. Hao G, Ding Y, Wen HJ *et al.* Attenuation of deregulated miR-369-3p expression sensitizes non-small cell lung cancer cells to cisplatin via modulation of the nucleotide sugar transporter SLC35F5. *Biochemical and Biophysical Research Communications* 2017;**488**:501–8.
97. Harding CV, Heuser JE, Stahl PD. Receptor-mediated endocytosis of transferrin and recycling of the transferrin receptor in rat reticulocytes. *Journal of Cell Biology* 1983;**97**:329–39.
98. Hartman AD, Wilson-Weekes A, Suvannasankha A *et al.* Constitutive c-jun N-terminal kinase activity in acute myeloid leukemia derives from Flt3 and affects survival and proliferation. *Experimental Hematology* 2006;**34**:1360–76.
99. Harvard Health. Radiation risk from medical imaging. *Harvard Health* 2021.

100. He M, Jia Y, Wang Y *et al.* Dysregulated MAPK signalling pathway in acute myeloid leukemia with RUNX1 mutations. *Expert Review of Hematology* 2022;**15**:769–79.

101. Hill MA. Radiation Track Structure: How the spatial distribution of energy deposition drives biological response. *Clinical Oncology* 2020;**32**:75–83.

102. Hillig RC, Sautier B, Schroeder J *et al.* Discovery of potent SOS1 inhibitors that block RAS activation via disruption of the RAS–SOS1 interaction. *Proceedings of the National Academy of Sciences of the United States of America* 2019;**116**:2551–60.

103. Hilton MJ, Tu X, Wu X *et al.* Notch signaling maintains bone marrow mesenchymal progenitors by suppressing osteoblast differentiation. *Nature Medicine* 2008;**14**:306–14.

104. Hsieh C-H, Yang JC-S, Jeng JC *et al.* Circulating microRNA signatures in mice exposed to lipoteichoic acid. *Journal of Biomedical Science* 2013;**20**, DOI: 10.1186/1423-0127-20-2.

105. Hsu CC, Yang AYP, Chen JY *et al.* Lysine deprivation induces AKT-AADAT signalling and overcomes EGFR-TKIs resistance in EGFR-Mutant Non-Small cell lung cancer cells. *Cancers* 2021;**13**:272.

106. Hsu W-L, Preston DL, Soda M *et al.* The Incidence of Leukemia, Lymphoma and Multiple Myeloma among Atomic Bomb Survivors: 1950–2001. *Radiation Research* 2013;**179**:361.

107. Hu L, Xie X, Xue H *et al.* MiR-1224-5p modulates osteogenesis by coordinating osteoblast/osteoclast differentiation via the Rap1 signalling target ADCY2. *Experimental and Molecular Medicine* 2022;**54**:961–72.

108. Hu N, Cheng Z, Pang Y *et al.* High expression of MiR-98 is a good prognostic factor in acute myeloid leukemia patients treated with chemotherapy alone. *Journal of Cancer* 2019;**10**:178–85.

109. Huang X, Schwind S, Santhanam R *et al.* Targeting the RAS/MAPK pathway with*miR-181a*in acute myeloid leukemia. *Oncotarget* 2016;**7**:59273–86.

110. Humbert M, Seiler K, Mosimann S *et al.* Reducing FASN expression sensitizes acute myeloid leukemia cells to differentiation therapy. *Cell Death and Differentiation* 2021;**28**:2465–81.

111. ICRP.

112. Indrieri A, Carrella S, Carotenuto P *et al.* The pervasive role of the MIR-181 family in development, neurodegeneration, and cancer. *International Journal of Molecular Sciences* 2020a;**21**:2092.

113. Indrieri A, Carrella S, Carotenuto P *et al.* The pervasive role of the MIR-181 family in development, neurodegeneration, and cancer. *International Journal of Molecular Sciences* 2020b;**21**:2092.

114. International Atomic Energy Agency. *ANNUAL REPORT 2002*. IAEA, 2002.

115. International Ministerial Conference on Nuclear Power in the 21st Century.

116. Ishikawa K, Yamashiro T, Ariga T *et al.* Predictive factors of posttreatment fracture by definitive radiotherapy for uterine cervical cancer. *Japanese Journal of Radiology* 2020;**39**:93–9.

117. Islam A, Ghimbovschi S, Zhai M *et al.* An exploration of molecular correlates relevant to radiation combined Skin-Burn trauma. *PLOS ONE* 2015;**10**:e0134827.

118. Jang H, Park Y, Jang J. Serum and glucocorticoid-regulated kinase 1: Structure, biological functions, and its inhibitors. *Frontiers in Pharmacology* 2022;**13**, DOI: 10.3389/fphar.2022.1036844.

119. Jeffrey Willey Lab – Radiation-Induced bone fracture. *Wake Forest University School of Medicine*.

120. Jelonek K, Widlak P, Pietrowska M. The influence of ionising radiation on exosome composition, secretion and intercellular communication. *Protein and Peptide Letters* 2016;**23**:656–63.

121. Jia Y, Liu J, Wang G-Q *et al.* MIR-484: a potential biomarker in health and disease. *Frontiers in Oncology* 2022;**12**, DOI: 10.3389/fonc.2022.830420.

122. Jiang F, Liu T, He Y *et al.* MiR-125b promotes proliferation and migration of type II endometrial carcinoma cells through targeting TP53INP1 tumor suppressor in vitro and in vivo. *BMC Cancer* 2011;**11**, DOI: 10.1186/1471-2407-11-425.

123. Jin B, Jin D, Zhuo Z *et al.* MiR-1224-5p Activates Autophagy, Cell Invasion and Inhibits Epithelial-to-Mesenchymal Transition in Osteosarcoma Cells by Directly Targeting PLK1 Through PI3K/AKT/mTOR Signalling Pathway *OncoTargets and Therapy* 2020;**Volume 13**:11807–18.

124. Jin Y, Chen Z, Dong J *et al.* SREBP1/FASN/cholesterol axis facilitates radioresistance in colorectal cancer. *FEBS Open Bio* 2021;**11**:1343–52.

125. Johnson SM, Dempsey C, Chadwick AL *et al.* Metabolic reprogramming of bone marrow stromal cells by leukemic extracellular vesicles in acute lymphoblastic leukemia. *Blood* 2016;**128**:453–6.

126. Johnson SM, Dempsey C, Parker C *et al.* Acute lymphoblastic leukaemia cells produce large extracellular vesicles containing organelles and an active cytoskeleton. *Journal of Extracellular Vesicles* 2017;**6**:1294339.

127. Jokar S, Marques IA, Khazaei S *et al.* The footprint of exosomes in the Radiation-Induced Bystander effects. *Bioengineering* 2022;**9**:243.

128. Kastelowitz N, Yin H. Exosomes and Microvesicles: Identification and Targeting By Particle Size and Lipid Chemical Probes. *ChemBioChem* 2014;**15**:923–8.

129. Kaur S, Raggatt LJ, Batoon L *et al.* Role of bone marrow macrophages in controlling homeostasis and repair in bone and bone marrow niches. *Seminars in Cell & Developmental Biology* 2017;**61**:12–21.

130. Khan SY, Tariq M, Perrott JP *et al.* Distinctive microRNA expression signatures in proton-irradiated mice. *Molecular and Cellular Biochemistry* 2013;**382**:225–35.

131. Kim E-J, Kang I-H, Lee J-W *et al.* MiR-433 mediates ERRγ-suppressed osteoblast differentiation via direct targeting to Runx2 mRNA in C3H10T1/2 cells. *Life Sciences* 2013;**92**:562–8.

132. Kornblau SM, Singh N, Qiu YH *et al.* Highly phosphorylated FOXO3A is an adverse prognostic factor in acute myeloid leukemia. *Clinical Cancer Research* 2010;**16**:1865–74.

133. Krause M, Rak-Raszewska A, Naillat F *et al.* Exosomes as secondary inductive signals involved in kidney organogenesis. *Journal of Extracellular Vesicles* 2018;**7**:1422675.

134. Krishnan KV, Steptoe AL, Martin HC *et al.* miR-139-5p is a regulator of metastatic pathways in breast cancer. *RNA* 2013;**19**:1767–80.

135. Kuchenbauer F, Morin RD, Argiropoulos B *et al.* In-depth characterization of the microRNA transcriptome in a leukemia progression model. *Genome Research* 2008;**18**:1787–97.

136. Kumar B, Garcia M, Weng L *et al.* Acute myeloid leukemia transforms the bone marrow niche into a leukemia-permissive microenvironment through exosome secretion. *Leukemia* 2017;**32**:575–87.

137. Láinez-González D, Serrano-López J, Alonso-Domínguez J-M. Understanding the notch signalling pathway in acute myeloid leukemia stem cells: From hematopoiesis to neoplasia. *Cancers* 2022;**14**:1459.

138. Lall R, Ganapathy S, Yang M *et al.* Low-dose radiation exposure induces a HIF-1-mediated adaptive and protective metabolic response. *Cell Death and Differentiation* 2014;**21**:836–44.

139. Le MV, Shyh-Chang N, Khaw SL *et al.* Conserved Regulation of p53 Network Dosage by MicroRNA–125b Occurs through Evolving miRNA–Target Gene Pairs. *PLOS Genetics* 2011;**7**:e1002242.

140. Lee HC, Her NG, Kang D *et al.* Radiation-inducible miR-770-5p sensitizes tumors to radiation through direct targeting of PDZ-binding kinase. *Cell Death and Disease* 2017a;**8**:e2693.

141. Lee J, Hong BS, Ryu HS *et al.* Transition into inflammatory cancer-associated adipocytes in breast cancer microenvironment requires microRNA regulatory mechanism. *PLOS ONE* 2017b;**12**:e0174126.

142. Li C, Zheng X, Li W *et al.* Serum miR-486-5p as a diagnostic marker in cervical cancer: with investigation of potential mechanisms. *BMC Cancer* 2018;**18**, DOI: 10.1186/s12885-017-3753-z.

143. Li H, Xie H, Liu W *et al.* A novel microRNA targeting HDAC5 regulates osteoblast differentiation in mice and contributes to primary osteoporosis in humans. *Journal of Clinical Investigation* 2009;**119**:3666–77.

144. Li J, Hu C, Han L *et al.* MiR-154-5p regulates osteogenic differentiation of adipose-derived mesenchymal stem cells under tensile stress through the Wnt/PCP pathway by targeting Wnt11. *Bone* 2015;**78**:130–41.

145. Li J, Shen Z, Chen W *et al.* Screening of mIRNAs in white blood cell as a radiation biomarkers for rapid assessment of acute radiation injury. *Dose-response* 2022;**20**:155932582211236.

146. Li J, Xia W, Su X *et al.* Species-specific mutual regulation of p53 and miR-138 between human, rat and mouse. *Scientific Reports* 2016a;**6**, DOI: 10.1038/srep26187.

147. Li M, Fu W, Wo L *et al.* miR-128 and its target genes in tumorigenesis and metastasis. *Experimental Cell Research* 2013;**319**:3059–64.

148. Li X, Ji Q, Zhang C *et al.* miR-30a acts as a tumor suppressor by double-targeting COX-2 and BCL9 in H. pylori gastric cancer models. *Scientific Reports* 2017;**7**, DOI: 10.1038/s41598-017-07193-w.

149. Li X, Lv Y, Gao N *et al.* microRNA-802/Rnd3 pathway imposes on carcinogenesis and metastasis of fine particulate matter exposure. *Oncotarget* 2016b;**7**:35026–43.

150. Li X, Wu J, Liu S *et al.* miR-384-5p Targets *Gli2* and Negatively Regulates Age-Related Osteogenic Differentiation of Rat Bone Marrow Mesenchymal Stem Cells. *Stem Cells and Development* 2019;**28**:791–8.

151. Lima JF, Cerqueira L, Figueiredo C *et al.* Anti-miRNA oligonucleotides: A comprehensive guide for design. *RNA Biology* 2018;**15**:338–52.

152. Ling K-H, Brautigan PJ, Hahn C *et al.* Deep sequencing analysis of the developing mouse brain reveals a novel microRNA. *BMC Genomics* 2011;**12**, DOI: 10.1186/1471-2164-12-176.

153. Liu X, Cheng Y, Zhang S *et al.* A necessary role of MIR-221 and MIR-222 in vascular smooth muscle cell proliferation and neointimal hyperplasia. *Circulation Research* 2009;**104**:476–87.

154. Liu X, Du B, Zhang P *et al.* miR-380-3p regulates melanogenesis by targeting SOX6 in melanocytes from alpacas (Vicugna pacos). *BMC Genomics* 2019a;**20**, DOI: 10.1186/s12864-019-6343-4.

155. Liu X, Xiao J, Zhu H *et al.* miR-222 Is Necessary for Exercise-Induced Cardiac Growth and Protects against Pathological Cardiac Remodeling. *Cell Metabolism* 2015;**21**:584–95.

156. Liu X, Ye Q, Zhao X-P *et al.* RAS mutations in acute myeloid leukaemia patients: A review and meta-analysis. *Clinica Chimica Acta* 2019b;**489**:254–60.

157. Liu Y, Cheng Z, Pang Y *et al.* Role of microRNAs, circRNAs and long noncoding RNAs in acute myeloid leukemia. *Journal of Hematology & Oncology* 2019c;**12**, DOI: 10.1186/s13045-019-0734-5.

158. Liu Y, Li Y, Ren Z *et al.* MicroRNA-125a-3p is involved in early behavioral disorders in stroke-afflicted rats through the regulation of Cadm2. *International Journal of Molecular Medicine* 2017, DOI: 10.3892/ijmm.2017.3179.

159. Looi CK, Hii L-W, Ngai SC *et al.* The role of RAS-Associated protein 1 (RAP1) in cancer: Bad actor or good player? *Biomedicines* 2020;**8**:334.

160. Lu D, Xu Y, Liu Q *et al.* Mesenchymal stem Cell-Macrophage crosstalk and maintenance of inflammatory microenvironment homeostasis. *Frontiers in Cell and Developmental Biology* 2021;**9**, DOI: 10.3389/fcell.2021.681171.

161. Lu Y, Zhou J, Pei R *et al.* Expression and clinical significance of phospholipase D1 in de novo acute myeloid leukemia. *Hematology* 2020, DOI: 10.1080/16078454.2020.1786971.

162. Lukasheva EV, Babayeva G, Каршиева СШ *et al.* L-Lysine α-Oxidase: Enzyme with Anticancer Properties. *Pharmaceuticals* 2021;**14**:1070.

163. Luo A, Xu Z, Shi X *et al.* Exosome-derived miR-339-5p mediates radiosensitivity by targeting Cdc25A in locally advanced esophageal squamous cell carcinoma. *Oncogene* 2019;**38**:4990–5006.

164. Lysine and Malignant Growth: I. The Amino Acid Lysine as a Factor Controlling the Growth Rate of a Typical Neoplasm on JSTOR.

165. Ma F, Zhang M, Gong W *et al.* MIR-138 suppresses cell proliferation by targeting BAG-1 in gallbladder carcinoma. *PLOS ONE* 2015;**10**:e0126499.

166. Mancuso M, Pasquali E, Giardullo P *et al.* The Radiation Bystander Effect and its Potential Implications for Human Health. *Current Molecular Medicine* 2012;**12**:613–24.

167. Marchitti SA, Brocker C, Stagos D *et al.* Non-P450 aldehyde oxidizing enzymes: the aldehyde dehydrogenase superfamily. *Expert Opinion on Drug Metabolism & Toxicology* 2008;**4**:697–720.

168. Marin AC, Martín M, Liñan O *et al.* Bystander effects and radiotherapy. *Reports of Practical Oncology & Radiotherapy* 2015;**20**:12–21.

169. Mavragani IV, Nikitaki Z, Souli M *et al.* Complex DNA damage: a route to Radiation-Induced Genomic instability and carcinogenesis. *Cancers* 2017;**9**:91.

170. McLaughlin TP, Monahan SP, Pruvost NL *et al. A Review of Criticality Accidents 2000 Revision*., 2000.

171. Menon SS, Uppal M, Randhawa S *et al.* Radiation Metabolomics: Current status and future directions. *Frontiers in Oncology* 2016;**6**, DOI: 10.3389/fonc.2016.00020.

172. Mens MMJ, Ghanbari M. Cell cycle regulation of stem cells by MicroRNAs. *Stem Cell Reviews and Reports* 2018;**14**:309–22.

173. Mercuri M, Sheth T, Natarajan MK. Radiation exposure from medical imaging: A silent harm? *Canadian Medical Association Journal* 2011;**183**:413–4.

174. MicroRNA-466 regulates the proliferation, migration and invasion of the human lung cancer cells by targeting transcription factor RUNX2. *PubMed* 2020.

175. Milella M, Kornblau SM, Estrov Z *et al.* Therapeutic targeting of the MEK/MAPK signal transduction module in acute myeloid leukemia. *Journal of Clinical Investigation* 2001;**108**:851–9.

176. Miyamoto Y, Mauer AS, Kumar S *et al.* MMU-MIR-615-3P regulates lipoapoptosis by inhibiting C/EBP homologous protein. *PLOS ONE* 2014;**9**:e109637.

177. Miyazaki T, Ikeda K, Sato W *et al.* Extracellular vesicle-mediated EBAG9 transfer from cancer cells to tumor microenvironment promotes immune escape and tumor progression. *Oncogenesis* 2018;**7**, DOI: 10.1038/s41389-017-0022-6.

178. Morgan WF. RADIATION-INDUCED GENOMIC INSTABILITY. *Health Physics* 2011;**100**:280–1.

179. Morris V, Zhang A, Yang T *et al.* MicroRNA-150 expression induces myeloid differentiation of human acute leukemia cells and normal hematopoietic progenitors. *PLOS ONE* 2013;**8**:e75815.

180. Nam RK, Benatar T, Amemiya Y *et al.* MicroRNA-652 induces NED in LNCaP and EMT in PC3 prostate cancer cells. *Oncotarget* 2018;**9**:19159–76.

181. Nehrbas JF, Butler JT, Chen D-W *et al.* Extracellular vesicles and chemotherapy resistance in the AML microenvironment. *Frontiers in Oncology* 2020;**10**, DOI: 10.3389/fonc.2020.00090.

182. Nepstad I, Hatfield KJ, Grønningsæter IS *et al.* The PI3K-Akt-MTOR signalling pathway in human acute myeloid leukemia (AML) cells. *International Journal of Molecular Sciences* 2020;**21**:2907.

183. Neubauer A, Maharry K, Mrózek K *et al.* Patients With Acute Myeloid Leukemia and *RAS* Mutations Benefit Most From Postremission High-Dose Cytarabine: A Cancer and Leukemia Group B Study. *Journal of Clinical Oncology* 2008;**26**:4603–9.

184. Nogales-Cadenas R, Cai Y, Lin JR *et al.* MicroRNA expression and gene regulation drive breast cancer progression and metastasis in PyMT mice. *Breast Cancer Research* 2016;**18**, DOI: 10.1186/s13058-016-0735-z.

185. Novitskiy SV, Pickup MW, Chytil A *et al.* Deletion of TGF-β signaling in myeloid cells enhances their anti-tumorigenic properties. *Journal of Leukocyte Biology* 2012;**92**:641–51.

186. O'Brien G, Cruz-Garcia L, Zyla J *et al.* Kras mutations and PU.1 promoter methylation are new pathways in murine radiation-induced AML. *Carcinogenesis* 2019;**41**:1104–12.

187. O'Brien JA, Hayder H, Zayed Y *et al.* Overview of MicroRNA biogenesis, mechanisms of actions, and circulation. *Frontiers in Endocrinology* 2018;**9**, DOI: 10.3389/fendo.2018.00402.

188. Ogawa H, Wu X, Kikuchi K *et al.* MicroRNAs induce epigenetic reprogramming and suppress malignant phenotypes of human colon cancer cells. *PLOS ONE* 2015;**10**:e0127119.

189. Ohyashiki JH, Umezu T, Kobayashi C *et al.* Impact on cell to plasma ratio of miR-92a in patients with acute leukemia: in vivo assessment of cell to plasma ratio of miR-92a. *BMC Research Notes* 2010;**3**, DOI: 10.1186/1756-0500-3-347.

190. Olme C -h., Finnon R, Brown N *et al.* Live cell detection of chromosome 2 deletion and Sfpi1/PU1 loss in radiation-induced mouse acute myeloid leukaemia. *Leukemia Research* 2013;**37**:1374–82.

191. Ookhtens M, Kannan R, Lyon I *et al.* Liver and adipose tissue contributions to newly formed fatty acids in an ascites tumor. *American Journal of Physiology Regulatory, Integrative and Comparative Physiology* 1984;**247**:R146–53.

192. Ørom UA, Nielsen FC, Lund AH. MicroRNA-10A binds the 5′UTR of ribosomal protein mRNAs and enhances their translation. *Molecular Cell* 2008;**30**:460–71.

193. Pan B-T, Johnstone RM. Fate of the transferrin receptor during maturation of sheep reticulocytes in vitro: Selective externalization of the receptor. *Cell* 1983;**33**:967–78.

194. Pan J, Zhou C, Zhao X *et al.* A two-miRNA signature (miR-33a-5p and miR-128-3p) in whole blood as potential biomarker for early diagnosis of lung cancer. *Scientific Reports* 2018;**8**, DOI: 10.1038/s41598-018-35139-3.

195. Pandita A, Ramadas P, Poudel A *et al.* Differential expression of miRNAs in acute myeloid leukemia quantified by Nextgen sequencing of whole blood samples. *PLOS ONE* 2019;**14**:e0213078.

196. Pando A, Reagan JL, Quesenberry PJ *et al.* Extracellular vesicles in leukemia. *Leukemia Research* 2018;**64**:52–60.

197. Paolicelli RC, Bergamini G, Rajendran L. Cell-to-cell communication by extracellular vesicles: focus on microglia. *Neuroscience* 2019;**405**:148–57.

198. Park JH, Kim YH, Shim S *et al.* Radiation-Activated PI3K/AKT pathway promotes the induction of cancer Stem-Like cells via the upregulation of SOX2 in colorectal cancer. *Cells* 2021;**10**:135.

199. Pepe F, Pagotto S, Soliman S *et al.* Regulation of miR-483-3p by the O-linked N-acetylglucosamine transferase links chemosensitivity to glucose metabolism in liver cancer cells. *Oncogenesis* 2017;**6**:e328.

200. Pierre S, Bats A-S, Coumoul X. Understanding SOS (Son of Sevenless). *Biochemical Pharmacology* 2011;**82**:1049–56.

201. Pomeroy EJ, Eckfeldt CE. Targeting Ras signalling in AML: RALB is a small GTPase with big potential. *Small GTPases* 2017;**11**:39–44.

202. Qin Y, Wu L, Ouyang Y *et al.* MiR-125a Is a critical modulator for neutrophil development. *PLOS Genetics* 2017;**13**:e1007027.

203. Quiles JM, Narasimhan M, Shanmugam G *et al.* Differential regulation of miRNA and mRNA expression in the myocardium of Nrf2 knockout mice. *BMC Genomics* 2017;**18**, DOI: 10.1186/s12864-017-3875-3.

204. RADIATION EXPOSURE FROM MEDICAL DIAGNOSTIC IMAGING PROCEDURES: HEALTH PHYSICS SOCIETY FACT SHEET. *hps.org*.

205. Rae C, Fragkoulis GI, Chalmers AJ. Cytotoxicity and radiosensitizing activity of the fatty acid synthase inhibitor C75 is enhanced by blocking fatty acid uptake in prostate cancer cells. *Advances in Radiation Oncology* 2020;**5**:994–1005.

206. Rae C, Fragkoulis GI, Chalmers AJ. Cytotoxicity and radiosensitizing activity of the fatty acid synthase inhibitor C75 is enhanced by blocking fatty acid uptake in prostate cancer cells. *Advances in Radiation Oncology* 2020;**5**:994–1005.

207. Rafat M, Moraghebi M, Afsa M *et al.* The outstanding role of miR-132-3p in carcinogenesis of solid tumors. *Human Cell* 2021;**34**:1051–65.

208. Rajasegaran Y, Aziz AA, Rosli AA *et al.* Footprints of microRNAs in cancer biology. *Biomedicines* 2021;**9**:1494.

209. Raposo G, Nijman H, Stoorvogel W *et al.* B lymphocytes secrete antigen-presenting vesicles. *Journal of Experimental Medicine* 1996;**183**:1161–72.

210. Raposo G, Stoorvogel W. Extracellular vesicles: Exosomes, microvesicles, and friends. *Journal of Cell Biology* 2013;**200**:373–83.

211. Read GH, Bailleul J, Vlashi E *et al.* Metabolic response to radiation therapy in cancer. *Molecular Carcinogenesis* 2021;**61**:200–24.

212. Reisz JA, Bansal N, Qian J *et al.* Effects of Ionizing radiation on Biological Molecules—Mechanisms of damage and emerging Methods of detection. *Antioxidants & Redox Signaling* 2014;**21**:260–92.

213. Rodríguez A, Yang C, Furutani E *et al.* Inhibition of TGFβ1 and TGFβ3 promotes hematopoiesis in Fanconi anemia. *Experimental Hematology* 2021;**93**:70-84.e4.

214. Rodriguez GV, Abrahamsson A, Turkina MV *et al.* Lysine in combination with estradiol promote dissemination of estrogen receptor positive breast cancer via upregulation of U2AF1 and RPN2 proteins. *Frontiers in Oncology* 2020;**10**, DOI: 10.3389/fonc.2020.598684.

215. Rommer A, Steinleitner K, Hackl H *et al.* Overexpression of primary microRNA 221/222 in acute myeloid leukemia. *BMC Cancer* 2013;**13**, DOI: 10.1186/1471-2407-13-364.

216. Rouas R, Merimi M, Badram B *et al.* Identification of the Microrna Signature of Acute Myeloid Leukemia Patient s Regulatory T Lymphocytes. *Blood* 2015;**126**:4967.

217. Rzepiel A, Horváth A, Kutszegi N *et al.* MiR-128-3p as blood based liquid biopsy biomarker in childhood acute lymphoblastic leukemia. *Molecular and Cellular Probes* 2023;**67**:101893.

218. Saludas L, Garbayo E, Ruiz-Villalba A *et al.* Isolation methods of large and small extracellular vesicles derived from cardiovascular progenitors: A comparative study. *European Journal of Pharmaceutics and Biopharmaceutics* 2022;**170**:187–96.

219. Schaue D, Micewicz ED, Ratikan JA *et al.* Radiation and inflammation. *Seminars in Radiation Oncology* 2015;**25**:4–10.

220. Shaffi K, Galas DJ, Etheridge A *et al.* Role of MicroRNAs in Renal Parenchymal Diseases—A new dimension. *International Journal of Molecular Sciences* 2018;**19**:1797.

221. Shi Z-Z, Wang W, Chen Y *et al.* The miR-1224-5p/TNS4/EGFR axis inhibits tumour progression in oesophageal squamous cell carcinoma. *Cell Death and Disease* 2020;**11**, DOI: 10.1038/s41419-020-02801-6.

222. Sinder BP, Pettit AR, McCauley LK. Macrophages: their emerging roles in bone. *Journal of Bone and Mineral Research* 2015;**30**:2140–9.

223. Singh S, Brocker C, Koppaka V *et al.* Aldehyde dehydrogenases in cellular responses to oxidative/electrophilicstress. *Free Radical Biology and Medicine* 2013;**56**:89–101.

224. Singh VK, Newman VL, Romaine PLP *et al.* Use of biomarkers for assessing radiation injury and efficacy of countermeasures. *Expert Review of Molecular Diagnostics* 2015;**16**:65–81.

225. Song N, Pei Z, Gui F. MiR-1224-5p acts as a tumor suppressor via inhibiting the malignancy of rectal cancer through targeting SLC29A3. *Iubmb Life* 2020;**72**:2204–13.

226. Song Y, Yue Z, Wang Z *et al.* MicroRNA-148b is frequently down-regulated in gastric cancer and acts as a tumor suppressor by inhibiting cell proliferation. *Molecular Cancer* 2011;**10**, DOI: 10.1186/1476-4598-10-1.

227. Sun M, Song H, Wang S *et al.* Integrated analysis identifies microRNA-195 as a suppressor of Hippo-YAP pathway in colorectal cancer. *Journal of Hematology & Oncology* 2017;**10**, DOI: 10.1186/s13045-017-0445-8.

228. Sun S, Wang X, Xing X *et al.* MiR-433-3p suppresses cell growth and enhances chemosensitivity by targeting CREB in human glioma. *Oncotarget* 2016;**8**:5057–68.

229. Sun X-L, Liu H, Li T *et al.* MicroRNA-339-5p inhibits cell proliferation of acute myeloid leukaemia by directly targeting SOX4. *Molecular Medicine Reports* 2018, DOI: 10.3892/mmr.2018.9552.

230. Surendran S, Jideonwo V, Merchun C *et al.* Gene targets of mouse miR-709: regulation of distinct pools. *Scientific Reports* 2016;**6**, DOI: 10.1038/srep18958.

231. Szatmári T, Kis D, Bogdándi EN *et al.* Extracellular vesicles mediate Radiation-Induced systemic bystander signals in the bone marrow and spleen. *Frontiers in Immunology* 2017;**8**, DOI: 10.3389/fimmu.2017.00347.

232. Szatmári T, Persa E, Kis E *et al.* Extracellular vesicles mediate low dose ionising radiation-induced immune and inflammatory responses in the blood. *International Journal of Radiation Biology* 2018;**95**:12–22.

233. Tang F, Zhang R, He Y *et al.* MicroRNA-125B induces metastasis by targeting STARD13 in MCF-7 and MDA-MB-231 breast cancer cells. *PLOS ONE* 2012;**7**:e35435.

234. Tanizaki R, Katsumi A, Kiyoi H *et al.* Mutational analysis of SOS1 gene in acute myeloid leukemia. *International Journal of Hematology* 2008;**88**:460–2.

235. Tao J, Ji J, Li X *et al.* Distinct anti-oncogenic effect of various microRNAs in different mouse models of liver cancer. *Oncotarget* 2015;**6**:6977–88.

236. TargetScanMouse 8.0.

237. Tetta C, Ghigo E, Silengo L *et al.* Extracellular vesicles as an emerging mechanism of cell-to-cell communication. *Endocrine* 2012;**44**:11–9.

238. Théry C, Duban L, Segura E *et al.* Indirect activation of naïve CD4+ T cells by dendritic cell–derived exosomes. *Nature Immunology* 2002;**3**:1156–62.

239. Tian T, Wang M, Ma D. TNF-α, a good or bad factor in hematological diseases? *PubMed* 2014;**1**:12.

240. Tomasik B, Fendler W, Chowdhury D. Serum microRNAs - potent biomarkers for radiation biodosimetry. *Oncotarget* 2018;**9**:14038–9.

241. Toulany M. Targeting K-Ras-mediated DNA damage response in radiation oncology: Current status, challenges and future perspectives. *Clinical and Translational Radiation Oncology* 2023;**38**:6–14.

242. Trissal M, Wong TN, Yao J-C *et al. MIR142* Loss-of-Function Mutations Derepress ASH1L to Increase *HOXA* Gene Expression and Promote Leukemogenesis. *Cancer Research* 2018;**78**:3510–21.

243. Truesdell SS, Mortensen RD, Seo M *et al.* MicroRNA-mediated mRNA translation activation in quiescent cells and oocytes involves recruitment of a nuclear microRNP. *Scientific Reports* 2012;**2**, DOI: 10.1038/srep00842.

244. Turner RM, Ristau BT, Nelson JB. Should Gleason score 6 still be called cancer? *Elsevier eBooks*. 2016, 41–7.

245. UniProt.

246. UNSCEAR 2006 Report Volume I. *United Nations : Scientific Committee on the Effects of Atomic Radiation*.

247. Valadi H, Ekström KM, Bossios A *et al.* Exosome-mediated transfer of mRNAs and microRNAs is a novel mechanism of genetic exchange between cells. *Nature Cell Biology* 2007;**9**:654–9.

248. Verbiest T, Bouffler S, Nutt SL *et al.* PU.1 downregulation in murine radiation-induced acute myeloid leukaemia (AML): from molecular mechanism to human AML. *Carcinogenesis* 2015;**36**:413–9.

249. Verbiest T, Finnon R, Brown N *et al.* Tracking preleukemic cells in vivo to reveal the sequence of molecular events in radiation leukemogenesis. *Leukemia* 2018;**32**:1435–44.

250. Vidal M. Exosomes: Revisiting their role as “garbage bags.” *Traffic* 2019;**20**:815–28.

251. Vishnubalaji R, Hamam R, Yue S-J *et al.* MicroRNA-320 suppresses colorectal cancer by targeting SOX4, FOXM1, and FOXQ1. *Oncotarget* 2016;**7**:35789–802.

252. Volk A, Li J, Xin J *et al.* AML Cells Utilize TNF-Driven JNK Signalling As a Critical NF-κB-Independent Survival Signal. *Blood* 2013, DOI: 10.1182/blood.v122.21.2890.2890.

253. Wang C, Lu H, Luo C *et al.* miR-412-5p targets Xpo1 to regulate angiogenesis in hemorrhoid tissue. *Gene* 2019;**705**:167–76.

254. Wang J, Chen T, Shan G. MIR-148B regulates proliferation and differentiation of neural stem cells via WNT/B-Catenin signalling in RAT ischemic stroke model. *Frontiers in Cellular Neuroscience* 2017;**11**, DOI: 10.3389/fncel.2017.00329.

255. Wang J, Hu Y, Ye C *et al.* miR-1224-5p inhibits the proliferation and invasion of ovarian cancer via targeting SND1. *Human Cell* 2020a;**33**:780–9.

256. Wang J, Jiang M, Xia S. MIR-339-5P increases radiosensitivity of lung cancer cells by targeting phosphatases of regenerating liver-1 (PRL-1). *Medical Science Monitor* 2018;**24**:8408–16.

257. Wang J, Zhu Q, Cao D *et al.* Bone marrow-derived IGF-1 orchestrates maintenance and regeneration of the adult skeleton. *Proceedings of the National Academy of Sciences of the United States of America* 2022a;**120**, DOI: 10.1073/pnas.2203779120.

258. Wang K, Long B, Li N *et al.* MicroRNA-2861 regulates programmed necrosis in cardiomyocyte by impairing adenine nucleotide translocase 1 expression. *Free Radical Biology and Medicine* 2016;**91**:58–67.

259. Wang L, Li C, Li R *et al.* MicroRNA-764-3p regulates 17β-estradiol synthesis of mouse ovarian granulosa cells by targeting steroidogenic factor-1. *In Vitro Cellular & Developmental Biology – Animal* 2015a;**52**:365–73.

260. Wang L, Niu N, Li L *et al.* H3K36 trimethylation mediated by SETD2 regulates the fate of bone marrow mesenchymal stem cells. *PLoS Biology* 2018a;**16**:e2006522.

261. Wang M, Dingler FA, Patel K. Genotoxic aldehydes in the hematopoietic system. *Blood* 2022;**139**:2119–29.

262. Wang S, Mi R, Cai Z *et al.* DAPK1 Interacts with the p38 Isoform MAPK14, Preventing Its Nuclear Translocation and Stimulation of Bone Marrow Adipogenesis. *Stem Cells* 2022b;**40**:508–22.

263. Wang T, Liu Y, Yuan W *et al.* Identification of microRNAome in rat bladder reveals miR-1949 as a potential inducer of bladder cancer following spinal cord injury. *Molecular Medicine Reports* 2015b;**12**:2849–57.

264. Wang X, Beute WK, Harrison JS *et al.* JNK1 as a signaling node in VDR-BRAF induction of cell death in AML. *Journal of Steroid Biochemistry and Molecular Biology/˜ the œJournal of Steroid Biochemistry and Molecular Biology* 2018b;**177**:149–54.

265. Wang X, Zhao Y, Lu Q *et al.* MIR-34A-5P inhibits proliferation, migration, invasion and epithelial-mesenchymal transition in esophageal squamous cell carcinoma by targeting LEF1 and inactivation of the Hippo-YAP1/TAZ signalling pathway. *Journal of Cancer* 2020b;**11**:3072–81.

266. Watahiki A, Wang Y, Morris J *et al.* MicroRNAs Associated with Metastatic Prostate Cancer. *PLOS ONE* 2011;**6**:e24950.

267. Waters PS, McDermott AM, Wall D *et al.* Relationship between Circulating and Tissue microRNAs in a Murine Model of Breast Cancer. *PLOS ONE* 2012;**7**:e50459.

268. Weng H, Lal K, Yang FF *et al.* The pathological role and prognostic impact of miR-181 in acute myeloid leukemia. *Cancer Genetics* 2015;**208**:225–9.

269. Wilkinson AC, Igarashi KJ, Nakauchi H. Haematopoietic stem cell self-renewal in vivo and ex vivo. *Nature Reviews Genetics* 2020;**21**:541–54.

270. Witkowska M, Majchrzak A, Cebula-Obrzut B *et al.* The distribution and potential prognostic value of SMAD protein expression in chronic lymphocytic leukemia. *Tumor Biology* 2017;**39**:101042831769455.

271. World Health Organization: WHO. Ionising radiation and health effects. *www.who.int* 2023.

272. Wu J, Lv Q, He J *et al.* MicroRNA-188 suppresses G1/S transition by targeting multiple cyclin/CDK complexes. *Cell Communication and Signalling* 2014;**12**, DOI: 10.1186/s12964-014-0066-6.

273. Wu S-C, Yang JC-S, Rau C-S *et al.* Profiling circulating MicroRNA expression in experimental sepsis using CECAL ligation and puncture. *PLOS ONE* 2013;**8**:e77936.

274. Wu Y, Fu Y, He K *et al.* Pan-cancer analysis of nemo-like kinase (NLK) expression convergence to pancreatic adenocarcinoma that has diagnostic, prognostic and treatment value. *Gene Reports* 2021;**24**:101260.

275. Wu Y, Su M, Zhang S *et al.* Abnormal expression of TGF-beta type II receptor isoforms contributes to acute myeloid leukemia. *Oncotarget* 2016;**8**:10037–49.

276. Xiao Y, Su C, Deng T. miR-223 decreases cell proliferation and enhances cell apoptosis in acute myeloid leukemia via targeting FBXW7. *Oncology Letters* 2016;**12**:3531–6.

277. Xie M, Qin H, Luo Q *et al.* MicroRNA-30a regulates cell proliferation and tumor growth of colorectal cancer by targeting CD73. *BMC Cancer* 2017;**17**, DOI: 10.1186/s12885-017-3291-8.

278. Xie M-Z, Shoulkamy MI, Salem AMH *et al.* Aldehydes with high and low toxicities inactivate cells by damaging distinct cellular targets. *Mutation Research: Fundamental and Molecular Mechanisms of Mutagenesis* 2016;**786**:41–51.

279. Xu W, Lucas FAS, Wang Z *et al.* Identifying microRNA targets in different gene regions. *BMC Bioinformatics* 2014;**15**, DOI: 10.1186/1471-2105-15-s7-s4.

280. Yadav M, Bhayana S, Liu J *et al.* Two-miRNA–based finger-stick assay for estimation of absorbed ionising radiation dose. *Science Translational Medicine* 2020;**12**, DOI: 10.1126/scitranslmed.aaw5831.

281. Yan J, Zhang Y-N, Liao J *et al.* MiR-497 suppresses angiogenesis and metastasis of hepatocellular carcinoma by inhibiting VEGFA and AEG-1. *Oncotarget* 2015;**6**:29527–42.

282. Yang J, Dong W-K, Zhang H *et al.* Exosomal microRNA panel as a diagnostic biomarker in patients with hepatocellular carcinoma. *Frontiers in Cell and Developmental Biology* 2022;**10**, DOI: 10.3389/fcell.2022.927251.

283. Yang J, Nie J, Ma X *et al.* Targeting PI3K in cancer: mechanisms and advances in clinical trials. *Molecular Cancer* 2019;**18**, DOI: 10.1186/s12943-019-0954-x.

284. Yang L, Guo Y, Liu X *et al.* The tumor suppressive miR-302c-3p inhibits migration and invasion of hepatocellular carcinoma cells by targeting TRAF4. *Journal of Cancer* 2018a;**9**:2693–701.

285. Yang R, Liu M, Liang H *et al.* miR-138-5p contributes to cell proliferation and invasion by targeting Survivin in bladder cancer cells. *Molecular Cancer* 2016a;**15**, DOI: 10.1186/s12943-016-0569-4.

286. Yang S, Liu B, Ji K *et al.* MicroRNA-5110 regulates pigmentation by cotargeting melanophilin and WNT family member 1. *The FASEB Journal* 2018b;**32**:5405–12.

287. Yang S, Wu Y, Zheng Z *et al.* MIR-191-5P disturbed the angiogenesis in a mice model of cerebral infarction by targeting inhibition of BDNF. *Neurology India* 2021;**69**:1601.

288. Yang W, Zhou C, Luo M *et al.* MiR-652-3p is upregulated in non-small cell lung cancer and promotes proliferation and metastasis by directly targeting Lgl1. *Oncotarget* 2016b;**7**:16703–15.

289. Yang Y, Xu J, Chen H *et al.* MiR-128-2 inhibits common lymphoid progenitors from developing into progenitor B cells. *Oncotarget* 2016c;**7**:17520–31.

290. Yang Y, Xu J, Chen H *et al.* MiR-128-2 inhibits common lymphoid progenitors from developing into progenitor B cells. *Oncotarget* 2016d;**7**:17520–31.

291. Yang Y. Role of fatty acid synthase in gemcitabine and radiation resistance of pancreatic cancers. *PubMed Central (PMC)* 2011.

292. Yang Z, Zhong W, Yang L *et al.* The emerging role of exosomes in radiotherapy. *Cell Communication and Signaling* 2022;**20**, DOI: 10.1186/s12964-022-00986-1.

293. Yanovskiy K, Shaki YY, Socol Y. Ethics of adoption and use of the linear No-Threshold model. *Dose-response* 2019;**17**:155932581882260.

294. Ying X, Zhang W, Fang M *et al.* miR-345-5p regulates proliferation, cell cycle, and apoptosis of acute myeloid leukemia cells by targeting AKT2. *Journal of Cellular Biochemistry* 2018, DOI: 10.1002/jcb.27461.

295. Yu G, Yin Z, He H *et al.* Low serum miR-223 expression predicts poor outcome in patients with acute myeloid leukemia. *Journal of Clinical Laboratory Analysis* 2020a;**34**, DOI: 10.1002/jcla.23096.

296. Yu J, Leung WK. 10 Loss of cyclin D2 expression in gastric cancer. *Handbook of Immunohistochemistry and in Situ Hybridization of Human Carcinomas*. 2005, 161–8.

297. Yu Y, Zhou H, Zhang G *et al.* Targeting the canonical Wnt/β-catenin pathway in cancer radioresistance: Updates on the molecular mechanisms. *Journal of Cancer Research and Therapeutics* 2019;**15**:272.

298. Yuan K, Ai W-B, Wan L-Y *et al.* The miR-290-295 cluster as multi-faceted players in mouse embryonic stem cells. *Cell & Bioscience* 2017;**7**, DOI: 10.1186/s13578-017-0166-2.

299. Yuan Z-H, Liu T, Wang H *et al.* Fatty acids metabolism: the bridge between ferroptosis and ionizing radiation. *Frontiers in Cell and Developmental Biology* 2021;**9**, DOI: 10.3389/fcell.2021.675617.

300. Zeng H, Hu M, Lu Y *et al.* MicroRNA 34a promotes ionising radiation–induced DNA damage repair in murine hematopoietic stem cells. *The FASEB Journal* 2019;**33**:8138–47.

301. Zhai L, Wu R, Han W *et al.* miR-127 enhances myogenic cell differentiation by targeting S1PR3. *Cell Death and Disease* 2017;**8**:e2707.

302. Zhang A, Hu H. A Novel Blood-Based microRNA Diagnostic Model with High Accuracy for Multi-Cancer Early Detection. *Cancers* 2022;**14**:1450.

303. Zhang H, Wang J, Wang Y *et al.* Long Non-Coding LEF1-AS1 sponge MIR-5100 regulates apoptosis and autophagy in gastric cancer cells via the MIR-

5100/DEK/AMPK-MTOR axis. *International Journal of Molecular Sciences* 2022;**23**:4787.

304. Zhang J, Li S, Li L *et al.* Exosome and Exosomal MicroRNA: Trafficking, sorting, and function. *Genomics, Proteomics & Bioinformatics* 2015;**13**:17–24.

305. Zhang J, Zhang L, Cui H *et al.* High expression levels of SMAD3 and SMAD7 at diagnosis predict poor prognosis in acute myeloid leukemia patients undergoing chemotherapy. *Cancer Gene Therapy* 2018;**26**:119–27.

306. Zhang L, Bailleul J, Yazal T *et al.* PK-M2-mediated metabolic changes in breast cancer cells induced by ionizing radiation. *Breast Cancer Research and Treatment* 2019;**178**:75–86.

307. Zhang L, Dong Y, Zhu N *et al.* microRNA-139-5p exerts tumor suppressor function by targeting NOTCH1 in colorectal cancer. *Molecular Cancer* 2014;**13**, DOI: 10.1186/1476-4598-13-124.

308. Zhang L, Liao Y, Tang L. MicroRNA-34 family: a potential tumor suppressor and therapeutic candidate in cancer. *Journal of Experimental & Clinical Cancer Research* 2019;**38**, DOI: 10.1186/s13046-019-1059-5.

309. Zhang M, Lan H, Peng S *et al.* MiR-223-3p attenuates radiation-induced inflammatory response and inhibits the activation of NLRP3 inflammasome in macrophages. *International Immunopharmacology* 2023;**122**:110616.

310. Zhang P, Li X, Zhang S *et al.* miR-370-3p Regulates Adipogenesis through Targeting Mknk1. *Molecules* 2021a;**26**:6926.

311. Zhang S, Li D, Zhao M *et al.* Exosomal MIR-183-5P shuttled by M2 polarized Tumor-Associated macrophage promotes the development of colon cancer via targeting THEM4 mediated PI3K/AKT and NF-KB pathways. *Frontiers in Oncology* 2021b;**11**, DOI: 10.3389/fonc.2021.672684.

312. Zhang X, Tamasi J, Lu X *et al.* Epidermal growth factor receptor plays an anabolic role in bone metabolism in vivo. *Journal of Bone and Mineral Research* 2010;**26**:1022–34.

313. Zhang Y, Liu J, Zhou L *et al.* Exosomal small RNA sequencing uncovers Dose-Specific MIRNA markers for ionising radiation exposure. *Dose-response* 2020;**18**:155932582092673.

314. Zhao P, Zhao L, Zhang K *et al.* Infection with street strain rabies virus induces modulation of the microRNA profile of the mouse brain. *Virology Journal* 2012;**9**, DOI: 10.1186/1743-422x-9-159.

315. Zhou W, Zou B, Liu L *et al.* MicroRNA-98 acts as a tumor suppressor in hepatocellular carcinoma via targeting SALL4. *Oncotarget* 2016;**7**:74059–73.

316. Zitvogel L, Regnault A, Lozier A *et al.* Eradication of established murine tumors using a novel cell-free vaccine: dendritic cell derived exosomes. *Nature Medicine* 1998;**4**:594–600.

317. Zuber J, Radtke I, Pardee TS *et al.* Mouse models of human AML accurately predict chemotherapy response. *Genes & Development* 2009;**23**:877–89.

8. Appendix

Below are Western Blots demonstrating common microvesicle and exosome markers (Calnexin, CD63, ALIX and TSG101). The following image manipulations were performed on all Western Blots prior to presentation here:

- Saturation correction: removal of original blue hue for black and white.
- Increased brightness and increased contrast (brightness increased to 55, contrast to 40).
- Introduction of protein size ladder (whereas previously it was manually drawn onto the film negative).
- Placement of protein labels.
- Manual removal of residual stains (e.g. dark stains at top of loading wells).

No excision of bands has been performed. Residual noise surrounding the sample has been left intact.

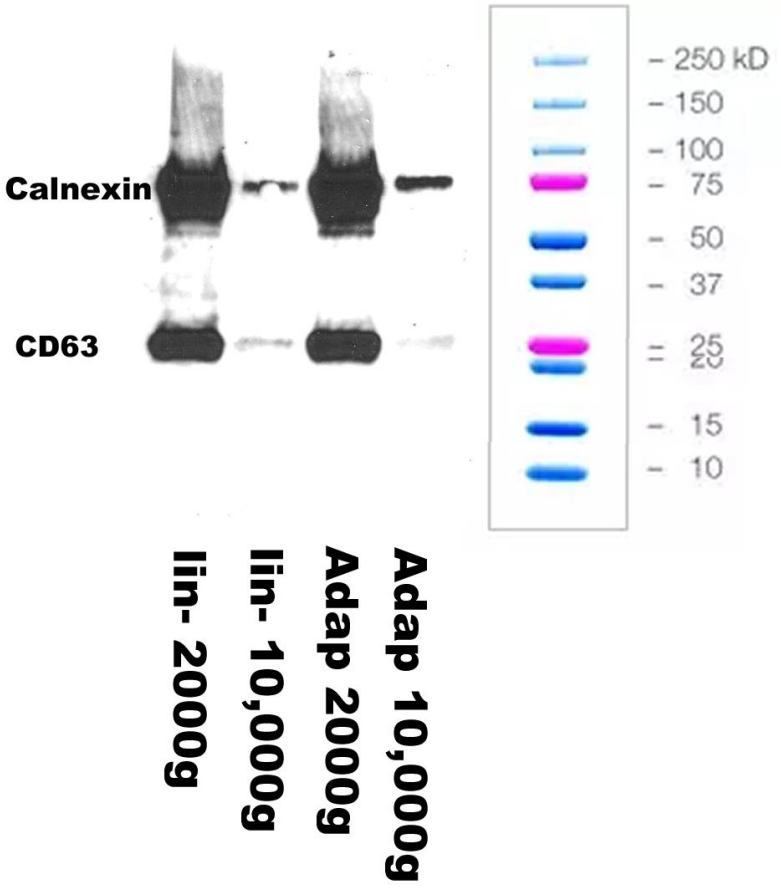


Figure A.01: Lineage depleted and adaptive media-derived EVs. Adaptive media was a succession of medias designed to deplete lineage+ cells, while lin- refers to direct lineage depletion. The purpose was to see the impact of a) lineage depletion and b) different centrifugation protocols on EV yield, marked here by CD63 (commonly found on small EVs) and calnexin, which can be a cellular contaminant, but also found on larger EVs (Saludas *et al.,* 2022, European Journal of Pharmaceutics and Biopharmaceutics). As seen, while 10,000g largely depletes calnexin, it also drastically depletes CD63. We ultimately compromised and settled on two centrifugation steps: 250g to remove cells, followed by 2000g to remove leftover cells.

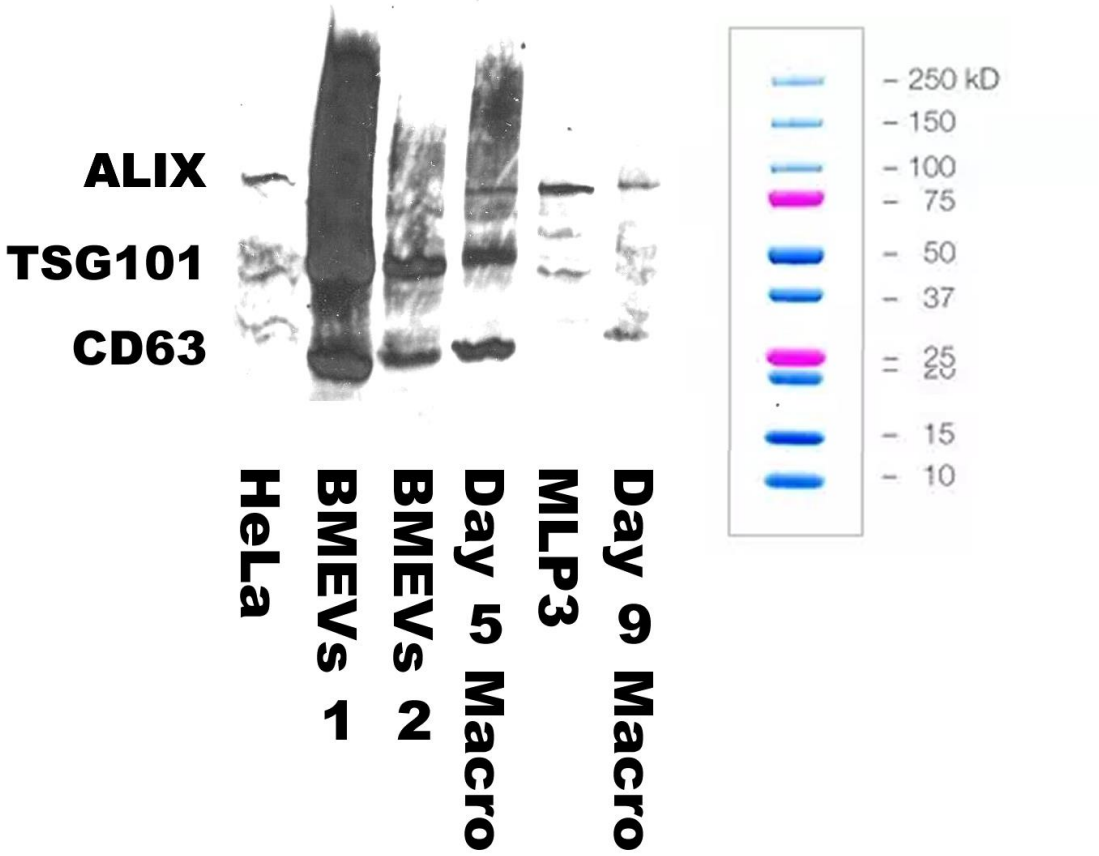


Figure A.02: Staining of different EV samples with ALIX, TSG101 and CD63. HeLa was used as a control sample, with presence of ALIX, TSG101 and CD63 confirmed, which are all membrane markers for EV presence. BM EVs 1 was a murine BM-derived EV preparation without prior centrifugation steps to ExoQuick addition. BM EVs 2 was a sample after 250g followed by 2000g centrifugation, then ExoQuick addition. Day 5 macrophages were BM-derived macrophages prepared as described in section **2.11** after 5 days of culture**.** MLP3 was a further control, a leukaemia stem cell line. Day 9 macro were the same macrophages but after 9 days in culture. Given the stark drop off in EV signal, we ultimately decided that 5 days was the maximum amount of time we would have macrophages in culture.

Appendix A: 3.01 Genetic targets involved in MAPK, Hippo, Wnt and FoxO pathways

The below tables are a collection of the KEGG-predicted miRNA and their predicted gene targets in different signalling pathways found in high clonal expansion CBA mCh/GFP mice. As seen, a wide range of genes are targeted for regulation, as opposed to a single subset of genes identically found across pathways. As demonstrated in chapter 3 however, an overlap exists, suggesting a core regulatory component.

Table 3.01a: Hippo pathway gene targets

miRNA	Gene target			
mmu-miR-181c-5p	Bmpr2	Mob1b	Lats1	Smad7
	Mpp5	Tcf7l2	Tead1	Crb1
	Ywhag	Tgfbr1	Dlg2	
mmu-miR-1897-3p	Wnt16			
mmu-miR-154-5p	Gdf6	Ppp2r2a		
mmu-miR-128-3p	Pard6b	Ywhab	Dlg2	Crb1
	Ppp2r2d	Tgfbr1	Wnt3a	Ppp1cc
	Mob1b	Tgfb3	Bbc3	
mmu-miR-497a-5p	Gsk3b	Axin2	Ywhaq	Smad7
	Ywhah	Lats1	Ccnd2	
	Amot	Wnt7a	Wnt3a	
mmu-miR-370-3p	Wnt10b	Smad1	Gdf5	
mmu-miR-132-3p	Sox2	Gdf5		
mmu-miR-138-5p	Tcf7	Tead1	Gdf5	
mmu-miR-540-3p	Crb2	Yap1		
mmu-miR-710	Gsk3b	Tcf712	Fzd7	
	Fzd2			
mmu-miR-302c-3p	Tgfbr2	Ccnd2		
mmu-miR-486a-5p	Sav1	Tead1		
mmu-miR-139-5p	Ppp2ca	Ywhaq		
mmu-miR-423-5p	Dvl3			
mmu-miR-382-5p	Tcf712	Tgfbr1		
mmu-miR-1198-5p	Tead1			
mmu-miR-345-5p	Tead1			
mmu-miR-2861	Ppp2r1b			

Table 3.01b: MAPK pathway gene targets

miRNA	Gene target			
mmu-miR-382-5p	Ppp3cc	Cacna1e	Traf6	Map3k8
	Ppp3r2	Braf	Hspa2	Tgfbr1
mmu-miR-326-3p	Pak1	Cacna1e	Fgf18	Fgfr2
mmu-miR-139-5p	Jun	Cacna2d1	Rap1b	
	Map3k1	Prkx	Mapk8	
mmu-miR-128-3p	Mapk14	Grb2	Egfr	Rap1b
	Fgf14	Rapgef2	Map2k4	Mapkapk3
	Rps6ka5	Ntrk2	Map3k14	Map2k7
	Cacna2d3	Tgfbr1	Sos1	Tgfb3
	Map3k1	Nf1	Cacng2	Cacna1f
	Zak	Map3k2	Dusp5	
mmu-miR-302c-3p	Fgf10	Rps6ka5	Dusp2	Mecom
	Mef2c	Rps6ka1	Rps6ka3	Sos1
	Rap1a	Mknk2	Tgfbr2	Fgf9
	Map3k2			
mmu-miR-497a-5p	Sos2	Nfatc3	Mapk3	Cacna1f
	Map2k1	Cacnb1	Braf	Mapk8
	Ppm1a	Cacna1i	Mapk9	
	Rps6ka3	Nf1	Nras	
mmu-miR-486a-5p	Mef2c	Nf1	Stk4	Map3k7
mmu-miR-370-3p	Mef2c	Nf1	Map2k7	Arrb1
mmu-miR-154-5p	Sos2	Rps6ka5		
mmu-miR-1198-5p	Rps6ka3	Cacnb4	Hspa2	
mmu-miR-181c-5p	Map2k1	Nlk	Braf	Tnf
	Fos	Tgfbr1	Rap1b	Pp3r1
	Rps6ka3	Il1a	Rras2	
mmu-miR-132-3p	Cacnb4	Sos1	Rras2	
	Nlk	Cacng2	Mapkapk2	
	Dusp9	Hspa1b	Cacna1c	
mmu-miR-1224-5p	Rps6ka3	Braf	Sos1	Cacna1f
mmu-miR-138-5p	Braf	Rela		
mmu-miR-423-5p	Cacnb3	Mras	Cacna1f	Cacna1c
mmu-miR-1949	Mef2c			
mmu-miR-1897-3p	Tab2			
mmu-miR-1983	Mapk10	Mapk9	Flna	
mmu-miR-710	Fgf15	Nras		
mmu-miR-1902	Ppm1a	Dusp5		

Table 3.01c: Wnt pathway gene targets

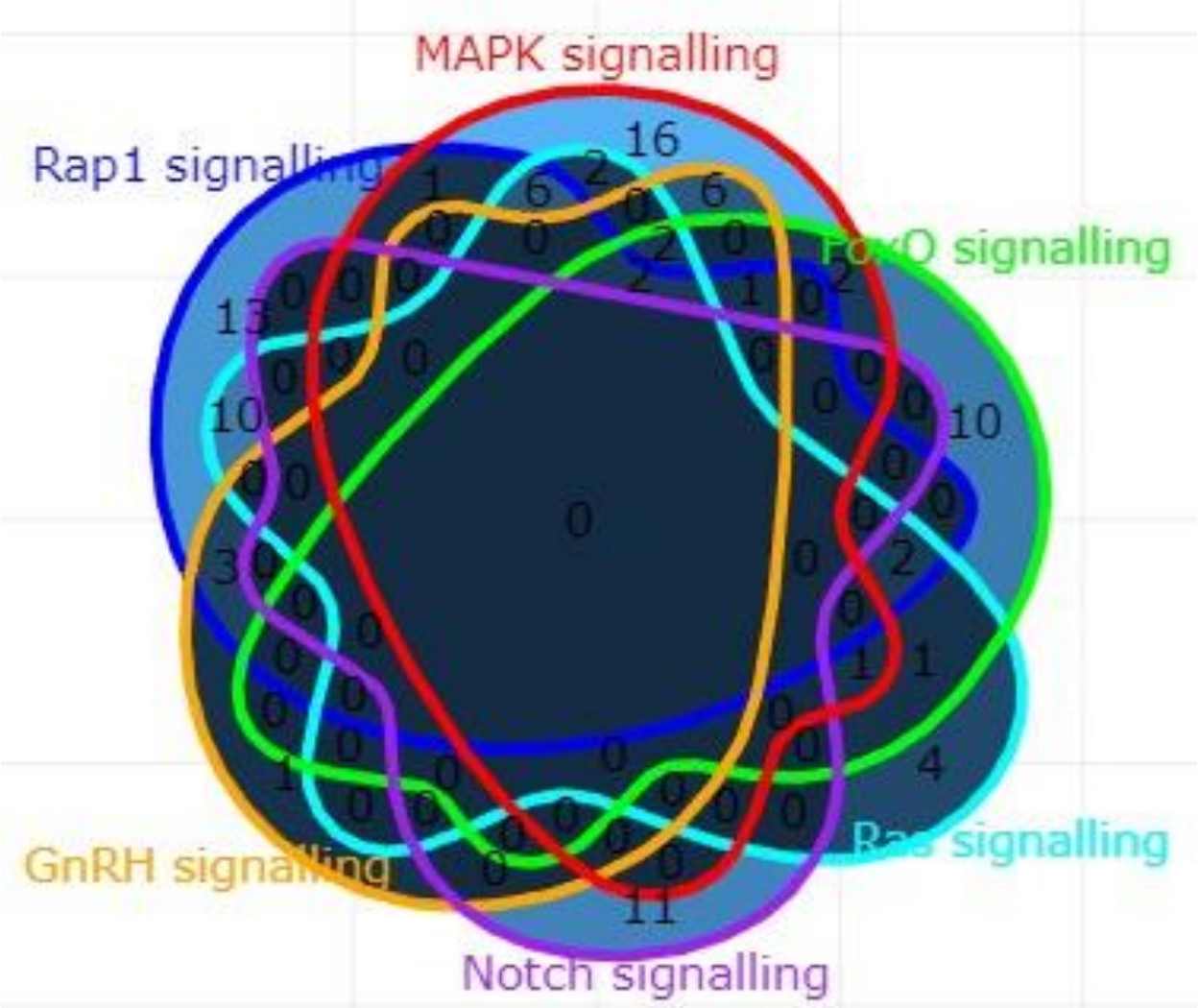
miRNA	Gene target			
mmu-miR-710	Ep300 Gsk3b	Fzd2	Tcf712	Fzd7
mmu-miR-154-5p	Camk2g			
mmu-miR-181c-5p	Senp2 Camk2g	Tcf7l2 Nlk	Csnk1a1 Ppp3r1	Plcb1
mmu-miR-128-3p	Sfrp1 Vangl2	Vangl1 Wnt3a	Plcb1 Dkk2	
mmu-miR-423-5p	Dvl3	Lrp5	Camk2a	Plcb2
mmu-miR-497a-5p	Gsk3b Lrp6 Nfatc3	Axin2 Siah1a Mapk9	Wnt7a Ccnd2 Wnt3a	Mapk8
mmu-miR-345-5p	Chd8			
mmu-miR-132-3p	Ep300	Nlk	Daam1	
mmu-miR-1983	Mapk10	Mapk9		
mmu-miR-1949	Wif1			
mmu-miR-139-5p	Jun	Prkx	Plcb1	Mapk8
mmu-miR-2861	Ctbp2			
mmu-miR-138-5p	Tcf7	Rock2	Daam2	
mmu-miR-486a-5p	Dkk2	Map3k7		
mmu-miR-382-5p	Camk2d	Ppp3cc	Ppp3r2	Tcf712
mmu-miR-302c-3p	Rock2	Ccnd2		
mmu-miR-1224-5p	Psen1			
mmu-miR-1198-5p	Rock2			
mmu-miR-370-3p	Wnt10b			
mmu-miR-1897-3p	Wnt16			

Table 3.01d: FoxO pathway gene targets

miRNA	Gene target			
mmu-miR-128-3p	Mapk14	Plk2	Irs1	Sos1
	Pik3r1	Foxo1	Tgfbr1	Tgfb3
	Pdpk1	Insr	Egfr	Setd7
	Grb2	Grm1	Foxo4	
mmu-miR-497a-5p	Sos2	Insr	Mapk9	Sgk1
	Pik3r1	Usp7	Nras	Mapk8
	Irs4	Mapk3	Ccnd2	
	Map2k1	Braf	Prkag2	
mmu-miR-710	Pik3r3	Ep300	Foxo1	Nras
mmu-miR-132-3p	Ep300	Sos1	Pten	
	Nlk	Sirt1	Sod2	
mmu-miR-302c-3p	Tgfbr2	Sos1	Ccnd2	Rbl2
mmu-miR-181c-5p	Pik3r3	Nlk	Braf	S1pr1
	Map2k1	Tgfbr1	Bcl2l11	Pten
mmu-miR-1983	Mapk10	Mapk9		
mmu-miR-154-5p	Sos2			
mmu-miR-1198-5p	Irs4	Pck2		
mmu-miR-486a-5p	Pik3r1	Pdpk1	Stk4	Pten
mmu-miR-139-5p	Homer2	Mapk8		
mmu-miR-1897-3p	Irs4			
mmu-miR-370-3p	Foxo1			
mmu-miR-382-5p	Pdpk1	Tgfbr1	Braf	
mmu-miR-1224-5p	Braf	Sos1		
mmu-miR-138-5p	Braf			
mmu-miR-540-3p	Pten			

Appendix 4.01A

Figure 4.01A: Notch signalling in mesenchymal stem cells. As seen, targeted genes in the Notch pathway (of which there are 11) do not overlap with MAPK, Rap1, FoxO, Ras, or GnRH signalling within MSCs 48 hours post-IR insult.



Appendix A:6.01 Protocol for analysing the effect of post-IR EVs on cytogenetic aberrations

Materials:

- ¼ fresh human peripheral blood Leukopak (BioIVT, but other suppliers e.g. StemCell, Sanbio can also be used)
- Acid citrose dextrose solution (ACD) (C3821, Sigma-Aldrich)
- RPMI1640 (Gibco)
- Penicillin/Streptomycin (Gibco)
- 70% Ethanol
- RBC lysis buffer 1X (Invitrogen)
- PBS
- FBS
- Panexin Basic (Pan-Biotech)
- T-125/T-75 suspension culture flasks (Sarstedt)
- Merck-Millipore 10,000kDa spin filters (Merck)
- Syto RNASelect Green Fluorescent Cell Stain, 5mM solution in DMSO (S3 2703, Invitrogen)
- 7-AAD Viability Staining Solution (00-6993-50, Invitrogen)
- Swinging bucket rotor centrifuge with 50ml Falcon Tube adaptors
- FACS machine

Protocol:

Day 1:

1. Prepare 1X Pen-Strep, 10%FBS RPMI 1640 media. Store at 4C.
2. Prepare 1X Pen-Strep, 10% Panexin Basic RPMI1640 media. Store at 4C.
3. Upon delivery of ¼ size Leukopak, immediately clamp to stand in sterilized BSC class II, such that the drainage tubes face downwards.

4. Sterilize the exterior of the Leukopak with 70% ethanol and allow to dry.
5. Record the estimated total blood volume within the Leukopak.
6. Prepare an appropriate container e.g. 50ml Falcon tube containing 15% by volume ACD
7. Sterilize a pair of scissors with 70% ethanol and allow to dry OR use sealed, autoclaved scissors.
8. Placing Falcon tube beneath the Leukopak, cut the drainage tube and remove tie, allowing blood to drain into Falcon tube. Repeat as necessary depending on total volume in the Leukopak. Cap and store in rack.
9. Cut open the top of the Leukopak and flush with 20ml RPMI 1640 prepared in step 1, draining into fresh 50ml Falcon tube.
10. Spin at 1200 RPM for 5 minutes in swinging bucket rotor to pellet cells. Remove supernatant, leaving 5ml volume above pellet to not disturb it.
11. Wash with 45ml RPMI1640 back up to 50ml, resuspending cell pellet.
12. Repeat steps 10 and 11 2X for a total of 3 washes, ending with a pellet suspended in 5ml.
13. Add 2ml RBC lysis buffer and incubate for 2-3 minutes. The solution will be a turbid red. Visually check if it becomes a clear red.
14. After 3 minutes, add PBS up to 50ml and spin at 1200 RPM for 5 minutes to pellet cells. Discard supernatant. If pellet is still a deep red, repeat step 13 once.
15. Count remaining cells e.g. using Incucyte automated cell counter and resuspend at $5x10^6$ cells/ml in complete RPMI1640 media.
16. Split into two halves, hereafter referred to as donor and recipient. Label accordingly.
17. Dispense recipient cells into T-125 or T-75 flasks. Incubate at 37C, 5% CO_2.
18. Split donor population into two halves: One half for 2Gy irradiation, the other for sham irradiation.
19. Irradiate samples as per labelled dose. Return to incubator.
20. Prepare a 1mM DMSO stock of Syto RNASelect Green.

21. Dispense 50ml of the culture into labelled 50ml Falcon tubes.

22. Add 50µl stock solution to 50ml of culture medium to obtain a final dye concentration of 1µM.

23. Incubate at 37C for 20 minutes. Protect from light.

24. Spin at 1200RPM for 5 minutes, resuspend in PBS.

25. Spin at 1200RPM for 5 minutes and remove PBS.

26. Repeat steps 24 and 25 2X for a total of 3 washes.

27. Resuspend in 50ml 10% Panexin-Basic RPMI1640. Dispense into labelled culture tube.

28. Incubate both donor and recipient cultures for 24 hours.

Day 2:

1. Add 2ml sterile PBS to 10,000kDa Merck-Millipore spin filter.
2. Centrifuge at 4,000g in a swinging bucket rotor for 15 minutes.
3. Aspirate and discard pre-filter. Discard filtrate. The spin filter is now primed.
4. Spin donor cell cultures at 1200RPM for 5 minutes. Remove supernatant and dispense maximum 15ml into labelled spin filter. Place remaining supernatant in fresh labelled 50ml Falcon tube. Store supernatant and pellet on ice.
5. Centrifuge spin filter with supernatant at 4000g for 30 minutes. Discard filtrate.
6. Repeat until all supernatant volume has been passed through.
7. Add 14ml sterile PBS and centrifuge at 4000g for 30 minutes. Discard filtrate. EV sample is now ready for further processing.
8. Using 200µl pipette, aspirate pre-filter, concentrated EVs. Dispense into recipient PBMC cell culture, labelling the donor (e.g. 2Gy EVs, 0Gy EVs). Do not dispense into at least 3 control flasks.
9. Incubate at 37C, 5% CO_2 for 24 hours.

10. Depending on further user-specific applications, either retain or discard pelleted cells from step 4.

Day 3:

1. Spin down recipient cell cultures at 1200 RPM, discarding supernatant and retaining pellet. Count and resuspend to $1x10^6$ cells/100µl in sterile PBS in FACS tubes.
2. Stain with 5µl 7-AAD per 100µl volume. Incubate for minimum 30 minutes on ice, protected from light.
3. Set gates on FACS machine: set thresholds using unstained cells (no 7-AAD) and stained cells with no donor EVs. Use FITC fluorescence channel for Syto RNASelect Green fluorescence.
4. Sort cell populations based on the following gates: Live, followed by segregation into two populations, FITC+ and FITC-. FITC+ represents cells with significant EV uptake, FITC- represents cells without EVs.
5. There will be 5 populations: FITC+/FITC- 2Gy donors, FITC+/FITC- 0Gy donors, and a control population with no donors.
6. Submit populations for downstream cytogenetic protocols e.g. dicentric breaks (CHO method) and γH2AX counting.

The protocol seemed to function up until step 6 of Day 3, hence why the cytogenetic protocols have not been replicated here. It is our suggestion to troubleshoot from this point onward to achieve a fully functional protocol allowing for cytogenetic damage characterization of cells within the same population that have and have not endocytosed IR-derived EVs.